Compositional and Genomic Factors Underlying the Efficiency of Corn Stover Bioconversion by *Ustilago maydis*

Dissertation

Stefan Josef Robertz

November 2025

Compositional and Genomic Factors Underlying the Efficiency of Corn Stover Bioconversion by *Ustilago maydis*

Inaugural-Dissertation

zur Erlangung des Doktorgrades
der Mathematisch-Naturwissenschaftlichen Fakultät
der Heinrich-Heine-Universität Düsseldorf

vorgelegt von

Stefan Josef Robertz

aus Düren

Düsseldorf, November 2025

Aus dem Institut für Pflanzliche Zell Biologie und Biotechnologie
der Heinrich-Heine-Universität Düsseldorf

Gedruckt mit der Genehmigung der
Mathematisch-Naturwissenschaftlichen Fakultät der
Heinrich-Heine-Universität Düsseldorf

Berichterstatter:

1. Prof. Dr. Markus Pauly

2. Prof. Dr. Michael Feldbrügge

Tag der mündlichen Prüfung: 05.03.2026

Eidesstattliche Versicherung

Ich versichere an Eides Statt, dass die Dissertation von mir selbständig und ohne unzulässige fremde Hilfe unter Beachtung der „Grundsätze zur Sicherung guter wissenschaftlicher Praxis an der Heinrich-Heine-Universität Düsseldorf". Die Dissertation wurde in ihrer jetzigen oder vergleichbaren Form noch bei keiner anderen Hochschule eingereicht. Ich habe zuvor keinen erfolglosen Promotionsversuch unternommen.

Düsseldorf, 04.11.2025 _____

Stefan Josef Robertz

Funding, publications and collaborations

This work was conducted during my time as research assistant at the Institute for Plant Cell Biology and Biotechnology at Heinrich Heine University, Düsseldorf. My project was performed within the project “NextVegOil – Production of a sustainable and tailor-made microbial palm oil substitute from agricultural residues” (Boost Fund 2.0 “NextVegOil” 2021_04), funded by the Strategieprojekt BioSC (No. 313/323-400-002 13). Funding is gratefully acknowledged.

By the time of submission, most of the first chapter (section 4.1) of this thesis was published under the Creative Commons license CC BY, while the other chapters are unpublished. The publications are:

Wang, S., Robertz, S., Seven, M., Kraemer, F., Kuhn, B. M., Liu, L., Lunde, C., Pauly, M., & Ramirez, V. (2023). A large-scale forward genetic screen for maize mutants with altered lignocellulosic properties. *Frontiers in Plant Science*, *14*(March), 1–12. https://doi.org/10.3389/fpls.2023.1099009

Robertz, S., Philipp, M., Schipper, K., Richter, P., Miebach, K., Magnus, J., Pauly, M., & Ramirez, V. (2024). Monitoring corn stover processing by the fungus *Ustilago maydis*. *Bioresources and Bioprocessing*, *3*. https://doi.org/10.1186/s40643-024-00802-3

Plant research is a highly interdisciplinary field; thus, the work often depends on close collaboration with other institutes of different disciplines. The *Ustilago maydis* strains used throughout this work were generated and provided by colleagues of the Institute for Microbiology, Prof. Dr. Michael Feldbrügge, HHU Düsseldorf. Furthermore, the BioLector® platform used for corn stover fermentation experiments was also provided by the Institute for Microbiology. The research on the activity and subcellular localization of *Zm*SWEET2a in different organisms was possible thanks to the support of the Institute for Molecular Physiology, Prof. Dr. Wolf B. Frommer, HHU Düsseldorf, by providing the necessary technical equipment (including all vectors and organisms) and operating the confocal microscope. The support of these collaborators throughout my work is gratefully acknowledged, especially of Dr. Magnus Philipp and Dr. Till Moritz Schladt.

Abstract

A key aspect of a sustainable bioeconomy is the bioconversion of renewable, agricultural waste streams by microorganisms for the production of high-value compounds. A promising approach is the bioconversion of corn stover by the fungus *Ustilago maydis*. *U. maydis* is able to grow on corn stover as the sole nutrient source. However, the utilization of this abundant agricultural waste is often hindered by its complex and heterogeneous nature and the need for an efficient breakdown into a suitable feedstock. The specific corn stover components utilized by *U. maydis* and the bottlenecks in the fermentation process remain largely unexplored.

To tackle this challenge, the first chapter of this thesis describes a platform to monitor *U. maydis* performance growing on corn stover. It uses online measurements of scattered light, fluorescence and pH to track fungal growth, combined with a detailed biochemical characterization of the post-fermentation biomass. The results reveal that *U. maydis* primarily feeds on the water-soluble carbohydrates present in corn stover, while the lignocellulosic fraction remains underutilized. To improve conversion of the abundant lignocellulosic fraction the effect on fungal performance of different lignocellulose corn mutants and different lignocellulose pretreatments was evaluated. The use of a lignin mutant (*bm3*) in combination with a commercial cellulolytic enzyme cocktail proofed to be the most efficient performance boost and combined, increased fungal performance by 120 % compared to wildtype corn stover (variety B73).

The second chapter focuses on the water-soluble carbohydrate fraction in corn stover, which is the most influential on *U. maydis* biomass production. The results highlight the substantial variability of this important fraction across a corn natural variation panel. To identify the genetic basis of this variation, a genome wide association study was conducted, which identified 37 quantitative trait loci associated with water-soluble carbohydrate related traits. Haplotype-chemotype association studies identified three candidate genes potentially involved in corn stover water-soluble carbohydrate traits. Functional studies in *Saccharomyces cerevisiae*, *Nicotiana benthamiana* or *in vitro* validated the roles of two of the candidate genes and revealed haplotype-specific differences in protein activity for one candidate gene. These insights lay a foundation for further studies to increase water-soluble carbohydrate content in corn stover and thereby enhancing bioconversion by *U. maydis*.

Abbreviations

Abbreviation	Description
A. tumefaciens	*Agrobacterium tumefaciens*
3-PGA	3-phosphoglycerate
A. niger	*Aspergillus niger*
a.u.	Arbitrary units
ADP	Adenosine-diphosphate
AIR	Alcohol-insoluble residue
Ara*f*	Arabinofuranosyl
At	Arabidopsis thaliana
ATP	Adenosine-triphosphate
AX	Arabinoxylan
bm	brown-midrib
$CaCl_2$	Calcium chloride
CAD	Cinnamyl alcohol dehydrogenase
cal1	candy-leaf 1
CAZyme	Carbohydrate active enzymes
CC	Crystalline cellulose
CCR	Cinnamoyl CoA reductase
CDS	Coding sequence
CM	Complete medium
COMT	O-methyltransferase
DOG	2-deoxy-d-glucose
E. coli	*Escherichia coli*
F6P	Fructose-6-phosphate
FA	Ferulic acid
Fru	Fructose
G6PDH	Glucose-6-phosphate dehydrogenase
Gal	Galactose
GAX	O-acetylated glucuronoarabinoxylan
GC-MS	Gas chromatograph coupled with a mass analyzer
Gfp	Green-fluorescent protein
Glc	Glucose
GlcA	Glucuronic acid
GlcN	Glucosamine
G-lignin	Guaiacyl
GOPOD	Glucose oxidase peroxidase
GT	Glycosyltransferase
GWAS	Genome-wide association study
H_2SO_4	Sulfuric acid
HC	Hemicellulose
HCl	Hydrochloric acid
H-lignin	p-hydroxyphenyl

HPAEC	High-performance anion-exchange chromatography
KOH	Potassium hydroxide
LD	Linkage disequilibrium
LiAc	Lithium acetate
M6P	Mannose-6-phosphate
MeGlcA	4-O-methylglucoronic acid
MES	2-(N-Morpholino) ethanesulfonic acid
$MgCl_2$	Magnesium chloride
MLG	Mixed-linkage glucan
MS	Murashige & Skoog media
MT	Million tons
N. benthamiana	*Nicotiana benthamiana*
NADP/NADPH	Nicotinamide adenine dinucleotide phosphate (hydrogen)
NaOH	Sodium hydroxide
OD	Optical density
Os	*Oryza sativa*
PAD	Pulsed amperometric detector
pCA	p-coumaric acid
PCR	Polymerase chain reaction
PEG	Polyethylenglycol
PGI	Phosphoglucose isomerase
PMI	Phosphomannose isomerase
QTL	Quantitative trait loci
rpm	rounds per minute
RT	room temperature
S. cerevisiae	*Saccharomyces cerevisiae*
SD	Standard deviation
SDS	Sodium dodecyl sulphate
S-lignin	Syringyl
SNP	Single nucleotide polymorphism
Srt1	High-affinity sucrose transporter
Suc	Sucrose
SWEET	Sugars Will Eventually be Exported Transporters
TFA	Trifluoracetic acid
U. maydis	*Ustilago maydis*
UDP-Glc	Uridine diphosphate glucose
Ura	Uracil
wt%	weight percent
Xyl	Xylose
Xyl*p*	Xylopyranosyl
Zm	*Zea mays*

Table of contents

List of figures

List of tables

1 Background

Increasing world population and ongoing depletion of fossil resources make the transition towards a bio-based economy more and more relevant. A bio-based economy focuses on replacing fossil-derived materials with renewable, environment-friendly resources, thereby reducing dependence on non-sustainable energy sources and mitigating the environmental impact. A central strategy in this transition is “bioconversion”, the microbial transformation of plant biomass, preferably agricultural waste streams, into high-value products. Bioconversion involves breaking down the complex polysaccharides in plant biomass into smaller, fermentable sugars, ideally by the enzymatic repertoire of the employed microorganism. These sugars are then taken up by the microorganism and metabolized into target compounds of industrial or commercial interest. Therefore, selecting both an efficient microorganism and a suitable plant biomass source is critical to optimizing the bioconversion process.

Among various plant families, the grasses, or Poaceae, are of major importance to modern agriculture, as many of the world´s most essential crops, such as sugarcane, maize, wheat, rice and barley, are grasses (Soreng et al., 2022; van der Weijde et al., 2013). Most crops are grown for their seeds, while their by-products, comprising stems and leaves, referred to as “stover”, are often underutilized through inefficient practices like burning. In Germany, maize (or corn; *Zea mays*) is among the most important crops, and its stover, represents its most abundant by-product. Based on previous calculations (Bichot et al., 2018) and FAO data (Food and Agriculture Organization of the United Nations) (FAO, 2025), corn stover production in Germany reached nearly 1.5 million tons (MT) in 2023 (Table 1). Considering that approximately 25 % of stover remains on the field post-harvest to enhance soil quality (Bichot et al., 2018), around 1.1 MT of corn stover was available for bioconversion in 2023, without taking into account the relatively minor amounts already utilized for such processes.

Table 1: **Corn stover production in Germany in 2023.** Data sourced from FAO (FAO, 2025) and calculations based on (Bichot et al., 2018).

Area (ha)	Corn cob production (t)	Yield (t/ha)	Ratio crop residues	Residue production (t)	Residue left on the ground (%)	Residue left on the ground (t)	Residue available for bioconversion (t)
466,400	4,498,900	9.65	0.33	1,484,637	25	371,159	1,113,478

While real-world data may slightly differ from these calculations, especially as the crop to residue ratio applied here is rather conservative compared to other studies (Scarlat et al., 2010), it underscores the enormous, locally-available feedstock potential of corn stover for bioconversion processes. Of the stover, the stems - long, straight structures (“internodes”) interrupted by swollen joints (“nodes”) - constitute the largest fraction and represent the most important agricultural residue for bioconversion processes (Bichot et al., 2018; Pordesimo et al., 2005).

After harvest, the major components of corn stover are structural compounds (60 - 80 wt%) of the plant cell walls, also referred to as “lignocellulose”, giving structural support to the cells and the whole plant (Akter et al., 2020; Sekhon et al., 2016; Templeton et al., 2009; Vogel, 2008). The lignocellulose consists of a mixture of carbohydrates (mostly glucan ~32 wt% and xylan ~19 wt%), bound within the complex polysaccharides cellulose and hemicellulose, the hydrophobic polymer lignin (~13 wt%), minor fractions of proteins (>5 wt%) and inorganic residues, also called ash, which are intracellular accumulated residues from soil or water contaminants (>5 wt%) (Lacey et al., 2016; Templeton et al., 2009). The non-structural compounds (18 - 35 wt%) comprise water-soluble carbohydrates (5 - 35 wt%, mostly glucose (Glc), sucrose (Suc) and fructose (Fru)), extractible inorganic residues from soil, collected during harvest (~3 wt%) and organic acids (~2 wt%) (Akter et al., 2020; Bian et al., 2015; Cazetta & Revoredo, 2018; S. F. Chen et al., 2007; Sekhon et al., 2016; Templeton et al., 2009; Vogel, 2008). Furthermore, the storage polysaccharide starch is present in corn stover, solely consisting of Glc monomers, however only in small quantities 0 - 2 wt% (Sekhon et al., 2016). While the water-soluble carbohydrates are readily fermentable, the plant cell wall polysaccharides require breakdown into fermentable carbohydrates prior bioconversion. Some microorganisms, particularly fungi that naturally grow on plant biomass, possess the necessary enzymatic repertoire to break down these complex polysaccharides into fermentable carbohydrates and convert them into higher-value products.

As the main focus of this work will be on the suitability of corn stover as an agricultural residue for the bioconversion by *U. maydis*, the following chapters will give a more detailed overview of the major carbohydrate sources in corn stover potentially relevant for bioconversion processes: water-soluble carbohydrates, starch and lignocellulose.

1.1 Water-soluble carbohydrate metabolism and bioconversion potential in grasses

In corn, the three major water-soluble carbohydrates are the disaccharide Suc, and its monosaccharide building blocks Glc and Fru (Akter et al., 2020). Suc is the main product of photosynthesis and the main transport sugar (Ruan, 2014). Furthermore, it acts as an osmotic regulator, a signaling and response molecule, a modulator of gene expression or as a storage molecule (Ruan, 2014). It is predominantly generated in the mesophyll cells of “source” tissues, the carbohydrate producing tissues, from photosynthetically fixed CO_2 (Seifert, 2004). The CO_2 fixation is catalyzed by the enzyme ribulose-1,5-bisphosphat-carboxylase/oxygenase (RubisCO), which uses CO_2 for carboxylation of ribulose-1,5-bisphosphat and generation of two 3-phosphoglycerate (3-PGA) (Bräutigam & Gowik, 2016; Gowik & Westhoff, 2011). 3-PGA enters the Calvin-Benson cycle and is reduced and transformed via isomerases into triose-phosphate (Schlüter & Weber, 2020). Triose-phosphate is either used to regenerate the CO_2 acceptor ribulose-1,5-bisphosphate, serves as precursor for starch synthesis or is exported into the cytosol and condensed into hexose-phosphates, the main precursors for uridine diphosphate glucose (UDP-Glc) (Jiang et al., 2015; Miyake, 2016; X. Ren & Zhang, 2013; Schlüter & Weber, 2020; Verbančič et al., 2018). UDP-Glc and additionally fructose-6-phosphate (F6P) are catalyzed by Suc-phosphate synthases into Suc-6-phosphate (Lunn, 2016). Afterwards, Suc-phosphate phosphatases transform Suc-6-phosphate into Suc (Ruan, 2014).

Suc is translocated from mesophyll cells into the phloem via two different pathways in grasses, the symplasmic loading, via plasmodesmata that directly connect the cytosols of adjacent cells, or the apoplastic loading, via first export into the apoplast, followed by import into the phloem (Braun et al., 2014; Ruan, 2014). Most grasses, including corn, wheat, barley and sugarcane, use apoplastic phloem loading, where Suc is exported from the mesophyll cells into the apoplast via SWEET transporters (“Sugars Will Eventually be Exported Transporters”) across a concentration gradient (Bihmidine et al., 2015; Braun et al., 2014). From the apoplast, Suc is imported into the phloem by Suc transporters, which simultaneously transport H^+ and Suc (Braun et al., 2014; Ruan, 2014).

In the phloem, Suc is transported from the source tissues, to the “sink” tissues such as meristems, developing leaves, roots, flowers and seeds that consume carbohydrates (Verbančič et al., 2018). Furthermore, Suc concentration in the phloem is one of the main osmotic driving forces, causing the translocation of all other solutes in the phloem (Braun et al., 2014; Eom et al., 2015). Upon arrival in the destination tissue, Suc is unloaded from the phloem via the same pathways as for phloem loading (Ruan, 2014). In the apoplast, cell wall-localized invertases degrade Suc into Glc and Fru, lowering the Suc concentration and thereby enhancing transport and unloading efficiency by increasing the concentration gradient (Lunn, 2016). Alternatively, Suc transporters facilitate direct cellular uptake into the cytosol (L. Q. Chen et al., 2015; Ruan, 2014). In the cytosol, Suc is either hydrolyzed by invertases into Glc and Fru or cleaved into Fru and UDP-Glc (the main building block for cell wall synthesis) by Suc synthases (Jiang et al., 2015; Lunn, 2016; Ruan, 2014). Suc can also be transported further into the vacuole, where it can be stored or alternatively degraded by vacuolar invertases into Glc and Fru (Eom et al., 2015; Ruan, 2014).

In the context of bioconversion processes, especially the role of Suc as a storage carbohydrate is of particular importance (Slewinski, 2012). Carbohydrate storage and partitioning in plants are governed by a fine-tuned balance between source production and sink demand relationships (Slewinski, 2012). When production exceeds the metabolic demands, plants store surplus carbohydrates in their leaves, mostly in the form of starch (Miyake, 2016). Some grasses, such as the tribes Bromeae or Triticeae, or the subfamily Danthonioideae, also store Suc or Fru-oligosaccharides (Miyake, 2016). These storage pools are dynamic and subject to diurnal fluctuations, primarily serving as carbon reserves to sustain metabolism during the night (Stitt & Zeeman, 2012). However, the grasses exhibit an additional strategy by storing considerable quantities of excess carbohydrates not just in leaves, but also in the vacuoles of stem parenchyma cells (Slewinski, 2012). The most notable example is sugarcane, which can accumulate up to 54 % Suc by dry weight in mature stems (Alves et al., 2019; Glassop et al., 2010). Other grasses similarly store Suc, along with Glc and Fru, in their stems, with reports ranging from 5 % up to 35 % in mature maize (Akter et al., 2020; Bian et al., 2015; Cazetta & Revoredo, 2018; S. F. Chen et al., 2007).

Unlike the transient carbohydrate storage in leaves, stem carbohydrate reserves in grasses represent a long-term storage system (Slewinski, 2012). These reserves do

not compete directly with other sink tissues for assimilated carbohydrates, as they mainly sequester surplus carbohydrates (Slewinski, 2012). They function as a carbohydrate “buffering system” to complement periods of drought, low light, or nutrient limitation, when photosynthetic carbon assimilation may be compromised during the plant´s life cycle (Cazetta & Revoredo, 2018; Sekhon et al., 2016; Setter et al., 2001; Slewinski, 2012).

The reserve of water-soluble carbohydrates in grass stems has a high potential as substrate for bioconversion processes. They are soluble in water and do not require additional processing. Furthermore, they can be fermented by most microorganisms, without the need of specialized carbohydrate active enzymes (CAZymes; (Drula et al., 2022)).

1.2 Starch metabolism and bioconversion potential in grasses

Starch is the main carbohydrate storage in plants that ensures a consistent supply of carbon in a variety of different tissues (López-González et al., 2022). Starch is either generated in source tissues to store Glc generated from photosynthesis directly in the chloroplasts, in sink tissues as dedicated starch storage (seeds and tubers), or as a temporary storage (flowers or fruits) in plastids (Apriyanto et al., 2022; López-González et al., 2022).

Starch consists of two types of glucan polymers - amylose (15 – 35 % of total starch) and amylopectin - whose relative quantities differ among plants, tissues and developmental stages (Apriyanto et al., 2022; Pérez & Bertoft, 2010). Amylose mostly consists of a α-(1,4)-linked Glc backbone with a few α-(1,6)-linked glucan branches, whereas amylopectin is highly branched with α-(1,6)-linkages (Pérez & Bertoft, 2010). In source tissues, the Calvin-Benson cycle generates the starch precursor F6P, which is converted by phosphoglucose isomerase (PGI) into Glc-6-phosphate (G6P) and further into G1P by phosphoglucomutase (Apriyanto et al., 2022). In sink tissues, G1P originates predominantly from Suc degradation by Suc synthases (Stein & Granot, 2019). G1P is converted by adenosine diphosphate-Glc (ADP-Glc) pyrophosphorylases into ADP-Glc, the main building block for starch synthesis (Apriyanto et al., 2022). In the plastids, starch synthases and plastidial phosphorylases synthesize the α-(1,4)-linked Glc backbone and starch branching and debranching enzymes introduce the α-(1,6)-linkages generating highly complex interconnected

starch granules (Apriyanto et al., 2022; Pérez & Bertoft, 2010). The granules contain regions of crystalline starch, which comprise highly ordered α-(1,4)-linked Glc chains interconnected via hydrogen bonds in a helical structure, alternating with amorphous starch, which are less ordered and less dense regions due to the intersection of α-(1,6)-linkages (Apriyanto et al., 2022; Pérez & Bertoft, 2010).

Starch degradation happens during the night to provide a continuous supply of carbohydrates and is more a combination of multiple reactions rather than a linear degradation pathway (Stitt & Zeeman, 2012). It is initiated by glucose phosphorylation at the granule surface via glucan water dikinases and phosphoglucan water dikinases (Stitt & Zeeman, 2012). This disrupts the crystalline structure and enables access of starch degrading enzymes (Stitt & Zeeman, 2012). The α-(1,4)-linkages are cleaved by amylases and phosphorylases, and the α-(1,6)-linked branches are cleaved by starch debranching enzymes (Apriyanto et al., 2022). The major starch breakdown products are maltose and Glc, which are exported to the cytosol and further metabolized (Stitt & Zeeman, 2012).

Since starch consists solely of Glc, the bioconversion potential is high (Van Zyl et al., 2012). However in crops, most starch is stored in the seeds, while the content in other tissues such as stems is minimal (Miyake, 2016). In maize, starch levels in mature stems range from 0 -2 wt% (Sekhon et al., 2016). Thus, the relevance of starch as a carbohydrate source for bioconversion processes based on corn stover is limited.

1.3 Lignocellulose metabolism and bioconversion potential in grasses

After harvest, 45 – 70 wt% of the corn stover is plant cell wall or “lignocellulose” (Templeton et al., 2009). Throughout their development, plant cell walls undergo substantial compositional and structural changes (Loqué et al., 2015). During early growth, grass cells are surrounded by primary cell walls which are composed mainly of cellulose microfibrils, hemicellulosic polysaccharides and pectins (Loqué et al., 2015). The water content of primary cell walls is around 60 – 70 % of total mass (Loqué et al., 2015). As grass cells mature and cell elongation ceases, secondary cell wall growth begins (Rao & Dixon, 2018). These secondary grass cell walls, contain primarily the polysaccharides cellulose and hemicellulose and the hydrophobic polyphenol lignin (Bulone et al., 2019; Gao et al., 2020; van der Weijde et al., 2013; Vogel, 2008). The

water content is significantly reduced to around 5 % of the total mass (Christensen & Rasmussen, 2019; Loqué et al., 2015).

As corn stover is senescent tissue, these secondary cell walls will be the focus of this work. The following sections will focus on the individual components found in the secondary cell walls of corn stover in more detail. Starting with the main component cellulose (~35 % dry weight), followed by the main hemicellulosic polysaccharide glucuronoarabinoxylan (GAX, ~20 % dry weight) and the minor hemicellulosic polysaccharide mixed-linkage glucan (MLG, ~3 % dry weight) (Vogel, 2008; S. Wang et al., 2023). Then the highly hydrophobic polyphenol lignin (12 - 14 % dry weight) will be explained (Templeton et al., 2009; Vogel, 2008), followed by a section about the three-dimensional interconnection within this lignocellulosic material.

Cellulose

To develop a deeper understanding of the bioconversion potential of corn stover, it is necessary to examine its individual components. The best understood example of synthesis and molecular architecture in lignocellulose is cellulose (Simmons et al., 2016). It is the most abundant polysaccharide in nature and a fundamental component of all plant cell walls, providing structural integrity and rigidity (Keegstra, 2010; Rongpipi et al., 2019). In cell walls of corn stover, cellulose makes up ~35 % of the dry weight and consists of hundreds to thousands unbranched β-(1,4)-glucose (Glc) units (Bichot et al., 2018; Bulone et al., 2019; Vogel, 2008).

The pre-cursor for cellulose synthesis is the nucleotide sugar UDP-Glc, which is used by plasma membrane localized cellulose synthase complexes, to create long unbranched Glc chains (Cosgrove, 2014; Marriott et al., 2016). The cellulose synthase complexes consist of multiple non-redundant cellulose synthase A proteins that enable the synthesis of all 18 – 24 Glc chains necessary to form a single cellulose microfibril towards the external membrane surface (Cosgrove, 2024; Marriott et al., 2016; R. Zhong et al., 2019). These microfibrils are stabilized by extensive hydrogen bond cross-linking (D. Harris et al., 2010; Somerville, 2006) and are deposited into the cell wall in well-aligned distinct layers, whose orientations differ between adjacent layers (Cosgrove, 2024). The microfibrils exhibit regions of high crystallinity, where the cellulose chains are tightly packed and form an ordered structure, intersected with amorphous regions that are less structured (Cosgrove, 2014).

For bioconversion processes, cellulose has the highest substrate potential, but only when it is broken down into Glc monomers (Bichot et al., 2018). Three different activities of carbohydrate active enzymes (CAZymes; (Drula et al., 2022)) are necessary to hydrolyze cellulose (Glass et al., 2013). Endo-(1,4)-β-glucanases cleave internal bonds in the cellulose chain, exo-(1,4)-β-glucanases or cellobiohydrolases cleave cellobiose from either the reducing or the non-reducing end of a cellulose chain and β-glucosidases cleave cellobiose into two Glc molecules (Glass et al., 2013). The crystallinity of cellulose greatly influences its degradability, as only the amorphous regions of cellulose are easily accessible for CAZymes (Gao et al., 2020; Perrot et al., 2022). Furthermore, the crystallinity of cellulose influences cross-linking with the other two main building blocks of grass cell walls, xylan and lignin, and thus has a strong impact on the three-dimensional structure of lignocellulose (Gao et al., 2020).

Glucuronoarabinoxylan

Glucuronoarabinoxylan (GAX), the main hemicellulosic polysaccharide in corn (~20 % dry weight), consists of a β-(1,4)-xylose (Xyl) backbone decorated with various substituents, including acetate, glucuronic acid (GlcA), 4-*O*-methylglucuronic acid (MeGlcA), hydroxycinnamic acids and arabinose (Ara) (Rennie & Scheller, 2014). Their occurrence and quantity varies depending on the analyzed tissue (Rennie & Scheller, 2014). The precursor for xylan biosynthesis is UDP-Glc, which is converted into the necessary glycosidic building blocks UDP-Xyl, UDP-GlcA, UDP-Arafuranosyl (Ara*f*) or UDP-Arabinopyranosyl by specific cytosol localized enzymes (Reiter & Vanzin, 2001; Seifert, 2004; R. Zhong et al., 2019). From the cytosol, these nucleotide sugars are transported into the Golgi apparatus, where the xylan backbone and its side chains are assembled before being transported to the cell wall via vesicles (R. Zhong et al., 2019). The backbone is synthesized by xylan synthase complexes composed of glycosyltransferase (GT) 47 proteins and two nonredundant groups of family GT43 proteins (R. Zhong et al., 2019). Substituents are added by specific enzymes: xylan *O*-acetyltransferases mediate *O*-acetylation, xylan glucuronyltransferases of the GT8 family add GlcA, glucuronoxylan methyltransferases methylate GlcA and clade A GT61 arabinosyltransferases attach Ara residues (R. Zhong et al., 2019).

There are two major xylan types in grasses: GAX, the predominant xylan type in maize, and arabinoxylan (AX) (Gille & Pauly, 2012; Pauly et al., 2013). AX is a Xyl backbone

decorated with *O*-acetyl, α-(1-2)- and/or α-(1-3)- (Ara*f*) and very few α-(1-2)-GlcA/MeGlcA residues, while GAX contains substantially more (Me)GlcA substituents (Gille & Pauly, 2012; Pauly et al., 2013; Peña et al., 2016). The Ara*f* residues of both GAX and AX can be further decorated with Ara*f* or xylopyranosyl (Xyl*p*) units (Saulnier et al., 1995). Furthermore, hydroxycinnamic acids, like ferulic acid (FA) or *p*-coumaric acid (*p*CA), can be esterified to the *O*-5 position of Ara*f* residues (Feijao et al., 2022; Tryfona et al., 2023). However, the regulation of patterns of these various side chains is not clearly understood in grasses and it might be related to functional specializations of individual xylan polysaccharides (Tryfona et al., 2023).

Enzymatic degradation of GAX involves the activity of several enzymes, depending on the side chain decorations (Van Den Brink & De Vries, 2011). The xylan backbone can be cut into Xyl oligosaccharides by β-(1,4)-endoxylanases and further into Xyl by β-(1,4)-xylosidases (F. Ren et al., 2024; Van Den Brink & De Vries, 2011). GlcA sidechains are cleaved off by α-glucuronidases, Ara side chains by arabinoxylan α-arabinofuranohydrolases, acetyl by acetylxylanesterases, FA by feruloyl esterases and *p*CA by *p*-coumaric acid esterases (F. Ren et al., 2024; Van Den Brink & De Vries, 2011). These enzymes are required to work in synergy, as the presence of some sidechains might interfere with the activity of specific hydrolases, e.g. the presence of GlcA sidechains prevents the release of Ara from adjacent xylose with an *Aspergillus niger* (*A. niger*) arabinoxylanhydrolase (Van Den Brink & De Vries, 2011; Verbruggen et al., 1998).

Since the main building block of xylan is Xyl, a pentose, the bioconversion potential compared to cellulose is lower, as many microorganism do not metabolize pentoses as efficiently as hexoses (Van Vleet & Jeffries, 2009). Furthermore, the different xylan substituents and its structural complexity increase the required metabolic variability in the microbe for an efficient bioconversion process (Van Vleet & Jeffries, 2009).

Mixed-linkage glucan

One feature of grass cell walls is the presence of mixed-linkage glucan (MLG), another hemicellulosic polysaccharide, which consists solely of Glc monomers, and can accumulate up to 20 % of the dry mass in rapidly growing tissues (Carpita, 1996; Pauly et al., 2013). Typically MLG is formed of β-cellotriosyl or β-cellotetraosyl units intersected by β-(1,3)-linkages, but longer oligosaccharides were also observed

(Bulone et al., 2019; Coomey et al., 2020). Three protein families were shown to be involved in plant MLG biosynthesis from the substrate UDP-Glc, namely cellulose synthase like F, H and J proteins (Bulone et al., 2019; Coomey et al., 2020; Kraemer et al., 2021). In maize, antibody labelling showed β-(1,3)(1,4)-D-glucan oligosaccharides localized at the Golgi apparatus, indicating Golgi-localized synthesis, followed by vesicle transport of the oligosaccharides to the cell walls (Carpita & McCann, 2010). In other grasses antibody detection indicated plasma membrane localized synthesis, which would indicate a direct synthesis of MLG towards the extracellular surface, similar to cellulose synthesis (Wilson et al., 2015).

The MLG content in cell walls fluctuates between developmental stages and diurnal changes and its accumulation is a balance between constant synthesis and degradation (Carpita, 1996; Kraemer et al., 2021; Pauly et al., 2013). MLG abundance is high in expanding tissues, but it gets degraded concomitant with cell elongation (Pauly et al., 2013). Licheninases (or (1,3)(1,4)-β-D-glucan 4-glucanohydrolase) cleave the MLG specific β-(1,3)-linkages and cellulases or β-glucosidases hydrolyze the β-(1,4)-linkages of the resulting Glc oligosaccharides (Fincher, 2009; Kraemer et al., 2021; Pauly et al., 2013; Perrot et al., 2022). Due to this turnover, its function was proposed to be a storage polysaccharide rather than a structural polysaccharide (Bulone et al., 2019; Carpita, 1996; Pauly et al., 2013). However, due to the presence of MLG in senescent stem tissues of rice its function might be dual (Vega-Sánchez et al., 2013).

MLG has a high potential for bioconversion processes, as it is built solely from Glc in a rather simple structure, which reduces the necessary CAZyme repertoire in the microbe (Kraemer et al., 2021). However, the MLG content in mature corn stems is rather low compared to the other polysaccharides (Kraemer et al., 2021).

Lignin

The last major component of secondary corn cell walls is lignin, a highly hydrophobic, phenolic polymer (12 - 14 % dry weight) (Christensen & Rasmussen, 2019; Templeton et al., 2009; Vogel, 2008). Lignin is composed of three monolignols, *p*-coumaryl alcohol, coniferyl alcohol and sinapyl alcohol (Ralph et al., 2019). These monolignols are synthesized in the cytosol through the phenylpropanoid pathway from phenylalanine and tyrosine, the latter substrate is grass-specific (Vanholme et al.,

2019). Phenylalanine and tyrosine are converted into cinnamate or *p*-coumaric acid, respectively, and further into *p*-coumaroyl CoA by 4-coumarate coenzyme A ligase (4CL) (Christensen & Rasmussen, 2019). Then, *p*-coumaroyl CoA is either converted into *p*-coumaryl alcohol via a two-step reaction catalyzed by cinnamoyl CoA reductase (CCR) and cinnamyl alcohol dehydrogenase (CAD) or it is converted into feruloyl-CoA via four enzymatic reactions (Christensen & Rasmussen, 2019). Feruloyl-CoA is converted to coniferaldehyde by CCR and further into coniferyl alcohol by CAD, or into sinapaldehyde via ferulate 5-hydroxylase and caffeic acid/5-hydroxyferulic acid *O*-methyltransferase (COMT) and then converted to sinapyl alcohol by CAD (Christensen & Rasmussen, 2019). From the cytosol, the monolignols *p*-coumaryl alcohol, coniferyl alcohol and sinapyl alcohol are exported to the cell walls, incorporated into the lignin molecule and then termed *p*-hydroxyphenyl (H), guaiacyl (G) and sinapyl (S) units, respectively (Marriott et al., 2016; R. Zhong et al., 2019). Depending on the monolignol, the linkages in the final polymer differ, as H- and G-units link via β-5 or 5-5 coupling with C-C linkages, while S-units are added via β-*O*-4 linkages (Christensen & Rasmussen, 2019). The lignin polymer is elongated by non-enzymatic radical coupling, making the resulting polymer very heterogeneous and complex (Ralph et al., 2019).

In nature, lignification of the cell wall serves the plant as a mechanical, defensive barrier against pathogens (Christensen & Rasmussen, 2019). Since lignin is not a polysaccharide, its bioconversion potential is very limited and furthermore, it blocks the access of CAZymes and presents the main hurdle for efficient bioconversion processes (Chang & Holtzapple, 2000). Among all lignocellulosic components, enzymatic depolymerization of lignin is the most complex, as it requires a range of different enzymes that are capable of oxidizing lignin and opening its phenyl rings (F. Ren et al., 2024). The most prominent enzymes are laccases, which are capable of forming radicals of phenolic compounds (F. Ren et al., 2024). As such, they are involved in lignin biosynthesis, however, fungal laccases are effective in depolymerizing lignin (Andlar et al., 2018; Hatfield et al., 2017). Peroxidases are another class of important lignin-degrading enzymes that utilize H_2O_2 to oxidize lignin (Andlar et al., 2018; F. Ren et al., 2024). Lignin-peroxidases oxidize nonphenolic methoxyl-substituted lignin units and manganese-dependent peroxidases oxidize Mn^{2+} to Mn^{3+}, which can diffuse into the lignin polymer and oxidize phenolic and nonphenolic compounds (Andlar et al., 2018).

This brief overview of lignin biosynthesis and its depolymerization highlights the complex role of this polymer in lignocellulose biomass utilization. Additionally, the entire overview of the main lignocellulosic building blocks shows the potential of lignocellulose as feedstock for bioconversion processes, as it consists mostly of carbohydrates bound into complex polysaccharides. However, in nature these polysaccharides do not occur isolated, but in a highly interconnected three-dimensional structure, which will be described in the next section.

Cross linking of corn stover lignocellulose

The lignocellulose of corn secondary cell walls gives structural support to the cells and the whole plant and evolved as a structural barrier protecting the plant against microbial degradation (F. Ren et al., 2024; Vogel, 2008). Its three-dimensional structure is based on a cellulosic grid-like backbone, embedded in a variable matrix of structural hemicellulosic polysaccharides crosslinked with lignin (Hatfield et al., 2017). The interaction of xylan with cellulose varies depending on the Ara*f* substitution pattern of the xylan backbone, as different arrangements of Ara*f* sidechains influence hydrogen bonding with cellulose or other xylan chains (Kang et al., 2019; Tryfona et al., 2023). A uniform distribution of Ara*f* and acetyl-sidechains results in a linear xylan backbone and enhances cross-linking with cellulose (Busse-Wicher et al., 2014; Tryfona et al., 2023). In contrast, clusters of GlcA substitutions, or uneven distributed acetyl groups disrupt the structured, linear xylan-backbone and thereby prevent xylan crosslinking to cellulose (Busse-Wicher et al., 2014; Gao et al., 2020; Tryfona et al., 2023). In consequence, this distorted xylan backbone, which is the predominant form in grasses, could extend into the matrix and interact with other cell wall components, predominantly lignin, but also other hemicelluloses and amorphous cellulose (Gao et al., 2020; Kang et al., 2019; Tryfona et al., 2023).

The hydroxycinnamic acids FA and *p*CA are essential binding molecules between different lignocellulosic compounds (Hatfield et al., 2017). FA enables xylan-xylan crosslinking via ferulic acid dimers and enables xylan-lignin crosslinking via diferulates (Hatfield et al., 2017; Tryfona et al., 2023). Alternatively, FA participates in lignin polymerization through free radical coupling, forming covalent lignin-carbohydrate complexes, or serves as nucleation sites for lignin assembly (Hatfield et al., 2017). *p*CA can generate cyclodimers that link xylan to lignin or it functions as a radical transfer

system, aiding in the formation of monolignol radicals, without directly integrating into the lignin polymer (Hatfield et al., 2017).

This intricate and heterogeneous architecture of the lignocellulose contributes to the recalcitrance of plant biomass, posing a significant challenge for microbial degradation and industrial bioconversion processes.

1.4 Strategies to enhance the bioconversion potential of corn stover

There are two main strategies to increase the bioconversion potential of corn stover. One focuses on pretreating the harvested biomass to alter cell wall structure and improve enzymatic digestibility. The other seeks to modify the plant itself, either through naturally occurring variants or targeted genetic approaches that for example change lignocellulose composition or enhance polysaccharide breakdown. The following sections will outline different pretreatment method applied to corn stover and, subsequently, approaches that exploit natural or engineered maize lines with improved bioconversion potential. Often the efficiency of these strategies is evaluated by comparing the saccharification yield of the biomass, *i.e.* how efficient is the release of fermentable sugars from the lignocellulosic polysaccharides by means of enzymatic hydrolysis (S. Wang et al., 2023).

Pretreatment of corn stover prior bioconversion

Pretreating lignocellulosic biomass enhances enzymatic degradation by disrupting the plant cell wall architecture, and partially hydrolyzing polysaccharides (Fansuri et al., 2024). A common initial step in most pre-treatment strategies is the particle size reduction via cutting or milling (Kumar et al., 2020; Vu et al., 2020). While this does not degrade the lignocellulosic polysaccharides into fermentable sugars, it enhances the effect of follow up physical and/or chemical treatments (Kumar et al., 2020; Vu et al., 2020).

Acid-based pretreatments of corn stover typically employ sulfuric acid (H_2SO_4), acetic acid or phosphoric acid, at various temperatures (50 C – 200 °C) and different concentrations (typically between 0.5 % and 10 % (w/v)), which directly hydrolyze the hemicellulose or cellulose into fermentable carbohydrates, yielding between 60 % to 90 % of fermentable monosaccharides from the complex polysaccharides (Fansuri et al., 2024; Galbe & Wallberg, 2019; Lorenci Woiciechowski et al., 2020). In comparison

enzymatic hydrolysis of untreated biomass usually yields less than 20 % of fermentable monosaccharides (Sindhu et al., 2016). The most common alkaline pretreatments are based on sodium hydroxide (NaOH), lime or sodium carbonate, again with a wide range of process conditions (Fansuri et al., 2024). Alkali-based processes mainly deacetylate the hemicellulose and solubilize parts of lignin and hemicellulosic fraction prior enzymatic degradation, by cleaving linkages between lignin and polysaccharides (Y. Chen et al., 2013; Y. He et al., 2008; Lorenci Woiciechowski et al., 2020). These alkali-based methods significantly increase saccharification yields e.g., NaOH pretreatment of mature maize stem tissues from different genotypes resulted in a 6-fold increased fermentable sugar yield compared to untreated material (S. Wang et al., 2023). One downside of most chemical pretreatments is the formation of by-products, like furfural, which originate from monosaccharide hydrolysis and inhibit microbial growth through the blocking of glycolysis (Jablonowski et al., 2022; Jilani & Olson, 2023).

Beyond chemical methods, physical pretreatments such as microwave irradiation have also been explored (L. Wang et al., 2024). Microwave irradiation causes rapid heating of polar bonds inside the lignocellulosic structure and increases enzymatic accessibility (Jablonowski et al., 2022). Coupling this physical treatment with chemical treatment further enhanced lignin removal and up to 87 % of the Glc was released from cellulose in corn stover (L. Wang et al., 2024). Among the most widely adopted approaches is steam explosion, where biomass is treated with high-pressure steam followed by rapid depressurization (Fansuri et al., 2024; Galbe & Wallberg, 2019). This results in rupture of cell wall structures and yields up to 75% of fermentable sugars, due to enhanced enzymatic accessibility of the polysaccharides (Fansuri et al., 2024; Galbe & Wallberg, 2019).

Biological pretreatments offer an alternative approach without the need for specialized equipment that withstands high temperature, corrosion or high pressure (Sindhu et al., 2016). These methods exploit the CAZyme potential of microorganisms and often focus on the capabilities of lignin-degrading fungi, like white rot fungi *Pleutorus ostreatus*, *Trametes versicolor* or *Ceriporiopsis subvermispora* (Mustafa et al., 2016; Taniguchi et al., 2005; Vasco-Correa et al., 2016; Vu et al., 2020). Lignin removal up to 45 % is possible in corn stover, which in turn enhances the accessibility and

degradability of hemicellulose and cellulose and boosts saccharification yields 7-fold (Song et al., 2013).

Alternatively, instead of employing living organisms, the secretome of lignocellulose-degrading fungi, like *Aspergillus nidulans* or *Aspergillus niger*, *Trichoderma reesei* or *Penicillium decumbens* can be purified and used to degrade lignocellulose (Couturier et al., 2012; G. Liu et al., 2013; Vu et al., 2020). Additionally, there are commercial lignocellulolytic enzyme cocktails available, such as Cellic® CTec2 (Novozymes) or Celluclast® (Novozymes). Compared to chemical or physical pretreatments, biological processes including living organisms and enzyme cocktails, are usually the slowest, especially those focusing on delignification which can take up to several weeks (Sharma et al., 2019; Song et al., 2013; W. Zhong et al., 2011). However, these biological pretreatments have benefits over other strategies, as they usually do not form inhibitory by-products and since no toxic chemicals are used in these processes, which could inhibit microbial growth, there is also no need for waste recycling (Sindhu et al., 2016). While pretreatment with living organisms requires sterile conditions, which is difficult on larger process scales, these requirements are eliminated when using the secretome of fungi, which substantially reduces costs and process complexity (Sindhu et al., 2016).

This overview shows that there is a wide variety of available pretreatment strategies for corn stover. Importantly, the choice of the most suitable pretreatment is not universal but depends strongly on the microorganism that will be employed in the bioconversion process, as the pretreatment must increase accessibility without inhibiting microbial metabolism.

Biotechnological strategies to increase bioconversion efficiency of corn stover *in planta*

An alternative strategy to improve the bioconversion efficiency of corn stover is to modify plant properties, either through naturally occurring mutants or genetically engineered maize lines with altered lignocellulose composition or enhanced biomass production.

The major barrier to efficient bioconversion is the presence of lignin. Several naturally occurring lignin mutants have been identified in maize. They are named *brown-midrib* (*bm*) mutants, for their characteristic reddish- brown pigmentation of the leaf midrib

and stalk pith, and exhibit modified lignin contents and compositions, resulting in increased feeding value for cows or other animals without compromising plant biomass yield (Barrière, 2017). Of the *bm* mutants, *bm3* is the most extensively studied, which contains a mutation in the COMT gene, resulting in altered monolignol composition, due to a reduced synthesis of S-lignin and increased saccharification yield (+ 25 % compared to reference material) (Vignols et al., 1995; S. Wang et al., 2023). Another example is the variety *bm1* with a mutation in CAD2, resulting in reduced lignin content, reductions in S- and G-lignin and increased saccharification yield (+ 25 % compared to reference material) (Halpin et al., 1998; S. Wang et al., 2023). Four additional *bm* mutants have been described in maize, which all exhibit increased saccharification potential, without severe growth defects (Barrière, 2017). Several *bm* double mutants were generated by crossing different *bm* mutants, however, these double mutants showed increased susceptibility to pathogens or reduced growth rates compared to the single mutants and wildtype maize (Christensen & Rasmussen, 2019; Tanaka et al., 2014; Vermerris et al., 2010). In addition to the natural *bm* mutants, a lot of research focused on reducing lignin content *in planta* by targeting the genes involved in lignin biosynthesis (section 1.3) e.g., via RNA interference or antisense downregulation (Christensen & Rasmussen, 2019). Key targets have included COMT (X. He et al., 2003; Piquemal et al., 2002), CAD (Fornalé et al., 2012) or CCR (Park et al., 2012). While these approaches often succeeded in altering lignin composition or reducing its overall content, they were frequently accompanied by undesirable trade-offs such as reduced plant growth or diminished resistance to pathogens (Christensen & Rasmussen, 2019; Vanhevel et al., 2024).

Beyond lignin-focused strategies, efforts have also targeted cell wall polysaccharides to improve saccharification yields. For example modifications to xylan, as its structure and side chain decorations strongly influence cross-linking with lignin and cellulose, thereby impacting bioconversion efficiency (Tryfona et al., 2023). In maize, efforts have concentrated on reducing cross-linking between xylan and lignin via FA and *p*CA (Buanafina et al., 2025, 2020; Chandrakanth et al., 2023; Fanelli et al., 2021). The overexpression of a fungal ferulic acid esterase in senescent maize plants resulted in increased saccharification yields (up to 125 % more fermentable carbohydrate yield compared to reference material) without growth defects, potentially due to reductions in polymer cross-linking (Buanafina et al., 2025). And the overexpression of a

sugarcane BAHD acetyltransferase in maize resulted in reduced FA levels, which could benefit biomass utilization due to decreased polymer cross-linking (Fanelli et al., 2021). However in the same study, no improved digestibility of non-pretreated biomass was detected (Fanelli et al., 2021). Other xylan modifications were explored in other crops, for example, in rice it was attempted to reduce the xylan *O*-acetylation by knocking down genes involved in this pathway in rice, which enhanced the saccharification yield up to 20 % compared to reference material of rice biomass (B. Zhang et al., 2017). However, xylan hypoacetylation often results in severe growth defects, as acetylation is essential for the cross-linking of xylan to cellulose (Pauly et al., 2019; Ramírez et al., 2018). Furthermore, increased saccharification of rice stover was achieved by knock-out of UDP-xylose epimerase and xylan arabinosyl-transferase, which decreased xylan arabinose decorations without growth defects, which could be an interesting approach for other crops, including maize (C. Chen et al., 2021).

Many microbes convert hexoses more efficiently than pentoses (Van Vleet & Jeffries, 2009), consequently, a lot of research focused on increasing the hexose/pentose ratio in lignocellulose. The most simple structured cell wall polysaccharide is MLG and increasing the MLG content in mature maize stems could result in increased bioconversion potential and an increased hexose/pentose ratio (Kraemer et al., 2021). Increased MLG accumulation was achieved by reducing MLG degradation by mutating the MLG hydrolase 1 (Kraemer et al., 2021). The so called “*cal1*” (candy-leaf 1) mutants showed enhanced MLG content in young and adult tissues, accompanied with an increased saccharification yield (+ 30 % compared to reference material) (Kraemer et al., 2021). In other grasses attempts were made to increase MLG content by overexpression of MLG synthases in barley or *Brachypodium dystachlon* (Burton et al., 2011; Kim et al., 2018; Vega-Sánchez et al., 2015). However, this resulted in severe growth defects (Burton et al., 2011; Kim et al., 2018; Vega-Sánchez et al., 2015). Similarly in other species, it was attempted to reduce *in planta* cellulose crystallinity, which would increase cell wall digestibility due to increased fermentability of cellulose. Attempts were made by mutating cellulose synthases or UDP-Glc epimerases in rice (D. M. Harris et al., 2012; R. Zhang et al., 2020). However, the success was limited as it severely restricts plant growth and development leading to a low plant biomass yield (D. M. Harris et al., 2012; R. Zhang et al., 2020).

An alternative approach to increase lignocellulose utilization is the expression of microbial CAZymes directly *in planta*, which could increase bioconversion efficiency and reduce the amount of enzymes necessary for biomass pretreatment (Biswas et al., 2006; Brunecky et al., 2011; D. Zhang et al., 2011). For example, the thermostable endocellulase Cel5A from *Acidothermus cellulolyticus* was expressed in maize and resulted in 10 % increased saccharification yield of the stover after acid pretreatment (Brunecky et al., 2011). Similarly, the expression of a xylanase from *Dictyoglomus thermophilum* resulted in increased saccharification yield by 10 % of corn stover, which was further increased (up to 20 %) by additionally expressing a feruloyl esterase from *A. niger* in the same transgenic maize line (D. Zhang et al., 2011).

Bioconversion efficiency can additionally be enhanced by increasing the water-soluble carbohydrate content in the stover as these carbohydrates can be directly utilized by microbes. In the past a few agronomic strategies targeted this fraction. Increasing the water-soluble carbohydrate content can be achieved by removing the plant´s ears before maturity (Ralph Singleton, 1948), however, this practice would render the plant useless for kernel harvest. Alternatively, it was attempted to delay the production of fertile ears in the plant to decrease the ear sink strength and accumulate surplus carbohydrates in the stem (Marten & Westerberg, 1972). This however, resulted in an overall carbon loss for the plant compared to normal grain varieties (Marten & Westerberg, 1972; Slewinski, 2012). Furthermore, increasing plant density in the field increased the stem sugar content in some high stem sugar hybrid lines, however, these lines are usually accompanied by reduced grain yield and higher susceptibility for smut infections (B. L. Ma et al., 2017).

Altogether, these examples highlight how genetic engineering and breeding strategies can alter the composition and accessibility of maize lignocellulose, thereby increasing bioconversion potential. But, the efficiency of bioconversion potential is not only determined by the feedstock, but similarly by the employed microorganism, which either directly metabolizes the monosaccharides released by pretreating the plant biomass, or is capable of further degrading the plant biomass into fermentable carbohydrates.

1.5 The potential of *U. maydis* for the bioconversion of corn stover

For bioconversion processes, plant pathogenic fungi are particularly interesting, due to their host-specific sets of lignocellulolytic enzymes, which enable efficient degradation of lignocellulose and utilization of the resulting monosaccharides for growth (King et al., 2011). As mentioned above, corn stover lignocellulose consists mostly of cellulose, hemicellulose, especially GAX, and lignin (Vogel, 2008). Thus, effective bioconversion of corn stover requires organisms capable of producing a variety of CAZymes, including cellulases, xylanases and lignin-modifying enzymes (Knežević et al., 2013). One promising candidate for these processes is the biotrophic fungus *U. maydis*, a natural pathogen of maize and its ancestor teosinte, causing agent of the corn smut disease, with a highly specialized enzymatic repertoire for maize tissue degradation (Lanver et al., 2014). *U. maydis´* genome encodes for 33 cell wall degrading enzymes (Kämper et al., 2006), comprising five endo-glucanases, three endo-xylanases, three arabinofuranosidases and two acetylxylan esterases, β-galactosidases and β-glucosidases (Geiser et al., 2013; X. Li et al., 2022; Mueller et al., 2008). Furthermore, six lignin-modifying enzymes were identified, *i.e.* four laccases and two chloroperoxidases, of which one was shown to cleave the linkage between Ara*f* and FA (Mueller et al., 2008; Nieter et al., 2015).

The expression and secretion of *U. maydis* CAZymes can be induced by the addition of complex plant-derived substrates to the growth medium (Cano-Canchola et al., 2000; Couturier et al., 2012; Mueller et al., 2008). For example, maize apical meristem tissue induced high pectate lyase and cellulase activities, while maize leave tissue induced xylanase and cellulase activities (Cano-Canchola et al., 2000; Mueller et al., 2008). Furthermore, in a comparative study, *U. maydis´* secretome induced with maize bran showed superior wheat straw degradation compared to *Trichoderma reesei* (*T. reesei*), the most investigated and industrially relevant plant biomass degrader (Couturier et al., 2012). In this study, fungal CAZyme secretion was induced by addition of maize bran to the growth media, followed by isolation and concentration of the culture supernatant, containing the secreted CAZymes (Couturier et al., 2012). The secretomes were then tested and compared for their release of glucose from wheat straw, and *U. maydis* showed superior degradation abilities over *T. reesei* (Couturier et al., 2012). The most abundant CAZymes in *U. maydis* secretome exhibit arabinoxylan degrading activity, when induced with maize bran (Couturier et al., 2012;

Reyre et al., 2022). In addition, *U. maydis* secretes a high number of oxido-reductases (8 % of total protein) whose activity was shown to assist in lignocellulose degradation (Andlar et al., 2018; Couturier et al., 2012). Together, these results suggest that *U. maydis* has great lignocellulolytic potential for the degradation of complex plant substrates.

Over the last decade, *U. maydis* emerged as a promising candidate for biotechnological applications (Feldbrügge et al., 2013; Regestein et al., 2018; Schlembach et al., 2020; Wierckx et al., 2021). In nature, *U. maydis* has a biphasic life-cycle, which can be divided into a non-pathogenic, yeast-like phase outside the host plant and a biotrophic, infectious and filamentous phase dependent on the host plant (Banuett, 1992). For biotechnological applications, especially its yeast-like growth is of interest due to easy handling under laboratory conditions (Wierckx et al., 2021). In axenic cultures, it propagates through budding and is tolerant to media impurities and hydromechanical stress (Feldbrügge et al., 2013; Wierckx et al., 2021). Furthermore, the fungus naturally produces a variety of industrially relevant compounds, including organic acids, polyols, lipids, and biosurfactants (Geiser et al., 2014; Paulino et al., 2017; Richter et al., 2024; Wierckx et al., 2021). The publication of its genome in 2006 (Kämper et al., 2006) has facilitated genetic engineering, leading to strains with significantly improved yields compared to the wildtype isolates (Paulino et al., 2017). In addition, *U. maydis* can utilize a wide variety of different carbon sources ranging from monosaccharides, like Glc, Fru, Xyl, Ara, over disaccharides, like Suc and cellobiose to complex substrates such as maize bran or freeze-dried maize leaves (Cano-Canchola et al., 2000; Couturier et al., 2012; Geiser et al., 2016; Richter et al., 2024).

This supports the notion that *U. maydis* is a fungus with substantial potential for the bioconversion of corn stover. However, critical details, such as the specific carbohydrate nutrient sources utilized by the fungus and the efficiency of corn stover lignocellulose degradation have yet to be determined

2 Aims of this thesis

Previous studies demonstrated that *U. maydis* can partially metabolize isolated polysaccharides, such as cellulose and birch xylan (Geiser et al., 2013, 2016). However, its capacity to utilize these polysaccharides within the complex, heterogeneous structure of corn stover remains unclear. To address this, the first chapter of this thesis will establish a small-scale microtiter plate cultivation platform (BioLector®) to monitor the bioconversion performance of *U. maydis* in degrading corn stover. By combining online monitoring data with a detailed compositional analysis of the post-fermentation lignocellulosic residue, this approach aims to identify the carbohydrate sources that are predominantly consumed by *U. maydis*, as well as those that remain underutilized. Additionally, investigating the bioconversion of specific corn lignocellulosic mutants and evaluating various pretreatment methods will help to identify and overcome bottlenecks in lignocellulose degradation.

Building on the findings of the first chapter, the second chapter will focus on the discovery that *U. maydis* is predominantly utilizing the abundant water-soluble carbohydrates Glc, Suc and Fru in corn stover. This section will investigate how the composition of water-soluble carbohydrates fluctuates in corn stover throughout the day and varies across the genetic diversity of corn. By combining water-soluble carbohydrate quantification with genetic data in a genome-wide association study, potential genes involved in water-soluble carbohydrate metabolism in corn stover will be identified. In the chapters three to five, the association between haplotypes and chemotypes will be analyzed for each candidate gene and they will be functionally characterized in different heterologous systems.

3 Materials and Methods

3.1 Plant materials and growth

Zea mays

The maize material (varieties B73, *bm3*, *bm1*, *cal1*) used for the BioLector© screening platform (section 4.1) was grown in the greenhouse under a 16 h/8 h light/dark-regiment and temperatures between 20 °C and 25.6 °C. The plants were watered twice per day and fertilized twice per week with 0.5 % (v/v) Wuxal® (S. Wang et al., 2023). The maize material B73 and *bm3* used for analyzing the influence of harvest time on the water-soluble sugar content (section 4.2) were grown in the botanical garden at the Heinrich Heine University Düsseldorf in the year 2023 and 2024. Seedlings were pre-cultivated for 2 weeks in a Fitotron® SGC 120 (Weiss Technik) before transferring them to the soil. In the year 2023, the plants were not fertilized. In the year 2024, the plants were fertilized every two weeks with a 7.5 % solution of “Wuxal Top N” fertilizer (composition N/P/K: 12/4/6). Maize material used for the water-soluble carbohydrate screening (section 4.2) was grown in the year 2021 at Corteva™ Agriscience (Eschbach, Germany) as part of the project “Cornwall” (BMBF, grant 031B1303A). Based on plant maturity, the internode below the first ear was harvested, dried and used for subsequent analyses.

Arabidopsis thaliana

Arabidopsis thaliana plants (section 4.4), were grown either in soil, on plates or hydroponic systems. Prior sowing in any system, the seeds were sterilized with chlorine gas. Tubes containing the seeds were placed open in a desiccator jar. Within the desiccator, 100 mL of bleach (Colgate Palmolive GmbH, Hamburg, Germany) was mixed with 3 mL of 37 % hydrochloric acid (HCl, Carl Roth GmbH + Co. KG, Karlsruhe, Germany). Immediately afterwards, the desiccator was sealed air-tight and incubated for 3 h, before ventilating. After 30 min of ventilation, the tubes were closed and the seeds stored at room temperature.

For soil growth *A. thaliana* seeds were stratified in 2 mL of 0.1 % plant agar at 4 °C for 2 to 4 days in the dark, before placing individual seeds on water-soaked 44 mm Jiffy-7 peat pellets. The plants were grown in walk-in climate chambers (2207_435_SON, regineering GmbH) with a 12/12 h light/dark regimen, a temperature of 20/19 °C and a

humidity of 75/40 %. The first week, the plant trays were covered with a lid to ensure sufficient humidity. The plants were watered twice per week. If not otherwise stated, after 8 weeks, seeds, stems or leaves were harvested for subsequent analyses.

For plate growth, sterilized seeds were placed on ½ MS (Murashige & Skoog) plates (Table 5) (pH 5.6 adjusted with 1 M KOH, Merck KGaA, Darmstadt, Germany) and varying Glc (Merck KGaA) concentrations, ranging from 0 % to 5 % (w/v) (H. Y. Chen et al., 2015). After stratification for 4 days (4 °C, dark), the plates were incubated at the same conditions mentioned before for soil growth and grown for 14 days. Afterwards, the plates were imaged and the total plant area determined with ImageJ (version 1.54), by manually marking the plant area in the software. Then, the plants were individually collected, freeze-dried for 1 day (Coolsafe™ system (Scanvac)) and used for subsequent compositional analyses of the water-soluble fraction.

For growth in hydroponic systems, sterile plastic cones (Araponics, Liege, Belgium) were filled with ½ MS media + 0.7 % plant agar (w/v; final concentration) without carbon source, at room temperature. The filled cones were inserted into the holes of 1000 µL pipette tip racks (Sarstedt) and transferred to pipette tip boxes containing 700 mL of ½ MS liquid media with either 0.5 % or 5 % (w/v) final Glc concentration. With a sterilized tweezer, single *A. thaliana* seeds were placed on each individual cone. Once, all cones were filled, the box was closed and wrapped three times with Micropore™ tape (3M™; VWR, cat. No. 115-8172). The boxes were placed at 4 °C in the dark for two days and then transferred to a Fitotron® SGC 120 (Weiss Technik) for 17 days with a 16 h/8 h light dark regimen. Light intensity was set to 9000 Lux, and the humidity was 65 % (light) and 80 % (dark). After completion of the growth phase, the roots were separated from the plants by cutting and the root length was determined by taking pictures with a scale bar and subsequent measurement using ImageJ (version 1.54). Afterwards, media residues were washed away with water and roots and plants separately freeze-dried for 1 day, the materials weighed and used for subsequent compositional analyses of the water-soluble carbohydrate fraction.

Two different T-DNA insertion *A. thaliana* lines were obtained from the European Arabidopsis Stock Centre (Table 2).

Table 2: ***A. thaliana*** **TDNA knock-out lines and specific primers.**

T-DNA line	NASC ID	AGI code	Name in this work	References
SALK_048430C	N670685	At3g14770	*Atsweet2-3*	(H. Y. Chen et al., 2015)
SALK_044600C	N674782	At3g14770	*Atsweet2-1*	

Homozygous plants were identified via PCR-based genotyping (Table 3 and Appendix Figure 26) with T-DNA insert specific primers (Table 4), designed with the online tool "T-DNA Primer Design" (http://signal.salk.edu/tdnaprimers.2.html).

Table 3: **PCR protocol for genotyping of *A. thaliana* lines.**

Cycles	Step	Temperature (°C)	Time
	Initial Denaturation	95	2 min
10	Denaturation	95	7 sec
	Annealing	62	30 sec
	Elongation	72	30 sec
25	Denaturation	95	7 sec
	Annealing	56	30 sec
	Elongation	72	30 sec
	Final Elongation	72	7 min

Table 4: **Specific primers used to identify T-DNA insertion plants.** Primer sequences are provided in Table 29. Exp. Size refers to the expected amplicon size.

T-DNA line	Name in this work	T-DNA primers	Exp. size	WT spec. primers	Exp. size	Gel picture
SALK_048430C	*Atsweet2-3*	P1 + P3	464-764	P2 + P3	1143	Appendix Figure 26
SALK_044600C	*Atsweet2-1*	P1 + P5	608-908	P4 + P5	1144	

Nicotiana benthamiana

Nicotiana benthamiana (section 4.4) was grown by the green-house responsible personnel at the Heinrich Heine University Düsseldorf as described in (Gombos et al., 2023). Seeds were soaked in water for 24 h at 20°C before being sown in a peat moss substrate for growing in a growth chamber. After two weeks, uniform seedlings were selected and transferred to a greenhouse for three weeks under long-day conditions 16 h/8 h light/dark cycle at 22°C/20°C and approximately 90 µmol/m^2/s light intensity and 60 % humidity.

3.2 Plant biomass preparation

Milling

Individual corn stems were collected and processed as described in (S. Wang et al., 2023). In short, the material was ground into powder in a GM200 mixer mill (Retsch) and freeze-dried. The powder was then milled in 2 mL screw cap tubes containing two 5 mm steel balls for 3x2 min at 30 Hz in a MM400 mixer mill (Retsch). The fine powder was resuspended in water (50 mg/mL) and sterilized by autoclaving (VX-120 autoclave (Systec), 15 min, 121 °C) for fermentation experiments or used as powder for the preparation of alcohol-insoluble residues (sections 4.1 and 4.2). Alternatively, for the water-soluble carbohydrate screening across the natural variation panel, a 1 cm section of the middle of the internode below the first ear was manually cut into small pieces. These pieces were then milled in 2 mL screw cap tubes containing two 5 mm steel balls for 3x2 min at 30 Hz in the MM400 mixer mill. The following procedure was similar to the process described above.

A. thaliana materials (stems, leaves, roots, (section 4.4)) were freeze-dried for 1 day, followed by the addition of two 5 mm steel balls and milling for 2x1 min at 30 Hz in a MM400 mixer mill. The fine powder was resuspended to a final concentration of 5 mg/mL and used for further analyses.

Lignocellulosic pretreatments

To test the effect of different lignocellulosic pretreatments (section 4.1), 70 mg of dried and milled corn material (variety B73) were weighed into 2 mL screw cap tubes and 1 mL of sulfuric acid (H_2SO_4, Carl Roth GmbH + Co. KG) or sodium hydroxide (NaOH, Sigma-Aldrich) were added to final concentrations of 0.39 and 0.05 g H_2SO_4 per g B73 or 0.16 g or 0.05 g NaOH per g B73. The samples were heated for 45 min at 121 °C with subsequent cooling on ice. The hydrolyzed samples were neutralized by addition of NaOH or H_2SO_4, respectively, and diluted to a final biomass concentration of 50 mg/mL by addition of 2-(N-Morpholino) ethanesulfonic acid (MES, Sigma-Aldrich) buffer (pH 6) to a final concentration of 50 mM.

For trifluoracetic acid (TFA, Carl Roth GmbH + Co. KG) pretreatment, 15 mg dried and milled B73 material was weighed into 2 mL screw cap tubes and resuspended in 300 µL of 2 M TFA. The suspensions were heated to 121 °C for 90 min, cooled down and

the acid evaporated with air flow at 40 °C. The remaining pellet was washed twice with 2-propanol (Carl Roth GmbH + Co. KG), dried and resuspended in sterile water to a final concentration of 25 mg/mL.

Microwave pretreatment of 50 mg/mL biomass slurry preparations was performed in a household microwave (DOMO DO1059CG) at 1000 W for 30 s. Slurries were cooled to room temperature, the water loss during microwaving was measured gravimetrically, and the lost water was replaced to reach the initial concentration of 50 mg/mL.

3.3 Biochemistry

Water-soluble carbohydrate quantification

Maize (50 mg/mL, (sections 4.1 and 4.2)) or *A. thaliana* (5 mg/mL (section 4.4) material was centrifuged (10 min, 12000 rpm), and the solid was separated from the liquor for compositional analyses. Additionally, residual material after fungal fermentation (sections 4.1 and 4.2) was transferred from the fermentation plates to 2 mL screw-cap tubes, centrifuged (10 min, 12000 rpm), and the solid was separated from the liquor for compositional analyses.

The liquor fractions were filtered through PTFE membrane filters (0.2 µm) and used directly for soluble sugar analysis on a high-performance anion-exchange chromatography (HPAEC) (Metrohm or Knauer Azura) equipped with a CarboPac PA20 column (3 x 150 mm) and a pulsed amperometric detector (PAD) (Metrohm or Antec Scientific Decade Elite). The following gradient was used: 21 min 1 mM NaOH, 9 min 700 mM NaOH and 13 min 1 mM NaOH, with a flow rate of 0.5 mL/min. Fucose (Sigma-Aldrich) was used as an internal standard for maize material, and glucosamine (GlcN, Sigma-Aldrich) for *A. thaliana*.

Solid fraction

Alcohol-insoluble residue preparation

The separated solid residue was dried with air flow. Alternatively, dried and milled plant biomass powder was used (section 4.1) and alcohol-insoluble residue (AIR) was prepared as described in (Foster et al., 2010a). In short, the material was washed once with 70 % (v/v) aqueous ethanol (Carl Roth GmbH + Co. KG), three times with chloroform methanol (1:1) (Carl Roth GmbH + Co. KG) and once with acetone (Carl Roth GmbH + Co. KG). Each centrifugation was done at 12000 rpm for 10 min, to pellet

the AIR. After the acetone wash, the material was dried at 40℃ with air flow and resuspended in water to a final concentration of 10 mg/mL.

Hemicellulosic monosaccharide and cellulose quantification

The simultaneous quantification of hemicellulosic monosaccharides and cellulose content in the solid was performed according to (S. Wang et al., 2023), using fucose as an internal standard. In short, paired AIR samples (1 mg) were resuspended with internal standard and dried at 40℃ with air flow. 50 µL 72 % (w/v) H_2SO_4 were added to one sample and after an incubation of 1 h at room temperature (RT), 1.4 mL water were added. The second sample was resuspended in 1.45 mL 4 % (w/v) H_2SO_4 and incubated at RT for 1 h. Both samples were autoclaved at 121℃ for 1 h in a VX-120 autoclave (Systec) and diluted with 0.5 M sodium acetate (Sigma-Aldrich) buffer pH 5.2. Afterwards, monosaccharide mixtures were separated using the same HPAEC system described above for the liquor fraction but using the following gradient: 23 min 2 mM NaOH, 7 min 490 mM NaOH, 3 min 700 mM NaOH, 24 min 2 mM NaOH, with a flow rate of 0.4 mL/min.

Acetate quantification

Cell wall-bound acetate content was determined as described in (Ramírez et al., 2018). In short, 1 mg AIR material was incubated in 0.25 M NaOH at 25℃ for 1 h. After neutralization HCl, acetic acid content was quantified using an Acetic Acid Assay Kit (K-ACET, Megazyme), following the adaptation to a 96-well plate published in (Gille et al., 2011). Solution 1 and 2 were mixed (30 µL + 12 µL per sample), added to each sample and incubated at RT for 3 min with constant shaking. The absorption was read at 340 nm (A0). Solution 3 was diluted in water (1:10) and 12 µL were added. The solution was incubated at RT for 4 min with constant shaking and the absorption read at 340 nm (A1). Finally, solution 4 was diluted 1:10 in water, 12 µL were added and the sample incubated at RT for 12 min with constant shaking. The absorption was read at 340 nm (A2) and the amount of acetate was calculated with an acetic acid standard curve according to the kit manual.

Starch quantification

The total amount of starch was quantified based on the Total Starch Kit (K-TSTA) method (Megazyme) with slight modifications. AIR (1 mg) was treated with a

thermostable α-amylase for 15 min at 100 °C with inversion every 5 min. After cooling down, 50 µL amyloglucosidase were added, vortexed and incubated for 30 min at 50 °C. The Glc content was then quantified in 10 µL of the supernatant with the glucose oxidase peroxidase (GOPOD) method according to (Kraemer et al., 2021). 300 µL of the GOPOD reagent were added and the samples incubated at 50 °C for 20 min. The absorption was measured at 510 nm and the Glc content calculated based on a Glc standard curve. The starch content was calculated from the difference between sample with and without addition of α-amylase.

Lignin quantification

Acetyl bromide soluble lignin content was determined according to (Foster et al., 2010a). 1 mg AIR material was resuspended in 100 µL 25 % v/v acetyl bromide (Sigma-Aldrich) in glacial acetic acid (Sigma-Aldrich) and incubated at 50 °C for 2 h, followed by 1 h with thorough mixing every 15 min. Afterwards, 400 µL 2 M NaOH and 70 µL 0.5 M hydroxylamine hydrochloride (Sigma-Aldrich) were added and the solution mixed. The volume was filled to 2 mL with acetic acid and centrifuged for 2 min at 10000 rpm. 200 µL were transferred to UV-specific 96-well plates and the absorption monitored at 280 nm. The percentage of acetyl bromide soluble lignin was calculated with the formula provided in (Foster et al., 2010a) using the grass specific coefficient 17.75.

Lignin composition analysis

Lignin composition was determined as published in (Foster et al., 2010a). 1 mg AIR material of unfermented corn stover was resuspended in 200 µL of 2.5 % boron trifluoride diethyl etherate (Sigma-Aldrich), 10% ethanethiol (VWR) in dioxane (Merck) and the vials gas phase was replaced with nitrogen. The samples were heated for 4 h at 100 °C with gentle mixing every 60 min. After cooling for 5 min on ice, 150 µL of 0.4 M sodium bicarbonate (Sigma-Aldrich) were added and the solutions mixed. 1 mL water and 0.5 mL ethyl acetate (Sigma-Aldrich) were added for phase separation. 150 µL of the ethyl acetate phase were transferred to 2 mL screw cap tubes and the solvent was evaporated with air flow, followed by washing the samples twice with 200 µL acetone and evaporation. For trimethylsilyl derivatization, 500 µL of dry ethyl acetate, 20 µL of pyridine (Sigma-Aldrich) and 100 µL of N, O- bis(trimethylsilyl) acetamide (Merck) were added and the samples incubated for 2 h at 25 °C. 100 µL of

the solution were transferred to a GC-MS compatible vial containing 100 µL acetone, and 2 µL were injected to gas chromatograph (7890B, Agilent) equipped with a quadrupole electronic ionization mass analyzer (5977A) equipped with a 30 m x 250 µm x 0.25 µm Slb-5MS column (Sigma-Aldrich) and a helium flow rate of 1.1 mL/min. The oven gradient followed this protocol: initial temperature 210 °C for 3 min, followed by a ramp of 3 °C/min to 250 °C and a final hold at 250 °C for 5 min. The mass analyzer screened for the three ions 239, 269 and 299 m/z.

Plant and fungal biomass separation

The following method was published before in (Robertz et al., 2024). For the estimation of *U. maydis* biomass material in the solid residue, first, *U. maydis* was grown in equivalent BioLector® conditions with 1 % (w/v) Glc as a carbon source instead of corn stover. Monosaccharide composition from the solid residue was determined as described before. Under these conditions, galactose (Gal), Glc, mannose, GlcN, and ribose were detected.

The identity of the monosaccharides was confirmed by the alditol acetate method based on (Foster et al., 2010b). In short, 1 mg of AIR was hydrolyzed with 2 M TFA, the acid was evaporated, and the remaining pellet was washed once with propanol. Next, the monosaccharides were reduced by the addition of sodium borohydride (Sigma-Aldrich) in 1 M ammonium hydroxide (Sigma-Aldrich). The mixtures were neutralized by addition of acetic acid and five washing steps with 9:1 (v:v) methanol acetic acid and methanol were conducted. Acetylation was done by addition of acetic anhydride (Sigma-Aldrich) and pyridine to the pellet. The solvents were evaporated, and the samples were washed twice with toluene. Ethyl acetate and water were added, and the organic phase was quantitatively transferred to a 2 mL screw cap tube, evaporated and the pellet resuspended in acetone. The resulting alditol acetates were injected into the above-mentioned GC-MS system. A Supelco SP-2380 (30 mm x 0.25 mm x 0.20 µm film thickness) column was used with a helium flow rate of 1.5 mL/min. The oven gradient followed this protocol: initial temperature 80 °C for 3 min followed by a ramp to 170 °C with 30 °C/min, afterwards a ramp to 240 °C with 4 °C/min, and a final hold at 240 °C for 15 min.

In addition, a constant amount of corn stover AIR was mixed with increasing amounts of *U. maydis* AIR grown on Glc, and the GlcN content was quantified, establishing a

linear correlation between *U. maydis* AIR and the detected GlcN content. Finally, the GlcN content in the solid residue from fermented samples (mixture of plant and fungus) was used to estimate the amount of fungal material. Given that Gal and Glc are present in both plant and fungal material, conversion factors were applied to determine the proportion of these monosaccharides originating from each source based on the GlcN-estimated fungal material.

Mass balance in glass flasks

For quantitative determinations of the post-fermentation residue, corn stover (variety B73) fermentations were also carried out in pre-weighed glass shake flasks (100 mm x 13 mm), with the same compositional setup used for the BioLector® fermentations. The cultures were shaken horizontally at 300 rpm, 28 °C, angled at 44 °. At the end of the fermentation, the flasks were centrifuged, and the liquor was separated from the solid, which was dried by speedvac (Concentrator Plus, Eppendorf) for 60 min at 45 °C and quantified gravimetrically. Subsequently, AIR was prepared and the remaining solid was quantified gravimetrically. Solid analyses were conducted as described above to determine the hemicellulosic monosaccharide composition, cellulose, lignin, acetate and starch content, as well as the amount of fungal material.

3.4 Microbiology

Growth media

All media was autoclaved prior use (Table 5). If a specific concentration of carbohydrates, or amino acids was required in the final media, these components were filter-sterilized (0.2 µm) before addition to the autoclaved media.

Table 5: **Growth media components.**

Media Name	Components	Manufacturer
LB broth (Luria/Miller)	Tryptone (10 g/L), yeast extract (5 g/L), sodium chloride (10 g/L), pH 7.0 ± 0.2	Roth (cat. No. X968)
LB agar (Luria/Miller)	Tryptone (10 g/L), yeast extract (5 g/L), sodium chloride (10 g/L), agar-agar (15 g/L), pH 7.0 ± 0.2	Roth (cat. No. X969)
YPM	Yeast extract (10 g/L), peptone (20 g/L), maltose (20 g/L) For plates: agar-agar (20 g/L) was added	
YNB – Ura	Yeast nitrogen base without amino acid and ammonium sulfate (Sigma-Aldrich cat. No. Y1251) (1.7 g/L), ammonium sulfate (5 g/L), maltose (20 g/L), histidine (76 mg/L), tryptophan (76 mg/L), Leucine (360 mg/L) For plates: agar-agar (20 g/L) was added	
CM	Detailed component list is shown in appendix Table 29.	
½ MS (Murashige and Skoog)	Cat. No. M0245	Duchefa Biochemie

Agar containing media was liquified before pouring into petri dishes by microwaving and cooling down to 60°C before addition of either carbohydrates, amino acids or antibiotics (not sterile; Table 6). After addition, the media was not heated again, to prevent thermal degradation of these components.

Table 6: **Antibiotics used in this work.**

Antibiotic	Concentration	Purpose
Ampicillin	100 µg/mL	*E. coli* selection
Kanamycin	50 µg/mL	*E. coli* and *A. tumefaciens* selection
Rifampicin	50 µg/mL	*A. tumefaciens* selection
Spectinomycin	50 µg/mL	*E. coli* and *A. tumefaciens* selection

Ustilago maydis strain and corn stover fermentation

All fermentation experiments (sections 4.1 and 4.2) were performed with the *Ustilago maydis* strain MB215^{Gfp}P$_{oma}$bgl1. Therefore, the MB215P$_{oma}$bgl1 strain described in (Geiser et al., 2016) was further modified to express a cytoplasmic green fluorescent protein (Gfp). This was achieved by collaborators in the Institute for Microbiology, HHU, Düsseldorf, by stable genomic integration of the *gfp* open reading frame under control of the constitutive promoter P$_{otef}$ into the *ip* locus using the integrative plasmid pOTEF-SG (Spellig et al., 1996), according to previously described protocols (Stock et al., 2012).

For the *U. maydis* inoculum, overnight pre-cultures were inoculated with *U. maydis* grown on complete medium (CM) agar plates supplemented with 1 % (w/v) Glc (Holliday, 1974) and used to inoculate main cultures to an optical density (OD_{600}) of 0.2. The main cultures were grown for 5 h, washed once, and resuspended in sterile water to a final OD_{600} of 1.5. MTP-R48-BOH 1 round well microtiter plates were filled with 1.5 mL suspension per well consisting of 600 µL corn stover (50 mg/mL), 750 µL 2x CM without Glc, 50 µL sterile water and 100 µL *U. maydis* inoculum (final OD_{600} of 0.1). The plates were incubated at 28°C with 1000 rpm constant shaking in a BioLector® device (Beckman Coulter Life Sciences, Aachen, Germany). To test the effect of Celluclast® (Novozymes) addition, 0.5 µL per mg plant biomass was included in the suspension. Scattered light was measured at a wavelength of 620 nm and a gain of 15. Additionally, Gfp fluorescence ($\lambda_{Ex.}$ = 488 nm; $\lambda_{Em.}$ = 520 nm, gain = 80), and pH ($\lambda_{Ex.}$ = 470 nm; $\lambda_{Em.}$ = 525 nm, gain = 23) were measured, with readings every 30 min.

Scattered light and Gfp fluorescence values were normalized to those obtained 2.5 h after inoculation, once the corn stover particles in the wells had reached homogeneous distribution.

Other microorganisms

Different strains of *Escherichia coli* were used throughout this work (Table 7).

Table 7: ***E. coli* strains used in this work.**

Strain name	Company	Use
E. coli TOP10F´		Restriction cloning; Plasmid amplification
E. coli One Shot® MAX Efficiency® DH5α™ -T1R	ThermoFisher; cat. No. 12297016	Gibson cloning; Gateway cloning, Plasmid amplification
E. coli DB3.1		Amplification of empty Gateway Vectors, as this strain is resistant to the toxic effect of the ccdB gene

The *Saccharomyces cerevisiae* strain EBY4000 [hxt1-17Δ::loxP gal2Δ::loxP stl1Δ::loxP agt1Δ::loxP ydl247wΔ::loxP yjr60cΔ::loxP] (Wieczorke et al., 1999) was used for growth assays and localization of the SWEET2a transporter (section 4.4). This strain is deficient in hexose transport and thus will be termed “transport deficient strain” in the following. As comparison, the background strain CEN.PK2-1C [MATα leu2-1,112 ura3-52 trp1-289 his3-Δ1 MAL2-8^{c} SUC2 hxt17Δ], used to create the transport deficient strain, was used (Wieczorke et al., 1999). Both strains were kindly provided by the Institute for Molecular Physiology, HHU Düsseldorf.

For transient expression of the *SWEET2a* gene in *Nicotiana benthamiana* three different *Agrobacterium tumefaciens* strains were used (section 4.4). The background of all strains was *A. tumefaciens* GV3101 (pMP90). One strain contained the p19 silencing suppressor from the tomato bushy stunt virus to enhance transgene expression (Sawaguchi et al., 2001). Two other strains either contained the pSOUP vector (Addgene plasmid #165419) or no additional plasmid and were used as carriers for the binary plant expression vectors. All strains were kindly provided by the Institute for Molecular Physiology, HHU Düsseldorf.

For long term storage of all microorganisms, cultures of interest were grown overnight in appropriate media. On the following day, 800 µL of the culture were mixed with 200 µL 80 % glycerol in CryoPure tubes (Sarstedt) and stored at -60 °C.

3.5 Primers and vectors

In general, primers were designed based on the gene/vector sequence of interest using the Primer3 Web tool (https://primer3.ut.ee/) (Koressaar et al., 2018; Koressaar & Remm, 2007; Untergasser et al., 2012), with, if possible, a length of 20-24 bp, a G/C content of 40-60 % a melting temperature around 55-62°C and a 3´-GC clamp. If primers were used for Gibson cloning, they were designed with the NEBuilder online tool (https://nebuilder.neb.com). Primers were ordered desalted from Sigma-Aldrich (Merck KGaA, Darmstadt, Germany) at a scale of 0.025 µmol

The following vectors were used in this work (Table 8). A list of primers is provided in the appendix (Table 29).

Table 8: **Vector backbones used in this work.**

Vector backbone	Use	Source	Sequence
pDONR™-221	Gateway entry vector	Provided by the Institute for Molecular Physiology, HHU Düsseldorf	Thermo Fisher Scientific Cat. Nr. 12536017
pDRf1-GW	Gateway destination vector; EBY4000 expression	pDRf1-GW was a gift from Wolf Frommer & Dominique Loque (Loqué et al., 2007)	Addgene plasmid #36026
pDRf1-GFP-GW	Gateway destination vector; EBY4000 localization	Provided by the Institute for Molecular Physiology, HHU Düsseldorf	Page 172
pMDC7NtmVenus	Gateway destination vector; *N. benthamiana* localization; N-terminal tag mVenus	Provided by the Institute for Molecular Physiology, HHU Düsseldorf	Page 173
pRD04 i. mVenus in pAB111	Gateway destination vector; *N. benthamiana* localization; C-terminal tag mVenus	Provided by the Institute for Molecular Physiology, HHU Düsseldorf	Page 175
pF3A WG (BYDV) Flexi®	TNT® SP6 High-Yield Wheat Germ Protein Expression System	Promega	Promega Cat. Nr. L5671

3.6 Microbial transformation

Escherichia coli

Chemically competent *E. coli* cells of the strain TOP10F´ and DB3.1 were provided by Felix Roth, Institute for Plant Cell Biology and Biotechnology, HHU Düsseldorf. They were prepared as follows, single colonies were picked from a LB plate and used as inoculum of a 10 mL LB broth overnight culture at 37°C and 225 rpm. 1 L of LB broth was inoculated with the overnight culture and grown to an OD of 0.4, before placing the culture on ice for 20 – 30 min. Afterwards, the cells were harvested by

centrifugation in pre-cooled flasks for 15 min, 3000 g, 4°C. The pellet was carefully resuspended in 100 mL ice cold 100 mM $MgCl_2$ (Sigma-Aldrich) and centrifuged at 2000 g for 15 min, 4°C. The supernatant was replaced with 200 mL ice cold 100 mM calcium chloride ($CaCl_2$, Sigma-Aldrich) and the cells incubated on ice for 20 min prior another centrifugation (2000 g for 15 min, 4°C). The pellet was resuspended in 50 mL of ice cold 85 mM $CaCl_2$, 15 % glycerol (v/v, Sigma-Aldrich) and centrifuged at 1000 g for 15 min, 4°C, before a final resuspension in 2 mL of 85 mM $CaCl_2$, 15 % glycerol (v/v). Aliquots of 50 µL were frozen in liquid nitrogen and stored at -60°C until use.

Competent *E. coli* cells of all strains (Table 7) were transformed with heat-shock, by slowly defrosting them on ice. Up to max. 5 µL ligation reaction, Gateway reaction or plasmid DNA (max. 100 ng) were added and the solution mixed by gently tapping the tubes. The cells were incubated on ice for 30 min, before heat-shock in a water bath at 42°C for 30 s. Afterwards, the cells were cooled on ice for 2 min and 500 µL LB broth or SOC outgrowth media (New England Biolabs® cat. No. B9020S) were added. The mixtures were incubated horizontally shaking at 37°C, 225 rpm for 60 min and finally plated on LB + antibiotic selection plates and incubated at 37°C. After 1-2 days, positive colonies were picked and the presence of the correct plasmid verified by colony PCR with vector specific primers.

Saccharomyces cerevisiae

Chemically competent cells of the yeast EBY4000 were created and transformed with the lithium acetate (LiAc, Sigma-Aldrich)/polyethylenglycol (PEG, Sigma-Aldrich) method (Gietz & Schiestl, 2007) with minor modifications. Overnight YPM liquid cultures of EBY4000 were inoculated from YPM plates and incubated at 30°C, 225 rpm. On the following day, the cultures were diluted to an OD of 0.1 in 50 mL YPM and incubated for another 5-6 h until they reached an OD of 0.8 – 1.0. The cultures were pelleted 5 min, 3000 rpm and washed once with water and once with 1 mL sterile 0.1 M LiAc. After resuspension in 0.5 mL 0.1 M LiAc, 50 µL aliquots were taken, pelleted and used for transformation. To each sample, individual transformation mixtures were added, containing 240 µL 50 % PEG, 36 µL 1 M LiAc and 10 µL denatured single stranded DNA from salmon testes (heated to 100°C for 10 min and cooled on ice prior using; Sigma-Aldrich, cat. No. D7656). 0.5 to 2 µg plasmid DNA were added and the mixture filled to a final volume of 360 µL. After mixing thoroughly, the cells were

incubated at 30 °C for 30 min, heat shocked at 42 °C for 30 min and centrifuged shortly. The transformation mixtures were replaced by water and the cells streaked out on selective media (YNB – Ura, Table 5). After 2-4 days, positive colonies were picked and the presence of the correct plasmid verified by colony PCR with vector specific primers.

For microscopy, yeast cells were grown over night in YNB – Ura medium (Table 5) and resuspended in distilled water to a final OD_{600} of 2.0 prior imaging. 10 µL were added to the microscopy slide.

Agrobacterium tumefaciens

Competent *Agrobacterium tumefaciens* cells were provided by the Institute for Molecular Physiology, HHU Düsseldorf. The cells (stored at -60 °C) were defrosted on ice, mixed with 100 – 200 ng of plasmid DNA and incubated for 30 min on ice. Afterwards, the cells were heat-shocked in a water bath for 5 min at 37 °C and incubated for another 40 min on ice. 500 µL LB medium was added without antibiotics and the mixtures incubated horizontally shaking, at 28 °C for 2-3 h. Finally, the cell suspensions were plated on selective LB plates and incubated at 28 °C until colonies formed (2-3 days). The presence of the correct plasmid was verified via colony PCR with vector specific primers.

3.7 Molecular Biology

Genomic DNA extraction from *A. thaliana*

Leaf material of *A. thaliana* was collected in a 1.5 mL tube, 2-3 glass beads were added and the material milled with a Retsch MM400 mixer mill for 2x 30s at 30 Hz. The milled material was collected at the bottom and 500 µL extraction buffer (100 mM Tris-HCl pH 8.0, 50 mM EDTA, 100 mM sodium chloride, 0.35% (w/v) sodium dodecyl sulphate (SDS) were added (all chemicals from Sigma-Aldrich), and the solution mixed. 130 µL ice-cold 5 M potassium acetate (Sigma-Aldrich) was added, and the tubes inverted several times before the plant material was pelleted at 15000 g for 15 min. 450 µL of the supernatant was mixed with 350 µL of ice-cold isopropanol and the tubes inverted and centrifuged for 10 min at 16000 g to pellet the DNA. The DNA pellet was washed with 500 µL 70 % ethanol and dried before resuspension in 100 µL TE buffer.

Plasmid DNA extraction

Plasmid DNA was extracted from *E. coli* overnight cultures using the Zyppy Plasmid Miniprep Kit (Zymo Research, cat. No. D4019) acc. to the manual.

DNA quantification and concentration

The DNA or RNA content was quantified using an Eppendorf BioSpectrometer (µCuvette® G1.0, standard dsDNA settings or standard RNA settings). If necessary, the DNA concentration was increased with the Zymoclean DNA Clean & Concentrator Kit (Zymo Research, cat. No. D4003) acc. to the kit manual.

PCR

Throughout this work, two different polymerases were used for different purposes. Red Taq DNA Polymerase (VWR) was used for colony PCRs of transformed microbes or genotyping of *A. thaliana* plants. Phusion™ High-Fidelity DNA-Polymerase (ThermoFisher Scientific, cat. No. F530S) and GC buffer (ThermoFisher Scientific, cat. No. F539L) were used for single nucleotide polymorphism (SNP) confirmation in *Zea mays* genomic DNA, Gibson cloning or addition of Gateway overhangs to DNA fragments. In general, both polymerases were diluted according to the manufacturer's instruction. Primers were added to a final concentration of 0.2 µM and, if necessary, dimethyl sulfoxide (Sigma-Aldrich) was added to a final concentration of 3 % (v/v). The Thermocycler conditions were based on the manufacturers protocol. 2-5 min of initial denaturation at 95°C, followed by 25 - 35 cycles of I) 30 s denaturation at 95°C; II) 30 s annealing at primer dependent temperatures (calculated with the ThermoFisher Scientific Tm calculator); III) various time of elongation at 72 °C depending on amplicon size (Red Taq 1 kb/min, Phusion 2 kb/min). These cycles were followed by a final elongation at 72°C for 5 min.

For colony PCRs, cell material was mixed in 10 µL of water. 1 µL of this mixture was used as template. For plasmid amplifications 10 ng of template plasmid was used.

Gel electrophoresis

DNA fragments were separated by size via gel electrophoresis using 1 % agarose in 1x TRIS-acetate-EDTA buffer gels and 1x TRIS-acetate-EDTA as running buffer. DNA was detected by addition of 2.5 µL GelRed™/50 mL to the gel. After a run time of 25-45 min at 110-120 V, the DNA bands were visualized using the Bio-Rad ChemiDoc™

XRS+, and compared to ready-to-use Gene Ruler 1kb or 1 Kb Plus DNA ladder (ThermoFisher Scientific, cat. No. SM0313 or Invitrogen, cat. No. 10787018, respectively). For DNA recovery from the gel, the bands of interest were cut out and the DNA recovered using the Zymoclean Gel DNA recovery Kit (Zymo Research, cat. No. D4002).

Sequencing

DNA fragments or plasmids were prepared and sent to Eurofins Genomics acc. to their instructions. DNA samples for sanger sequencing were diluted based on the amplicon length and mixed with 25 pmol of appropriate primer in a final volume of 10 µL. Whole plasmid sequencing sample were diluted to 600 ng DNA in 20 µL final volume. The obtained sequencing results were aligned with *in silico* generated templates in Benchling.

3.8 Restriction/Ligation cloning and Gibson assembly of *PMI3* haplotypes

The coding sequence of the *PMI3* gene (haplotype 1) (acc. Nr. EU974512.1) flanked C-terminally by the SfaAI restriction site (GCGATCGC) and N-terminally by the MssI restriction site (GTTTAAAC) was ordered synthesized in the pDONR™-221 vector (GeneArt gene synthesis, ThermoFisher Scientific). The expression vector pF3A WG (BYDV) Flexi® (Table 8) was obtained from Promega.

Both plasmids were digested with FastDigest DNA restriction enzymes SfaAI and MssI (ThermoFisher Scientific) in FastDigest Green Buffer (ThermoFisher Scientific, cat. No. B72) at 37°C for 30 min to 2 h, followed by inactivation at an enzyme dependent temperature. Dephosphorylation of the pF3A WG (BYDV) Flexi® vector backbone was achieved by adding FastAP Thermosensitive Alkaline Phosphatase (ThermoFisher Scientific, cat. No. EF0654) to the mixture, acc. to the manufacturer's instructions. The resulting DNA fragments were separated and isolated by gel electrophoresis and gel extraction, followed by the Zymoclean DNA Clean & Concentrator Kit (Appendix Figure 27). The products were ligated using Thermo Scientific T4 DNA Ligase (New England Biolabs®, cat. No M0202S). The ligation mix composition was set up according to the NEBio Calculator (nebiocalculator.neb.com), and the reaction incubated at 16°C for 16 h followed by 10 min inactivation at 65°C. The final product was directly used to transform competent *E. coli* cells. The presence of the correct plasmid was checked

via colony PCR with vector backbone (P23 + P44) specific primers that flank the insertion site (Figure 28) and additionally confirmed by whole plasmid sequencing.

To create the other haplotypes from the pF3A::*PMI*3_hap1 template, a two-fragment Gibson assembly approach was used. The mutation-carrying primers for each haplotype were created with the NEBuilder tool (nebuilder.neb.com). The primer combinations are given below (Table 9) and the primer sequences are given in the appendix (Table 29).

Table 9: **Primer combination for two-fragment Gibson assembly of PMI haplotypes.**

Haplotype	Primer combination fragment 1	Primer combination fragment 2
pF3A::*PMI3*_hap2	P21 + P16; amplicon 2228 bp	P22 + P15; amplicon 2409 bp
pF3A::*PMI3*_hap3	P21 + P18; amplicon 2549 bp	P22 + P17; amplicon 2088 bp
pF3A::*PMI3*_hap4	P21 + P20; amplicon 3273 bp	P22 + P19; amplicon 1364 bp

The fragments were amplified in a 50 µL PCR setup with Phusion™ High-Fidelity DNA-Polymerase using 0.5 ng/µL template. The PCR protocol for the individual haplotypes is shown below (Table 10). Furthermore, in parallel the same PCR setup was prepared in 10 µL reactions with gradually increasing annealing temperatures. These temperatures were 59.6°C, 61.9°C, 64,7°C, 68,6°C, 71,7°C (Figure 29).

Table 10: **PCR conditions to amplify Gibson fragments.**

Cycles	Step	Temperature (°C)	Time
	Initial denaturation	95	2 min
25	Denaturation	95	30 s
	Annealing	PMI3_hap2: 67 PMI3_hap3: 65 PMI3_hap4: 65	30 s
	Elongation	72	PMI3_hap2: 1:45 min PMI3_hap3: 2:15 min PMI3_hap4: 2:15 min
	Final elongation	72	10 min

The fragments were separated via gel electrophoresis, cut out and pooled from the two different PCR setups mentioned above and purified as described before. Finally, the two isolated fragments for each haplotype were mixed with 2x DNA assembly mix according to the recommendations of the NEBuilder assembly tool to a total amount of 0.5 pmol DNA in a total volume of 10 µL. The mixtures were incubated at 50°C overnight. 2 µL of the assembly mix were used to transform *E. coli* DH5α. Positive transformants were selected on ampicillin containing plates and used for plasmid amplification followed by plasmid extraction and whole plasmid sequencing to confirm the correct sequences.

3.9 Gateway cloning of *SWEET2a*

The coding sequence of *ZmSWEET2a* (haplotype 1) (acc. nr. Zm00001eb155660_T003) was ordered synthesized in the pDONR™-221 vector (GeneArt gene synthesis, ThermoFisher Scientific). This plasmid was used as a template to amplify the complete coding sequence (CDS) with the primer combination P34 + P35 (Table 29) via PCR with Phusion™ High-Fidelity DNA-Polymerase using 0.5 ng/µL vector as template.

Table 11: **PCR protocol used to amplify CDS of SWEET2a_hap1.**

Cycles	Step	Temperature (°C)	Time
	Initial denaturation	95	2 min
25	Denaturation	95	30 s
	Annealing	66	30 s
	Elongation	72	45 s
	Final elongation	72	10 min

The cleaned and concentrated PCR product was used as template to create the SWEET2a_hap2 coding sequence, as well as both haplotype coding sequences without the stop codon containing the attB sites, via a two-step PCR protocol using the following primer combinations (Table 12) and Phusion™ High-Fidelity DNA-Polymerase with 0.5 ng/µL template. The primer sequences are provided in the appendix (Table 29).

Table 12: **Primer combinations for *SWEET2a* haplotype generation with and without stop codon.**

Construct	Primer combination step1	Primer combination step2
SWEET2a_hap1	P32 + P30	P28 + P29
SWEET2a_hap1 w/o stop	P32 + P31	P28 + P29
SWEET2a_hap2	P33 + P30	P28 + P29
SWEET2a_hap2 w/o stop	P33 + P31	P28 + P29

The PCR protocol is shown below (Table 13). After step 1, the PCR product was purified and eluted in 10 µL elution buffer. 5 µL was used as template for step 2.

Afterwards, all DNA fragments were cloned into the pDONR™221 vector in a BP reaction, catalyzed by the Gateway™ BP Clonase™ II Enzyme mix (ThermoFisher Scientific, cat. No. 11789020) according to the manufacturer´s instructions, but all volumes reduced by half and the incubation time was overnight. Of the reaction mixture, 2 – 4 µL were used to transform *E. coli* DH5α and positive transformants were selected on kanamycin containing medium. From the entry clones, the different

haplotype constructs were subcloned into the destination vectors for the different systems via LR reaction catalyzed by the Gateway™ LR Clonase™ II Enzyme mix (ThermoFisher Scientific, cat. No. 11791020) according to the manufacturer´s instructions, but all volumes reduced by half.

Table 13: **PCR conditions to add Gateway overhangs to *SWEET2a* haplotype CDS.**

Step	Cycles	Step	Temperature (°C)	Time
Step 1		Initial denaturation	95	2 min
	13	Denaturation	95	30 s
		Annealing	SWEET2a_hap1: 66 SWEET2a_hap2: 64	30 s
		Elongation	72	1 min
		Final elongation	72	2 min
Step 2		Initial denaturation	95	2 min
	21	Denaturation	95	30 s
		Annealing	60	30 s
		Elongation	72	1 min
		Final elongation	72	2 min

For subcellular localization in *N. benthamiana*, SWEET2a_hap1 and SWEET2a_hap2 were N-terminally tagged with mVenus by subcloning into the pMDC7NtmVenus vector (Table 8). Both haplotypes without stop codon were cloned into the pRD04 i. mVenus in pAB111 vector to add a C-terminal mVenus tag. For growth experiments in EBY4000, both haplotypes were cloned into the pDRf1-GW and for subcellular localization, both haplotypes without stop codon were cloned into the pDRf1-eGFP-GW vector.

After the LR reactions, 4 µL of the reaction mixtures were used to transform *E. coli* DH5α or TOP10F´ and positive colonies were selected on spectinomycin (pMDC7NtmVenus and pRD04 i. mVenus in pAB111) or ampicillin (pDRf1-GW and pDRf1-eGFP-GW) containing medium. Positive transformants were used to amplify the plasmids, followed by plasmid extraction and whole plasmid sequencing to confirm correct sequences.

3.10 Phosphomannose isomerase expression and activity studies

For *in vitro* expression of PMI3_hap1 – PMI3_hap4, the TnT® SP6 High-Yield Wheat Germ Protein Expression System (Promega, catalogue nr. L3261) was used, following the manufacturer´s instructions. The master mix was stored at -60°C and prior use quickly thawed by hand warming, before gentle mixing by pipetting up and down several times. Plasmid DNA (20 µL), isolated and purified in nuclease-free water

(provided with the Expression System Kit) directly prior use, was mixed with the master mix (30 µL) by pipetting, and the mixtures incubated at 25°C for 2 h. Alternatively, water without plasmid DNA was mixed with the master mix and used as negative control (named “no protein”). Afterwards, the mixtures were directly used for the following assays.

The catalyzation of the reaction from mannose-6-phosphate (M6P) to fructose-6-phosphate (F6P) (section 4.5; named “F6P synthesis”) was measured in a coupled enzymatic assay based on (Maruta et al., 2008), following the adaptations published in (Hu et al., 2016). All components were obtained from Sigma Aldrich. 10 µL NADP (Nicotinamide adenine dinucleotide phosphate, 13.5 mM, cat. No. N0505), 1 U phosphoglucose isomerase (PGI; *S. cerevisiae*, cat. No. 10128139001), 1 U glucose-6-phosphate dehydrogenase (G6PDH; *Leuconostoc mesenteroides*, cat. No. 346774) were mixed in 50 mM Tris-HCl buffer pH 7.5 to a final volume of 265 µL. 25 µL M6P was added in different concentrations ranging from 0 – 2800 µM final concentration in the assay and the mixtures equilibrated at 30°C with absorption measurements every minute at 340 nm for 5 min. Once the readings were constant, 10 µL containing 1.5 µL or 2.5 µL of protein extract from the TnT® expression system in 50 mM Tris-HCl buffer pH 7.5 or 10 µL containing 0.5 U phosphomannose isomerase (PMI; *E. coli*, cat. No. P2621) were added. The absorption increase was monitored for 90 min at 30°C, with readings every minute at 340 nm. The increase in NADPH was determined from the initial linear absorption increase rates of cofactor reduction after subtraction of background PMI activity measured in the no protein control. The applied molar extinction coefficient of NADPH corrected for the path length was 3.38 L/mmol. The protein activity was then calculated as µmol (cofactor reduction) per min per total protein, with the total protein concentration determined via a Bradford assay. The data points for the Michaelis-Menten plots were generated by plotting the activity over the substrate concentration. Furthermore, Lineweaver Burk plots were generated by plotting the reciprocal activity over the reciprocal substrate concentration and with the linear regression the Vmax value was calculated in units per mg total protein as the reciprocal value of the y-intercept, and Km was determined by multiplying the slope with Vmax. Both kinetic values (Km and Vmax) were then used to plot the curves in the Michaelis-Menten graphs.

The reverse reaction from F6P to M6P (termed “M6P synthesis” in section 4.5) was measured as an endpoint reaction by mixing water, 5 µL of the TnT® cell free expression system mixture and 25 µL of F6P as substrate to a final volume of 200 µL and incubating at 25°C for 40 min. Additionally, a ”no protein” control samples was included in this assay. The resulting mixtures of phosphate sugars were separated on the HPAEC system mentioned before equipped with a CarboPac PA20 column (3 x 150 mm) and a PAD detector (Metrohm). The following gradient was used: 30 min 420 mM NaOH followed by flushing with 700 mM NaOH for 10 min and an equilibration phase of 15 min at 420 mM NaOH. The phosphate sugar concentration was then determined via a standard curve with known concentrations of M6P, F6P and G6P.

3.11 Bradford

The total protein content (section 4.5) was determined based on the Coomassie Plus (Bradford) Assay Kit manual (ThermoFisher Scientific, cat. No. 23236) with minor modifications. 10 µL of the unknown protein sample in appropriate dilutions were mixed with 200 µL of Bradford reagent (1:5 diluted in water) in a 96-well plate. After short incubation at RT, the absorbance was read at 595 nm. The total protein content was calculated based on a bovine serum albumin standard curve.

3.12 Transient gene expression in *Nicotiana benthamiana*

The day prior *N. benthamiana* infiltration (section 4.4), liquid *A. tumefaciens* overnight cultures (5 mL LB + antibiotics) were inoculated in 50 mL Falcon tubes and incubated at 28°C shaking at 225 rpm (rounds per minute). The overnight cultures were diluted to an OD_{600} of 0.1 in the morning and incubated for another 5-6 hours, until an OD_{600} of 0.8 was reached. The cultures were centrifuged and the media replaced with infiltration buffer (10 mM magnesium chloride, 10 mM MES pH 5.6, 450 µM acetosyringone (Carl Roth)). Expression vector carrying *A. tumefaciens* strains were mixed with the p19 carrying strain to final ODs of 0.1 in a volume of 5 mL and the mixtures incubated in the dark for at least 2 h. Leaves from 3-week-old *N. benthamiana* plants were infiltrated on the abaxial side, using a 1 mL syringe. If not otherwise stated, infiltrated leaves were sprayed two to three days after infiltration with β-estradiol (20 µM β-estradiol (Sigma-Aldrich), 0.1 % v/v Tween-20 (Carl Roth) (Zuo et al., 2001)). Induction times ranged from 30 min to 5 h. Prior microscopy, the leaves were infiltrated

with 0.1 % (w/v) aniline blue and imaged immediately. A 1 cm section of the leave was placed with the abaxial side facing up on microscope slides.

3.13 Confocal fluorescence microscopy

Confocal images (section 4.4) were obtained using a Zeiss LSM900 microscope, equipped with Airyscan GaAsp-PMT detectors and diode lasers using a C-Apochromat 40x/1.20 W Korr FCS water objective or a Plan-Apochromat 63x/1.40 Oil DIC M27 objective. To visualize proteins of interest, mVenus was excited with a 488 nm laser (0.5 -4 % laser power) and emission was detected at 538 nm. To visualize Gfp the same excitation laser was used, but the emission set to 509 nm. Autofluorescence was detected with excitation at 506 nm and emission at 751 nm.

3.14 Genome-wide association study

The R-script for computing the genome-wide association study (GWAS) (section 4.2) associating the water-soluble carbohydrate content in corn stover with genomic variations across a natural variation panel was provided by the Institute for Quantitative Genetic and Genomics of Plants, HHU Düsseldorf, within the scope of the “Cornwall” project (BMBF; 031B0193A). First, the influence of the genotype on the phenotypic trait was analyzed, while accounting for the effect of the field position and the replicate, by fitting a linear mixed-effect model (using lme4 package in R), to identify genotypes with significantly higher or lower traits. The analyzed traits were water-soluble glucose, sucrose, fructose content, the total water-soluble carbohydrate content and the relative water-soluble carbohydrate composition with relative parts of glucose, sucrose and fructose. To account for the unequal distribution of group sizes, the estimated marginal means were calculated, which were then used as input values for the GWAS. Further, a principal component analysis was conducted to reduce the dimensionality and capture genetic variation among the genotypes and to account for genetic relatedness based on the SNP data, a genetic relationship matrix was computed. Then, the GWAS was conducted (Mixed Linear Model, using the sommer::GWAS() function in R) by modelling the average trait value as a function of the first two principal components, accounting for the relationship of the genotypes using the genetic relationship matrix and the residual variance of the trait. In the last step, significant SNP identifiers ($p < 0.0001$) and their physical position in the maize genome were extracted. Furthermore, the results were plotted in a Manhattan-Plot (using the ggplot2 package

in R). Since the SNP ID and their physical position were based on B73 RefGen_v2, they were converted into B73 RefGen_v5, by copying the SNP identifiers into MaizeGDB.org (Woodhouse et al., 2021) and extracting their respective v5 synonyms and position.

The decay of linkage disequilibrium (LD) was calculated for each chromosome based on the SNP data, using the built-in function in TASSEL5 (Bradbury et al., 2007) with the LD threshold set to 0.1 and used to define an individual quantitative trait loci (QTL) for each SNP. The physical position of each significant SNP from the GWAS was taken as central reference point for its respective QTL. The boundaries of each QTL were then determined by adding or subtracting the LD distance. The identified QTLs were then transferred to the “EnsemblPlants” database (Yates et al., 2022), where gene identifiers within each QTL were extracted. Using the “MaizeMine” platform (version 1.5), the gene identifiers were matched to their corresponding annotation based on MaizeGDB. Based on the gene annotation data, candidate genes potentially involved in water-soluble carbohydrate metabolism were selected for further analysis.

3.15 Haplotype-chemotype analysis

The physical position and the genomic DNA and cDNA sequences of each candidate gene were obtained from their respective entries in MaizeGDB and imported into Benchling. The introns and exons were then manually annotated based on the alignment of genomic DNA with cDNA using the inbuild function in Benchling. To check each candidate gene for SNP occurrence across the natural variation panel, whole genome sequence data of 135 corn varieties were used, which were previously published (Grzybowski et al., 2023). The SNPs in the coding sequence were then filtered for non-synonymous SNPs, resulting in an amino acid change in the final protein. Based on non-synonymous SNP occurrence, the 135 varieties were then grouped into haplotypes. The haplotype detected in the reference variety B73 was always set to haplotype 1. For each haplotype the average and standard deviation was calculated for all seven traits analyzed in the GWAS (absolute glucose, fructose, sucrose and total water-soluble carbohydrate content and relative glucose, sucrose, fructose content). Then, the averages were compared for significant differences. For the candidate genes *ZmSWEET2a* and *ZmSWI3C1* a pairwise comparison to haplotype 1 was conducted with a two-tailed Students T-Test. For *ZmPMI3* the data

were first tested for a normal distribution with a Shapiro-Wilk test ($p < 0.05$). Since the data for haplotype 1 and haplotype 2 were non-normal distributed for the absolute fructose content, a Kruskal-Wallis Test was used for group comparisons, followed by a Dunn´s multiple comparison test with an adjusted p-value according to Bonferroni ($p < 0.008$). Additionally, the total water-soluble carbohydrate content was compared for this candidate gene. Since the data followed a normal distribution for each haplotype, a One-way ANOVA followed by Tukey-HSD test was conducted with $p < 0.05$.

3.16 Software and analysis tools

Chromatograms from HPAEC were integrated either with ChlarityChrom (version 7.4.2.107, Kanuer) or MagIC Net (version 3.3, Metrohm). GC/MS data were analyzed in the MSD ChemStation Data Analysis software (version F.01.03, Agilent). Fermentation data from the BioLector system were exported as .csv files from the BioLection 2 software (m2p-labs GmbH, now Beckman Coulter) and further analyzed in Excel (Office 2019). In general, all numerical data analysis was done in Excel (Office 2019) or in R (v4). For statistics in excel, the Real Statistics Resource Pack (real-statistics.com) was used. If not otherwise stated, *in silico* molecular biology was done with Benchling. Confocal microscopy pictures were analyzed with Omero (version 5.6) or ImageJ (version 1.54). The grammar and wording of this thesis were improved with the assistance of the large language model ChatGPT-4o. The model was solely used to refine existing text. Sections of the text were copied into ChatGPT with the prompt to “rewrite”. The revised output was then manually reviewed and selectively integrated into the original text.

4 Results and Discussion

4.1 Chapter 1: Corn stover as substrate for *Ustilago maydis*

4.1.1 Background

It was shown before that the fungus *U. maydis* can grow on a variety of different carbon sources, ranging from easy-fermentable mono- and disaccharides to more complex substrates like maize bran or milled maize seedling tissues (Cano-Canchola et al., 2000; Couturier et al., 2012; Geiser et al., 2016; Richter et al., 2024). However, the studies that used complex substrates did not focus on substrate degradation, but the fungal secretome, thus, it is not known which carbohydrate-containing fractions of the substrates *U. maydis* utilized (Cano-Canchola et al., 2000; Couturier et al., 2012). Furthermore, it is unknown whether it can utilize corn stover for growth, which comprises mostly complex lignocellulose from senescent corn stem tissue. *U. maydis´* CAZyme repertoire points into the direction that it could be able to utilize this substrate, since the fungus expresses a variety of cellulose-, xylan- and lignin-acting enzymes (Couturier et al., 2012; Geiser et al., 2013; Kämper et al., 2006; X. Li et al., 2022; Mueller et al., 2008; Nieter et al., 2015). Furthermore, its ability to grow on other corn materials like seedling leaves and bran supports this notion (Cano-Canchola et al., 2000; Couturier et al., 2012), however, these substrates differ substantially in their composition from corn stover. Thus, to track potential fungal growth, an online monitoring platform is necessary that allows the detection of fungal growth in a highly turbid, complex media containing plant biomass particles.

Microtiter plate screening platforms play the predominant role for high-throughput process developments on laboratory scale (Kensy et al., 2009; Ladner et al., 2016). They allow the fast screening of a variety of different conditions *i.e.*, different media, strains, pretreatments, with less manual work than conventional Erlenmeyer flask setups, which substantially accelerates process development (Ladner et al., 2016). Conventional Erlenmeyer flasks require continuous probing during the fermentation to detect parameters like optical density or light scatter, substrate consumption or product production offline (X. Zhang et al., 2019). However, over the last decades, online monitoring systems, like the BioLector® system or the µ24 system, based on microtiter plates have been developed that use optical measurements to detect important process parameters, including scattered light, fluorescence, pH or dissolved oxygen

tension, without the need to stop the shaking process for the read-out (Isett et al., 2007; Kensy et al., 2009; Samorski et al., 2005). These systems allow the parallel culturing of multiple microbial cultures under controlled environmental conditions, constant shaking, and continuous online process monitoring, meaning that key parameters such as optical density, pH, or dissolved oxygen are measured in real time (Isett et al., 2007; Kensy et al., 2009; Samorski et al., 2005). Furthermore, it was shown that the results obtained in laboratory scale fermentations based on these systems can be transferred to larger scale fermenter systems, which simplifies process scale-up (Kensy et al., 2009; Wewetzer et al., 2015).

The BioLector® platform was chosen in this work to monitor potential fungal growth on corn stover. Due to the high turbidity of the fermentation media, optical density measurements are impossible without previous sample dilution, since the light beam has to pass through the entire culture liquid (Samorski et al., 2005). The BioLector® platform circumvents this issue, as it detects media turbidity based on scattered light. Scattered light measurements do not require penetration of the culture liquid, as only the reflected light is used for detection, which makes this reading more suitable for online monitoring of turbid media (Samorski et al., 2005). Additionally, the system allows the parallel detection of fluorescence, pH and dissolved oxygen tension all based on optical measurements (Ladner et al., 2016; Samorski et al., 2005). Furthermore, it was shown before that this system is suitable to monitor *U. maydis* growth in Glc or arabinose containing media (Hartmann et al., 2018; Hussnaetter et al., 2021; Philipp et al., 2022). However, online monitoring of *U. maydis* growth on complex substrates like corn stover was not attempted in this system before.

4.1.2 Results

Monitoring of *Ustilago maydis* performance growing on corn stover

To determine whether the BioLector® platform can monitor the fungal performance, the fungus was mixed with increasing concentrations of milled B73 material (Figure 1 A). Fungal growth was monitored via scattered light reading, as it correlated with cell density (Samorski et al., 2005). The previously characterized *U. maydis* P_{oma}bgl1 strain (Geiser et al., 2016) was modified to express the green fluorescent protein (Gfp) as a second method to monitor and quantify fungal growth (Robertz et al., 2024). In the control without corn stover, only a slight uptick in the scattered light signal was observed, reaching a maximum of 13.9 ± 0.1 a.u. (arbitrary units), after 22 h (Figure 1 A). This increase is likely attributable to residual nutrients still present in the media. In contrast, when the media was supplemented with corn stover, there was a notable boost in the scattered light signal, indicative of fungal biomass production. This surge begins around the 6 h mark in all corn stover concentrations tested. While the maximum values of scattered light using 3 g/L or 10 g/L corn stover were observed after 23 h, increasing the corn stover material to 20 g/L resulted in a maximum signal (140.9 ± 6.1 a.u.) after 14 h, followed by a stationary phase where the signal slightly decreased to 131.7 ± 5.7 a.u. until the conclusion of the experiment (Figure 1 A). This decrease is most likely caused by plant biomass particles sticking to the walls of the microtiter plate, which results in decreasing turbidity of the media over time.

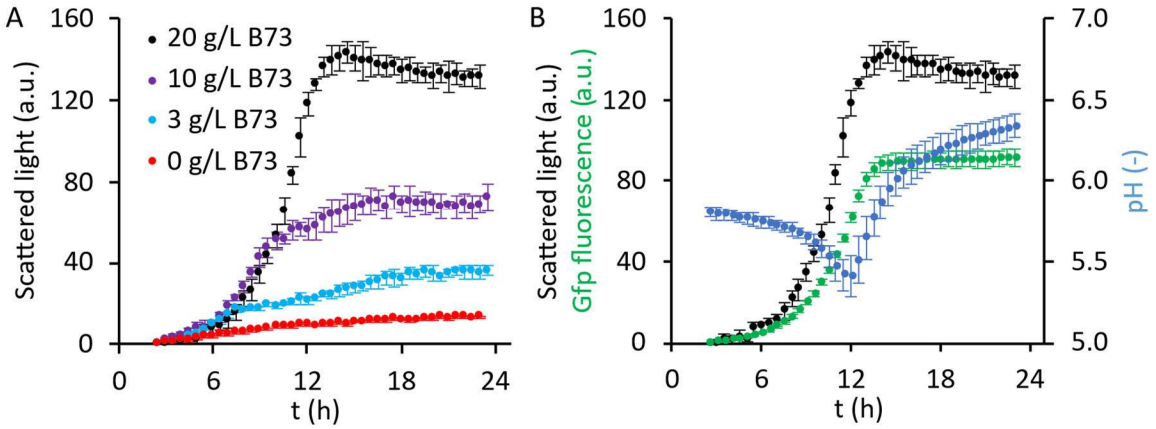

Figure 1: **Online performance monitoring of *Ustilago maydis* on B73 corn stover.** (A) Scattered light reading of fungal growth in medium supplemented with 3 g/L (blue), 10 g/L (purple) or 20 g/L (black) ground B73 corn stem material from 4 individual plants in comparison to medium without addition of B73 stem material (red) (n = 2). (B) Scattered light (black), Gfp fluorescence (green) and pH (light blue) monitoring of fungal growth in medium supplemented with 20 g/L of B73 plant material as carbon source. The data are shown as scattered light and Gfp fluorescence in arbitrary units (a.u.) and pH over time (t) in hours (h) and are the results of two independent fermentation experiments with independent fungal inoculums and 4 plants variety B73. The average ± SD is calculated from the resulting n = 8.

The growth performance of *U. maydis* on 20 g/L corn stover was further characterized (Figure 1 B). Scattered light measurements in cultures can be influenced by cell shape, cell size and the corn stover particles in the system (Kunze et al., 2014), so the Gfp fluorescence was monitored as additional fungal biomass production indicator. Furthermore, the pH was monitored throughout the fermentation, to gain insights into the fungal metabolic activity. Together with the increase in scattered light signal after 6 h, the pH of the media dropped from an initial 5.8 to a minimum of 5.4 by 12 h. As the cultures reached the stationary phase, the pH increased, reaching 6.3 by the end of the cultivation period (Figure 1 B). Furthermore, the Gfp fluorescence signal emitted by the fungus increased correlating to the scattered light signal, reaching the stationary phase at 89.0 ± 4.1 a.u. after 14 h. Unlike the scattered light reading, the Gfp signal remained constant until conclusion of the experiment, highlighting that the Gfp fluorescence is not influenced by potential changes in media turbidity caused by plant biomass particles (Figure 1 B).

These results indicate that the BioLector® platform allows a detailed characterization of the fungal growth performance on corn stover. In addition, the simultaneous monitoring of growth (scattered light and Gfp fluorescence) and metabolic activity (pH) confirmed that *U. maydis* can grow on B73 corn stover as sole carbon source. Based

on these results, the next step was to identify which of the carbohydrate sources present inside corn stover *U. maydis* utilized for growth. As introduced before, these can be separated into the non-structural carbohydrates, which comprise the water-soluble carbohydrates and starch, and the lignocellulosic polysaccharides cellulose and hemicellulose.

U. maydis´ utilization of water-soluble carbohydrates in corn stover

To identify, which corn stover components were utilized by *U. maydis*, a compositional analysis was conducted on the residue remaining after fermentation in the presence ("post-fermentation residue") and absence ("pre-fermentation residue") of the fungus. The suspensions were collected from the BioLector® plate at the end of cultivation and the liquor fraction was separated from the solid fraction and dried for further analysis. The pre-fermentation liquor fraction contained high amounts of water-soluble carbohydrates, Glc, Suc and Fru (Table 14).

Table 14: **Carbohydrate composition of the liquor fraction of B73 [wt%].** Soluble carbohydrate quantification of not autoclaved, pre- and post-fermentation B73 material. Data of the not autoclaved and pre-fermented water-soluble carbohydrate contents are shown as average ± SD of n = 4 plants. The data for post-fermented water-soluble carbohydrate contents are the results of two independent fermentation experiments with independent fungal inoculums and 4 plants. The average ± SD is calculated from the resulting n = 8. Bold values indicate statistically significant differences between -/+ *U. maydis* conditions determined by pairwise comparisons of not autoclaved vs. pre-fermented and pre-fermented vs. post-fermented biomass by a two-tailed students t-Test at *p*-value < 0.05.

Condition	Glucose	Sucrose	Fructose	Total
B73 not autoclaved	9.1 ± 1.1	2.3 ± 1.1	9.3 ± 1.0	20.7 ± 1.4
B73 pre-fermentation	9.0 ± 0.9	2.4 ± 0.9	9.6 ± 0.6	21.0 ± 0.8
B73 post-fermentation	**0.3 ± 0.04**	**0.1 ± 0.03**	**0.04 ± 0.03**	**0.4 ± 0.05**

Since the corn stover was autoclaved prior fermentation to prevent microbial contamination, the potential impact of autoclaving on the composition and availability of water-soluble carbohydrates was examined. No significant differences in Glc, Suc and Fru content were detected between not autoclaved (Glc: 9.1 ± 1.1 wt%, Suc: 2.3 ± 1.1 wt%, Fru 9.3 ± 1.0 wt%) and pre-fermented corn stover (Glc: 9.0 ± 0.9 wt%, Suc: 2.4 ± 0.9 wt%, Fru 9.6 ± 0.6 wt%) (Table 14). No differences were detected for the total water-soluble carbohydrate contents either (not autoclaved 20.7 ± 1.4 wt% versus pre-fermented 21.0 ± 0.8 wt%) (Table 14).

In the post-fermentation residue, only trace amounts of the carbohydrates were detected (Glc: 0.3 ± 0.04 wt%, Suc: 0.1 ± 0.03 wt%, Fru 0.04 ± 0.03 wt%), and the total

water-soluble carbohydrate content in the post-fermentation residue was reduced to 0.4 ± 0.05 wt% (Table 14). This indicates that *U. maydis* is utilizing these abundant water-soluble carbohydrates in corn stover for growth.

U. maydis´ utilization of corn stover lignocellulose

The other major source of carbohydrates in corn stover is lignocellulose. To identify, if *U. maydis* utilized specific compounds of this fraction, a detailed biochemical analysis of the post-fermentation solid residue was conducted. However, to determine specific utilization of lignocellulosic compounds, it is necessary to dissect the post-fermentation residue into plant and fungal material, due to the extensive growth of *U. maydis* during fermentation.

To achieve this, fungal markers are used as indirect measurements for fungal biomass production (Duong et al., 2022; Y. Li et al., 2007; Manter et al., 2001). To identify a suitable fungal carbohydrate marker, the cell wall monosaccharide composition of *U. maydis* AIR was analyzed via HPAEC and alditol acetates (Figure 2 A). The main carbohydrate detected in *U. maydis* cell walls was Glc (183.3 ± 15.4 µg/mg AIR) followed by Gal (29.9 ± 1.7 µg/mg AIR). Additionally, mannose (13.9 ± 1.6 µg/mg AIR), GlcN (12.2 ± 1.0 µg/mg AIR) and traces of ribose (6.6 ± 3.1 µg/mg AIR) were detected (Figure 2 A). Of these monosaccharides, GlcN was chosen as the most suitable *U. maydis* marker, as it is absent in corn biomass.

A

Monosaccharide	c (µg/mg AIR)
Glucosamine	12.2 ± 1.0
Galactose	29.9 ± 1.7
Glucose	183.3 ± 15.4
Mannose	13.9 ± 1.6
Ribose	6.6 ± 3.1

B

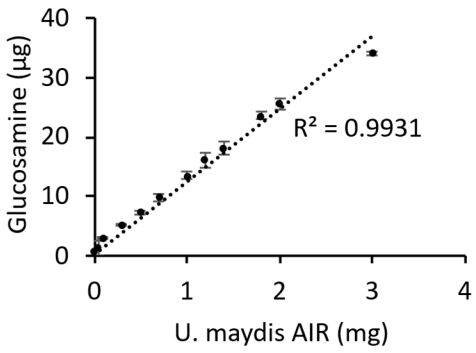

Figure 2: ***U. maydis* cell wall analysis. A) Monosaccharide composition of *U. maydis* AIR.** Data are shown as the average ± SD of 5 replicates grown on Glc containing CM media. The concentrations are based on 72 % sulfuric acid hydrolysis followed by HPAEC quantification, and the identity of galactose, glucose, mannose and ribose was confirmed via alditol acetate analysis. **B) Linear correlation between the GlcN content and 1 mg B73 AIR mixed with increasing amounts of *U. maydis* AIR (0 – 3 mg).** Data are shown as average ± SD of 3 replicates. R^2 represents the coefficient of determination.

Next, the suitability of GlcN as *U. maydis* marker in plant and fungal biomass mixtures, similar to the post-fermentation biomass collected from the BioLector® plates, was analyzed by mixing a constant amount of B73 AIR material with increasing amounts of *U. maydis* AIR, grown on Glc-containing media (Figure 2 B). No GlcN was detected in samples without fungal biomass addition, but the amount of GlcN increased linearly with increasing amounts of *U. maydis* AIR material (R^2 = 0.99) (Figure 2).

These results show that the GlcN content detected in plant and fungal biomass mixtures is a suitable indicator for *U. maydis* biomass production. Furthermore, the presence of Gal and Glc in *U. maydis* material needs to be considered when analyzing the post-fermentation residue, as these monosaccharides are present in both, fungal and plant cell walls.

Based on these results, conversion factors were calculated that allow the estimation of *U. maydis* biomass, *U. maydis* Glc and *U. maydis* Gal (µg/mg total AIR), based on the amount of detected GlcN in the post-fermentation residue (µg/mg total AIR). The detected GlcN content was multiplied by 80.65 to get the total *U. maydis* material, by 14.79 for *U. maydis* Glc and by 2.41 for *U. maydis* Gal.

Next, the amounts of *U. maydis* Gal and *U. maydis* Glc were subtracted from the total Gal and Glc detected in the post-fermentation residue, resulting in the plant derived Gal and Glc, which are shown below (Table 15). Furthermore, the other hemicellulosic monosaccharides Ara and Xyl, the main lignocellulosic building blocks crystalline cellulose and lignin, as well as acetate and starch were quantified, to analyze the individual utilization of each component (Table 15).

Table 15: **Relative biomass composition [% of AIR] of the pre- and post-fermentation B73 residue.** Data are the results of two independent fermentation experiments with independent fungal inoculums and 4 plants of B73. The average ± SD is calculated from the resulting n = 8. Bold values indicate statistically significant differences between the material determined by a two-tailed students t-Test at *p*-value < 0.05.

Condition	Arabinose	Galactose	Glucose	Xylose	HC	CC	Lignin	Acetate	Starch	*U. maydis*	Total
B73 pre-fermentation	2.5 ± 0.1	0.7 ± 0.0	2.6 ± 0.3	23.1 ± 0.7	29.0 ± 0.9	33.4 ± 2.5	15.8 ± 0.9	5.0 ± 0.3	0.5 ± 0.2	n.d.	83.7 ± 3.4
B73 post-fermentation	2.6 ± 0.2	**0.8 ± 0.0**	2.8 ± 0.3	**18.6 ± 0.1**	**25.0 ± 0.2**	32.6 ± 1.2	16.5 ± 0.6	**3.9 ± 0.2**	0.8 ± 0.0	11.2 ± 1.4	90.0 ± 1.1

n.d. = not detected; HC = sum of hemicellulosic monosaccharides; CC = crystalline cellulose; Total = Sum of plant and fungal components

No significant reduction in lignin content between post- and pre-fermented residues was observed. Starch was similarly unaffected, although only trace amounts of this polymer were present in the pre-fermentation biomass (Table 15). A slight reduction in total hemicellulose (-15 %) was detected in the post-fermentation samples. Analysis of the hemicellulosic monosaccharide composition (Ara, Gal, Glc and Xyl) revealed that the reduction in total hemicellulose was primarily attributed to a decrease in Xyl (-21 %). The strongest decrease was observed in the proportion of wall-bound acetate (-22 %, Table 15), mostly found as a substituent on the xylan backbone in corn stover.

In summary, the utilization of the lignocellulosic fraction is rather limited, with a preferential reduction in Xyl and acetate (Table 15), indicating the utilization of acetylated xylan. The quantification of fungal biomass in the post-fermentation residue is essential, to distinguish between plant and fungal components and the use of GlcN as a marker for fungal biomass quantity proved to be suitable method.

Mass balance of lignocellulose utilization in shake glass flasks

As it is virtually impossible to quantitatively harvest the post-fermentation solid fraction from the BioLector® plate, parallel cultures were grown on material from one B73 plant in shake glass flasks. These flasks are compatible with mass balance calculations and were used to validate the calculations for the post-fermentation solid fraction from the BioLector® fermentations. The analysis showed that the solid residue constituted most of the post-fermentation residue, increasing from 67.8 ± 2.7 wt% in pre-fermented samples to 80.1 ± 1.2 wt% in post-fermented samples (Table 16). Further dissection revealed that the solid fraction mainly consists of AIR. Of the AIR, 11.2 ± 0.1 % corresponded to *U. maydis* biomass (Table 17), which closely matches the fungal biomass estimated in the BioLector® samples (11.2 ± 1.4 %) (Table 15).

Table 16: **Composition of the solid fraction of B73 material [mg] fermented in shake glass flask experiments.** Data are shown as the average ± SD of 3 replicates from one B73 plant. Bold values indicate statistically significant differences between the material determined by a two-tailed students t-Test at *p*-value < 0.05.

Condition	Starting weight	Solid total	Solid plant	Solid *U. mayds*	AIR total	AIR plant	AIR *U. maydis*
Pre-fermentation	30	21.6 ± 1.2	21.6 ± 1.2	n.d.	17.1 ± 0.6	17.1 ± 0.6	n.d.
Post-fermentation	30	25.6 ± 0.5	19.2 ± 0.3	6.4 ± 0.3	21.5 ± 0.7	19.1 ± 0.6	2.4 ± 0.1

The composition of the post-fermentation biomass corroborated the results observed in the BioLector® plate (Table 15). The Xyl and acetate content decreased by 15.8 % and 22.3 %, respectively, indicating a utilization of acetylated xylan (Table 17). Significant decreases in crystalline cellulose and lignin content were detected, however, the pre-fermented material showed an unexpectedly high proportion of both components, compared to previous analyses (Table 15). Interestingly, both applied methods detected a small but significant increase in Gal content in the post-fermentation residue.

Table 17: **Relative biomass composition [% of total AIR] of the pre- and post-fermentation residue in shake glass flasks.** Data are shown as the average ± SD of 3 replicates from one B73 plant. Bold values indicate statistically significant differences between the material determined by a two-tailed students t-Test at *p*-value < 0.05.

Condition	Ara	Gal	Glc	Xyl	CC	Lignin	Acetate	Starch	*U. maydis*	Total
Pre-fermentation	2.5 ± 0.1	0.7 ± 0.0	2.4 ± 0.1	22.3 ± 1.5	41.1 ± 2.6	19.6 ± 0.8	5.2 ± 0.1	0.8 ± 0.0	n.d.	94.5 ± 3.1
Post-fermentation	**1.9 ± 0.2**	**0.9 ± 0.0**	**3.7 ± 0.3**	**16.8 ± 0.5**	**30.6 ± 1.0**	**17.0 ± 0.9**	**3.8 ± 0.2**	0.7 ± 0.1	11.2 ± 0.1	86.6 ± 0.7

Ara: Arabinose; Gal: Galactose; Glc: Glucose; Xyl: Xylose; CC: crystalline cellulose; Total: Sum of all components

Overall, these results indicate that *U. maydis* is predominantly utilizing all easy-accessible, water-soluble carbohydrates Glc, Suc and Fru (Table 14), accounting for the rapid fungal growth and metabolic activity detected in the BioLector® platform (Figure 1). The efficient utilization of the complex lignocellulosic fraction requires further optimization, as only a limited degradation of acetylated xylan was detected. Crystalline cellulose and lignin content remained unaffected in the BioLector® fermentations (Table 15), and only slightly decreased in the shake flasks experiment (Table 17). This restricted utilization of lignocellulosic components likely explains the cessation of growth and decline in fungal metabolic activity during the later stages of fermentation, as observed through online monitoring (Figure 1). The next two sections will focus on exploring different optimization strategies to enhance lignocellulosic utilization by *U. maydis*. First, different pretreatment strategies of the corn stover biomass prior fermentation will be tested and in a second step, different corn stover mutants, exhibiting alterations in their lignocellulosic composition will be used as substrate.

Effect of pretreatments on *U. maydis* performance

Pretreating lignocellulosic biomass prior fermentation is a possible way to increase its bioconversion potential. Thus, to assess if common pretreatments would enhance *U. maydis* performance, several strategies were picked. The selected pretreatment strategies were hydrolysis with acids (sulfuric acid (H_2SO_4) and trifluoracetic acid (TFA)) or base (sodium hydroxide (NaOH)), as chemical pretreatments. Furthermore, microwave irradiation was tested as physical pretreatment in comparison to the standard autoclaving treatment. And as biological treatment, the direct addition of a commercial CAZyme cocktail (Celluclast®) to the fermentation was tested. The effect of these strategies on *U. maydis* performance was then monitored and evaluated in the BioLector® platform. (Figure 3).

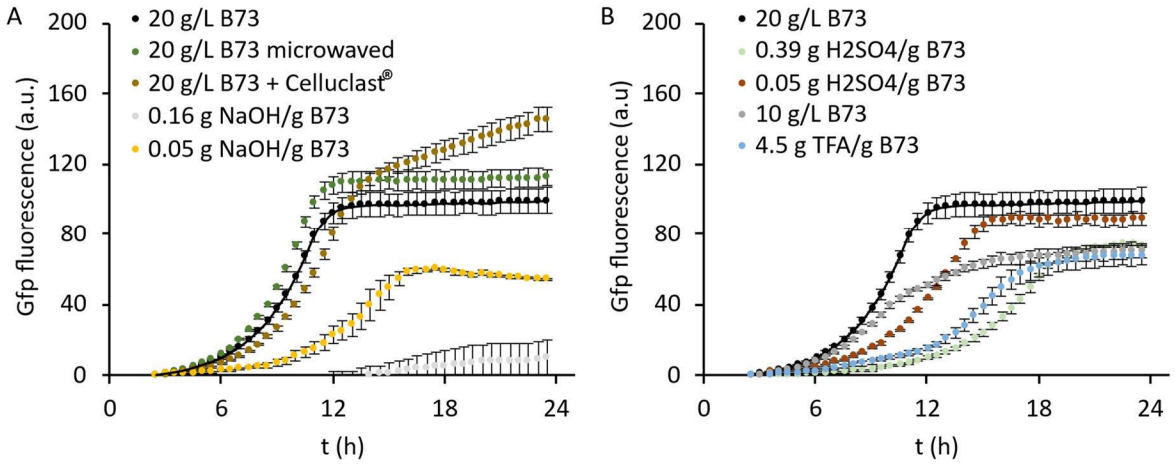

Figure 3: **Gfp fluorescence monitoring of *Ustilago maydis* fermenting variously treated B73 corn stover.** A) Standard autoclave treatment compared to microwave, alkaline hydrolysis and enzyme supplementation. B) Standard autoclave treatment compared to acid hydrolyses. Depicted is the increase in Gfp fluorescence in arbitrary units (a.u.) over time (t) in hours (h). Standard autoclave treatment (20 g/L black line with dots (A/B); 10 g/L grey (B)), microwave treatment (dark green) and Celluclast® addition (brown) was tested with 1 fungal inoculum on 4 plants variety B73. TFA hydrolysis (4.5 g/g (light blue) was tested with 1 fungal inoculum on duplicates of 4 plants variety B73. The sodium hydroxide (NaOH) (0.16 g/g (light grey) and 0.05 g/g (yellow)) and sulfuric acid (H2SO4) (0.39 g/g (light green) and 0.05 g/g (red)) hydrolyses were tested with material of one B73 plant in duplicates and the pH buffered to 6 with the addition of 50 mM MES.

The fungus growing on 20 g/L autoclaved material showed normal growth performance, reaching the stationary phase after 13 h (95.8 ± 6.4 a.u.). Hydrolyzing the corn stover with 0.16 g NaOH/g B73 before fermentation resulted in barely any fungal growth, showing a maximum Gfp fluorescence at 9.9 ± 9.9 a.u. (-90 %) at conclusion of the experiment (Figure 3 A). Reducing the NaOH concentration to

0.05 g/g slightly improved fungal performance, reaching the stationary phase after 16 h at 58.1 ± 2.1 a.u. (-38 %) (Figure 3 A). The hydrolysis with 0.39 g H_2SO_4/g B73 resulted in an extended lag phase. The stationary phase started after 14 h and reached a maximum at 69.9 ± 0.1 a.u. (-28 %) after 20 h. Reducing the acid concentration to 0.05 g/g B73 increased the fungal performance to 88.2 ± 3.0 a.u. after 16 h, however this was still 8 % lower than the performance on autoclaved material (Figure 3 B).

Another tested hydrolysis was 2 M (TFA) hydrolysis, a standard method used to hydrolyze matrix polysaccharides from plant cell walls into monosaccharides (Foster et al., 2010b). One potential advantage of this hydrolysis is the volatility of TFA; thus, it can be evaporated after hydrolysis. In comparison to autoclaved B73 material (10 g/L), *U. maydis* showed similar maximum Gfp fluorescence (autolclaved 70.3 ± 4.2 a.u. vs. TFA hydrolyzed 67.5 ± 5.5 a.u.). However, the initial lag phase was elongated and the exponential growth started after 12 h of fermentation, compared to 6 h for autoclaved material (Figure 3 B). In summary, none of the tested acid or base hydrolyses resulted in increased growth performance of the fungus under the tested conditions.

Microwaving the material prior fermentation resulted in a slightly accelerated growth compared to the autoclaved reference material. Furthermore, the stationary phase was reached at 109.4 ± 5.8 a.u. after 12.5 h, which represents a performance increase of +14 % (Figure 3 A). The supplementation of the commercial CAZyme mixture Celluclast® resulted in a slightly slower initial growth. However, while *U. maydis* fermenting the other biomasses reached the stationary phase until the end of the experiment, the cultures supplemented with Celluclast® were still growing after 24 h and reached a maximum Gfp fluorescence of 145.2 ± 7.1 a.u. (+51 %) (Figure 3 A).

In conclusion, of the tested strategies, the addition of the commercial CAZyme mixture Celluclast® was the most beneficial for fungal growth, with cultures continuing to grow until the conclusion of the experiment. Microwaving the biomass prior to fermentation modestly enhanced fungal growth performance, while the acid or alkaline hydrolyses hindered *U. maydis* growth under the tested conditions.

Effect of altered lignocellulose composition on *U. maydis* performance

Having observed the limited utilization of B73 lignocellulosic material, the question arose, if using material from different corn varieties would enhance fungal performance and lignocellulosic utilization. To address this, three well-described corn mutants, exhibiting alterations in their lignocellulosic composition, namely *cal1*, *bm1* and *bm3*, were grown in parallel to the B73 material and *U. maydis* performance was monitored (Figure 4).

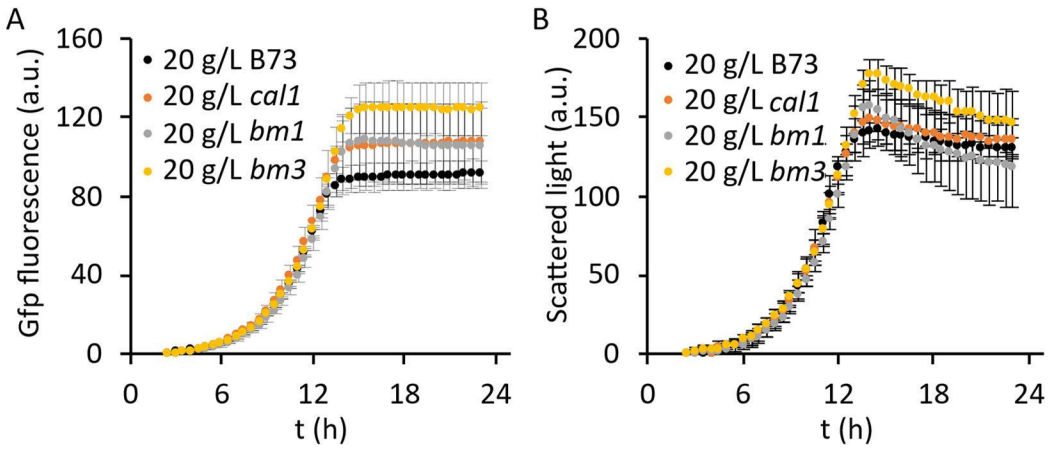

Figure 4: **Performance monitoring of *Ustilago maydis* fermenting corn stover exhibiting alterations in lignocellulosic composition.** A) Gfp fluorescence and B) scattered light monitoring of *U. maydis* fermenting B73 (black), *cal1* (orange), *bm1* (grey) and *bm3* (yellow). The data are shown Gfp fluorescence and scattered light in arbitrary units (a.u.) over time (t) in hours (h) and are the results of two independent fermentation experiments with independent fungal inoculums and 4 plants variety B73 and 6 plants of each *cal1*, *bm1* and *bm3*. The average ± SD is calculated from the resulting n = 8 (B73) or n = 12 (*cal1, bm1*, *bm3*).

Although there were no discernible differences in initial fungal growth between the different mutants and the B73 material, the maximum scattered light and Gfp fluorescence values differed. Fermenting B73 material, *U. maydis* reached stationary growth after 14 h at a Gfp fluorescence of 89.0 ± 4.1 a.u. (Figure 4 A) and a scattered light reading of 140.9 ± 6.1 a.u. (Figure 4 B). The fungus fermenting *cal1* reached the stationary phase after 14.5 h with a Gfp fluorescence reading of 104.6 ± 19.1 a.u. (+18%). *U. maydis* reached an even higher maximum growing on the lignin mutants *bm1* or *bm3*. The stationary phases were reached after 14.5 h at 106.7 ± 17.0 a.u. (+20%) and 121.0 ± 6.5 a.u. (+36 %), for *bm1* and *bm3*, respectively (Figure 4 A). These improved fungal performances were supported by the scattered light readings showing increases of 6 % for *cal1*, 12 % for *bm1* and 26 % for *bm3* (Figure 4 B). In

conclusion, these results show that fungal performance is enhanced by using material of different lignocellulosic mutants.

This raised the question, whether the observed increase in fungal performance stems from enhanced degradation of lignocellulose due to the mutations, or from greater availability of other, more easily accessible carbohydrates in these mutants. To determine, which carbohydrate source was utilized by *U. maydis*, detailed biochemical analyses of the post-fermentation residues were conducted to identify utilization of the water-soluble carbohydrates and the lignocellulosic material (Table 18 and Table 19).

Table 18: **Carbohydrate composition of the liquor fraction of B73, *cal1*, *bm1* and *bm3* [% of raw material].** Data of the soluble carbohydrate contents of the pre-fermentation (pre-f.) samples are shown as average ± SD of n = 4 plants variety B73 and n = 6 plants variety *cal1*, *bm1* and *bm3*. Data of the post-fermentation (post-f.) samples are shown as the results of two independent fermentations with independent fungal inoculums and n = 4 plants variety B73 and n = 6 plants variety *cal1*, *bm1* and *bm3*. The average ± SD is calculated from the resulting n = 8 and n = 12. Bold values indicate statistically significant differences between the amount of carbohydrates detected for the mutants compared to B73 tissue, determined by two-tailed students T-tests. All values for the fermented tissue differ significantly from their respective value in unfermented tissue, determined by two-tailed students T-tests. For simplicity this is not indicated in the table.

Condition	Glucose	Sucrose	Fructose	Total
B73 pre-fermentation	9.0 ± 0.9	2.4 ± 0.9	9.6 ± 0.6	21.0 ± 0.8
cal1 pre-fermentation	12.7 ± 3.0	1.7 ± 0.4	12.3 ± 3.4	26.6 ± 6.3
bm1 pre-fermentation	**11.8 ± 1.4**	**8.6 ± 1.8**	10.9 ± 1.9	**31.3 ± 3.8**
bm3 pre-fermentation	**14.6 ± 0.5**	3.0 ± 0.8	**13.7 ± 0.8**	**31.2 ± 1.4**
B73 post-fermentation	0.3 ± 0.04	0.1 ± 0.03	0.04 ± 0.03	0.4 ± 0.05
cal1 post-fermentation	0.3 ± 0.1	0.1 ± 0.04	0.1 ± 0.1	0.5 ± 0.1
bm1 post-fermentation	0.4 ± 0.1	0.1 ± 0.1	0.2 ± 0.2	0.8 ± 0.3
bm3 post-fermentation	0.3 ± 0.1	0.03 ± 0.01	0.2 ± 0.1	0.6 ± 0.1

The reference material B73 contained 21.0 ± 0.8 % total water-soluble carbohydrates, consisting of 9.0 ± 0.9 % Glc, 2.4 ± 0.9 % Suc and 9.6 ± 0.6 % Fru (Table 18). The total water-soluble carbohydrate content of *cal1* material was slightly increased to 26.6 ± 6.3 % (+26 %), caused by slightly elevated amounts of Glc (+41 %) and Fru (+28 %), compared to B73. In the post-fermentation biomass, only traces of the water-soluble carbohydrates were detected (Table 18). In the post-fermentation lignocellulosic fraction of *cal1*, Xyl was reduced by -16 %, acetate by -22 %, and total hemicellulose by -11 %, which is similar to the reductions detected in B73 tissues (Xyl -21 %, acetate -22 %, total HC -15 %). Crystalline cellulose and lignin content remained unaffected (Table 19). The amount of *U. maydis* material detected in the

post-fermentation biomass was comparable between *cal1* (11.0 ± 3.0 %) and B73 (11.2 ± 1.4 %) (Table 19). The higher standard deviation in *cal1* samples reflects greater variability in fungal growth, consistent with the larger spread observed in Gfp fluorescence and scattered light data (Figure 4 A and B).

The *cal1* mutant was described to accumulate MLG in senescent stems (Kraemer et al., 2021). This increase was detected by an increased Glc content in the hemicellulosic fraction (Kraemer et al., 2021). However, in the plants analyzed in this work, no significant difference to B73 was detected in hemicellulosic Glc content (Table 19). In addition, the other hemicellulosic components Ara, Gal and Xyl were significantly reduced compared to B73 material (-20 %, -15 % and -9 %, respectively). Therefore, the slight improvement in fungal performance on *cal1* is most likely due to the slight increase in water-soluble carbohydrate content, rather than enhanced utilization of the lignocellulosic biomass.

Table 19: **Relative biomass composition [% of AIR] of the pre- and post-fermentation B73, *cal1*, *bm1* and *bm3* residue.** Comparison of the pre-fermentation biomass composition (- *U. maydis*) and post-fermentation biomass (+ *U. maydis*). Data are the results of two independent fermentation experiments with independent fungal inoculums and 4 plants of B73 and 6 plants of *cal1*, *bm1* and *bm3*. The average ± SD is calculated from the resulting n = 8 or n = 12. Italic values indicate statistically significant differences between the pre-fermentation biomasses of *cal1*, *bm1* or *bm3* compared to the pre-fermentation B73 material. Bold values indicate statistically significant differences between the pre- and post-fermentation materials of each genotype. The fungal material (column *U. maydis*) detected in *cal1*, *bm1* or *bm3* tissues was compared to the amount detected in B73 material. All statistically significant differences were determined by two-tailed Students t-Tests at *p*-value < 0.05 comparing the respective tissues.

Condition	Arabinose	Galactose	Glucose	Xylose	HC	CC	Lignin	Acetate	Starch	*U. maydis*	Total
B73 pre-f.	2.5 ± 0.1	0.7 ± 0.0	2.6 ± 0.3	23.1 ± 0.7	29.0 ± 0.9	33.4 ± 2.5	15.8 ± 0.9	5.0 ± 0.3	0.5 ± 0.2	n.d.	83.7 ± 3.4
B73 post-f.	2.6 ± 0.2	**0.8 ± 0.0**	2.8 ± 0.3	**18.6 ± 0.1**	**25.0 ± 0.2**	32.6 ± 1.2	16.5 ± 0.6	**3.9 ± 0.2**	0.8 ± 0.0	11.2 ± 1.4	**90.0 ± 1.1**
cal1 pre-f.	*2.0 ± 0.3*	*0.6 ± 0.1*	3.4 ± 0.9	*21.1 ± 1.0*	27.2 ± 2.1	33.7 ± 2.7	16.0 ± 2.8	4.9 ± 0.2	0.5 ± 0.2	n.d.	82.9 ± 5.4
cal1 post-f.	2.2 ± 0.3	**0.8 ± 0.1**	3.4 ± 0.5	**17.7 ± 1.1**	**24.2 ± 1.5**	33.8 ± 1.4	17.8 ± 1.4	**3.8 ±0.3**	**0.8 ± 0.1**	11.0 ± 3.0	**91.3 ± 3.7**
bm1 pre-f.	*2.1 ± 0.1*	0.7 ± 0.0	*3.3 ± 0.4*	21.7 ±0.9	27.9 ± 1.0	35.5 ± 1.5	*18.0 ± 1.0*	4.6 ± 0.3	0.6 ± 0.2	n.d.	86.4 ± 1.9
bm1 post-f.	2.2 ± 0.1	**1.0 ± 0.1**	3.6 ± 0.4	**16.5 ± 1.1**	**23.4 ± 1.3**	**31.7 ± 1.4**	17.9 ± 0.7	**3.1 ± 0.1**	0.8 ± 0.1	**15.5 ± 1.3**	**92.5 ± 1.3**
bm3 pre-f.	2.4 ± 0.2	*0.6 ± 0.0*	2.1 ± 0.3	23.6 ± 0.8	28.7 ± 0.8	35.4 ± 1.5	15.4 ± 1.2	5.0 ± 0.2	0.4 ± 0.2	n.d.	84.9 ± 2.9
bm3 post-f.	2.2 ± 0.1	**1.0 ± 0.1**	**3.0 ± 0.2**	**18.0 ± 1.0**	**24.2 ± 1.1**	**33.3 ± 0.8**	14.2 ± 0.8	**3.5 ± 0.2**	**0.7 ± 0.0**	**15.4 ± 1.5**	**91.2 ± 1.3**

n.d. = not detected; HC = sum of hemicellulosic monosaccharides; CC = crystalline cellulose; Total = Sum of plant and fungal components

The lignin mutant *bm1* showed increased total water-soluble carbohydrate content (+49 %), with high amounts of Suc (+258 %) and slightly increased Glc (+31 %) and Fru (+13 %) contents, compared to B73 (Table 18). Only traces were detected of these carbohydrates in the post-fermentation biomass. In the lignocellulosic fraction, the Xyl content was reduced by -24 % and the acetate content by -33 %, indicating slightly

improved degradation compared to B73 material B73 tissues (Xyl -21 %, acetate -22 %) (Table 19). Additionally, the crystalline cellulose content was significantly reduced by -11 %, while no significant reduction was observed in B73 material (Table 19). The *bm1* post-fermentation residue contained 15.5 ± 1.3 % *U. maydis* material, which is an increase by 38 % compared to B73. The increased fungal biomass production was also detected in the online monitoring (Figure 4 A and B).

The mutant *bm1* was described as containing reduced lignin content (Halpin et al., 1998). However, the pre-fermented material analyzed here did not show reduced lignin content, instead the lignin content was significantly increased by +13 %, compared to B73 stems (Table 19). Similar variations in the *bm1* lignin content were previously reported ranging from -20 % reductions to no differences, depending on the study and the methods used (Barrière et al., 2013; Halpin et al., 1998; Marita et al., 2003; S. Wang et al., 2023; Xiong et al., 2020). In summary, the increased fungal performance on *bm1* material is mostly attributable to the presence of significantly more water-soluble carbohydrates in the post-fermentation residues. In addition, a significant reduction in crystalline cellulose content indicates a slightly improved utilization of the lignocellulosic fraction of this mutant. The described *bm1* chemotype was not detected in the analyzed plants, thus, the reason for the improved utilization remains unclear from the data presented here.

The lignin mutant *bm3* contained slightly more Suc compared to B73 (+25 %), as well as significantly higher amounts of Glc (+62 %) and Fru (+42 %), which resulted in a significantly increased total water-soluble carbohydrate content by +49 % (Table 18). After fermentation with *U. maydis* only traces of all water-soluble carbohydrates were present, indicating that *U. maydis* is utilizing them as nutrient source (Table 18). In the lignocellulosic fraction, the Xyl content was reduced by -24 % and the acetate content decreased by -30 % (Table 19). This indicates slightly improved degradation compared to B73 material (Xyl -21 %, acetate -22 %) (Table 19). In addition, the crystalline cellulose content was significantly reduced by -6 %, while no reductions were detected in B73 material. The fungal material comprised 15.4 ± 1.5 % of the post-fermentation biomass (+38 % compared to B73) (Table 19). This increase in fungal biomass production was also detected in the online monitoring, where *U. maydis* showed the highest performance on *bm3* material (Figure 4 A and B).

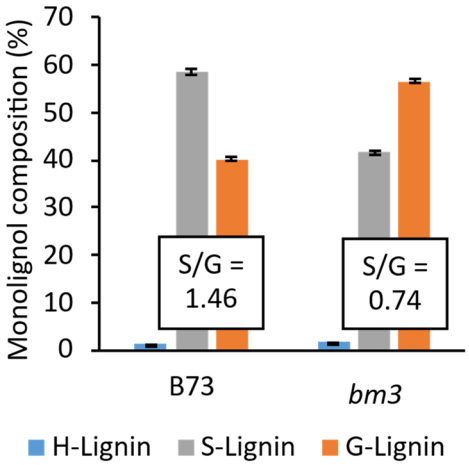

Figure 5: **Monolignol composition (%) of pre-fermentation B73 and *bm3* material.** Data are shown as the average ± SD of 2 plants per genotype for the three monolignols: H-lignin (*p*-hydroxyphenyl, blue), S-lignin (Syringyl, grey) and G-lignin (Guaiacyl, orange).

The mutant *bm3* was described as exhibiting a reduced S/G lignin ratio and slightly reduced lignin content compared to B73 (Vignols et al., 1995). The pre-fermented *bm3* material analyzed here showed a reduced S/G-lignin ratio of 0.74, compared to 1.46 of B73 (Figure 5), but the lignin content did not differ significantly. In summary, the improved fungal performance on *bm3* material is mostly attributable to the increased water-soluble carbohydrate content detected in the pre-fermentation biomass. The slightly increased reductions in Xyl, acetate and crystalline cellulose indicate that *U. maydis* is utilizing the lignocellulosic fraction of *bm3* material more efficiently than B73 material, which could be due to the altered lignin composition influencing the cross-linking of lignin to the other lignocellulosic components, like xylan.

In conclusion, these results show that the water-soluble carbohydrates are the most important carbohydrate source for *U. maydis* performance across all four genotypes B73, *cal1*, *bm1* and *bm3*. The improved performances on both lignin mutants *bm1* and *bm3* are attributable to significantly increased water-soluble carbohydrate contents. In addition, the altered lignin composition in *bm3* material most likely resulted in enhanced utilization of the lignocellulosic components xylan and crystalline cellulose.

Effect of combined assisted enzymatic lignocellulose degradation and altered lignin composition on *U. maydis* performance

The previous section identified two different strategies that enhance fungal performance: enzymatic pretreatment and lignin modification in corn stover. The most

effective strategy to enhance fungal performance on B73 material was the addition of Celluclast® directly to the fermentation mix. And increased fungal performance was detected on the lignin mutant *bm3* (+38 % compared to B73), associated to significantly more water-soluble carbohydrates and slightly increased utilization of the lignocellulosic fraction, likely due to an indirect effect of the altered lignin composition in the mutant. Now, both approaches were combined to analyze if *U. maydis* performance can be further enhanced due to potential synergistic effects of Celluclast® addition and altered lignin composition (Figure 6).

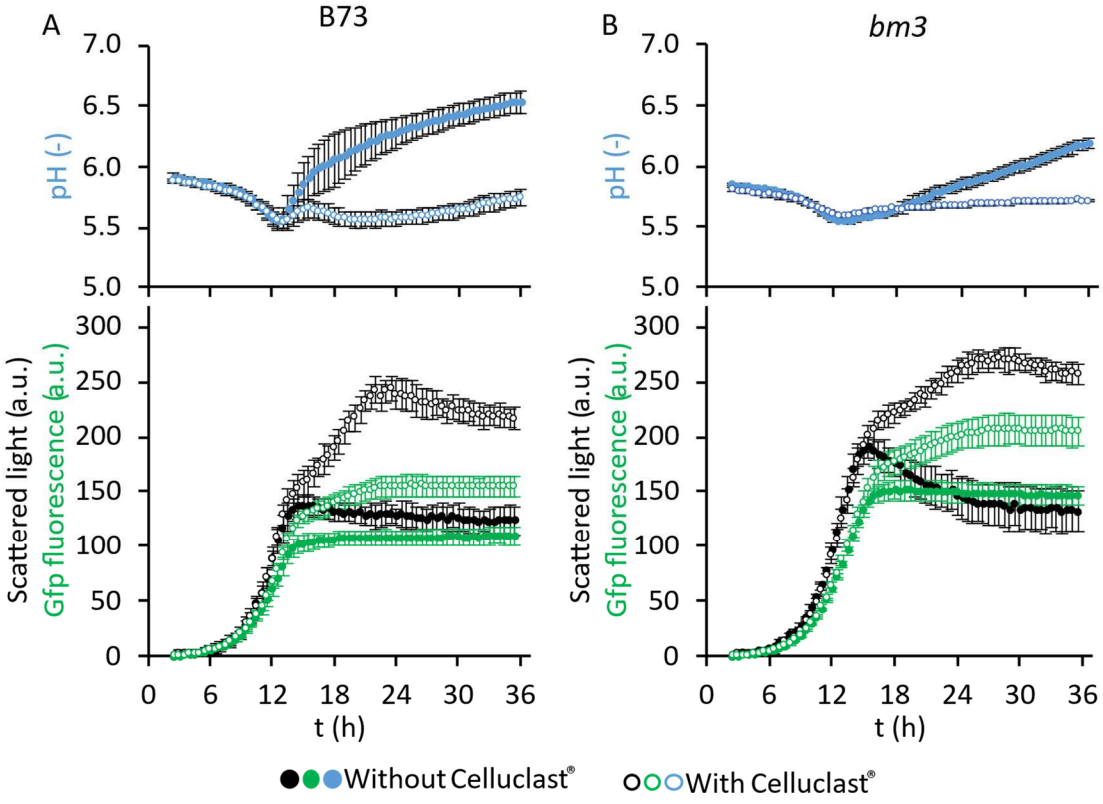

Figure 6: **Effect of Celluclast® addition on the growth performance of *U. maydis*.** Performance monitoring (scattered light (black), Gfp fluorescence (green) and pH (blue)) of *U. maydis* fermenting B73 (A) and *bm3* (B) material without (filled icons) and with (white icons) addition of Celluclast®. Depicted are scattered light and Gfp fluorescence in arbitrary units (a.u.) and pH over time (t) in hours (h). The data are the average ± SD of one fungal inoculum fermenting technical duplicates of 4 individual plants (variety B73) and 6 individual plants (variety *bm3*).

Fungal performance on B73 and *bm3* material without Celluclast® supplementation exhibited comparable growth patterns to previous experiments (Figure 1 B and Figure 4). The exponential growth phase on B73 material began after 6.5 h, reaching the stationary phase at 14.5 h, with scattered light and Gfp fluorescence readings of

136.1 ± 10.9 a.u. and 101.1 ± 8.2 a.u., respectively (Figure 6 A). *U. maydis* growing on *bm3* material reached the stationary phase at 15.5 h at a scattered light value of 190.0 ± 8.6 a.u. and a Gfp fluorescence at 140.7 ± 5.3 a.u. (Figure 6 B), highlighting the reproducibility of superior performance on *bm3* material. For both non-supplemented fermentations of B73 and *bm3*, the pH dropped from an initial value 5.9 for B73 and 5.8 for *bm3* to approximately 5.5 by the end of the exponential phase, after which it steadily increased to 6.5 for B73 and 6.2 for *bm3* (Figure 6 A and B). During the stationary phase, the non-supplemented *bm3* fermentation exhibited a decrease in scattered light, dropping from 190.0 ± 8.6 a.u. at 15.5 h to 132.4 ± 19.8 a.u. at 36 h, while the Gfp fluorescence slightly increased from 140.7 ± 5.3 a.u. to 146.2 ± 8.4 a.u. at 15.5 h and 36 h, respectively (Figure 6 B). A similar trend was also noticed before for *bm3* material (Figure 4), likely due to plant biomass adhering to the walls of the plate.

With the addition of Celluclast®, a noticeable shift in growth dynamics occurred in both substrates. The initial growth phase remained indistinguishable from the non-supplemented fermentations, but while they reached their stationary phase, the Celluclast®-supplemented samples entered a second, less rapid exponential phase, similar to the results shown before (Figure 3). For B73 material, fungal performance reached the stationary phase after 22 h, with fluorescence and scattered light readings increasing to 153.0 ± 9.0 a.u. (+51 %) and 242.3 ± 12.6 a.u. (+78 %), respectively (Figure 6 A), comparable to the results shown before (Figure 3 A).

In Celluclast®-supplemented *bm3* fermentations the second growth phase extended to 27 h, reaching a Gfp fluorescence and scattered light reading of 203.7 ± 13.1 a.u. and 268.8 ± 9.7 a.u, respectively (Figure 6 B). This corresponds to a Gfp fluorescence and scattered light increase of 101 % and 97 %, respectively, compared to non-supplemented B73 material. Furthermore, the pH in Celluclast® supplemented fermentations diverged from the non-supplemented fermentations. While the pH of non-supplemented fermentations increased steadily to final values of 6.5 (B73) and 6.2 (*bm3*), the pH in Celluclast® supplemented fermentations remained lower, with final values of 5.7 for B73 and *bm3* (Figure 6 A and B).

To further understand the impact of Celluclast® on fungal performance, a comprehensive compositional analysis of the post-fermentation residue was performed

following the established method, to identify increased utilization of individual lignocellulosic components (Table 20).

Table 20: **Relative biomass composition [% of AIR] of the post-fermentation residue of B73 and *bm3* supplemented without ("-") and with ("+") Celluclast®.** The supplementation of Celluclast® is shown as average ± SD of two technical replicates for each individual plant, *i.e.* n = 8. Bold values indicate statistically significant differences between the material determined by a two-tailed students t-Test at *p*-value < 0.05.

Condition	Arabinose	Galactose	Glucose	Xylose	HC	CC	Lignin	Acetate	Starch	*U. maydis*	Total
B73 - Celluclast®	1.7 ± 0.2	0.9 ± 0.1	2.5 ± 0.6	18.2 ± 1.6	23.2 ± 2.2	32.2 ± 2.7	15.3 ± 0.7	4.4 ± 0.3	0.7 ± 0.0	12.6 ± 1.5	88.4 ± 1.8
B73 + Celluclast®	**1.2 ± 0.1**	**0.6 ± 0.1**	**0.3 ± 0.3**	**14.7 ± 1.0**	**16.9 ± 1.2**	**27.5 ± 1.8**	**16.6 ± 0.9**	4.5 ± 0.7	**0.8 ± 0.1**	**24.1 ± 1.9**	90.4 ± 2.1
bm3 - Celluclast®	1.2 ± 0.1	0.8 ± 0.1	2.2 ± 0.4	15.9 ± 0.8	20.2 ± 1.0	31.7 ± 1.9	12.8 ± 0.8	4.4 ± 0.5	0.7 ± 0.1	18.2 ± 2.1	87.9 ± 2.2
bm3 + Celluclast®	**0.9 ± 0.1**	**0.5 ± 0.1**	n.d.	**12.9 ± 1.1**	**13.6 ± 1.7**	**25.1 ± 2.3**	**15.3 ± 0.5**	4.6 ± 0.4	**0.9 ± 0.1**	**37.4 ± 5.7**	96.9 ± 5.1

n.d. = not detected; HC = sum of hemicellulosic monosaccharides; CC = crystalline cellulose; Total = Sum of plant and fungal components

The analysis of the post-fermentation solid residue confirmed the improved performance detected in the online monitoring. In Celluclast®-supplemented B73 material, the amount of fungal material almost doubled (+91 %) compared to the non-supplemented samples (Table 20). Furthermore, Celluclast®-supplementation significantly decreased the relative abundances of all lignocellulosic carbohydrate sources present in corn stover. The proportions of crystalline cellulose and total hemicellulose decreased by -14 % and -27 %, respectively (Table 20). All hemicellulosic monosaccharides were reduced, particularly Glc where only trace amounts were found in Celluclast®-supplemented samples.

In Celluclast®-supplemented *bm3* material, the amount of fungal material reached 37.4 %, representing a 105 % increase compared to non-supplemented *bm3* material and a 196 % increase compared to non-supplemented B73 material (Table 20). This increase in fungal biomass production attributable to Celluclast®-supplementation was higher in *bm3* compared to B73. Similarly, the post-fermentation residue composition showed bigger reductions in the proportions of crystalline cellulose (-21 %) and total hemicellulose (-33 %). This suggests that the altered lignin composition of *bm3* mediates enhanced substrate accessibility and/or hydrolytic activity of the enzymes present in the Celluclast® cocktail.

Unexpectedly, increments in the relative abundance of lignin and starch were detected for both genotypes (Table 20). A possible explanation is that these values reflect the relative decrease of the other components of the solid residue. Alternatively, it could be due to fungal components influencing the measurements of these particular components, primarily if large amounts of fungal biomass are present in the post-

fermentation residue. Fungal cell membranes contain sterols which may interfere with the spectrophotometric lignin quantification (Baloch et al., 1984). Similarly, *U. maydis* might accumulate glycogen during corn stover fermentation which is indiscernible from starch in the employed assay.

In summary, these data indicate that Celluclast® treatment during cultivation results in additional substrates derived from the lignocellulosic fraction in corn stover for *U. maydis* to continue growing upon consumption of the water-soluble carbohydrates. Combining the lignocellulolytic activity supplementation with the use of *bm3* corn stover results in a synergistic effect, allowing a threefold build-up of fungal biomass compared to the initial conditions set for B73.

4.1.3 Discussion

Corn stover is an abundant agricultural byproduct, and its potential use as a substrate for bioconversion is of major interest for the transition towards a bio-based economy. Within the last decade, the natural corn pathogen *U. maydis* emerged as a promising candidate for bioconversion processes (Feldbrügge et al., 2013; Regestein et al., 2018; Schlembach et al., 2020; Wierckx et al., 2021). However, its ability to utilize corn stover as sole carbon source was not studied so far. Thus, the first chapter of this thesis focused on establishing a small-scale cultivation platform using the BioLector® system to assess *U. maydis* growth performance on corn stover and to identify the carbohydrate sources being metabolized.

The combination of online monitoring and biochemical quantification accurately determines *U. maydis* growth performance on corn stover

The results of this chapter demonstrated that *U. maydis* is capable of utilizing corn stover as a sole carbon source, making an important step towards its application in lignocellulose bioconversion. While earlier studies showed its ability to metabolize purified cellulose and birch xylan (Geiser et al., 2013, 2016), maize bran (Couturier et al., 2012), or maize seedling tissue (Cano-Canchola et al., 2000), the results here extend those findings by confirming fungal growth on the complex, heterogeneous substrate corn stover.

The BioLector® system proved to be a reliable platform for monitoring *U. maydis* growth in the turbid, corn stover-containing media (Figure 1). Despite the inherent turbidity, scattered light and Gfp fluorescence signals closely aligned, validating their use as complementary growth indicators. The observed pH dynamics, with a drop during exponential growth and a sharp rise in stationary phase, further corroborated metabolic activity and match previously reported shifts towards less acidic metabolic pathways under nutrient limitation (Geiser et al., 2013; Terfrüchte et al., 2018).

However, while online monitoring effectively captures growth trends, it provides only relative measures. This limitation becomes particularly critical when assessing substrate utilization, as increasing fungal biomass may dilute residual lignocellulose, leading to an overestimation of degradation efficiency. To address this, absolute biomass quantification was achieved through GlcN analysis, serving as a fungal cell wall-specific marker due to its presence in chitin-like structures of *U. maydis* (Sánchez-

Arreguin et al., 2022) and absence in corn stover. This approach not only confirmed biomass production independently of online metrics but also enabled estimation of fungal contributions to the post-fermentation residues.

Although GlcN serves as a suitable proxy for fungal biomass, it has inherent limitations. Fungal cell wall composition can vary with growth conditions (Mitchell et al., 2006; Steudler & Bley, 2015), which could mean that the cell wall compositions differ between samples cultivated on Glc containing media and samples cultivated on corn stover containing media. This could potentially introduce slight inaccuracies in the quantification of fungal cell wall components and is likely reflected in the increase in Gal and Glc content at higher fungal biomass concentrations (Table 19 and Table 20). Despite this, the combination of online monitoring and biochemical quantification of fungal biomass presents a robust framework for evaluating *U. maydis* performance on complex lignocellulosic substrates with an unprecedented level of detail. The suitability of this platform as a fast-screening system was exemplified by testing the impact of different lignocellulosic pretreatments or corn stover substrates on *U. maydis* performance. Furthermore, it can be utilized to screen fungal strains (Robertz et al., 2024), or potentially to assess the effect of heterologous CAZyme expression on *U. maydis* performance and dissect enzymatic mechanisms in complex lignocellulosic substrates. As such, the platform serves as a valuable tool to scale-up the bioconversion process of corn stover by *U. maydis* from laboratory to fermenter scale.

U. maydis primarily utilizes water-soluble carbohydrates, but only limited lignocellulose

Corn stover contains two primary carbohydrate fractions that can be potentially utilized by *U. maydis*: water-soluble carbohydrates and structural polysaccharides (hemicellulose and cellulose) within the cell walls. The platform developed here enabled a detailed assessment of carbohydrate consumption by comparing the pre- and post-fermentation composition of the biomass, while also accounting for the contribution of fungal biomass (Table 15).

U. maydis efficiently metabolized the water-soluble carbohydrate fraction (Table 18), likely due to the direct accessibility of these sugars. Furthermore, the water-soluble carbohydrates are *U. maydis* primary carbohydrate source during plant infection (Billett & Burnett, 1978; Doehlemann et al., 2008). In nature, the fungus hijacks the plants

carbohydrate metabolism by converting source tissue into sink tissues and feeds on the imported water-soluble carbohydrates, especially Suc (Billett & Burnett, 1978; Doehlemann et al., 2008). Thus, its ability to efficiently uptake and metabolize Glc, Fru and Suc is expected.

U. maydis possesses several well-described transporters that enable the uptake of Glc, Fru or Suc, however in some cases, their expression during haploid, yeast-like growth is unclear. Among them is a high-affinity Suc transport (Srt1) (Wahl et al., 2010). Srt1 expression has only been observed during pathogenic growth, not under laboratory conditions using mono- or disaccharides, suggesting its regulation may be dependent on plant-derived signals (Wahl et al., 2010). Despite this, the complete deletion of Suc from the post-fermentation biomass (Table 14 and Table 18) suggests that *U. maydis* consumes this disaccharide *in vitro*. This may be mediated by invertases, which cleave Suc into Glc and Fru for subsequent uptake via the hexose transporter Hxt1 (Horst et al., 2008; Voll et al., 2011). However, expression of these invertases has similarly been reported only during plant infection, but not in haploid growth (Horst et al., 2008; Voll et al., 2011).

From the lignocellulose, *U. maydis* is capable of partially degrading xylan and minor parts of cellulose (Table 19). This minimal utilization of this abundant fraction fits to the previous finding that *U. maydis´* CAZymes cause minimal damage to lignocellulose *in planta* to avoid plant immune responses triggered by degradation products (Geiser et al., 2013). The degradation pattern is in line with previous studies that identified when *U. maydis* was grown on media containing freeze-dried corn leaf or stem material from seedlings, xylanase and cellulase were the predominant activities in *U. maydis* secretome (Cano-Canchola et al., 2000). Furthermore, growth on maize bran resulted in secretion of xylanases, arabinofuranosidases and oxido-reductases (Couturier et al., 2012). While both studies focused on the fungal secretome, the work presented here focused on the degradation of the complex substrate, an approach that was not done before for *U. maydis*. This strategy allows the identification of enzymatic activities under the applied conditions in greater detail. Furthermore, the developed monitoring platform coupled with the biochemical substrate analysis could aid in characterizing further enzymes and their activities in more detail. The slight, but significant reductions in Xyl and acetate across all corn stover substrates suggests xylan degradation and deacetylation, likely by secreted xylanases and acetylxylan esterases, respectively

(Geiser et al., 2013; X. Li et al., 2022; Mueller et al., 2008). Degradation of xylan is in line with results published before that showed that *U. maydis* wildtype isolate MB215 is able to partially degrade commercial birchwood xylan (Geiser et al., 2016).

Despite the presence of genes encoding for secreted arabinofuranosidases in *U. maydis* genome (Couturier et al., 2012; Doehlemann et al., 2008; Geiser et al., 2013; Lanver et al., 2014), no utilization of Ara was detected in any tested variety. This could be due to the complex lignocellulose architecture, where Ara*f* often serves as a crosslink between the xylan backbone and lignin, via glycosidic and ester bonds to FA dimers, respectively (Hatfield et al., 2017; Tryfona et al., 2023). While the glycosidic bond might be cut by arabinofuranosidases, the ester bond requires additional enzymatic activity. It could potentially be cleaved by a chlorogenic acid esterase that was identified in *U. maydis* secretome (Nieter et al., 2015). However, its reduced activity at pH 5.5 – 6.5 or temperatures below 30 °C may limit efficiency under the applied conditions (Nieter et al., 2015).

A slight reduction in cellulose indicates that *U. maydis* is expressing and secreting cellulases under the applied conditions, however, potentially their access to the cellulose is limited. Cellulose degradation is mediated by three enzymatic activities: endo-1,4-β-glucanases cleave internal bonds in the cellulose chain, exo-1,4-β-glucanases or cellobiohydrolases cleave cellobiose from either the reducing or the non-reducing end of a cellulose chain and β-glucosidases cleave cellobiose into monomers (Glass et al., 2013). The applied *U. maydis* strain overexpressed a β-glucosidase (umag_00446), which was previously shown to hydrolyze cellobiose (Geiser et al., 2016). Thus, it is unlikely that this reaction is the limiting factor. Furthermore, it was shown that this strain is able to release small amounts of Glc from the synthetic microcrystalline cellulose substrate Avicel (Geiser et al., 2016). Considering the dense lignocellulosic structure in corn stover, it is more likely that the endo- or exo-1,4-β-glucanases or cellobiohydrolases are either not able to penetrate and cleave the cellulose chains or they are not active under the tested fermentation conditions.

In summary, the primary carbohydrate source for *U. maydis* are water-soluble carbohydrates, while the lignocellulose of corn stover remains underutilized. The expression of some genes potentially involved in water-soluble carbohydrate

consumption and lignocellulose degradation was not shown during haploid growth. Thus, a detailed profiling of the expressed and secreted enzymes would help to clarify, which specific *U. maydis* enzymes are expressed during the fermentation and characterize potential synergistic hydrolytic activities, especially focusing on xylanase and cellulase activities. Only a handful of *U. maydis´* CAZymes are characterized in detail so far. CAZyme knock-out or overexpressing strains could be developed and tested on the complex corn stover substrate. Within the last two decades, especially since the genome was published (Kämper et al., 2006), the genome editing tools for *U. maydis* were continuously expanded (Wierckx et al., 2021). Targeted gene deletion is possible via Golden Gate cloning (Terfrüchte et al., 2014). Alternatively, promotor exchange via homologous recombination, e.g. to the endogenous promoter P_{oma}, for the creation of overexpressing strains is a suitable method to test the catalytic potential of individual enzymes (Geiser et al., 2016). This was done before for the strain used in this work (overexpressing an endogenous β-glucanase under control of P_{oma}) and other strains overexpressing endogenous xylanases or endoglucanases, and their catalytic potential on cellulose, xylan or cellobiose was evaluated (Geiser et al., 2016). With the platform developed in this work, similar strain monitoring studies could be done and the substrates expanded to highly complex substrates, including stover from corn or other grasses.

U. maydis performance was significantly increased by enzymatic pretreatment of corn stover with modified lignin composition

While *U. maydis* demonstrated efficient and extensive utilization of water-soluble carbohydrates in corn stover, the lignocellulosic fraction remained largely underutilized. This observation underscores limitations in the fungus´ natural capacity to degrade the lignocellulosic fraction and highlights the potential for further strategies aimed at enhancing lignocellulose conversion efficiency. The online fermentation monitoring of the BioLector® system enabled the rapid screening of six strategies designed to improve fugal performance on corn stover, specifically targeting the recalcitrant lignocellulose.

One strategy was the use of maize mutants with altered lignocellulosic architecture. The tested corn varieties were: *cal1*, exhibiting increased MLG content; *bm1*, exhibiting reduced lignin content; and *bm3*, exhibiting altered lignin composition (Halpin et al.,

1998; Kraemer et al., 2021; Vignols et al., 1995). All three cell wall alterations were previously shown to increase saccharification efficiency of the lignocellulose (Barrière, 2017; Christensen & Rasmussen, 2019; S. Wang et al., 2023). Thus, these varieties were tested as substrate for *U. maydis*, to explore if the alterations in lignocellulose enhance utilization of this fraction and enhance fungal performance.

The pre- and post-fermentation biomasses of *cal1* corn stover did not show a difference in hemicellulosic Glc compared to B73 material, consequently fungal performance was also not improved on *cal1* corn stover (Table 15 and Table 19). Online monitoring revealed that *U. maydis* performed better on biomass from *bm* mutants, particularly *bm3*. However, further analysis indicated that this improvement was mostly due to increased levels of water-soluble carbohydrates rather than improved degradation of the lignocellulosic, as only minor lignocellulosic utilization differences were detected compared to the reference variety (Table 18 and Table 19). The slight increased utilization in *bm3* lignocellulose could also be attributed to the changed S:G monolignol ratio, which influences crosslinking of lignin to cellulose or xylan and overall cell wall architecture and increases the saccharification yield (Barrière, 2017; Vignols et al., 1995; S. Wang et al., 2023).

The other five tested strategies were lignocellulosic pretreatments. Pretreating the biomass is a well-established step in bioconversion workflows, primarily aimed at disrupting lignocellulose structure to improve enzymatic accessibility and release of fermentable carbohydrates (Da Silva et al., 2010; Kumar et al., 2020; Leroy et al., 2021; Lorenci Woiciechowski et al., 2020; Vu et al., 2020). Here, several strategies were evaluated for their ability to enhance *U. maydis* growth on B73 corn stover (Figure 3). These included alkaline treatment, acid hydrolysis and microwave irradiation. However, all chemical treatments resulted in reduced fungal performance, while the microwave irradiation only slightly increased fungal performance (Figure 3). The negative impact of NaOH and H_2SO_4 pretreatments is noteworthy, particularly since these treatments are widely reported to enhance lignocellulosic saccharification, i.e. the release of fermentable carbohydrates from the lignocellulose after digestion with CAZymes (Bichot et al., 2018; Y. Chen et al., 2013; Duguid et al., 2009; S. Wang et al., 2023). However, they also introduce potential inhibitory factors, e.g. by dissociating water-soluble carbohydrates (Akter et al., 2020). Despite pH neutralization and buffering to pH 6 with MES, a buffer widely used for *U. maydis* cultivation (Geiser et

al., 2014; Grebe et al., 2024; Richter et al., 2024; Volkmar et al., 2023), residual salts and degradation by-products such as furfural and hydroxymethylfurfural, known glycolysis inhibitors, may have negatively affected fungal growth or enzymatic activity (Akter et al., 2020; Bichot et al., 2018; Jablonowski et al., 2022; Jilani & Olson, 2023; Sharma et al., 2019). The observed improvement in fungal performance with reduced concentrations of NaOH and H_2SO_4 supports the hypothesis that both strategies exhibit inhibitory effects on fungal performance under the tested conditions. TFA pretreatment, which benefits from its volatility and does not require neutralization, also failed to improve fungal performance (Figure 3). Although TFA is effective in hydrolyzing hemicellulose into monosaccharides (Foster et al., 2010b), it may still generate inhibitory compounds during hydrolysis. These findings suggest that, despite theoretical improvements in lignocellulose accessibility, the tested chemical pretreatments were suboptimal for *U. maydis* fermentation. Future work could explore whether additional steps, such as desalting, detoxification or closely monitored pH controlling, might mitigate the negative effects observed here. Moreover, a comprehensive metabolite profiling of hydrolysates, aiming especially at toxic degradation products like furfurals, would help to clarify if substrate toxicity is the primary bottleneck.

In contrast to the chemical pretreatments, short-term microwave treatment led to a modest improvement in fungal growth compared to autoclaving (Figure 3). This aligns with previous reports indicating that microwave treatment can enhance enzymatic access by disrupting lignocellulose via selective heating of polar bonds (Jablonowski et al., 2022; H. Ma et al., 2009; Saleem et al., 2015; Xu, 2015). While the observed effect was relatively small, it nonetheless supports the broader conclusion that physical pretreatments which enhance substrate accessibility, without introducing toxic by-products, may offer more compatible strategies for improving *U. maydis* bioconversion performance.

By far the greatest improvement in *U. maydis* performance was achieved by the addition of Celluclast® to the fermentation, resulting in a 91 % performance increase on B73 material (Figure 6). By combining the *bm3* mutant with Celluclast®, fungal biomass production was enhanced by +196 % compared to the B73 reference material. The increased utilization of the lignocellulose in B73 and *bm3* material was most likely due to a complementary effect of *U. maydis* intrinsic enzymatic repertoire

and Celluclast®. As introduced before, to effectively degrade lignocellulose, multiple CAZymes must act in concert. *U. maydis* is superior in xylan degradation and secretes superior quantities of auxiliary enzymes acting on lignin depolymerization, while *T. reesei* (the production organism of Celluclast®) is a very efficient cellulose degrader (Couturier et al., 2012; King et al., 2011). Similar to the results obtained here, it was shown before that the combination of *T. reesei* and *U. maydis* secretomes shows synergistic effects for the degradation of wheat straw (Couturier et al., 2012). In the same study, it was hypothesized that *U. maydis* hemicellulases, especially the arabinofuranosidases, depolymerize wheat arabinoxylan, which facilitates access to cellulose for *T. reesei* cellulases, thus resulting in a higher saccharification yield of wheat straw (Couturier et al., 2012). For the data presented here, the significantly increased fungal performance on *bm3* with Celluclast® addition, is due to multiple synergistic effects. First, the *bm3* material is more susceptible to degradation by Celluclast®, due to the altered lignin composition, which enhances access to cellulose (Barrière, 2017; Vignols et al., 1995; S. Wang et al., 2023). And second, the *bm3* material contains more water-soluble carbohydrates compared to B73, which facilitate fungal growth.

Taken together, the results of this chapter underline the central role of water-soluble carbohydrates in the bioconversion of corn stover by *U. maydis*. Future work could explore the effect of heterologous CAZyme secretion by *U. maydis*, which would omit the need for enzymatic supplementation. Potential enzymes could be cellulases from *T. reesei* or other effective cellulose degraders, like *Aspergillus niger*. While this approach requires *U. maydis* strain engineering and potentially process optimization, the water-soluble carbohydrates in corn stover are easily and directly accessible for *U. maydis* and thus, an interesting target to immediately increase fungal performance by selecting or engineering corn varieties with elevated water-soluble carbohydrate levels.

4.2 Chapter 2: Variability of water-soluble carbohydrates in corn stover

4.2.1 Background

Synthesis and accumulation of water-soluble carbohydrates is strongly driven by photosynthetic activity, which in turn is dependent on the circadian rhythm (Liang et al., 2019). Carbohydrate storage in corn stems functions as a long-term reserve that buffers against suboptimal growth conditions during the plant´s life (Cazetta & Revoredo, 2018; Sekhon et al., 2016; Setter et al., 2001; Slewinski, 2012). This storage does not directly compete with other carbohydrate sinks, since it primarily stores surplus carbohydrates (Slewinski, 2012). However, the identity and demand of sink tissues vary across the maize life cycle, and little is known about the source-sink dynamics in senescent field grown plants (Liang et al., 2019). During early growth stages, the expanding stems serve as the primary carbohydrate sinks, whereas seeds become the dominant carbohydrate sink after the onset of the reproductive phase (Liang et al., 2019). Concomitant with this shift in sink priority, a decline in photosynthetic carbon assimilation in source tissues was observed in various maize hybrids (Liang et al., 2019). In consequence, it is possible that stem stored carbohydrates may be mobilized to support seed filling, helping to offset reduced carbohydrate production in the leaves. A similar physiological role was previously identified for the water-soluble carbohydrates stored in rice stems (D. R. Wang et al., 2017). However, in various maize hybrids it was identified that the total water-soluble carbohydrate content in stems remains relatively constant throughout one day in the reproductive phase, indicating that they do not contribute to seed filling (Liang et al., 2019). If this applies to other corn varieties and whether the individual carbohydrates Glc, Suc and Fru underly diurnal fluctuations in other growth phases is not known. Thus, the first objective of this chapter is to investigate how water-soluble carbohydrate content in corn stover is influenced by the circadian rhythm. By focusing on fluctuations of these carbohydrates throughout one harvest day, it will be identified if the water-soluble carbohydrate content in corn stover can be maximized by optimizing the harvest time.

The second objective of this chapter is to identify genomic regions in corn that influence the water-soluble carbohydrate content. This will be achieved by assessing the natural variability of water-soluble carbohydrate content in corn stover across a natural

variation panel of European maize lines. Based on these results, a genome-wide association study (GWAS) will be conducted for water-soluble carbohydrate-related traits. This GWAS could identify genomic regions associated with traits by linking the observed phenotypic variation with the diverse genetic background of the natural variation panel. The identified genomic regions will be analyzed in closer detail, and three candidate genes will be picked for further analysis.

4.2.2 Results

Fluctuation of water-soluble carbohydrate content in corn stover throughout the day

To identify, whether the carbohydrate storage in senescent stems underlies diurnal fluctuations, and if it is possible to predict the optimal harvest time for maximized carbohydrate content, material of the reference variety B73 was grown in the botanical garden (HHU Düsseldorf) in the year 2023 and 2024. Furthermore, *bm3* plants were grown under the same conditions, to additionally examine if the increased water-soluble carbohydrate content detected in the greenhouse-grown plants used in the previous chapter (Table 19) is reproducible in field-grown plants. Both genotypes were harvested on the same day after 5-month growth (May to October), at three and five timepoints in 2023 and 2024, respectively. The water-soluble carbohydrates Glc, Fru, Suc were quantified in the internode below the first ear (Figure 7).

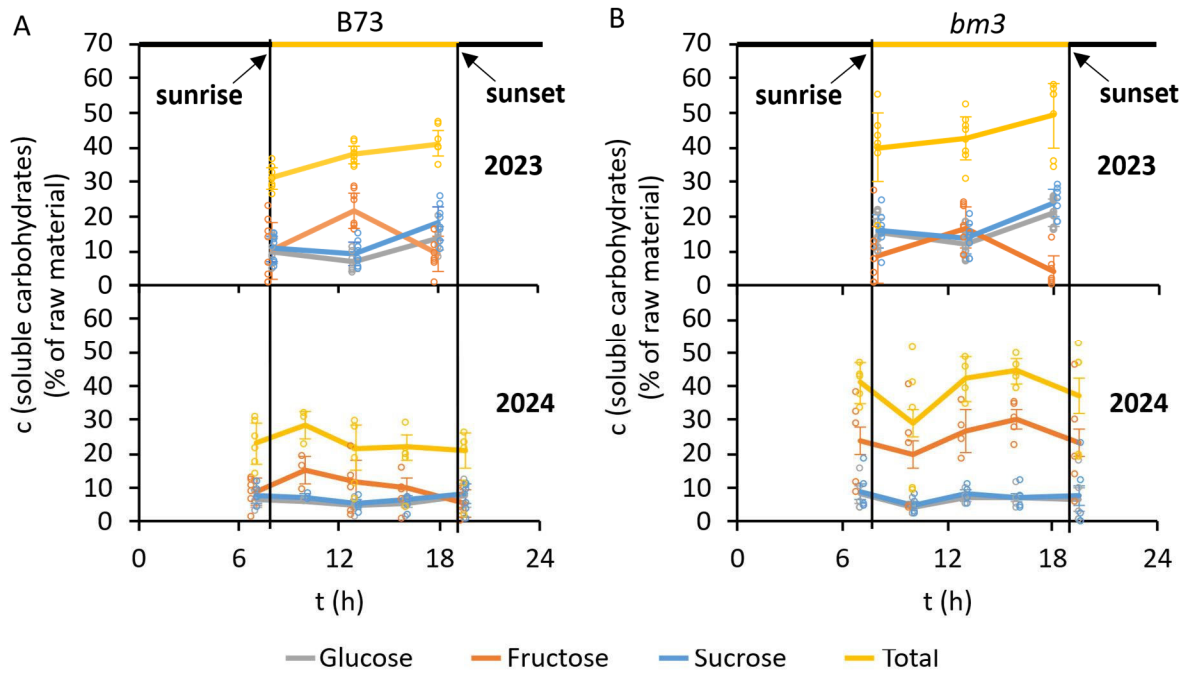

Figure 7: **Water-soluble carbohydrate content in the stems of B73 (A) and *bm3* (B) plants harvested at different timepoints throughout one day.** Data are shown as AVG ± SD (lines) as well as the individual datapoints for each individual plant (points) for glucose (grey), fructose (orange), sucrose (blue) and total water-soluble carbohydrate content (yellow) at different timepoints (t) within one day (h). In 2023, n = 8 per timepoint were harvested for B73 and bm3 (except *bm3* at 6 pm: n = 7). In 2024, 6 plants (n = 6) were harvested of B73 at 7 am and 7:30 pm, at 10 am: n = 3, at 1 pm and 4 pm: n = 5. In the case of *bm3*, n = 5 for all timepoints except at 1 pm (n = 4). Statistical analyses of these data are shown in Table 21.

In both years 2023 and 2024, diurnal fluctuations in water-soluble carbohydrate content were observed in B73 and *bm3* corn stover, with *bm3* exhibiting significantly higher total water-soluble carbohydrate content in the morning than B73 (Table 21), indicating that the results of the previous chapter 4.1 are reproducible in field-grown plants. Furthermore, the Glc and Suc content of *bm3* plants of the year 2023 was significantly higher compared to B73 throughout the whole day (Table 21).

In 2023, three harvest timepoints (8 am, 1 pm, and 6 pm) were selected, revealing an increase in total water-soluble carbohydrates throughout the day in both genotypes. In B73 (Figure 7 A), the content rose from 31.1 ± 3.0 % at 8 am to 41.2 ± 3.8 % at 6 pm, with Glc and Suc following similar trends. Both carbohydrates showed a slight dip from 8 am to 1 pm (Glc: 10.0 ± 3.8 % to 7.1 ± 2.8 %; Suc: 10.9 ± 3.7 % to 9.1 ± 3.3 %) before increasing significantly towards 6 pm (Glc: 13.8 ± 3.4 %; Suc: 18.1 ± 4.9 %) (Table 21). Fru, however, exhibited a distinct pattern, peaking at 1 pm (21.6 ± 5.1 %) before declining towards the evening (9.3 ± 4.9 %). The water-soluble carbohydrates in *bm3* followed a similar trend (Figure 7 B). The total water-soluble carbohydrate content increased from 40.0 ± 9.9 % at 8 am to 49.3 ± 9.3 % at 6 pm, with Glc and Suc reaching their highest levels in the evening (Glc: 21.2 ± 3.8 %; Suc: 24.1 ± 4.0 %). Fru peaked at 1 pm (16.9 ± 5.8 %) before decreasing sharply to 6 pm (4.0 ± 4.5 %) (Table 21).

Table 21: **Water-soluble carbohydrate content [wt%] and composition [%] of B73 and *bm3* stems harvested at different timepoints.** Data are shown as the average ± SD of the plants (n indicated in column "plants"). "wt%" refers to the weight percentage of the dried raw material and "%" refers to the relative composition of the total soluble carbohydrate fraction. For the year 2023, significant differences of one carbohydrate among the harvest timepoints are indicated by the letters "a" and "b", determined by one-way ANOVA followed by Tukey-HSD test ($p < 0.05$). In 2024, no significant differences were identified with the same tests. Bold values indicate statistically significant differences between B73 and *bm3* for the year 2023 or 2024, determined with a two-tailed Students T-Test ($p < 0.05$).

	Time	Glucose [wt%]	Fructose [wt%]	Sucrose [wt%]	Total [wt%]	Glucose [%]	Fructose [%]	Sucrose [%]	Plants
B73 2023	8 AM	10.0 ± 3.8**ab**	10.2 ± 8.1 **a**	10.9 ± 3.7 **a**	31.1 ± 3.0 **a**	32.5 ± 13.0 **a**	32.0 ± 25.3 **a**	35.5 ± 13.2 **ab**	8
	1 PM	7.1 ± 2.8 **a**	21.6 ± 5.1 **b**	9.1 ± 3.3 **a**	37.8 ± 2.7 **b**	18.7 ± 6.6 **b**	57.6 ± 14.4 **b**	23.7 ± 7.8 **a**	8
	6 PM	13.8 ± 3.4 **b**	9.3 ± 4.9 **a**	18.1 ± 4.9 **b**	41.2 ± 3.8 **b**	33.1 ± 5.7 **a**	23.6 ± 13.8 **a**	43.3 ± 8.4 **b**	8
bm3 2023	8 AM	**15.3 ± 4.2 a**	8.9 ± 8.2**ab**	**15.8 ± 4.8 a**	**40.0 ± 9.9 a**	40.1 ± 11.5 **a**	20.0 ± 14.9 **a**	39.8 ± 7.9 **ab**	8
	1 PM	**12.0 ± 3.6 a**	16.9 ± 5.8 **b**	**13.6 ± 4.3 a**	42.5 ± 6.3 **a**	**27.9 ± 6.2 b**	**40.2 ± 14.2 b**	31.9 ± 8.2 **a**	8
	6 PM	**21.2 ± 3.8 b**	4.0 ± 4.5 **a**	**24.1 ± 4.0 b**	49.3 ± 9.3 **a**	**43.3 ± 3.6 a**	**7.3 ± 7.6 a**	49.4 ± 4.4 **b**	7
B73 2024	7 AM	6.7 ± 2.7	7.7 ± 2.3	8.6 ± 4.0	23.0 ± 6.0	29.1 ± 8.8	33.9 ± 8.9	37.0 ± 17.4	6
	10 AM	6.1 ± 0.3	7.2 ± 0.7	15.1 ± 4.2	28.4 ± 4.2	21.9 ± 3.7	26.0 ± 4.5	52.1 ± 8.0	3
	1 PM	4.7 ± 1.2	5.3 ± 1.3	11.7 ± 6.3	21.7 ± 6.8	24.1 ± 10.0	26.6 ± 8.2	49.2 ± 18.0	5
	4 PM	5.1 ± 0.9	6.5 ± 0.9	10.1 ± 2.9	21.8 ± 3.7	23.7 ± 3.6	30.2 ± 4.3	46.0 ± 7.1	5
	7:30 PM	7.6 ± 3.3	8.0 ± 2.9	5.4 ± 4.0	21.0 ± 5.1	35.1 ± 11.0	37.4 ± 8.0	27.5 ± 18.7	6
bm3 2024	7 AM	8.1 ± 4.6	**8.8 ± 5.4**	24.1 ± 11.7	**41.1 ± 4.8**	20.3 ± 11.7	22.0 ± 13.3	57.7 ± 24.9	5
	10 AM	4.4 ± 1.7	5.0 ± 2.1	19.9 ± 14.0	29.2 ± 16.9	18.3 ± 6.0	21.1 ± 7.8	60.7 ± 13.6	5
	1 PM	7.0 ± 1.9	**8.4 ± 2.2**	26.8 ± 6.3	**42.2 ± 5.3**	16.9 ± 4.8	20.0 ± 5.6	63.1 ± 10.4	4
	4 PM	6.9 ± 2.6	**7.3 ± 2.9**	30.5 ± 4.7	**44.7 ± 3.5**	**15.4 ± 5.2**	**16.1 ± 6.0**	**68.5 ± 11.1**	5
	7:30 PM	6.4 ± 6.8	**7.6 ± 9.0**	23.2 ± 14.0	37.2 ± 14.5	15.2 ± 13.4	17.0 ± 18.3	67.7 ± 31.6	5

In 2024, the harvest time frame was expanded to include early morning (before sunrise) and evening (after sunset). Unlike in the previous year, B73 did not show an evening increase (Figure 7 A). The total water-soluble carbohydrate content started at 23.0 ± 6.0 % at 7 am, peaked at 10 am (28.4 ± 4.2 %), and then slightly decreased to 21.0 ± 5.1 % by 7:30 pm (Table 21). Glc and Suc followed the same trends as in 2023 but with less pronounced changes, decreasing from 7 am to 1 pm (Glc: 6.7 ± 2.7 % to 4.7 ± 1.2 %; Suc: 7.7 ± 2.3 % to 5.3 ± 1.3 %) before slightly increasing again towards the evening (Glc: 7.6 ± 3.3 %; Suc: 8.0 ± 2.9 %). Fru peaked at 10 am (15.1 ± 4.2 %, n = 3) before gradually declining to 5.4 ± 4.0 % at 7:30 pm (Table 21).

For *bm3* in 2024, fluctuations in total water-soluble carbohydrate content were less pronounced compared to 2023 (Figure 7 B), however the total water-soluble carbohydrate content was higher than in B73 in plants harvested in the morning, noon and afternoon (Table 21). The total water-soluble carbohydrate content in *bm3*

remained relatively stable throughout the day, from 41.1 ± 4.8 % at 7 am to 42.2 ± 5.3 % at 1 pm and 37.2 ± 14.5 % at 7:30 pm. Interestingly, the 10 am harvest exhibited significant plant-to-plant variation, ranging from 9.3 % to 51.6 %. Unlike in 2023, Glc and Suc levels remained constant throughout the day without statistically significant changes. Furthermore, Fru was consistently the dominant water-soluble carbohydrate, comprising around 50 % of the total content. It increased from 24.1 ± 11.7 % at 7 am to 30.5 ± 4.7 % at 4 pm before declining again to 23.2 ± 14.0 %.

Since the field was in the botanical garden, the use of fungicides was not possible. Thus, in 2023, roughly a third of the *bm3* plants was infected by *U. maydis*, while B73 infection was minimal, which is in line with the higher susceptibility of *bm3* for *U. maydis* infection detected before (Tanaka et al., 2014). In 2024, possibly due to the very wet months May and June (Table 30), roughly two thirds of the plants were infected regardless of the genotype, thus, influences of this biotic stress on the water-soluble carbohydrate metabolism of both genotypes cannot be excluded.

Despite this, the results of this section highlight two main findings. First, the water-soluble carbohydrate content in the stems of senescent corn plants is variable throughout one day, with especially the Fru content exhibiting the highest variations. Since the results of 2023 and 2024 are not consistent regarding the optimal harvest time for maximized water-soluble carbohydrate content, future work is necessary to clarify this relationship. The second highlight is that the genotype-specific increased water-soluble carbohydrate content of *bm3* observed in greenhouse-grown plants was reproducible in field experiments, despite the additional biotic and abiotic factors influencing plant metabolism.

Variability of water-soluble carbohydrate content across a natural variation panel of European maize lines

In the first chapter of this work, three greenhouse grown varieties (B73, *bm1*, *bm3*) exhibited significant differences in their water-soluble carbohydrate content (Table 18). Notably, the differences between B73 and *bm3* were reproduced in field experiments across two harvest seasons (Table 21). Building on these genotypic differences, the variability of the water-soluble carbohydrates Glc, Fru and Suc was examined across a broader range of maize varieties to evaluate their suitability for genome-wide association studies.

To do so, a natural variation panel comprising 289 corn varieties was cultivated in a field in southern Germany in the year 2021. Plants were harvested based on maturity and water-soluble carbohydrates were quantified in the internode below the first ear. While most varieties were harvested in groups of three plants grown closely together, a few varieties were grown and harvested in more replicates spread out across the field. This design allowed assessment of positional effects on the phenotype and determination of whether inter-genotypic variation within the population exceeded intra-genotypic variation, which would make the dataset suitable for a genome-wide association study (GWAS). The genotypes harvested at multiple locations across the field are: F268, F10, H49 (n = 6); B73 (n = 13); A619 (n = 14); F7, FAP1360A (n = 15) (Table 22 and Figure 8).

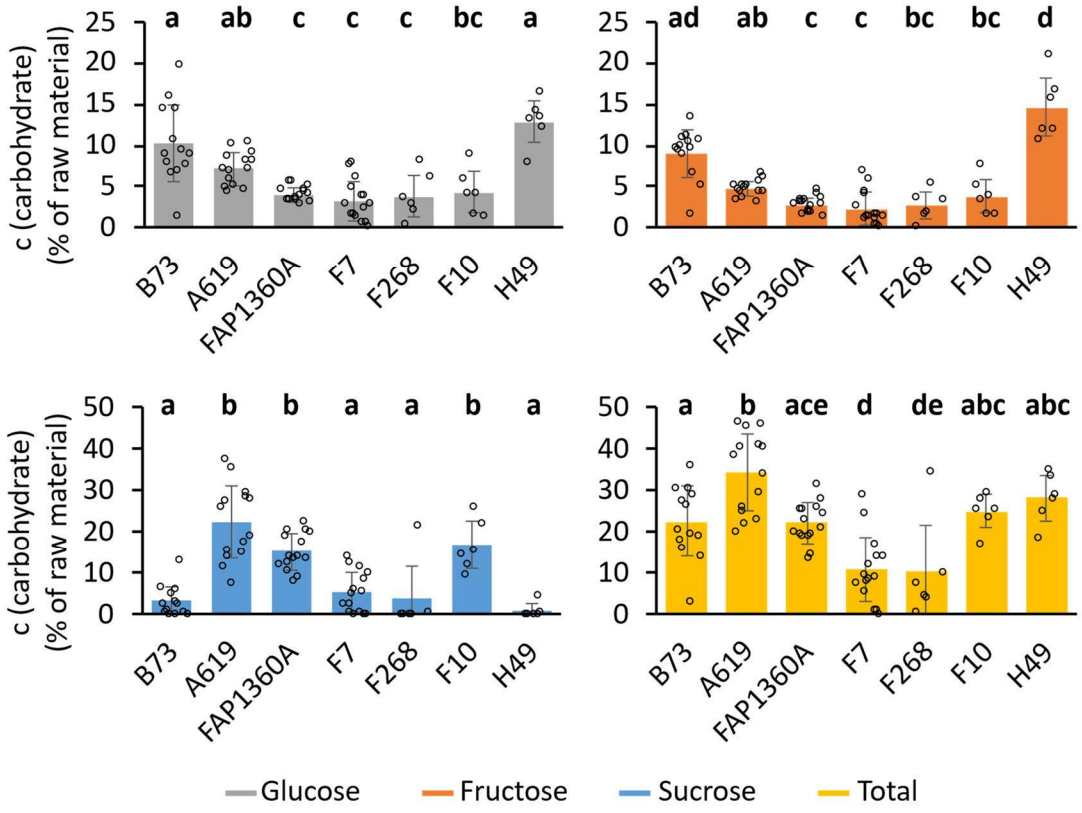

Figure 8: **Soluble carbohydrate composition (% of raw material) of 7 varieties with more than 3 biological replicates.** Data are shown as AVG ± SD and individual measurements of n = 6 for F268, F10, H49; n = 13 for B73; n = 14 for A619; n = 15 for F7 and FAP1360A. Depicted is the glucose (grey), fructose (orange), sucrose (blue) and total water-soluble carbohydrate content (yellow). Letters above the bars indicate statistically significant differences within one sugar among the genotypes, determined by a Kruskal-Wallis test followed by Dunn´s multiple comparison with a corrected alpha according to Bonferroni set to 0.002.

Among the varieties harvested in multiple replicates across the field, distinct differences in water-soluble carbohydrate compositions were detected (Table 22 and Figure 8). Of these seven varieties, F268 and F7 had the lowest total water-soluble sugar content, with an average of 10.8 % and 10.2 %, respectively, and their average Glc, Fru and Suc contents were consistently below the populations average (Table 22). In contrast, A619 and H49 had the highest total water-soluble carbohydrate contents, at 34.3 % and 28.3 %, respectively, with ranges of 27.0 % and 16.5 %, respectively (Figure 8). Interestingly, A619 was particularly high in Suc content (22.3 %, range 30.4 %), while H49 contained predominantly Glc (12.9 %, range 8.6 %) and Fru (14.6 %, range 10.2 %) (Table 22). F10 and FAP1360A showed a comparable composition to A619, with comparable Suc levels, but less Glc and Fru (Figure 8). And B73 and H49 exhibited low Suc levels but high Glc and Fru contents. Notably, the

water-soluble carbohydrate composition of B73 was very similar to the greenhouse B73 plants analyzed in the previous chapter (Table 14).

Table 22: **Descriptive statistics for the natural variation panel.** Glucose (Glc), fructose (Fru), sucrose (Suc) and total water-soluble carbohydrate content (Total) in the natural variation panel. Replicated varieties are shown separately. n indicates the number of individual plants per genotype.

	Trait	Minimum (wt%)	Average (wt%)	Maximum (wt%)	Standard deviation (wt%)	Range (wt%)
Natural variation panel 289 varieties	Glc	0.0	7.1	19.4	4.0	19.4
	Fru	0.1	5.9	16.9	3.6	16.8
	Suc	0.0	12.7	37.6	8.9	37.6
	Total	2.0	25.7	52.4	10.7	50.4
B73 n = 13	Glc	1.3	10.2	19.8	4.6	18.5
	Fru	1.6	9.1	13.5	2.9	11.9
	Suc	0.0	3.1	13.1	3.6	13.1
	Total	2.9	22.4	36.0	8.5	33.1
A619 n = 14	Glc	4.4	7.2	10.4	2.0	6.0
	Fru	3.1	4.7	6.5	1.0	3.4
	Suc	7.3	22.3	37.7	9.0	30.4
	Total	19.8	34.3	46.8	9.4	27.0
FAP1360A n = 15	Glc	3.0	4.1	5.7	0.9	2.7
	Fru	1.4	2.8	4.5	0.9	3.1
	Suc	7.8	15.2	22.5	4.4	14.7
	Total	13.5	22.1	31.7	4.8	18.2
F7 n = 15	Glc	0.0	3.2	7.9	2.4	7.9
	Fru	0.0	2.3	7.0	2.0	7.0
	Suc	0.0	5.3	14.3	4.8	14.3
	Total	0.0	10.8	28.9	7.9	28.9
F268 n = 6	Glc	0.4	3.8	8.0	2.6	7.6
	Fru	0.2	2.7	5.4	1.7	5.2
	Suc	0.0	3.7	21.3	7.9	21.3
	Total	0.6	10.2	34.8	11.3	34.2
F10 n = 6	Glc	1.5	4.4	8.8	2.5	7.3
	Fru	1.6	3.9	7.6	2.1	6.0
	Suc	9.6	16.7	26.2	5.8	16.6
	Total	17.1	24.9	29.5	4.0	12.4
H49 n = 6	Glc	7.9	12.9	16.5	2.6	8.6
	Fru	10.7	14.6	20.9	3.5	10.2
	Suc	0.0	0.8	4.6	1.7	4.6
	Total	18.5	28.3	35.0	5.5	16.5

For the entire population (289 varieties), Glc in the corn stem was on average 7.1 % with a wide range of 19.4 % (Table 22). The Fru content was similarly distributed across the entire population with an average of 5.9 % and a range of 16.8 % (Table 22). Both monosaccharides correlated with $r = 0.87$ across all varieties (Table 23). The Suc content was even more variable with an average of 12.7 % and a range of 37.6 % (Table 22). Furthermore, the Suc content weakly correlated to the other water-soluble carbohydrates (Table 23). Finally, the total water-soluble carbohydrate content across the entire population was on average 25.7 %, with a wide range of 50.4 % (Table 22). As Suc is the most abundant water-soluble carbohydrate in most analyzed varieties,

the correlation to the total water-soluble carbohydrate content is higher (0.74) than for Glc (0.57) and Fru (0.53) (Table 23).

Table 23: **Pearson correlations between the individual water-soluble carbohydrates in the natural variation panel.**

	Glucose	Fructose	Sucrose
Fructose	0.87		
Sucrose	-0.12	-0.14	
Total	0.57	0.53	0.74

In summary, these results show that the water-soluble carbohydrate content and composition are a highly variable trait in corn stover. Both are influenced by the plants' position in the field as can be seen intra-genotypic variability. However, the inter-genotypic variability across the entire natural variation population exceeds the intra-genotypic variation. Thus, this population is suitable for GWAS. Interestingly, while most corn varieties seem to accumulate Suc as main water-soluble carbohydrate in their stems, some varieties, such as H49 or B73 predominantly accumulate Glc and Fru, which also potentially explains differences in water-soluble carbohydrate contents in literature reported before (S. F. Chen et al., 2007; Setter & Flannigan, 1986; Slewinski, 2012).

Correlation of *U. maydis* performance to water-soluble carbohydrate content in corn stover

The water-soluble carbohydrate content is highly variable across the natural variation of corn, which in consequence could result in highly variable fungal performances across different corn varieties. To assess this relationship between *U. maydis* performance and the abundance of water-soluble carbohydrates, specific corn varieties were selected from the natural variation panel for fermentation experiments. For each individual water-soluble carbohydrate (Glc, Suc, Fru) and the total water-soluble carbohydrate traits, the three lines from the natural variation panel exhibiting the highest and lowest values were picked. In addition, as the lignocellulosic biomass exhibits substantial differences across these varieties, Xyl, total hemicellulose, crystalline cellulose and lignin traits were also selected (Appendix Table 31). The lignocellulosic composition data of the natural variation panel were kindly provided by Dr. Shaogan Wang (Institute for Plant Cell Biology and Biotechnology, HHU Düsseldorf), as they were quantified within the scope of the "Cornwall" project (BMBF;

031B0193A). *U. maydis* performance was monitored on the resulting 43 selected corn varieties. The fungal performance was evaluated based on the detected Gfp fluorescence, as it could not be excluded that the different biomass compositions of the corn varieties differentially influence the scattered light readings (Figure 9).

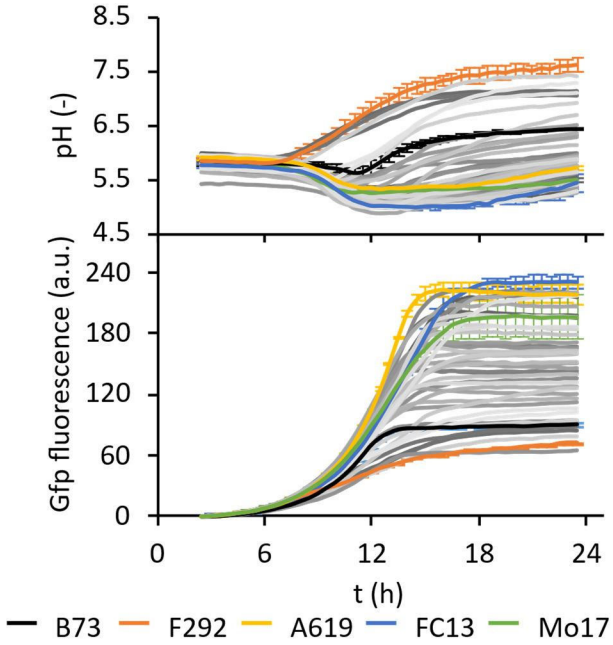

Figure 9: ***Ustilago maydis* growth performance on 43 different corn varieties.** The data are shown as the average of 3 plants of 41 corn varieties and 2 plants of 2 corn varieties for Gfp fluorescence in arbitrary units (a.u.) and pH over time (t) in hours (h). The material of the reference variety originated from one plant and was included as an internal control to assess the reproducibility of the different fermentations. Highlighted are the reference variety B73 (black), a low performing variety F292 (orange) and the best performing varieties A619 (yellow) and FC13 (blue) with their standard deviations.

U. maydis fermenting the reference variety B73, which was used as a control to ensure consistency of the fermentation setups, reached the stationary phase after 14 h with a Gfp fluorescence of 86.0 ± 2.0 a.u. (Figure 9). The least growth was detected on variety (F292) with a maximum Gfp fluorescence of 71.6 ± 0.6 a.u. by the end of the experiment. The pH increased from 5.8 at the start to 7.6 by the end, the highest across all tested varieties. Interestingly, the exponential growth phase ended after 16 h (59.9 ± 1.4 a.u.), however, the cultures continued into another less steep growth phase until the end of the experiment. This variety exhibited very low water-soluble sugar content, but the amount of hemicellulosic fraction and especially Xyl was among the highest across the whole sample set, which could serve as a carbohydrate source for *U. maydis* (Appendix Table 31). As identified in the previous chapter the *U. maydis*

strain used in this work is capable of digesting fractions of the arabinoxylan in corn stover. Thus, it is possible that the second, less rapid growth phase might be caused by *U. maydis* digesting the lignocellulosic fraction and especially the arabinoxylan of this variety.

The fastest fungal growth was observed with the variety A619 with a Gfp fluorescence of 219.5 ± 6.5 a.u., after 15 h and a minimal pH of 5.3 after 12 h. One variety (FC13) reached a slightly higher maximum Gfp fluorescence and a slightly lower pH (5.0), but the growth on this variety was slower (227.5 ± 3.1 a.u., 18 h) (Figure 9). Both of these varieties are among the highest in water-soluble carbohydrate content, with the highest amounts of Suc (Appendix Table 31). FC13 contains more total water-soluble carbohydrates than A619, which causes the increased Gfp fluorescence, however, potentially its slight increase in hexoses (27.5 %) compared to A619 (24.0 %) might result in slower growth due to metabolic shifts in *U. maydis* (Appendix Table 31).

Fermenting Mo17, a variety with high Glc and Fru, but low Suc levels (Appendix Table 31), *U. maydis* exhibited slightly reduced performance compared to A619 and FC13, achieving a stationary phase Gfp fluorescence of 192.1 ± 17.8 a.u. after 17 h (Figure 9). This aligns with its total water-soluble carbohydrate content compared to A619 and FC13 (Appendix Table 31). The exponential growth phase was less steep compared to A619, which would support that *U. maydis* growth slightly slower on Glc and Fru, compared to Suc.

To further clarify the correlation between fungal performance and water-soluble carbohydrates, the Gfp fluorescence was correlated with the pre-fermentation biomass composition (Table 24 and Figure 10).

Table 24: **Pearson correlation coefficients of *U. maydis* performance and the individual corn stover components in the pre-fermentation biomass.**

	Glucose	Fructose	Sucrose	Total	Xylose	HC	Cellulose	Lignin
U. maydis performance	0.46	0.37	0.76	0.92	-0.22	-0.02	0.16	-0.19

The highest correlation was detected for total water-soluble carbohydrate content ($r = 0.92$). The correlation to individual water-soluble carbohydrates was lower, with Suc content being the highest at $r = 0.76$ (Table 24 and Figure 10), which can be explained by Suc being the major water-soluble carbohydrate in most of the analyzed corn varieties across the entire population (Table 22).

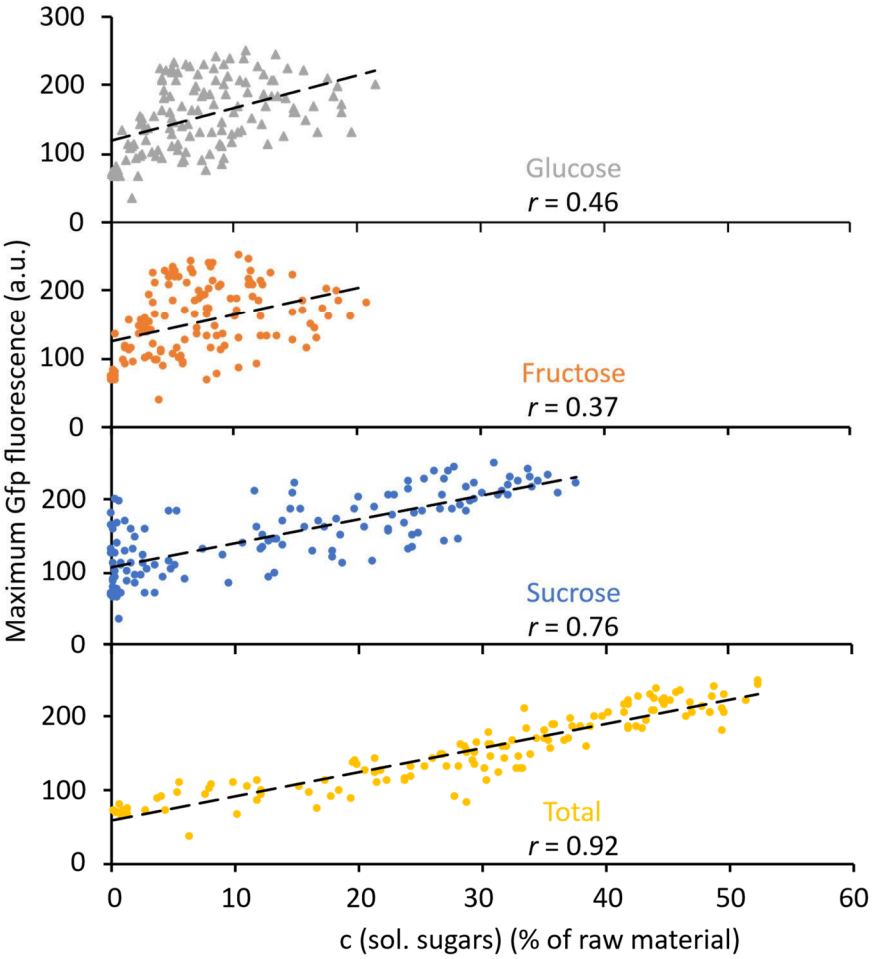

Figure 10: **Correlation of *Ustilago maydis* performance to water-soluble carbohydrates (% of raw material).** Fungal performance is determined by the maximum detected Gfp fluorescence. The data are shown as individual data points for maximum Gfp fluorescence in arbitrary units (a.u.) over the total water-soluble carbohydrate content (soluble sugars) (% of raw material) of 3 plants for 41 corn varieties and 2 plants for 2 corn varieties. *r* shows the Pearson correlation coefficients.

The correlations of fungal performance with Glc or Fru content were lower (Table 24 and Figure 10). However, this is mostly because varieties containing less Glc or Fru, still contained substantial amounts of Suc (Appendix Table 31), which served as carbohydrate source for *U. maydis*. Even lower were the correlations of fungal performance to the lignocellulosic components Xyl (r = -0.22), total hemicellulose (r = -0.02), crystalline cellulose (r = 0.16) and lignin (r = -0.19) (Table 31).

Overall, high levels of water-soluble carbohydrates were the most important factor for *U. maydis* performance (Table 31 and Figure 10). While the composition of these carbohydrates slightly affected growth speed, as shown for the different Gfp fluorescence curves of the varieties A619, FC13 and Mo17, maximum performance

remained largely unaffected. Low correlation coefficients were detected for the abundance of lignocellulosic components in pre-fermentation biomass and the fungal performance.

U. maydis utilization of the lignocellulosic fraction across a large set of corn varieties

Even though the correlations between fungal performance and lignocellulosic components were low, it is still possible that they represent a carbohydrate source for *U. maydis*. Thus, it was evaluated whether variations in lignocellulosic attributes present in a larger set of corn varieties influence corn stover utilization by *U. maydis*. A compositional analysis of the lignocellulosic material was conducted by comparing pre- and post-fermentation biomass. The difference between pre- and post-fermentation biomass of each individual lignocellulosic component was then correlated to the maximum Gfp fluorescence detected during the fermentation (Table 25). A positive Pearson correlation indicates that for higher Gfp fluorescence, the lignocellulosic component was reduced, which can be interpreted as *U. maydis* utilization. Contrary, a negative Pearson correlation indicates that for increasing Gfp fluorescence values, the lignocellulosic component was increased.

Table 25: **Pearson correlation coefficients between *U. maydis* performance and the utilization of lignocellulosic components of 43 different corn varieties.** The components are arabinose (Ara), galactose (Gal), glucose (Glc), xylose (Xyl), total Hemicellulose (HC), crystalline cellulose (CC), lignin and acetate.

	Ara	Gal	Glc	Xyl	HC	CC	Lignin	Acetate
U. maydis performance	0.61	-0.43	-0.46	0.61	0.39	0.57	0.27	0.52

Ara (r = 0.61), Xyl (r = 0.61), acetate (r = 0.52) and CC (r = 0.57) all positively correlate to fungal performance (based on Gfp fluorescence). This could indicate that *U. maydis* utilizes these components for growth (Table 25), which would be in line with the lignocellulose utilization identified in Chapter 1 (Table 17). The negative correlations for Gal (r = -0.43) and Glc content (r = -0.46) are most likely caused by increased contents of these components in the post-fermentation biomass.

Overall, *U. maydis* can utilize corn stover of all tested varieties, highlighting the flexibility and the potential of corn stover as substrate for *U. maydis* fermentation (Figure 9). While water-soluble carbohydrate content in the pre-fermented biomass is the primary influence on fungal performance, the composition of these carbohydrates

has limited impact (Table 31 and Figure 10). For the lignocellulosic fraction, the results show that fungal performance correlates mostly to a reduction in acetylated arabinoxylan and cellulose (Table 25), which is in line with the lignocellulose utilization results of chapter 1. However, in comparison to the water-soluble carbohydrate fraction, the impact on overall fungal performance is limited (Appendix Table 31).

Genome-wide association study of the water-soluble carbohydrate content in corn stover

The correlation between fungal performance and water-soluble carbohydrate content highlights the importance of this trait for further investigation, as it is a main contributor to the bioconversion potential of corn stover by *U. maydis*. Furthermore, the detected high variability of this trait across the natural variation panel makes it a suitable basis for GWAS. In this work, a SNP matrix comprising 44,293 SNPs across 212 corn varieties of the natural panel served as the genomic dataset. The phenotypic traits were absolute glucose (Glc), fructose (Fru), sucrose (Suc) and total water-soluble carbohydrate content (Total), as well as the relative composition of the water-soluble carbohydrate fraction (Glc%, Fru%, Suc%). The SNP information, as well as the GWAS R-script was provided by the Institute for Quantitative Genetic and Genomics of Plants, HHU Düsseldorf, within the scope of the “Cornwall” project (BMBF; 031B0193A).

First, Manhattan plots were generated to visualize the association between each individual SNP and the trait, plotted against the physical SNP position in the maize genome (Appendix Figure 30). In total, 40 SNPs showed significant associations with the seven analyzed traits. Three of these SNPs were excluded due to annotation inconsistencies in the updated MaizeGDB database annotation (RefGen_v2 versus RefGen_v5) (Table 32). For the remaining 37 SNPs, quantitative trait loci (QTL) were defined by taking the SNP position as the central point and extending the region upstream and downstream according to the linkage disequilibrium (LD) decay for the corresponding chromosome ($r^2 = 0.1$) (Table 26 and Appendix Figure 31). The distribution of QTLs varied across chromosomes, with the highest number (12) detected on chromosome 1, followed by six QTLs each on chromosomes 3 and 7 (Figure 11). Chromosomes 4, 8, and 9 each contained three QTLs, chromosome 5 had two, and chromosomes 2 and 6 had one each (Figure 11). No QTLs were identified on chromosome 10 (Figure 11).

Table 26: **Overview of all QTL regions for water-soluble carbohydrate traits and candidate genes in maize.**

Name	Trait	Chr.	Physical position B73 RefGen_v5		QTL detected for multiple traits?	Putative genes in QTL	Candidate gene	Bin locus
			5´ start	Size				
Glc_1_1	Glc	1	244978795	400 Kb		9		
Glc_2_1	Glc	2	33085853	600 Kb		13		
Glc_3_1	Glc	3	3455532	600 Kb	**Overl.** Glc%_3_1	32		
Glc_5_1	Glc	5	84614765	400 Kb		6		
Glc_6_1	Glc	6	42714540	500 Kb		8		6.01
Glc_7_1	Glc	7	182224830	600 Kb		29		
Glc_8_1	Glc	8	3067614	800 Kb		20		
Glc_8_2	Glc	8	102980217	800 Kb		17		
Glc%_1_1	Glc%	1	42713701	400 Kb		13		
Glc%_1_2	Glc%	1	207073252	400 Kb	**Eq.** Suc%_1_1; Fru%_1_1	9		1.07
Glc%_3_1	Glc%	3	3454820	600 Kb	**Overl.** Glc_3_1	32		
Glc%_3_2	Glc%	3	210446242	600 Kb		20	***SWEET2a***	
Glc%_4_1	Glc%	4	230857952	800 Kb	**Overl.** Suc%_4_1; **Eq.** Suc%_4_2	11		
Glc%_5_1	Glc%	5	189123384	400 Kb		14		5.05
Glc%_9_1	Glc%	9	156415497	800 Kb	**Eq.** Fru%_9_1; Suc%_9_1	37		
Suc_1_1	Suc	1	248016003	400 Kb		9		
Suc_3_1	Suc	3	140863822	600 Kb		9	***SWI3C1***	
Suc_3_2	Suc	3	209375293	600 Kb		25		
Suc_7_1	Suc	7	545208	600 Kb		16		
Suc%_1_1	Suc%	1	207073252	400 Kb	**Eq.** Glc%_1_2; Fru%_1_1	9		1.07
Suc%_1_2	Suc%	1	230398209	400 Kb		6		1.07
Suc%_4_1	Suc%	4	230857934	800 Kb	**Overl.** Suc%_4_2; Glc%_4_1	11		
Suc%_4_2	Suc%	4	230857952	800 Kb	**Overl.** Suc%_4_1; **Eq.** Glc%_4_1	11		
Suc%_7_1	Suc%	7	125030985	600 Kb	**Eq.** Fru%_7_1	19		
Suc%_9_1	Suc%	9	156415497	800 Kb	**Eq.** Glc%_9_1; Fru%_9_1	37		
Fru_1_1	Fru	1	193352471	400 Kb	**Overl.** Fru_1_2; Fru_1_3	16		
Fru_1_2	Fru	1	193583734	400 Kb	**Overl.** Fru_1_1; Fru_1_3	16		
Fru_1_3	Fru	1	193583872	400 Kb	**Overl.** Fru_1_1; Fru_1_2	16		
Fru_1_4	Fru	1	250499962	400 Kb		8		
Fru_1_5	Fru	1	277412674	400 Kb		8		
Fru_7_1	Fru	7	109596853	600 Kb		9		
Fru_8_1	Fru	8	11556275	800 Kb		13	***PMI3***	
Fru%_1_1	Fru%	1	207073252	400 Kb	**Eq.** Glc%_1_2; Suc%_1_1	9		1.07
Fru%_3_1	Fru%	3	139090412	600 Kb		7		
Fru%_7_1	Fru%	7	125030985	600 Kb		18		
Fru%_9_1	Fru%	9	156415497	800 Kb	**Eq.** Glc%_9_1; Suc%_9_1	37		
Total_7_1	Total	7	645208	600 Kb		12		

The traits are: the amount of glucose (Glc), fructose (Fru), sucrose (Suc) in absolute and relative (%) abundance and the total water-soluble carbohydrate content (Total); Overl.: overlapping QTLs, meaning their genomic region partially overlaps; Eq.: equal QTLs, meaning they are based on same SNP; the column Bin locus refers to the loci identified in (Bian et al., 2015) associated with maize stalk Suc content determined via Brix measurement.

Eight QTLs were associated with Glc, seven with Glc% and Fru, six with Suc%, four each with Suc and Fru% and one with total water-soluble carbohydrate content. Several QTLs were associated with multiple traits *i.e.*, the same SNP was significantly associated with multiple traits. These are: Glc%_1_2 equal to Suc%_1_1 and Fru%_1_1; Glc%_9_1 equal to Suc%_9_1 and Fru%_9_1. In addition, Suc%_7_1 is equal to Fru%_7_1 and Glc%_4_1 is equal to Suc%_4_2 (Table 26). Some QTLs overlap within or across traits *i.e.*, their genomic region partially overlaps. Fru_1_1, Fru_1_2, Fru_1_3 overlapped and were identified within the same trait, while Glc_3_1 overlapped with Glc%_3_1. Suc%_4_1 overlapped with the QTLs Glc%_4_1 and Suc%_4_2 (Table 26).

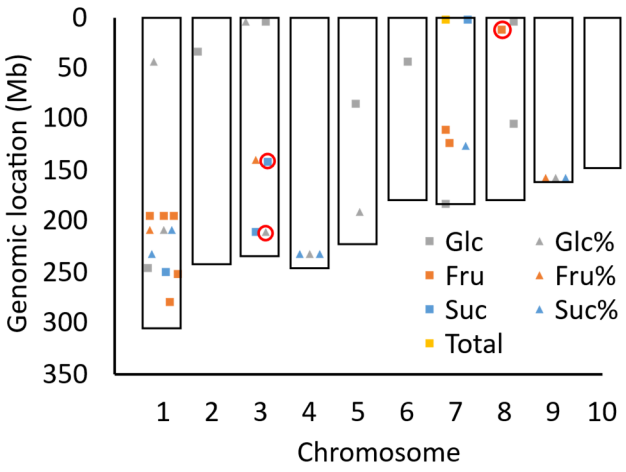

Figure 11: **Physical position of the significant quantitative trait loci across the maize genome.** Each data point represents one QTL detected for the different traits, i.e. the amount of glucose (Glc), fructose (Fru), sucrose (Suc) in absolute (squares) and relative (%; triangles) abundance and the total water-soluble carbohydrate content (Total). Red circles highlight QTLs containing candidate genes (Table 26).

Furthermore, a previous study identified several bin loci associated with corn stem Suc content, quantified by Brix measurement (Bian et al., 2015). Some of the QTLs identified in this work here, are located in the bin loci identified in (Bian et al., 2015). These are the three equal QTLs Glc%_1_2, Suc%_1_1 Fru%_1_1, as well as QTL Suc%_1_2 all located in bin locus 1.07 (Table 26). Furthermore, Glc%_5_1 was located in bin locus 5.05 and Glc_6_1 in bin locus 6.01 (Table 26).

The genome annotation data of all QTLs were then manually analyzed for genes putatively involved in water-soluble carbohydrate metabolism. Three candidate genes were picked for further detailed analyses. These candidate genes were: I) a putative

subunit of a chromatin remodeling complex (*ZmSWI3C1*, “SWITCH3C 1” Acc. Nr.: Zm00001eb138850) located in the genomic region defined by QTL Suc_3_1 (Table 26), which could be involved the transcriptional regulation of synthesis/accumulation of water-soluble carbohydrates; II) a putative bi-directional transporter from the SWEET family (“Sugars Will Eventually be Exported Transporter”) (*ZmSWEET2a*, Acc. Nr.: Zm00001eb155660), located in the region defined by QTL Glc%_3_2 (Table 26), which could be directly involved in water-soluble carbohydrate transport; and III) a putative phosphomannose isomerase (*ZmPMI3*, Acc. Nr.: Zm00001eb335020), located in the genomic region defined by QTL Fru_8_1 (Table 26), which could catalyze the reversible reaction of mannose-6-phosphate to fructose-6-phosphate, which are both central metabolites of carbohydrate metabolism as precursors for e.g. ascorbic acid and Suc.

4.2.3 Discussion

The previous chapter 1 identified the water-soluble carbohydrates as the most influential carbon source for *U. maydis* during the bioconversion of corn stover. Accordingly, this chapter focuses on this fraction, aiming to identify genomic regions and specific genes in maize associated with the accumulation and composition of water-soluble carbohydrates in corn stover.

The accumulation of substantial water-soluble carbohydrate reserves in the stems of senescent maize plants has been known for decades (Ralph Singleton, 1948; Van Reen & Singleton, 1952). Nevertheless, relatively few studies available in English have examined this trait across a wide range of field grown maize varieties. It is well established that water-soluble carbohydrate contents fluctuate over the plant´s life cycles, reflecting shifts in source-sink dynamics (Akter et al., 2020; Liang et al., 2019; Sekhon et al., 2016; Slewinski, 2012) and that they also differ between internodes of the same plant (Bian et al., 2014). To control for these temporal and tissue-specific variations, water-soluble carbohydrate content in this study was consistently measured in the internode immediately below the first ear at physiological maturity.

In the European natural variation panel examined here, all water-soluble carbohydrates showed considerable variability: 16.8 wt% for Fru, 19.4 wt% for Glc and 37.6 wt% for Suc content (Table 22). The variation in Suc content is particularly striking, exceeding the 7 wt% range previously reported across eighteen maize varieties (Sekhon et al., 2016). This broader range is likely attributable to the larger number of genotypes analyzed in the present study. Furthermore, the variation was substantially greater than the Brix (a proxy for Suc content) values of 10 -15 % (w/v) previously reported across 202 recombinant inbred lines (Bian et al., 2015). The discrepancy likely reflects methodological differences: Brix values were derived from juice pressed from maize stalks (Bian et al., 2015), whereas in this study, sections of the stem were finely milled and resuspended in water, thereby extracting all intracellular water-soluble carbohydrates. Differences in population structure, *i.e.* recombinant inbred line versus a natural variation panel, may also contribute to the contrasting results. Supporting the broad variation of the water-soluble carbohydrates identified here, another study reported that total water-soluble carbohydrate content in maize stems ranged from 0 to 450 mg/g dry weight, determined by near-infrared

spectroscopy, across 350 different samples collected from field grown plants (Goñi et al., 2024). This range is comparable to the 50.4 wt% observed here (Table 22). Taken together, this extensive phenotypic variation underscores the suitability of the analyzed panel as a basis for GWAS.

Apart from this substantial phenotypic variation, maize is further characterized by remarkable genetic diversity, coupled with high abundance of SNPs and rapid LD decay (Mazaheri et al., 2019). These features allow GWAS to detect trait-associated loci with high resolution, as abundant genetic variants provide markers for association and rapid LD decay narrows the genomic intervals linked to each trait. In this work, GWAS was performed using 44,293 SNPs of 212 diverse maize lines from a natural variation panel phenotyped in one harvest season. Seven traits related to water-soluble carbohydrate content in corn stover were analyzed and a total of 37 QTLs were identified across 9 of the 10 chromosomes (Figure 11). Given differences in population structures, experimental locations and trait measurements, substantial colocalization with previously reported QTLs was not expected. However, six QTLs identified here overlapped with bin loci reported by Bian et al. (2015). Especially interesting is that four of these QTLs were located in the bin loci 1.07 on chromosome 1: three QTLs (Glc%_1_2, Fru%_1_1, Suc%_1_1) linked to the same significant SNP, and one additional QTL Suc%_1_2 (Table 26). Because bin 1.07 has been associated with Brix (Suc) measurements of stalk juice, the colocalization of two Suc-related QTLs further reinforces the robustness of the present findings. The other two colocalizing QTLs were associated with absolute and relative Glc content (Glc_6_1 in bin 6.01 and Glc%_5_1 in bin 5.05) (Table 26). Importantly, the QTLs detected in this work refine the bin loci from multi-megabase regions to intervals of less than 500 Kb, substantially narrowing down the number of potential candidate genes involved in water-soluble carbohydrate metabolism. For example, the four QTLs colocalizing in bin 1.07 reduced potential candidates from 83 genes to fifteen genes (Table 26).

In addition to the colocalizing QTLs, 31 additional genomic regions were associated with water-soluble carbohydrate traits in corn stover. Future work could be done to adjust statistical models to better account for population structure, potentially uncovering additional loci from the presented data set. Additionally, expanding the phenotyping data from one harvest season to multiple seasons across different locations would further increase the GWAS strength. Nevertheless, the genomic

regions identified in this work provide a valuable starting point for a more detailed gene-level analysis, including haplotype-chemotype association and functional studies. The results for the three chosen candidate genes are presented in the following chapters (4.3 - 4.5).

4.3 Chapter 3: *ZmSWI3C1* is associated with sucrose content in corn stover

4.3.1 Background

The first identified candidate gene from the GWAS, *ZmSWI3C1* (Zm00001eb138850), was located in Suc_3_1 (Table 26) and is a predicted SWI3 subunit of a SWI/SNF adenosine triphosphate (ATP)-dependent chromatin remodeling complex (Depge-Fargeix et al., 2011). It is located on the negative strand of the long arm of chromosome 3 (B73 RefGen_v5; chr3: 141,362,300 – 141,370,233). In MaizeGDB, it is listed as *MYBR14* (MYB-related-transcription factor) and it was previously also named *ZmCHB106* (CHROMATIN REMODELING COMPLEX SUBUNIT B 106) (X. Yu et al., 2016) or *ZmSOC1* (SUPPRESSOR OF OVEREXPRESSION OF CONSTANTS 1) (C. Li et al., 2025). However, the name *SWI3C1* will be kept throughout this work in accordance to (Depge-Fargeix et al., 2011).

Four domains were previously identified in *ZmSWI3C1* (Figure 12 A) (Depge-Fargeix et al., 2011). These are: the SWIRM domain (named for its presence in SWI3, Rsc8, Moira proteins; amino acid (aa) 186 – 276) involved in DNA binding; the ZZ-type zinc finger domain (aa 364 – 390) potentially involved in protein-protein interactions; the SANT domain (named for its presence in SWI3/ADA2/N-Cor/TFIII proteins; aa 418 – 466) involved in histone interaction and the leucine rich domain (aa 585 – 654), which is shared across many SWI3 proteins (Depge-Fargeix et al., 2011). SWI/SNF complexes are highly conserved across eukaryotes and function by utilizing the energy from ATP hydrolysis to remodel chromatin structure, thereby influencing gene expression (Boyer et al., 2004; X. Chen et al., 2024; Han et al., 2020; Nelissen et al., 2015; Vercruyssen et al., 2014). The SWI3 subunit, a core component of these complexes is essential for their correct assembly and activity (Boyer et al., 2004; X. Chen et al., 2024; Han et al., 2020; Nelissen et al., 2015). Thus, this gene candidate could be involved in transcriptional regulation controlling water-soluble carbohydrate content in corn stover.

4.3.2 Results

MaizeGDB lists two transcript isoforms of this gene, differing in the presence of exon 10 (Figure 12 A), and both were considered in the haplotype-chemotype analysis. Whole genome sequences were available for 135 of the corn varieties used in this work (Grzybowski et al., 2023). Using this data, the CDS of *ZmSWI3C1* was compared to identify non-synonymous SNPs and group the 135 corn varieties into distinct haplotypes. These haplotypes were then compared for differences in Suc content, since *ZmSWI3C1* was identified in a region associated to Suc content in corn stover. This allows the detection of genetic variants that are associated with differences in Suc and helps identify genetic factors that contribute to the phenotypic variation across the tested varieties.

The predicted domains are marked in accordance with Depge-Fargeix et al. (2011) in Figure 12 B. It contains the SWIRM and the SANT domain (green and blue Figure 12 B). Furthermore, it contains a ZZ-type zinc finger domain and a leucine rich region, (orange and grey Figure 12 B). Across all varieties, transcript isoform 1 (T001) contained three non-synonymous SNPs: SNP1 (G/A; location chr3_141369544) in exon 2 (L133F), SNP2 (A/C; location chr3_141368966) in exon 3 (S290A) and SNP3 (C/T; location chr3_141362325) in exon 10 (S785N) (Figure 12 A to C). In contrast, transcript isoform 2 (T002) includes only SNP1 and SNP2, as exon 10 is absent (Figure 12 D). Due to the absence of SNP3 in T002, the three haplotypes identified in this isoform are more prevalent across varieties. In contrast, rare alleles in T001, formed by the presence of SNP3 in combination with either SNP1 or SNP2, are found in less than 5 % of the analyzed varieties and these rare alleles were excluded from the haplotype analysis.

SWI3C1 was located in the QTL Suc_3_1. In consequence, the average Suc contents of the three distinct haplotypes were compared (hap1 to hap3). For isoform T001, hap2 (17.3 ± 9.0 wt%; n = 33) contained significantly more Suc than hap1 (13.2 ± 9.5 wt%; n = 80), corresponding to an increase of + 31 % (Figure 12 E). For T002 however, hap1 (13.0 ± 9.5 wt%; n = 88) and hap2 (16.6 ± 9.1 wt%; n = 38) the Suc content did not differ significantly (Figure 12 F).

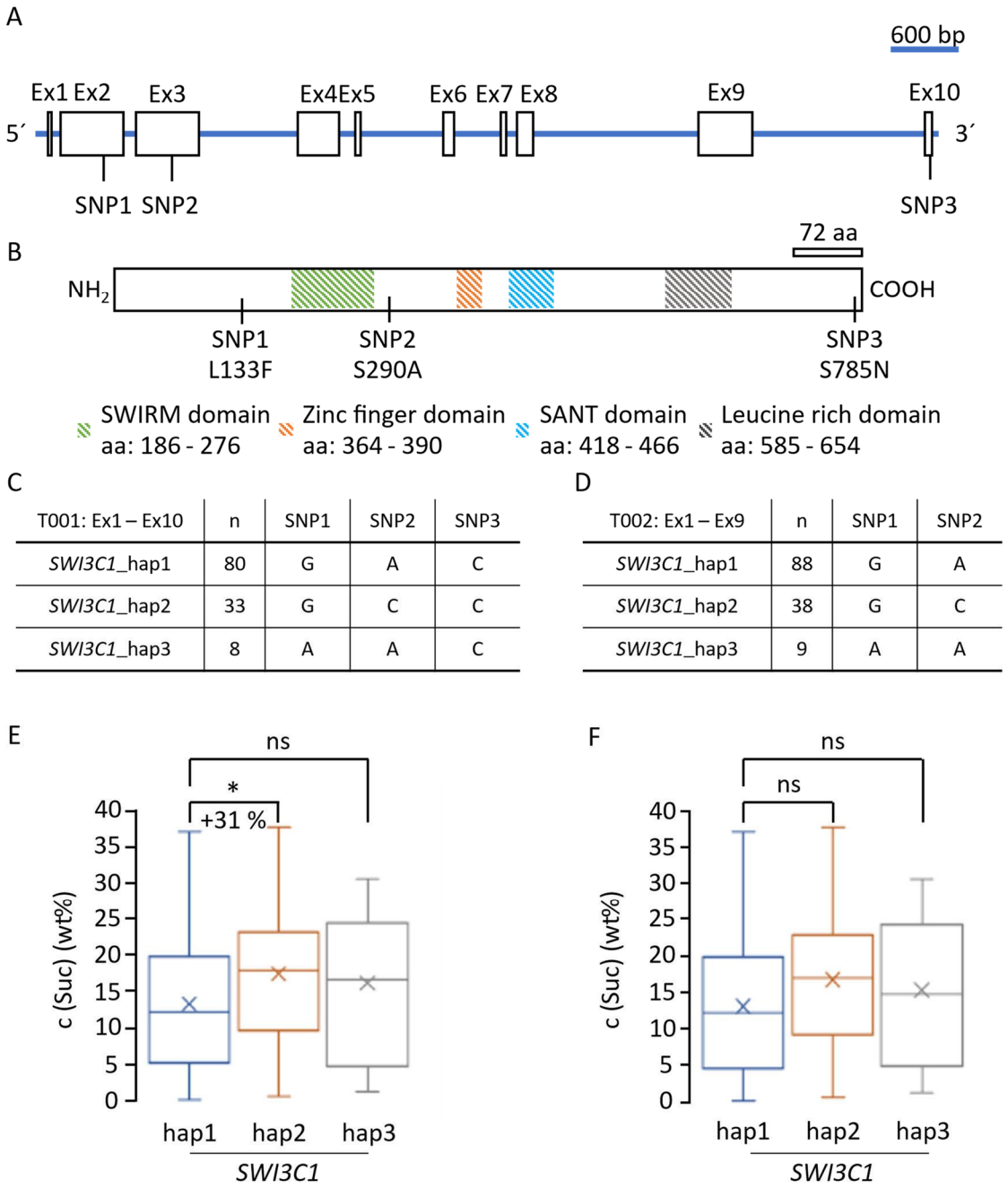

C

T001: Ex1 – Ex10	n	SNP1	SNP2	SNP3
*SWI3C1*_hap1	80	G	A	C
*SWI3C1*_hap2	33	G	C	C
*SWI3C1*_hap3	8	A	A	C

D

T002: Ex1 – Ex9	n	SNP1	SNP2
*SWI3C1*_hap1	88	G	A
*SWI3C1*_hap2	38	G	C
*SWI3C1*_hap3	9	A	A

Figure 12: ***SWI3C1* haplotype-chemotype analysis.** A) Schematic representation of the SNP positions in coding sequence of *SWI3C1*. The sizes of the exons (Ex) and introns are according to the scale bar. B) Schematic representation of the SNP positions and domain organization in the SWI3C1 protein sequence. The positions of the SWIRM (green), Zinc finger (orange), SANT (blue) and Leucine rich domain (grey) are according to (Depge-Fargeix et al., 2011). aa stands for amino acids. Sizes are according to the scale bar. C/D) Non-synonymous single nucleotide polymorphism and the distribution across the haplotypes for transcript isoform 1 (T001) (C) and 2 (T002) (D). n refers to the number of varieties for each haplotype. E/F) Suc content (wt%) of the individual haplotypes for T001 (E) and T002 (F). Data are shown as the AVG ± SD of the varieties. Asterisk indicates statistically significant differences identified with a two-tailed Students T-Test with $p < 0.05$ comparing hap2 and hap3 to hap1. ns indicates not significant differences.

4.3.3 Discussion

The *ZmSWI3C1* gene was identified within QTL Suc_3_1, which is associated to Suc content in corn stover. Three haplotypes of the *ZmSWI3C1* gene were defined across the studied maize varieties, with *SWI3C1*_hap2 showing a significant +31 % increase in Suc content for transcript isoform 1. This haplotype is defined by SNP2, which causes a substitution of serine, a polar and hydrophilic amino acid, with alanine, which is non-polar. SNP2 is located 14 amino acids downstream of the SWIRM domain, a region primarily involved in DNA binding (Depge-Fargeix et al., 2011). Such an amino acid change may influence local protein conformation and thereby indirectly affect SWIRM-mediated DNA-binding efficiency. Nonetheless, experimental validation is required to determine whether SNP2 exerts a functional effect.

Future work is also necessary to clarify whether *ZmSWI3C1* directly contributes to variation in Suc content. A possible explanation is that the gene influences tissue development, thereby indirectly promoting photosynthate production. In *A. thaliana*, the closest homolog *AtSWI3C* regulated cell proliferation during leaf development: overexpression increases leaf area, whereas knock-out mutants display dwarfism, aberrant morphology and delayed development (Sarnowski et al., 2005; Vercruyssen et al., 2014). Accelerated leaf development at early growth stages could extend the period of photosynthate production, thereby increasing the accumulation of Suc and other water-soluble carbohydrates stored in maize stems as a surplus photosynthate reserve (Slewinski, 2012). Supporting this, Bian et al. (2014) reported a QTL for stem Suc content that colocalized with a QTL for leaf area in maize (Bian et al., 2014). While the connection is only speculative, since no evidence is provided in the data presented here and the studies that worked on *AtSWI3C* did not focus on water-soluble carbohydrates metabolism, functional conservation across plants was shown before within the SWI3 family. For instance, loss of function in the closely related SWI3D subunit caused similar phenotypes (leaf curling, developmental defects) in both maize and *A. thaliana* (Sarnowski et al., 2005; X. Yu et al., 2016). So, it could be possible that *AtSWI3C* and *ZmSWI3C1* perform similar functions *in planta*. Thus, *ZmSWI3C1* could be associated with Suc content in the stems through the control of photosynthate production and vegetative growth.

To establish a causal relationship between *ZmSWI3C1* and corn stem Suc content, experimental validation is essential. For example, the maize BonnMu mutant lines (BonnMu0370552::Mu, BonnMu0370553::Mu or BonnMu0558913::Mu (Marcon et al., 2020)) harboring insertions in *SWI3C1* exons could be screened for the water-soluble carbohydrate content in their stover. Phenotypic screening for traits such as delayed development, semi-dwarf growth, or reduced root systems, similar to those observed in *A. thaliana swi3c* mutants, would provide additional insight (Sarnowski et al., 2005). Importantly, maize harbors a paralog, *ZmSWI3C2* (Zm00001eb201260) (X. Chen et al., 2024), which raises the possibility of functional redundancy. Thus, generating double knock-out lines of both *SWI3C* genes may be necessary. These lines could then additionally be complemented with individual *ZmSWI3C1* haplotypes to assess if the mutant phenotype could be recovered, and if the haplotypes mediate differential phenotype recovery. This would provide additional information about potential SNP effects. In addition, tissue- and stage-specific expression profiling of *ZmSWI3C1* in varieties carrying different haplotypes could help clarify whether changes in expression patterns contribute to variation in Suc content in the stover.

It should also be noted that the haplotype-chemotype analysis was based only on a subset of the natural variation panel for which whole-genome sequencing data were available. As more maize varieties are sequenced in the future, haplotype-chemotype associations can be refined, and rare alleles with potential effects may be identified.

4.4 Chapter 4: *ZmSWEET2a* is associated with glucose content in corn stover

4.4.1 Background

The second gene candidate from the GWAS was *ZmSWEET2a* (Zm00001eb155660), which encodes a putative member of the bi-directional sugar transporter family SWEET and is located on the negative strand of the long arm of chromosome 3 (B73 RefGen_v5; chr3: 210,739,191 – 210,741,096). Previously, it was also referred to as *Zm*SWEETb-2 (Zhu et al., 2022), as *Zm*SWEET7 (Vinodh Kumar et al., 2023) or as *Zm*SWEET2 in NCBI. However, in MaizeGDB.org and (Sun et al., 2024), it is referred to as *Zm*SWEET2a, which will also be used throughout this work.

According to the SWEET family nomenclature, the SWEET transporters should be numbered based on the closest homologous protein in *A. thaliana* or rice (Eom et al., 2015). Following this nomenclature, the number gives information about the putative subcellular localization of the SWEET transporter. For example, SWEET2 is a tonoplast localized transporter, whereas SWEET1 or SWEET7 are plasma membrane localized transporters (H. Y. Chen et al., 2015; L. Q. Chen et al., 2010; Eom et al., 2015; L. Zhang et al., 2021; X. Zhang et al., 2021). Due to the inconsistencies in naming *Zm*SWEET2a across the publications and since no biological evidence of its subcellular localization or function has been provided so far, it is unclear whether *Zm*SWEET2a is a plasma membrane or tonoplast localized transporter. Furthermore, it is similarly unclear which carbohydrate is preferentially transported as it was recently mentioned as a Suc transporter, without providing functional evidence (Kaderbek et al., 2025), however its closest homologs in rice and *A. thaliana* are Glc transporters (H. Y. Chen et al., 2015; Tao et al., 2015). Thus, both localization and transport specificity are controversial.

4.4.2 Results

Haplotype-chemotype analysis for *ZmSWEET2a*

MaizeGDB lists three transcript isoforms of *Zm*SWEET2a, but the canonical transcript is version 3, which comprises 6 exons, 5 introns (CDS: 693 bp; (Figure 13 A)) and encodes a 230 amino acid protein (25.17 kDa; isoelectric point 8.75). This transcript will be the focus of this section. The protein contains seven predicted transmembrane domains, which are characteristic for SWEET transporters (L. Q. Chen et al., 2010) and a C-terminal dileucine signal peptide DSSAPLLA (Bonifacino & Traub, 2003) (Figure 13 B).

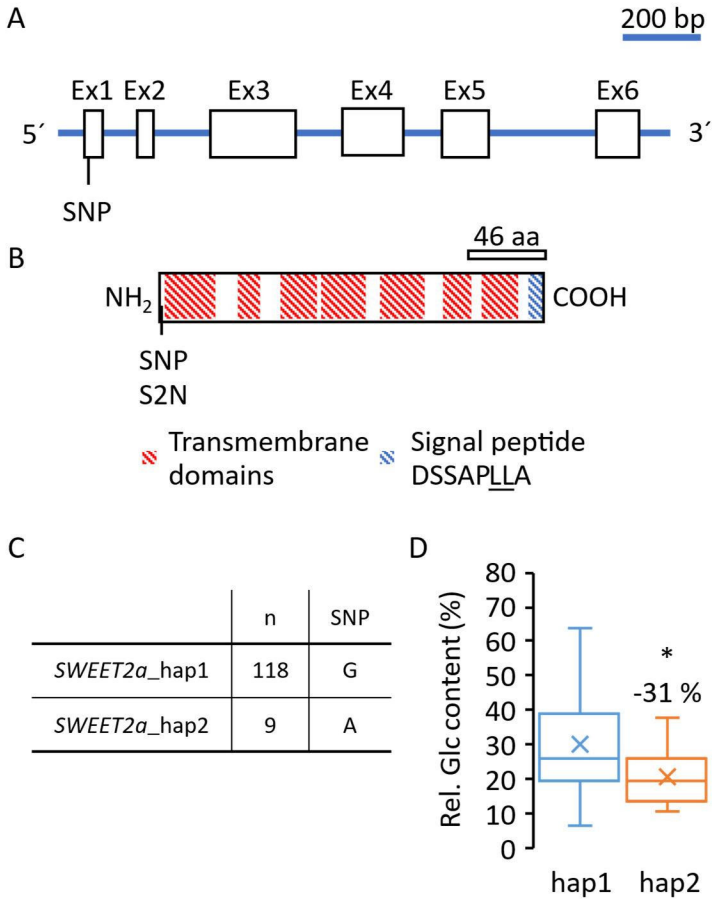

	n	SNP
*SWEET2a*_hap1	118	G
*SWEET2a*_hap2	9	A

Figure 13: ***SWEET2a* haplotype-chemotype analysis.** A) Schematic representation of the SNP position in the coding sequence of *SWEET2a*. The sizes of the exons (Ex) and introns are according to the scale bar. B) Schematic representation of the SNP position, the seven transmembrane domains (red) and the C-terminal signal peptide (blue) in the protein sequence of SWEET2a. Sizes are according to the scale bar. aa stands for amino acids. C) Non-synonymous single nucleotide polymorphism and the distribution across the haplotypes. n refers to the number of varieties representing each haplotype. D) Relative glucose content (% of total water-soluble carbohydrate) of both *Zm*SWEET2a haplotypes. Data are shown as the AVG ± SD of the varieties. Asterisk indicates statistically significant differences between hap1 and hap2 identified with a two-tailed Students T-Test with $p < 0.05$.

Two distinct haplotypes were detected across all varieties, distinguished by one non-synonymous SNP (G5A; location chr3_210740835) in exon 1 causing an S to N change in the second amino acid (Figure 13 A and B). Haplotype 1 comprised 118 varieties, including the maize reference variety B73, while haplotype 2 was much rarer and included 9 varieties (Figure 13 C).The candidate gene *SWEET2a* was located in the QTL Glc%_3_2 associated to relative Glc content (Table 26). In consequence, the relative Glc content was compared among the haplotyes, which was 31 % higher in hap1 varieties (30.1 ± 13.4 %) compared to hap2 varieties (20.9 ± 8.0 %) (Figure 13 D).

In summary, these results show that two distinct haplotypes were present for the *SWEET2a* gene, which differed by a SNP close to the N-terminal end. The significant differences in relative Glc content between hap1 and hap2 are in line with the QTL and the associated trait in the GWAS analysis, indicating that *Zm*SWEET2a might be involved in the transport of Glc in corn stover.

A. thaliana sweet2 mutants

The closest homolog to *ZmSWEET2a* in *A. thaliana* is *AtSWEET2*, a tonoplast localized Glc transporter (H. Y. Chen et al., 2015). Two T-DNA insertion mutants were previously described for the *AtSWEET2* gene, namely *sweet2-1*, carrying an insertion in the first intron, and *sweet2-3*, with an insertion in the fifth exon (H. Y. Chen et al., 2015). These insertions resulted in no detectable full-length *At*SWEET2 transcripts in homozygous mutants (H. Y. Chen et al., 2015).

One potential approach to examine the function of *ZmSWEET2a in planta* is to complement the knock-out mutations of the *A. thaliana sweet2-1* and *sweet2-3* lines, by inserting the *ZmSWEET2a* gene and analyzing, if the expression recovers the mutant phenotypes. Furthermore, both *ZmSWEET2a* haplotypes could be expressed in the knock-out mutants, and the resulting plants could be analyzed for differential phenotype recovery, which would indicate SNP-dependent differences in protein activity. Two phenotypes were previously described for *sweet2-1* and *sweet2-3*, a reduced total leaf area of plants grown on high Glc media and reduced water-soluble carbohydrate content in soil grown leaves (H. Y. Chen et al., 2015). Thus, these homozygous T-DNA insertion lines and Col-0 wildtype plants were obtained from the

European Arabidopsis stock center and examined for these mutant phenotypes, which in a second step could be complemented by the addition of the *ZmSWEET2a* gene.

First, the plants were grown on ½ MS plates with varying Glc concentrations (0 %, 1 %, 2.5 %, 5 %). Instead of total leaf area quantified in (H. Y. Chen et al., 2015), the total plant area was measured and additionally, the water-soluble Glc content was quantified in these plants (Figure 14).

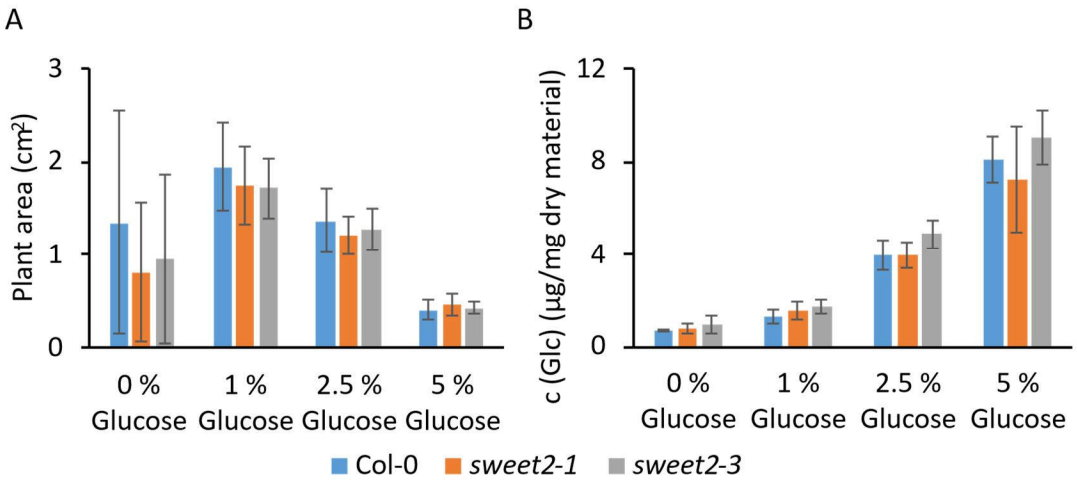

Figure 14: ***A. thaliana* phenotyping on ½ MS plates with increasing Glc concentrations.** A) Plant area (cm²) of *A. thaliana* plants grown on ½ MS plates supplemented with different glucose concentrations (indicated on the x-axis). Depicted are the average ± SD of 15 plants for the plant area. B) Soluble glucose content in the dried material (µg/mg dry material) in the same samples shown in A. For the glucose content, the material of 5 plants was pooled. The graph represents the average ± SD of the resulting three pools per genotype. No statistical differences were detected comparing the T-DNA insertion lines (*sweet2-1* and *sweet2-3*) to the Col-0 wildtype with a two-tailed Students T-Test with $p < 0.05$.

Plants growing on ½ MS media without Glc showed the highest variability in plant area, regardless of the genotype. From 1 % to 5 % Glc, the plant area showed greater consistency and decreased with increasing Glc concentrations. However, no significant differences in plant area were observed between Col-0 and the two T-DNA lines *sweet2-1* and *sweet2-3* (Figure 14 A). The water-soluble Glc content in plant material increased with higher Glc concentrations in the media, but no genotype-dependent differences were detected (Figure 14 B). In consequence, this mutant phenotype could not be reproduced under the tested conditions.

The mutant phenotyping was then extended to senescent stem tissue, and the water-soluble carbohydrate content was quantified in samples harvested after 8 weeks of

growth (Appendix Figure 32). However, no significant differences were observed within the water-soluble carbohydrate contents of the three genotypes (Appendix Figure 32).

In previous studies it was shown that *At*SWEET2 is predominantly expressed in the tonoplast of root cells (H. Y. Chen et al., 2015). The knock-out of *At*SWEET2 could potentially result in differences in root growth or carbohydrate accumulation. Thus, both *A. thaliana* T-DNA lines and the wildtype were analyzed for potential differences in root length and the water-soluble carbohydrate content in roots (Table 27). To obtain clean roots free from soil or agar contaminations, the plants were grown in a sterile hydroponic system using ½ MS liquid media supplemented with 5 % Glc. Root length was imaged after 17 days and measured with ImageJ, but no significant differences were detected between the genotypes (Table 27).

Table 27: **Root length of *A. thaliana* plants grown in hydroponic systems supplemented with 5 % glucose.** The data are shown as the average ± SD of 24 individual plants per genotype.

	Col-0	*sweet2-1*	*sweet2-3*
Root length (cm)	4.19 ± 0.97	4.05 ± 0.92	4.10 ± 1.35

To quantify the water-soluble carbohydrate content, roots from 2 or 3 plants were pooled, resulting in 8 individual pools per genotype. Root dry weight was determined by weighing the pools and normalizing values based on root number per pool. In addition to 5 % Glc media, plants grown in 0.5% Glc media were also included in the analysis. However, no significant differences were detected between the *A. thaliana* lines for root weight (Appendix Figure 33 A) or Glc and Fru content (Appendix Figure 33 B and C).

In addition to the roots, the above-ground material was also analyzed for the individual plant dry weight and water-soluble carbohydrate content (Glc and Fru) (Figure 15). Again, no differences were detected in plant dry weight at 0.5% Glc media (Figure 15 A). However, Col-0 plants growing in 5 % Glc weighed 3.4 ± 0.8 mg, while *sweet2-1* plants showed a significant reduced weight with 2.8 ± 0.6 mg, which corresponds to a reduction by 17.7 %. *sweet2-3* plants showed a reduction of 14.8 % (2.9 ± 0.6 mg), which was not significantly different from Col-0 (Figure 15 A).

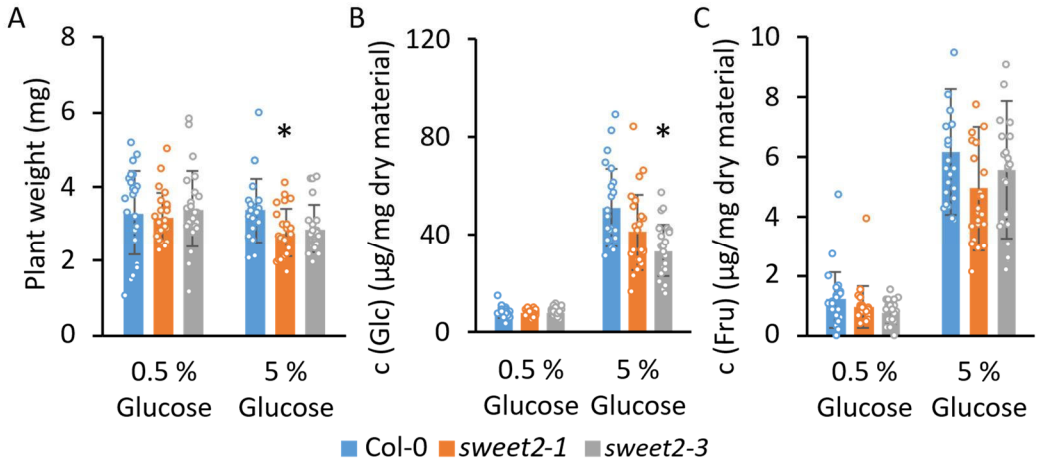

Figure 15: ***A. thaliana*** **phenotyping of hydroponics-grown plants at different Glc concentrations.** A) Dry Weight (mg) of A. thaliana plants grown in hydroponic systems supplemented with 0.5 % or 5 % glucose. B) Soluble glucose and C) Soluble fructose content (µg/mg dry material) of these plants. Data are depicted as the average ± SD of ≥ 23 plants. Datapoints show the individual measurements. Significant differences between a knock-out line (*sweet2-1* or *sweet2-3*) and Col-0 are indicated by an asterisk and determined by a one-way ANOVA followed by Tukey-HSD test with $p < 0.05$.

A similar trend was also detected for the Glc content. No differences were found for the plants grown at 0.5 % Glc. However, at 5 % Glc, the Glc content of *sweet2-1* (40.8 ± 15.4 µg/mg) was reduced by 20.0 % compared to Col-0 (50.9 ± 16.1 µg/mg). In *sweet2-3*, the Glc content was significantly reduced by 34.5 % to 33.2 ± 10.8 µg/mg (Figure 15 B). No significant differences in the Fru content were detected in any of the conditions tested (Figure 15 C), suggesting that the decrease in Glc was not due to an overall reduction in water-soluble carbohydrates, but a specific reduction in Glc content.

Overall, no significant differences were detected between the genotypes for most of the tested conditions. Only in plants growing in hydroponic systems at high Glc concentrations the T-DNA insertion line *sweet2-1* produced less biomass, whereas *sweet2-3* accumulated less water-soluble Glc than Col-0. Both results are in line with the hypothesized function of *At*SWEET2, as it was shown that *sweet2* knock-out plants develop smaller leaves and accumulate reduced Glc contents in leaf tissue (H. Y. Chen et al., 2015). However, it was not attempted to complement these phenotypes with *Zm*SWEET2a_hap1 and *Zm*SWEET2a _hap2. Although the data are significant, the variation between the individual plants is relatively large. As *Zm*SWEET2a_hap1 and *Zm*SWEET2a _hap2 differ only in one non-synonymous SNP a complete loss in activity

is highly unlikely. Thus, to determine differences between both haplotypes and determine slight variations in protein activity, the *A. thaliana* system is most likely not sensitive enough, and a different approach was tested to determine haplotype-specific differences in protein activity, based on a hexose transport deficient yeast strain.

Transport activity studies of SWEET2a in *S. cerevisiae*

One often used system to examine the activity and localization of potential Glc transporters is the heterologous expression in a hexose transport deficient *S. cerevisiae* EBY4000 strain, from now on called “transport deficient” strain (H. Y. Chen et al., 2015; L. Q. Chen et al., 2010; Sosso et al., 2015; Tao et al., 2015; Wieczorke et al., 1999). This transport deficient strain was generated by knocking-out 18 hexose transporters in the *S. cerevisiae* CEN.PK2-1C strain, from now on called “wildtype” (Wieczorke et al., 1999). The wildtype strain grows on Glc containing media, while the transport deficient strain can only grow on maltose containing media (Wieczorke et al., 1999). Expression of several plant plasma membrane hexose transports have been shown to successfully complement the growth on Glc of the transport-deficient strain. For example, this system was previously used to characterize the plasma membrane Glc transporter *At*SWEET1 (L. Q. Chen et al., 2010), the maize *Zm*SWEET4c (Sosso et al., 2015) or the poplar *Pag*SWEET7 (L. Zhang et al., 2021). Furthermore, it was used to analyze the influence of amino acid mutations in *At*SWEET1 (Xuan et al., 2013). Thus, the transport deficient strain could be a suitable system to clarify if *Zm*SWEET2a is involved in hexose transport and in how far the SNP affects transport, following the same approach as described for the *A. thaliana* mutants, by studying the complementation of the mutant phenotype.

The transport deficient strain was transformed with the non-integrative vector pDRf1 containing either of the two *Zm*SWEET2a haplotypes. *At*SWEET2, *Zm*SWEET2a closest homolog in *A. thaliana*, and the empty pDRf1 vector were also included as controls. The growth behavior of all strains was monitored under different growth conditions (Figure 16).The wildtype was able to grow on both Glc- and maltose-containing media, while the transport deficient strain only grew on maltose media as previously reported (Wieczorke et al., 1999) (Figure 16). The pDRf1 vector contains the URA3 gene, which complements uracil auxotrophy (Loqué et al., 2007). In consequence, under auxotrophic conditions (without uracil supplementation) only

successfully engineered strains grew, while growth of the wildtype and the transport deficient strain were inhibited, as these strains cannot synthesize uracil (Figure 16). However, growth in the successfully transformed strains was only detected on Maltose containing media, while no growth was detected on Glc containing media (Figure 16). Furthermore, no growth was detected under similar conditions on Fru or Suc containing media (Appendix Figure 34). This indicates that neither the *Zm*SWEET2a haplotypes nor the *At*SWEET2 control complement the transport deficiency of the transport deficient strain.

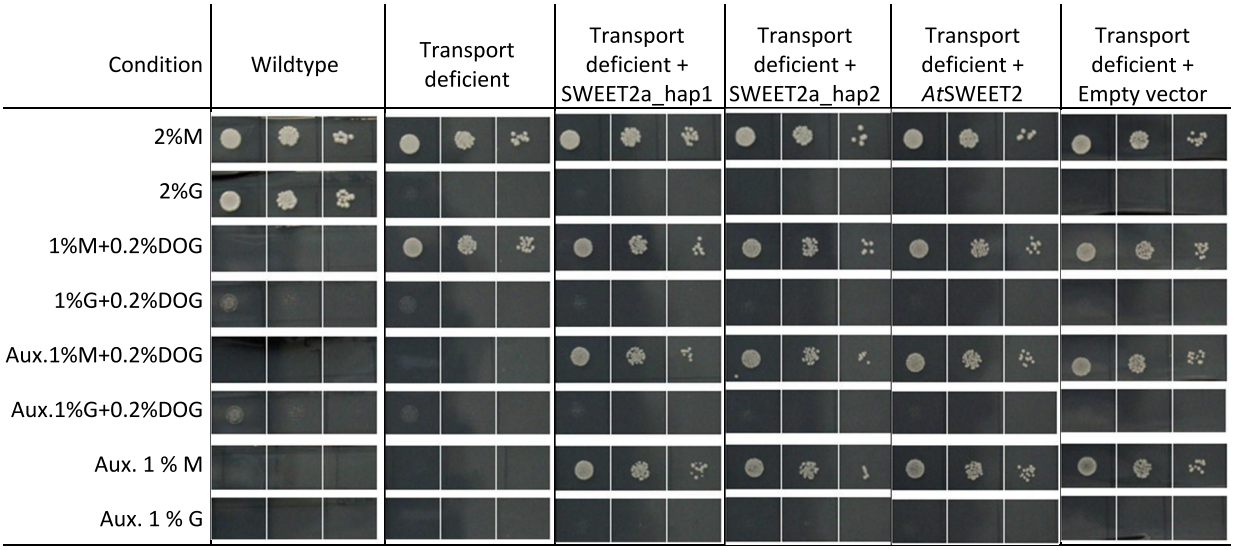

Figure 16: ***S. cerevisiae* growth assay.** Different yeast strains *i.e.*, the wildtype strain, the transport deficient strain and the transport deficient strain transformed with ZmSWEET2a_hap1, _hap2, AtSWEET2 or the empty pDRf1-vector were spotted on synthetic medium containing different carbon sources maltose (M), glucose (G) or 2-deoxy glucose (DOG). The amino acids histidine, tryptophan, leucine and uracil were added to the media. Uracil was used as selection marker for the pDRf1 vector and not added to the media indicated with Aux. The plates were incubated at 28 °C for four days before taking pictures. Individual spots from left to right show 10-fold dilutions. Brightness was adjusted for all pictures by +20 %.

The toxic Glc-analogue 2-deoxy glucose (DOG) is an often-used tool to characterize hexose transporters. If DOG is added to the media and taken-up by the yeast, it will block glycolysis and inhibit growth (Laussel et al., 2022). Previous studies showed that even though *At*SWEET2 did not recover Glc growth of the transport deficient strain, the transformed yeast cells were sensitive to the addition of DOG to the media, indicating that *At*SWEET2 mediated DOG import (H. Y. Chen et al., 2015). Thus, 0.2 % DOG was added to plates containing either Glc or maltose (Figure 16). The wildtype strain did not grow on media containing Glc + 0.2 % DOG, which confirms the toxicity of DOG for *S. cerevisiae* (Figure 16). The transport deficient strain was unaffected by the addition of 0.2 % DOG to maltose containing media, indicating that the strain is

unable to import it, reducing the toxicity of the compound (Figure 16). Similarly, none of the transformed transport deficient strains showed increased sensitivity to 0.2 % DOG (Figure 16), which further confirms that the *Zm*SWEET2a haplotypes do not complement the hexose transport deficiency under these conditions.

Previous results showed that the DOG sensitivity of the transport deficient strain transformed with *At*SWEET2 can be enhanced by increasing the pH of the synthetic media from 5 to 7 (H. Y. Chen et al., 2015). Thus, the pH was adjusted to 7, the growth assay repeated and the colony forming units (CFUs) were counted (Figure 17).

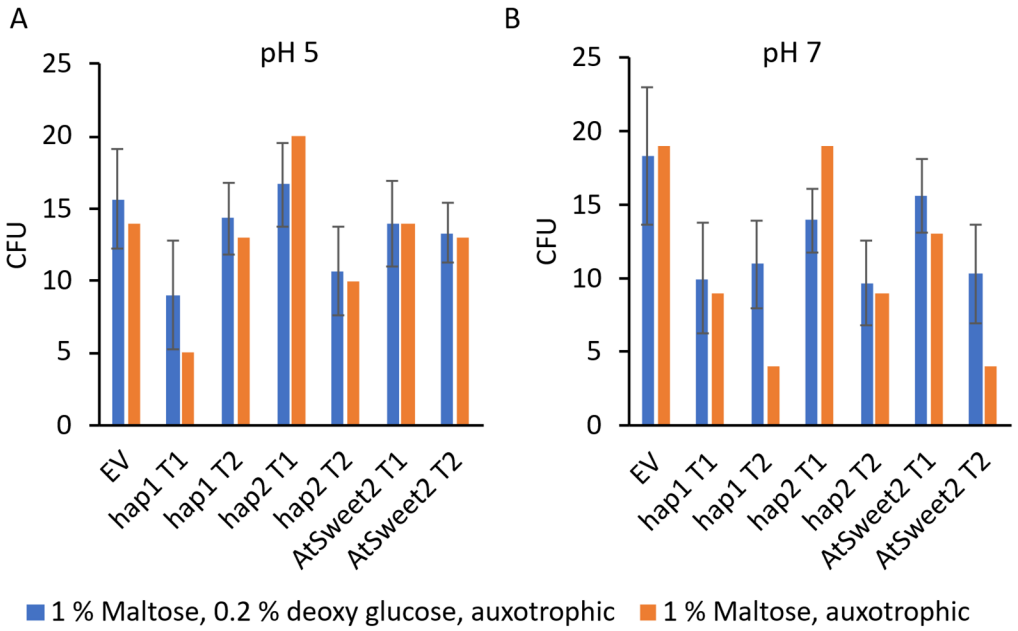

Figure 17: **Colony forming units (CFU) of *S. cerevisiae* strains expressing different SWEET transporters on deoxy glucose containing media at pH 5 (A) and pH 7 (B).** The media was supplemented with 1 % maltose, amino acids for auxotrophic growth requirements and with (blue) or without (orange) addition of 0.2 % deoxy glucose. Depicted are the CFUs of the transport deficient strain transformed with the empty pDRf1 vector (EV), two individual transformants of *Zm*SWEET2a_hap1 (hap1 T1 and T2), *Zm*SWEET2a_hap2 (hap1 T1 and T2) and *At*SWEET2 (T1 and T2). The blue bars are AVG and SD of 3 individual plates. The values were compared for each strain between pH5 and pH7 as well as each transformant to the empty vector at pH5 or pH7 with two-tailed Students T-Tests, $p < 0.05$, but no significant differences were detected. Orange bars are the CFUs counted on one plate.

However, no significant differences were detected between the DOG sensitivity of transport deficient strain expressing either the empty vector control or any of the SWEET constructs (Figure 17). In addition, the CFUs of the individual strains did not differ between pH 5 or pH 7, suggesting that under the tested conditions, the pH does

increase the DOG sensitivity. These results further indicate that neither of the *Zm*SWEET2a haplotypes nor the *At*SWEET2 mediates DOG transport.

In summary, the results of these experiments show that *Zm*SWEET2a does not complement the hexose transport deficiency of the yeast strain. This could have multiple reasons. For example, if *Zm*SWEET2a does not localize to the plasma membrane in yeast, but to another compartment, the transport deficiency cannot be recovered. Alternatively, the transporter might not be actively expressed in the yeast system, or it might not be a functional transporter. To further investigate the *Zm*SWEET2a transport it was next attempted to analyze its subcellular localization in the transport deficient strain.

Subcellular localization of SWEET2a in *S. cerevisiae*

As mentioned before, there is controversy regarding the subcellular localization of *Zm*SWEET2a in literature. The inability to complement the transport deficiency in the hexose transport deficient yeast strain indicates that *Zm*SWEET2a could be tonoplast localized. This hypothesis is further supported by the presence of the predicted C-terminal signal peptide (Figure 13 B and Appendix Figure 39).

To investigate *Zm*SWEET2a´s subcellular localization and assess potential SNP effects, both haplotypes were tagged with Gfp at the C-terminus and expressed in the transport deficient yeast strain. Although it is possible that the Gfp-tag masks the C-terminal signal peptide, previous work has shown that *Os*SWEET2b (the closest homolog of *Zm*SWEET2a in rice , which contains a similar C-terminal signal peptide (Appendix Figure 39)) localizes to the vacuole in the same system using a C-terminal Gfp-tag (Tao et al., 2015). This is in line with the postulation of (Wolfenstetter et al., 2012) that the distance between the signal peptide and the transmembrane domain is important for efficient tonoplast localization, rather than the length of the C-terminus. Furthermore, the same subcellular localization system was previously used to identify *At*SWEET1 localization to the plasma membrane (Zhu et al., 2022). Both, the *Os*SWEET2b and the *At*SWEET1 were used as subcellular localization controls here (Figure 18).

*At*SWEET1 localized to both the plasma membrane and the tonoplast (white arrows Figure 18 A) in the transport deficient yeast cells, consistent to previous reports on its localization (Tao et al., 2015). As anticipated, in the empty vector control, fluorescence

was detected throughout the yeast cell, indicating cytosolic localization of Gfp (Figure 18 B). Some cells expressing *Os*SWEET2b showed a fluorescent vacuole (white arrow Figure 18 C), while others exhibited a more diffuse fluorescent signal. In these cells, no distinct vacuole was visible in the transmission images. However, in line with previous data, *Os*SWEET2b did not localize to the plasma membrane (Tao et al., 2015).

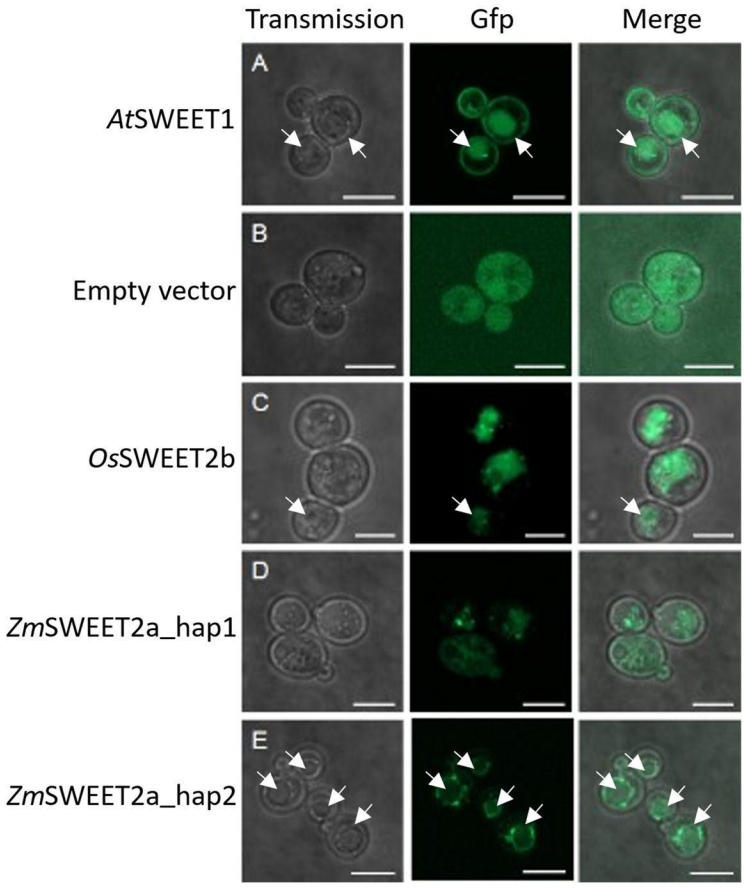

Figure 18: **Subcellular localization of GFP tagged SWEET transporters in transport deficient *S. cerevisiae* strain.** Transmission and GFP pictures were taken by laser scanning confocal microscopy. Depicted are transport deficient cells transformed with *At*SWEET1 (A), empty vector (B), *Os*SWEET2b (C), *Zm*SWEET2a_hap1 (D) and _hap2 (E). White arrows indicate clear vacuolar localization. Each picture is the overlay of 4 z-stack pictures. Scale bar: 5 µm.

The transport deficient cells expressing SWEET2a_hap2 displayed well-defined structures that could resemble vacuoles (white arrow Figure 18 E). The fluorescence signal in these structures suggests that SWEET2a_hap2 localizes to the tonoplast. Furthermore, no fluorescence was detected associated with the plasma membrane.

The cells expressing SWEET2a_hap1 did not exhibit similar defined structures. Instead, the Gfp signal appeared diffuse, making it difficult to attribute fluorescence to

a specific compartment in the transmission images. With the applied method, it cannot be ruled out that this diffuse fluorescence results from the yeast vacuole fragmenting into smaller vesicles, which can occur for example under hypertonic stress conditions (S. C. Li & Kane, 2009). Notably, no fluorescence was observed associated with the plasma membrane (Figure 18 D).

In order to better interpret the results in this experiment, multiple individual cells from each genotype were analyzed for their fluorescence signal pattern. Based on the observed Gfp signal, each cell was categorized as “Tonoplast”, “Diffuse” and “Not expressing” for both *Zm*SWEET2a haplotypes and *Os*SWEET2b (Figure 19). The number of cells in each category was then counted and plotted. Individual pictures are shown in the appendix (Appendix Figure 35 to Figure 37).

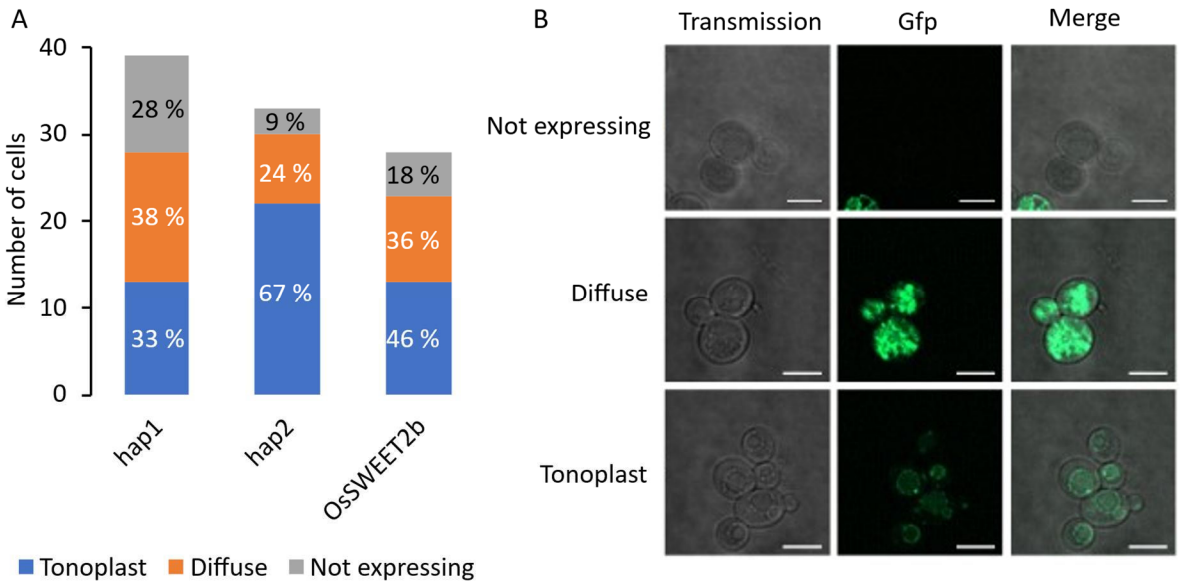

Figure 19: **Quantitative summary of subcellular localization of SWEET2a_hap1, SWEET2a_hap2 and *Os*SWEET2b in transport deficient strain.** A) Number of cells expressing SWEET2a_hap1:Gfp (hap1), SWEET2a _hap2:Gfp (hap2) or *Os*SWEET2b:Gfp showing tonoplast localized (blue), or diffuse (orange) Gfp fluorescence or no fluorescence (“Not expressing” grey). The individual bars represent the absolute number of cells, while the values represent the relative distribution. The data were compared with a Chi-square test of independence ($p < 0.05$), but no significant differences were detected. B) Example pictures of yeast cells not expressing the fusion protein or showing diffuse localization or tonoplast localization. Scale bar: 5 µm.

The majority of cells expressing *Os*SWEET2b:Gfp (46 %) showed a tonoplast localized fluorescence (Figure 19). In 36 % of the cells, the fluorescence appeared diffuse and in 18 % no fluorescence was detected, suggesting that the fusion protein was not properly expressed or to very low levels (Figure 19). Among the cells transformed with

the SWEET2a_hap1:Gfp construct, 28 % did not show fluorescence (Figure 19). Additionally, 38 % exhibited diffuse fluorescence, while 33 % of the cells displayed tonoplast localized fluorescence. For SWEET2a_hap2, 9 % of the cells showed no fluorescence (Figure 19), 24 % exhibited diffuse fluorescence, and 67 % showed tonoplast fluorescence (Figure 19). These data did not differ significantly, thus, it would be necessary to expand this analysis to a larger number of cells, before drawing conclusions regarding a potential SNP-effect on the subcellular localization in the transport deficient strain.

In conclusion, these results suggest that *Zm*SWEET2a localizes predominantly to the tonoplast in yeast, while no fluorescence was detected associated with the plasma membrane. The potential tonoplast localization is consistent with the previously published localization of *Zm*SWEET2a´s homologs *At*SWEET2 and *Os*SWEET2b (Tao et al., 2015), thus, the number “2” is more suitable for this putative transporter, than the previously used number “7” (Vinodh Kumar et al., 2023).

Subcellular localization of SWEET2a in *N. benthamiana*

In order to extend the results observed in the yeast system, subcellular localization was next attempted in *Nicotiana benthamiana*. Unlike yeast, *N. benthamiana* provides a plant-specific cellular environment including native endomembrane systems, trafficking pathways, and post-translational modifications that are more similar to those in maize. Additionally, transient expression in *N. benthamiana* allows for rapid assessment of protein localization without the need for stable transformation.

Both SWEET2a haplotypes were C-terminally tagged with mVenus (in the following named SWEET2a_hap1:mVenus and SWEET2a_hap2:mVenus). In addition, N-terminally tagged mVenus fusion proteins of both haplotypes were generated (in the following named mVenus:SWEET2a_hap1 and mVenus:SWEET2a_hap2), all constructs transiently expressed in *N. benthamiana* and imaged with laser scanning confocal microscopy. Furthermore, to avoid mislocalization artifacts related to protein overexpression in the cells, an inducible protein expression system was used. Initially, protein expression was induced 5 h before imaging and the mVenus fluorescence signal was detected for all constructs (Appendix Figure 38). However, for all four constructs punctuated agglomerations were detected across the entire cells (Appendix Figure 38). Comparable agglomerations were previously interpreted as side-effects of

protein overexpression or proteins that were still transported in the cell (Lin et al., 2014; Wolfenstetter et al., 2012; Xuan et al., 2013). To reduce this effect, the expression was not induced, and leaky expression was monitored (Figure 20).

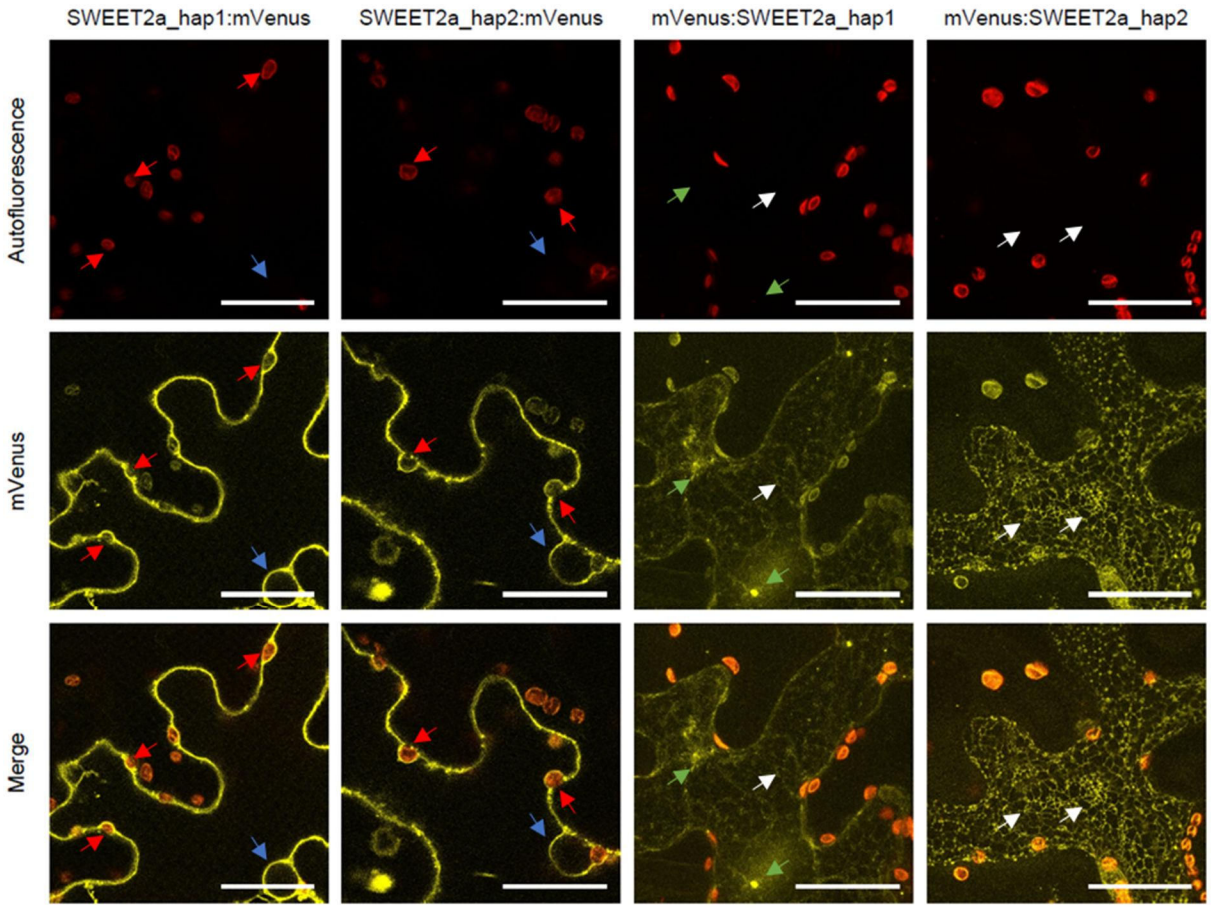

Figure 20: **Subcellular localization of mVenus tagged SWEET2a_hap1 and SWEET2a_hap2 in *N. benthamiana* leaf cells.** Pictures were taken 3 days post infiltration with laser scanning confocal microscopy. Red arrows indicate potential tonoplast localization, blue arrows indicate potential nuclear envelope, green arrows indicate agglomerations and white arrows indicate net-like structures. Scale bar = 50 µm. The pictures of both C-terminal fusion proteins are single layers, while the pictures of both N-terminal fusion proteins are the overlay of multiple z-stack images.

For all constructs, leaky expression of the fusion proteins was detected (Figure 20). The vacuoles of *N. benthamiana* cells are huge and fill most of the intercellular space. In consequence, it is difficult to distinguish tonoplast from plasma membrane, as they are tightly pressed together for most of the cell. However, the chloroplasts (visible in the autofluorescence pictures (Figure 20)) are located between tonoplast and plasma membrane and the tonoplast is dented around the chloroplasts, which aids in identification of the tonoplast (F. Li et al., 2024). For both SWEET2a_hap1:mVenus and SWEET2a_hap2:mVenus the fluorescence signal was mostly dented inwards

around the chloroplasts (white arrows Figure 20), which could indicate a predominant tonoplast localization of both fusion proteins. However, due to additional, weaker fluorescence signals on the plasma membrane facing side of the chloroplasts, a plasma membrane localization cannot be excluded. Furthermore, for both C-terminal fusion proteins structures that could indicate the nuclear envelope were fluorescent, which could either be again the dented tonoplast, or hint at a localization in the endoplasmic reticulum (ER) network (blue arrows Figure 20). Similar putative ER staining was previously associated to protein that was still in traffic (Wolfenstetter et al., 2012).

The N-terminal mVenus fusion proteins of both haplotypes showed net-like patterns across the entire cell (Figure 20). A similar pattern was previously also detected for N-terminal Gfp:*At*SWEET1 fusions in rice protoplasts 3-days post transformation and was interpreted as potential artifacts due to fusion protein misfolding, resulting in ER protein retention (Wolfenstetter et al., 2012). The di-leucine tonoplast localization motif is on the C-terminal end of the *Zm*SWEET2a protein (DSSAPLLA) (Bonifacino & Traub, 2003) (Appendix Figure 39). Thus, the tonoplast localization should not be influenced by the addition of an N-terminal tag. However, the N-terminal tag could influence the protein folding, or alternatively, the functional N-terminal end of the *Zm*SWEET2a fusion protein is required for ER release.

In summary, the results for the subcellular localization in *N. benthamiana* and the transport deficient yeast strain support the hypothesis that *Zm*SWEET2a localizes predominantly to the tonoplast. This also fits the localization of its closest homologs in *A. thaliana* and rice. While future work needs to determine the transported sugar molecule, it is likely that *Zm*SWEET2a similarly transports hexoses as its close homologs do. The influence of the non-synonymous SNP on the activity or the localization of *Zm*SWEET2a is not evident from the data presented here. Slight differences in subcellular localization were detected in the transport deficient yeast strain. However, it cannot be excluded that these originate from different vacuole physiologies. No obvious differences were identified in *N. benthamiana*, thus, other systems are necessary to clarify if the SNP causes differences in transport activity or localization.

4.4.3 Discussion

The second gene candidate identified by the GWAS was *ZmSWEET2a*, a putative member of the bi-directional sugar transporter family SWEET. *ZmSWEET2a* was identified in QTL Glc%_3_2 associated with the relative Glc content in corn stover (Table 26). Furthermore, the localization experiments showed that *Zm*SWEET2a predominantly localizes to the tonoplast in *S. cerevisiae* (Figure 18) and in *N. benthamiana* (Figure 20), providing the first experimental evidence for a previously controversial subcellular localization. These results, combined with its previously identified primarily expression in senescent stem tissue (Stelpflug et al., 2016), suggest that *Zm*SWEET2a could participate in vacuolar carbohydrate storage in mature maize stems.

Although the transported carbohydrate cannot be determined from the presented data, Glc is the most likely candidate based on protein homology with the two tonoplast localized Glc transports *Os*SWEET2b and *At*SWEET2 (H. Y. Chen et al., 2015; Tao et al., 2015). This would be consistent with the GWAS trait (relative Glc content), and with the identification of two *ZmSWEET2a* haplotypes, of which one exhibited significantly lower Glc levels in stover (Figure 13). The defining SNP of haplotype 2 lies near the vacuole-facing, N-terminal end of the protein and results in the exchange of serine to asparagine. Since many SWEET transporters interact with carbohydrates through hydrogen bonds involving asparagine residues (Tao et al., 2015; Vinodh Kumar et al., 2023), the additional asparagine at the vacuolar-facing N-terminus could strengthen carbohydrate binding. For *Zm*SWEET2a, this might favor enhanced Glc binding on the vacuolar side and increased efflux, leading to reduced vacuolar Glc accumulation. As the vacuole represents the major Glc storage compartment in senescing tissues, this could explain the significantly reduced relative Glc content in haplotype 2 maize varieties (Figure 13). In the cytosol, Glc could be further metabolized by hexokinase to G6P, which is the starting point of glycolysis as well as a known activator for Suc synthases (Ruan, 2014), which would promote energy production in plant cells or storage of Suc, respectively.

In addition to its potential role in substrate binding, the SNP may also affect tonoplast targeting or transporter activity. Localization experiments in the transport deficient yeast strain showed that SWEET2a_hap2:Gfp predominantly localized to the vacuole,

whereas SWEET2a_hap1:Gfp appeared more diffuse (Figure 18). While this pattern could suggest a haplotype-dependent difference in subcellular localization, the observed differences were not statistically significant and require future confirmation. The yeast vacuole itself is a highly dynamic organelle that alters its morphology in response to various internal and external stimuli (S. C. Li & Kane, 2009). Under normal conditions, cells usually contain multiple medium-sized vacuoles, which merge into a single vacuole during stationary phase, Glc deprivation or hypotonic stress (S. C. Li & Kane, 2009). In contrast, under hypertonic stress, the vacuole fragments into multiple smaller vesicles (S. C. Li & Kane, 2009; Zieger & Mayer, 2012). In this work, cells were resuspended in water prior imaging, creating hypotonic and carbohydrate depleted conditions. This typically results in vacuole merging and swelling (Desfougères et al., 2016; S. C. Li & Kane, 2009), and this vacuole morphology was observed in most cells expressing SWEET2a_hap2. However, vacuoles in cells expressing SWEET2a_hap1 were fragmented, resembling the vacuoles seen during hyper-osmotic stress (Zieger & Mayer, 2012). This difference, although not statistically significant, could indicate haplotype-specific changes in the osmotic regulation across the vacuolar membrane, potentially caused by differences in *Zm*SWEET2a´s vacuolar localization. Under hypotonic conditions, this imbalance could impair vacuole swelling and fusion (Desfougères et al., 2016; S. C. Li & Kane, 2009). However, the altered morphology might also reflect secondary effects on vacuolar fusion dynamics or stress signaling pathways, both of which are tightly linked to vacuolar stability and cellular responses (Bonangelino et al., 2002; Zieger & Mayer, 2012). Further quantitative analyses will therefore be required to clarify whether haplotype-specific effects impact the vacuole morphology observed here.

Lastly, the SNP could influence ER release of the protein *in planta*. Both N-terminal haplotype fusion proteins showed net-like patterns across the *N. benthamiana* cells (Figure 20). Similar patterns were previously interpreted as ER retention for Gfp:*At*SWEET1 in *A. thaliana* protoplasts (Wolfenstetter et al., 2012). This observation suggests that the N-terminal region could be important for correct ER export, and the serine-to-asparagine substitution might subtly influence this process. Such an effect could in turn impact the efficiency with which *Zm*SWEET2a reaches the tonoplast, thereby altering its functional abundance in planta. If so, this might contribute to the

observed differences in stem Glc levels between haplotypes, although further work is required to establish a direct mechanistic link.

To further clarify *Zm*SWEET2a´s function in maize, mutant varieties carrying insertions in *ZmSWEET2a*, like the BonnMu0382607::Mu or BonnMu0382608::Mu lines (Marcon et al., 2020), could be analyzed for their Glc content in mature stems. Additionally, other phenotypes as reduced Glc content in leaves or reduction in leaf size, similar to those observed in *Atsweet2* mutants (H. Y. Chen et al., 2015), could be explored. Functional redundancy is possible because maize contains another *ZmSWEET2* homolog (Acc. nr. Zm00001eb342040), so double knock-out lines may be required to reveal phenotypes. Complementation of the double knock-out lines with either the active *ZmSWEET2a* gene or an inactivated version would allow assessment of phenotypic recovery and evaluation of gene function *in planta*. To clarify the SNP effect on *Zm*SWEET2a protein activity, potentially reconstitution in lipid vesicles followed by ^{14}C-labelled Glc (or Suc, Fru) uptake assays could help, according to the protocol published for *Os*SWEET2b (Tao et al., 2015). Both haplotype proteins could be synthesized in *P. pastoris* and purified via a C-terminal His-tag and reconstituted into *E. coli* polar lipid (Avanti Research) (Tao et al., 2015). By incubation in labelled carbohydrate-containing solution followed by liquid scintillation measurement, potential differences in carbohydrate uptake activity can be determined. Furthermore, it could be tested to re-direct the *Zm*SWEET2a to the plasma membrane in e.g., the transport-deficient yeast strain, by exchanging the C-terminal localization signal peptide (DSSAPLLA). Replacing the di-leucine sequence with alanine was previously shown to results in an efficient re-routing of a tonoplast transporter to the plasma membrane (Wolfenstetter et al., 2012). This could be similarly tested in the transport-deficient yeast strain, followed by subcellular localization monitoring and growth assays as described in this work. If *ZmSWEET2a* is a functional Glc transporter, this would complement the hexose transport deficient phenotype of the yeast. Additionally, by monitoring growth via CFU counting on plates, or online monitoring of liquid cultures in growth systems like the BioLector®, SNP-effects on transport efficiency could be identified, due to differential growth.

In conclusion, *ZmSWEET2a* was identified in a QTL associated with relative Glc content in maize stover, and varieties carrying the two haplotypes showed differences in Glc levels. Experimental data showed its predominant localization to the tonoplast

in yeast and *N. benthamiana*. Together, these findings suggest that *ZmSWEET2a* may play a role in carbohydrate storage in corn stover and represents a promising target for further research on enhancing water-soluble carbohydrate content.

4.5 Chapter 5: *ZmPMI3* is associated with fructose content in corn stover

4.5.1 Background

The third candidate gene identified from the GWAS (Zm00001eb335020) encodes a putative phosphomannose-isomerase (*PMI*) and is located on the positive strand of the short arm of chromosome 8 (B73 RefGen_v5; chr8: 11,689,365 - 11,693,144). PMIs (enzyme commission number: 5.3.1.8) catalyze the reversible reaction between mannose-6-phosphate (M6P) and fructose-6-phosphate (F6P), a central reaction in plant carbohydrate metabolism, as F6P is a direct precursor for glycolysis and M6P for ascorbic acid (AsA) metabolism (Figure 21).

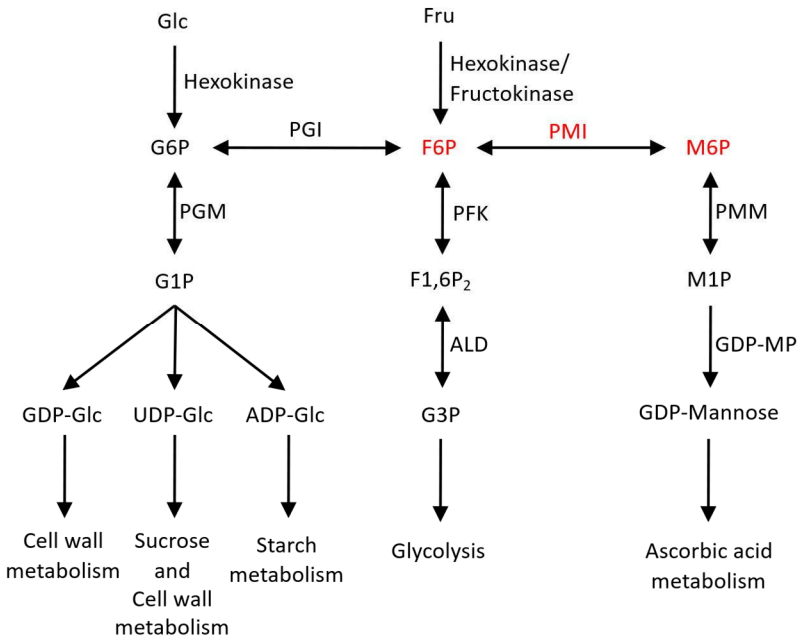

Figure 21: **Schematic representation of the central role of F6P and M6P in carbohydrate metabolism.** The figure is based on information from the KEGG PATHWAY database (Kanehisa, 2019; Kanehisa et al., 2024; Kanehisa & Goto, 2000) and is not exhaustive. Abbreviations are: Glc: Glucose; Fru: Fructose; G6P: Glucose-6-Phosphate; PGI: Phosphoglucose isomerase; F6P: Fructose-6-Phosphate; PMI: Phosphomannose isomerase; M6P: Mannose-6-Phosphate; PGM: Phosphoglucose mutase; PFK: 6-Phosphofructokinase; PMM: Phosphomannose mutase; G1P: Glucose-1-Phosphate; $F1,6P_2$: Fructose-1,6-bisphosphate; M1P: Mannose-1-Phosphate; GDP-Glc: Guanosine diphosphate Glucose; UDP-Glc: Uridine diphosphate glucose; ADP-Glc: Adenosine diphosphate Glucose; ALD: Fructose-1,6-bisphosphate Aldolase; GDP-MP: GDP Mannose Phosphorylase; G3P: Glycerinaldehyde-3-Phosphate

For a long time, PMIs were considered nonexistent in most higher plants, due to the absence of detectable enzyme activity (Hu et al., 2016; Reed et al., 2001; Stoykova & Stoeva-Popova, 2011). However, functional PMIs have been identified in *A. thaliana*

or rice (Hu et al., 2016; Maruta et al., 2008). In *A. thaliana* it was shown that PMI1 is essential for ascorbic acid synthesis *in planta* via the Smirnoff/Wheeler pathway from Glc to L-AsA (Wheeler et al., 1998), while PMI2 expression was only induced during sugar starvation conditions and might be related to plant cell wall polysaccharide degradation (Maruta et al., 2008).

MaizeGDB currently lists two other phosphomannose isomerase genes: *ZmPMI1* (B73 RefGen_v5 chr3: 23.825.301 – 23.834.443) and *ZmPMI2* (B73 RefGen_v5 (chr4: 7.870.887 – 7.879.674). However, besides that their expression levels are low during normal growth and under abiotic stress conditions, little is known about their function *in planta* (Forestan et al., 2016; C. Yu et al., 2021).

4.5.2 Results

Gene sequence analysis of *ZmPMI3*

The gene Zm00001eb335020 is located in the QTL Fru_8_1 and annotated as producing a single transcript. The gene comprises two exons and one intron and encodes a 168 amino acid protein. However, after closer inspection of the CDS from MaizeGDB, no stop codon was detected, raising questions about the completeness of the annotation. Interestingly, a second putative *PMI* gene, Zm00001eb335030 (B73 RefGen_v5; chr8: 11.717.745 - 11.721.770), is annotated 26 kb downstream. This gene consists of three exons and two introns and encodes a 244 amino acid protein. Both genes are marked in MaizeGDB as “possibly represents two tandemly repeated genes” and “NCBI LOC Annotation category: suggests misassembly”, indicating potential issues in genome assembly or gene annotation.

To assess whether these two genes represent distinct functional entities or fragments of a single gene, their predicted encoded protein sequences were aligned with known PMIs from rice (*Os*PMI1) (Hu et al., 2016) and *Candida albicans* (Cleasby et al., 1996) (Figure 22). The sequence alignment revealed that the protein sequences of the two putative genes do not align with each other, indicating that they are not a repetition of the same gene (Figure 22). Furthermore, it revealed high sequence conservation between both fragments and the described PMIs (Figure 22). The eukaryotic PMI class 1 consensus sequence “YxDxNHKPE”, characteristic of zinc-dependent PMI enzymes (Coulin et al., 1993), is present in protein sequence 1 (Zm00001eb335020). Additionally, four zinc-ligand binding residues were previously identified in *Ca*PMI (Cleasby et al., 1996) and also conserved in *Os*PMI1 (Hu et al., 2016). Three of these residues are present in protein sequence 1 (Zm00001eb335020), while the fourth is present in protein sequence 2 (Zm00001eb335030) (green dots in Figure 22 and Figure 23 B). Furthermore, the predicted catalytic domain, based on the domain identified in *Ca*PMI (Cleasby et al., 1996), is split between the two protein sequences and contains highly conserved amino acid sequences (black bars in Figure 22; blue boxes in Figure 23 B). In addition, both other predicted functional domains are similarly split between both protein sequences. These are the predicted C-terminal domain (green bars in Figure 22; green boxes in Figure 23 B) and the helical domain (grey

bars in Figure 22; grey box in Figure 23 B). This suggests that both protein sequences 1 and 2 are potentially two parts of a single PMI protein.

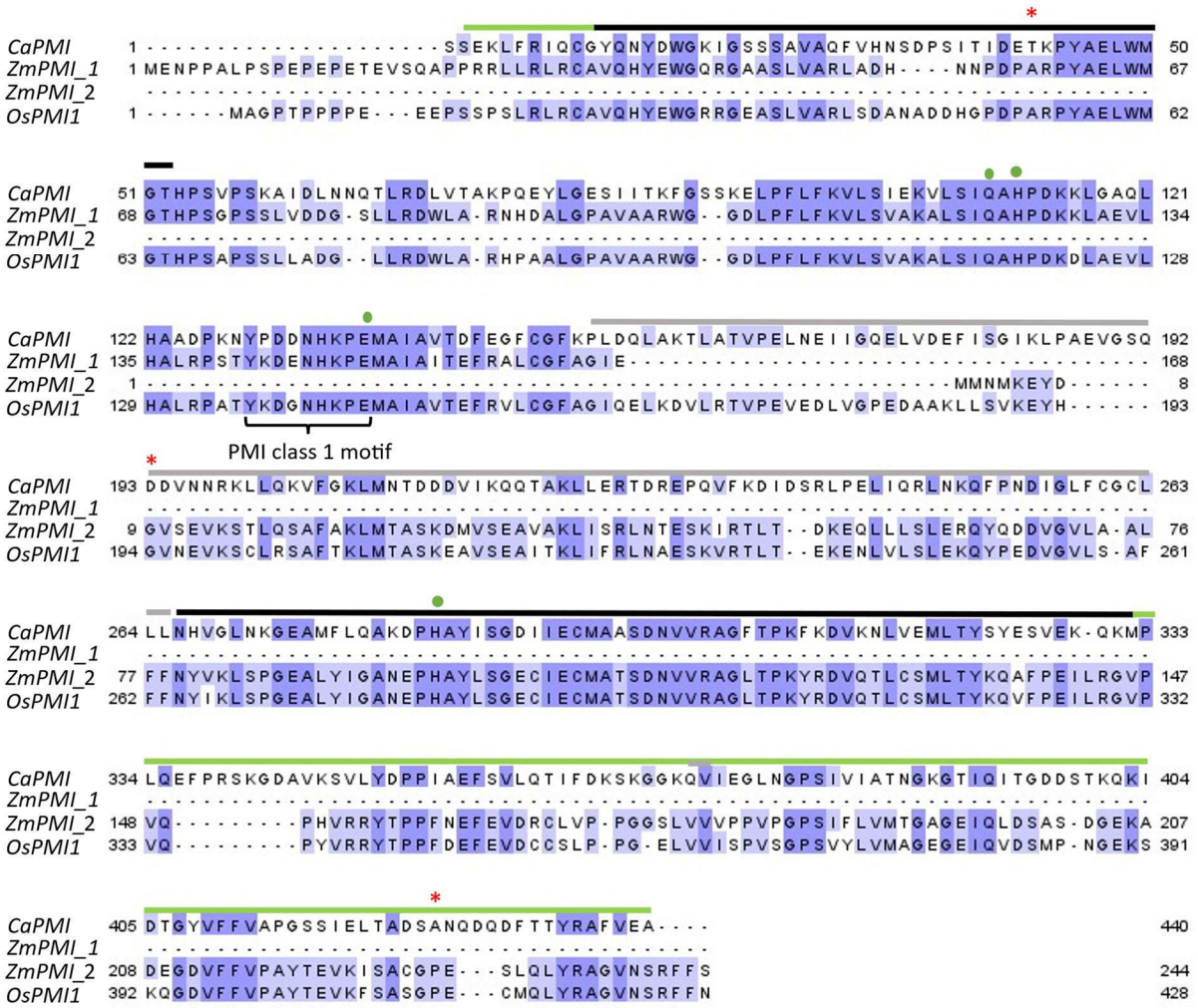

Figure 22: **Primary sequence alignment of the putative PMI amino acid sequence 1 (Zm00001eb335020) and sequence 2 (Zm00001eb335030) and the described *Ca*PMI and *Os*PMI1.** The alignment was done with Clustal Omega (1.2.4) using the default parameters and visualized with Jalview (2.11.4.1). Identical and conserved amino acids across sequences are color coded in dark and light blue, respectively. Four zinc-ligand binding residues (green dots; based on *Os*PMI1) and the PMI class 1 consensus sequence are indicated acc. to (Hu et al., 2016). Red asterisks indicate the positions of the non-synonymous SNPs. Black bars above the sequences indicate the catalytic domain, grey bars the helical domain and green bars the C-terminal domain based on *Ca*PMI (Cleasby et al., 1996).

The predicted molecular weights for protein sequences 1 and 2 are 18.5 kDa and 26.8 kDa, respectively. Individually, these values are considerably lower than those reported for other plants PMIs such as *Os*PMI1 (46.93 kDa), *Os*PMI2 (44.18 kDa) and *Chlorella variabilis* PMI1 (45.85 kDa) (Hu et al., 2016), as well as *At*PMI1 (48.5 kDa) and *At*PMI2 (49.2 kDa) (Maruta et al., 2008). However, the combined molecular weight

of protein sequences 1 and 2 is 45.3 kDa, closely aligning with the molecular weights of these plant PMIs. Furthermore, a closer inspection of available full-length cDNA sequencing data identified an entry (accession number EU974512.1), containing both gene sequences along with a small intervening segment within a single open reading frame (Alexandrov et al., 2009; Soderlund et al., 2009).

In conclusion, all these points suggest that the two MaizeGDB entries Zm00001eb335020 and Zm00001eb335030 could be misannotated and are part of one single PMI protein. This single predicted gene (LOC100272536) comprising five exons and four introns, including a 26 kb intron (Figure 23 A), encodes a 435 amino acid protein with a molecular weight of 48 kDa. From now on, the candidate gene will be named *ZmPMI3*.

Haplotype-chemotype analysis of *ZmPMI3*

The *PMI3* gene was further analyzed for genetic variation (Figure 23). Four distinct haplotypes were detected across all varieties and the non-synonymous SNPs are located in exon 1, exon 2 and exon 5 (Figure 23 A and asterisks in Figure 22). Furthermore, SNP1 is located in the sequence corresponding to the catalytic domain, SNP2 in the helical domain and SNP3 in the C-terminal domain (Figure 22 and Figure 23 B), according to the nomenclature used in (Cleasby et al., 1996). PMI3_hap1 was found in 85 varieties, PMI3_hap2 (SNP1 G/A; location chr8_11691207; aa seq: A59T) in 28 varieties (Figure 23 C). PMI3_hap3 (SNP2 G/T; location chr8_11691635; aa seq: G166C) and PMI3_hap4 (SNP3 C/A; location chr8_11721334; aa seq: P407Q) were much rarer and detected in 7 and 6 varieties, respectively (Figure 23 C). The *PMI3* was detected in the QTL Fru_8_1 associated with absolute Fru content in corn stover, thus, the Fru content was compared between the four haplotypes (Figure 23 D). However, no significant differences were detected (Figure 23 D), which could be due to the GWAS being conducted on 212 varieties, while the haplotype-chemotype analysis included only 135 varieties. In addition to the Fru content, the total water-soluble carbohydrate content was compared among the same haplotypes (Figure 23 E). PMI3_hap1 did not differ significantly to the other haplotypes (Figure 23 E). However, PMI3_hap2 and PMI3_hap3 exhibited on average +88 % and +107 % more total water-soluble carbohydrate content than PMI3_hap4, respectively (Figure 23 E).

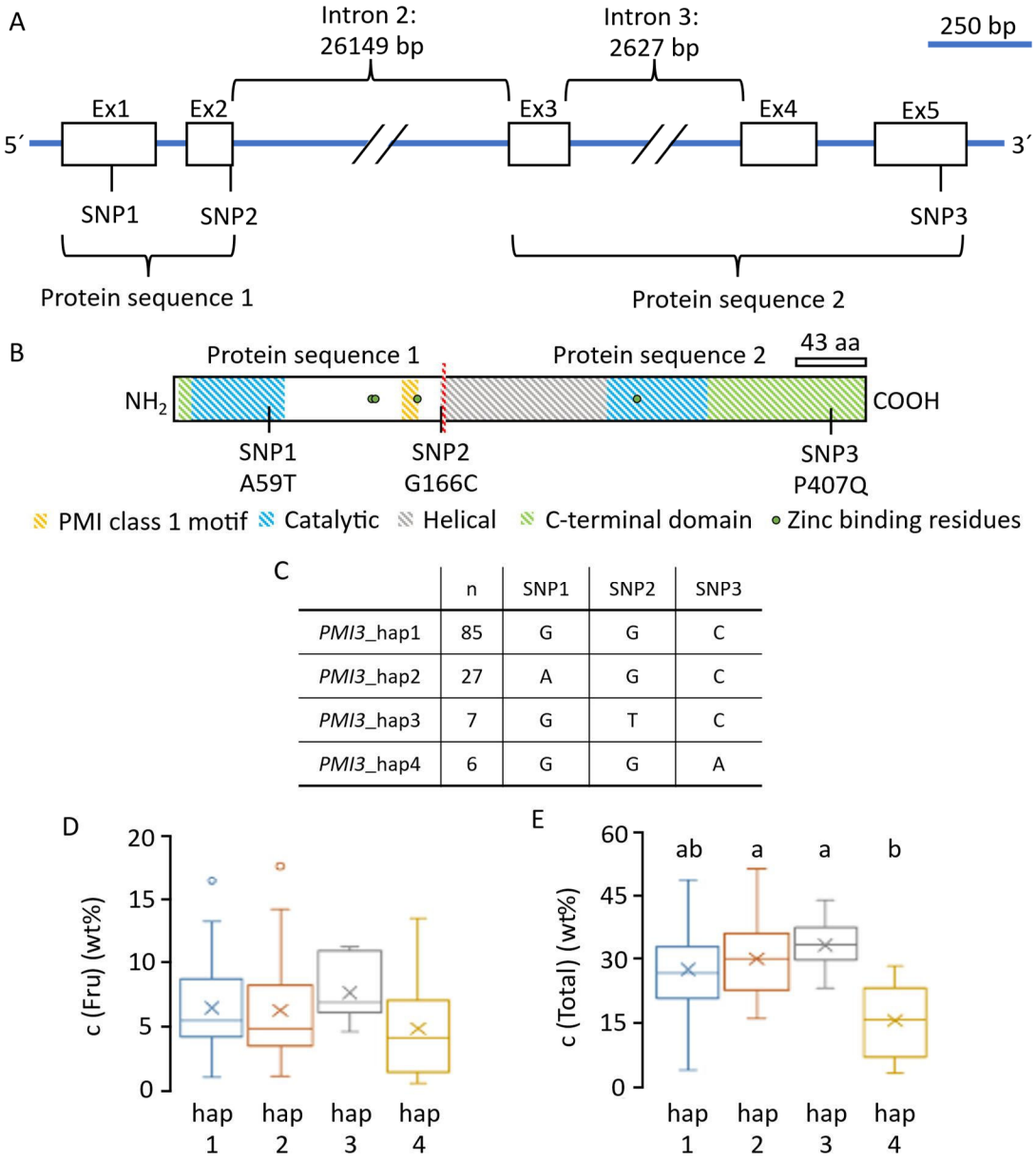

Figure 23: ***PMI3* haplotype-chemotype analysis.** A) Schematic representation of the SNP positions in the CDS of *PMI3*. If not specified, the sizes of the exons (Ex) and introns are acc. to the scale bar. B) Schematic representation of the SNP position, the PMI class 1 motif (orange), the predicted catalytic domains (blue), the helical domain (grey), the C-terminal domain (green), the Zinc binding residues (green dots) and the cut between protein sequence 1 and 2 (red) in the protein sequence of PMI3. Sizes are according to the scale bar. aa stands for amino acids. Domains are determined based on homology to *Ca*PMI and the results of (Cleasby et al., 1996). C) Non-synonymous single nucleotide polymorphisms and their distribution across the individual haplotypes. D) Fructose (Fru) content and E) total water-soluble carbohydrate content (Total) in wt% of ZmPMI_hap1 to ZmPMI_hap4. Data are shown as the AVG ± SD. No significant differences were found for Fru, determined with a Kruskal-Wallis test, followed by Dunn´s multiple comparison test with Bonferroni adjusted $p < 0.008$, due to non-normal data distribution. (D). Letters in E indicate statistically significant differences between the haplotypes, identified with a One-Way ANOVA followed by a Tukey-HSD test with $p < 0.05$.

F6P and M6P synthesis activity of PMI3 haplotypes

PMIs catalyze the reversible reaction converting mannose-6-phosphate (M6P) to fructose-6-phosphate (F6P). To assess PMI activity in the direction of F6P synthesis a coupled *in vitro* assay was employed, where phosphoglucose isomerase (PGI) converts F6P into G6P. G6P is then oxidized by D-glucose-6-phosphate dehydrogenase (G6PDH), into gluconate-6-phosphate, concomitantly reducing β-$NADP^+$ to NADPH, which is quantified spectrophotometrically as a measure of PMI activity (Hu et al., 2016; Maruta et al., 2008) (Figure 24 A). To test, if the identified maize PMI3 is a functional PMI and to confirm the prediction that it is one annotated protein, PMI3_hap1 (present in maize reference variety B73) was expressed in the the TnT® SP6 High-Yield Wheat Germ Protein Expression System. The total protein content was determined with a Bradford assay (Appendix Table 33) and the F6P synthesis activity tested without further purification. TnT® SP6 expression mix samples without expression vector were included as “no protein” control. Two different PMI3_hap1 protein concentrations were added to the reaction mixtures containing PGI, G6PDH, β-NADP and various concentrations of the M6P substrate. The absorption increase at 340 nm was monitored as a proxy for the reduction of β-$NADP^+$ to NADPH over time. The detected absorbance was blanked against the background absorbance measured in the no protein controls. The initial enzyme activity was determined based on the initial linear absorption increase and plotted over the substrate concentration (Figure 24 A). And the results show that PMI3_hap1 exhibits F6P synthesis activity (Figure 24 A). Furthermore, the reaction kinetic for F6P synthesis followed Michaelis-Menten kinetics. The Km and Vmax values of this reaction were then estimated from the Lineweaver Burk plot as 335.1 ± 35.9 µM and 217.7 ± 12.5 µmol/min/mg total protein, respectively (Figure 24 A).

To determine if PMI3_hap1 additionally exhibits M6P synthesis activity, an endpoint measurement was used. The protein produced in the TnT® SP6 expression system was incubated with F6P for one hour and the resulting sugar phosphate mixtures separated via HPAEC and quantified using standards (Figure 24 B). In the no protein control sample, no M6P was detected, indicating that the TnT® SP6 expression system has no background PMI activity (Figure 24). However, an unexpectedly high concentration of G6P (62.0 % of total phosphate sugars) was observed (Figure 24 B orange bar), which indicates that background PGI activity is present, further converting

F6P to G6P. For PMI3_hap1, M6P (3.6 % of total phosphate sugars) was detected (Figure 24 B black bar), which indicates that PMI3_hap1 exhibits M6P synthesizing activity. Due to the PGI background activity, G6P (62.3 % of total phosphate sugars) was also formed in the PMI3_hap1 sample (Figure 24 B). Since both PMI and PGI compete for the same F6P substrate (Figure 21), the presence of PGI could result in reduced M6P synthesis.

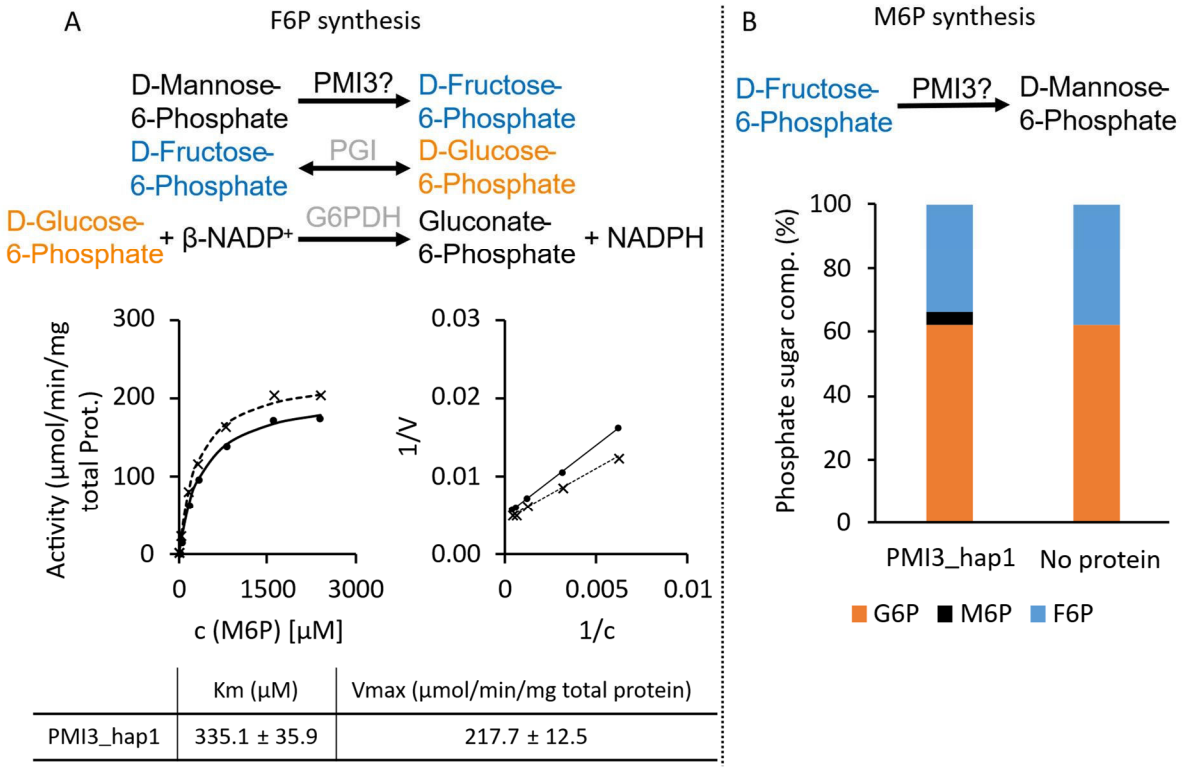

	Km (µM)	Vmax (µmol/min/mg total protein)
PMI3_hap1	335.1 ± 35.9	217.7 ± 12.5

Figure 24: **Characterization of PMI3_hap1 activity. A) Enzyme kinetics of PMI3_hap1 F6P synthesis activity measured in coupled enzymatic assay.** PMI: phosphomannose isomerase, PGI: phosphoglucose isomerase, G6PDH: D-glucose-6-phosphate dehydrogenase. In the final reaction NADP is reduced to NADPH, which results in an absorption increase at a wavelength of 340 nm. For the Michaelis-Menten plot, the results are depicted as the individual measurements of two different protein concentrations (points and crosses) in activity (µmol/min/mg total protein) over concentration of substrate M6P (µM). The curves are calculated based on the Vmax and Km values determined with the Lineweaver Burk plot, which is depicted in 1/activity over 1/substrate concentration. **B) M6P synthesis activity measurement of PMI3_hap1.** Phosphate sugar composition (% of total phosphate sugars) after mixing PMI3_hap1 and a negative control ("No protein") with F6P as substrate. Detected were fructose-6-phosphate (F6P, blue), mannose-6-phosphate (M6P, black) and glucose-6-phosphate (G6P, orange).

Together these results indicate that the produced PMI3_hap1 protein has both M6P and F6P synthase activities, which supports the hypothesis that it is a functional PMI and that the annotation of the two MaizeGDB entries as a single protein is correct. To now further analyze potential SNP-related effects on the protein activity, the different

haplotypes were expressed with the same TnT® SP6 system and their kinetic parameters for the F6P synthesis activity compared (Figure 25 and Appendix Figure 40). The high PGI background activity in the TnT® SP6 system interferes with the quantitative determination of M6P synthesis activity of PMI3. Hence, this reaction was not compared among the haplotypes.

Measuring the F6P synthesis, all four haplotypes showed increasing absorbance at 340 nm over time, indicating that M6P is converted to F6P by all protein versions. Based on this, the initial activity was calculated following the same procedure as described for PMI3_hap1. These values were then used to plot the Michaelis Menten and Lineweaver Burk graphs (Appendix Figure 40) to further calculate the haplotype-specific Vmax (µmol/min/mg total protein) and Km (µM) values (Figure 25).

	Km (µM)	Vmax (µmol/min/mg total protein)
PMI3_hap1	335.1 ± 35.9	217.7 ± 12.5 ac
PMI3_hap2	364.4 ± 31.5	286.3 ± 16.3 b
PMI3_hap3	412.6 ± 64.1	228.0 ± 2.7 ab
PMI3_hap4	417.7 ± 18.0	154.6 ± 7.8 c

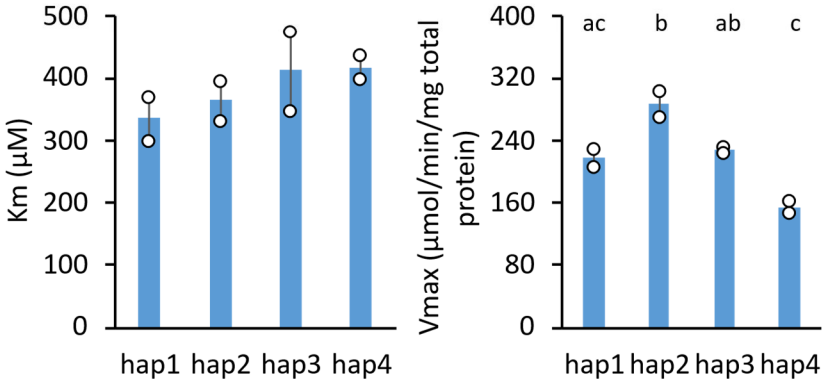

Figure 25: **Kinetics of F6P synthesis activity of distinct PMI3 haplotypes.** Significant differences are indicated by the letters and were determined with a one-way ANOVA followed by a Tukey HSD/Kramer test with $p < 0.05$. Data are shown as the average ± SD of the two concentrations tested in the activity assay for each haplotype. No significant differences were found for the Km values.

The Km values were not significantly different across all four haplotypes and ranged from 335.1 ± 35.9 µM for PMI3_hap1 to 417.7 ± 18.0 µM for PMI3_hap4 (Figure 25). However, the Vmax values differed significantly between the haplotypes, indicating that the proteins bind the substrate equally well, but their catalytic activities differ.

Compared to PMI3_hap1, PMI3_hap2 showed significantly higher Vmax (217.7 ± 12.5 vs. 286.3 ± 16.3 µmol/min/mg total protein, respectively) (Figure 25). PMI3_hap3 displayed similar Vmax at 228.0 ± 2.7 µmol/min/mg total protein as PMI3_hap1 and PMI3_hap2 (Figure 25). And PMI3_hap4 showed reduced Vmax at 154.6 ± 7.8 µmol/min/mg total protein, which did not differ significantly from PMI3_hap1, but from both PMI3_hap2 and PMI3_hap3 (Figure 25). SNP3 (differentiating PMI3_hap4 from PMI3_hap1) is not located in a predicted functional domain (Figure 23 B), the protein PMI3_hap4 exhibited the lowest Vmax (Figure 25). In addition, corn varieties that contained PMI3_hap4 showed significantly reduced total water-soluble carbohydrate content compared to PMI3_hap2 and PMI3_hap3 containing varieties (Figure 23 E), which could be an indication for an involvement of PMI3 in water-soluble carbohydrate metabolism in maize. Furthermore, the significant increase in Vmax detected for PMI3_hap2 compared to PMI3_hap1 and PMI3_hap4 is interesting, as the non-synonymous SNP1 is in the predicted active site (Figure 23 B). This could indicate that this SNP is beneficial for the F6P synthesis activity of PMI3.

4.5.3 Discussion

The third candidate gene identified from the GWAS was *ZmPMI3* identified in the QTL Fru_8_1, which was associated with the Fru content in corn stover. The sequence analysis suggests that *ZmPMI3* corresponds to the two entries in MaizeGDB, Zm00001eb335020 and Zm00001eb335030. While they are currently annotated as two repeated genes, the sequence alignment coupled with domain comparisons with characterized PMIs from rice and *C. albicans* indicates a missannotation in the database. Each fragment contains conserved elements typical of PMIs, but only together do they reconstitute the catalytical, helical and C-terminal domains described in other species (Figure 22 and Figure 23 B). Consistently, the combined predicted molecular weight of the two fragments matches that of other plant PMIs, while the individual fragments are considerably smaller. Mining of maize full length cDNA databases identified a reported open reading frame spanning both annotated regions (Alexandrov et al., 2009; Soderlund et al., 2009). Furthermore, the results presented here show that *Zm*PMI3 catalyzes the isomeric reaction between M6P and F6P, since both M6P- and F6P-synthesizing activities were detected in the respective assays (Figure 24). Taken together, these findings suggest that *ZmPMI3* could be a single gene encompassing both annotated entries.

In planta, PMIs occupy a central role in carbohydrate metabolism (Figure 21). *ZmPMI3* was identified in a QTL associated with the Fru content in corn stover. Furthermore, four distinct haplotypes of *ZmPMI3* were detected across the maize varieties. While no significant differences in Fru levels were detected between the haplotypes (Figure 23 D), it is still possible that changes in PMI activity could affect Fru accumulation in corn stover. Specifically, changes in PMI3 activity may alter the size of the F6P pool, a central glycolytic intermediate and the direct phosphorylated form of Fru generated by hexokinases or fructokinases (Figure 21) (Granot et al., 2014). A reduction in F6P via its conversion to M6P by *Zm*PMI3 could increase the demand for Fru phosphorylation, thereby lowering free Fru pools.

Interestingly, the haplotypes differed significantly in total water-soluble carbohydrate content (Figure 23 E), which correlated with differences in kinetic properties of the *Zm*PMI3 proteins (Figure 25). All haplotypes displayed F6P synthesis activity, but *Zm*PMI3_hap2 exhibited significantly higher catalytic activity compared to

*Zm*PMI3_hap1 and *Zm*PMI3_hap4 (Figure 25). Furthermore, varieties carrying *ZmPMI3*_hap2 accumulated significantly more water-soluble carbohydrates than *ZmPMI3*_hap4 varieties (Figure 23 E). Future work is needed to identify a link between PMI activity and total water-soluble carbohydrate content. One possible explanation is that increased *Zm*PMI3 activity enhances the interconversion between M6P and F6P, thereby influencing metabolic fluxes linked to carbohydrate homeostasis. Since this reaction provides intermediates for the Smirnoff-Wheeler pathway from Glc to L-Ascorbic acid (AsA) biosynthesis (Maruta et al., 2008; Wheeler et al., 1998), variation in *Zm*PMI3 activity could indirectly affect stress physiology. AsA mediates abiotic stress tolerance, including high light, drought, temperature, and salinity, and increased AsA levels have been linked to higher photosynthetic rates in rice and can support ATP production in maize chloroplasts (Ivanov et al., 2007; Y. Liu et al., 2011; Venkatesh & Park, 2014). Thus, it is conceivable that *Zm*PMI3 haplotypes indirectly affect water-soluble carbohydrate accumulation via stress responses. In maize, these carbohydrates act as reserves that buffer stress responses and only then contribute to seed filling and plant function (Cazetta & Revoredo, 2018; Sekhon et al., 2016; Setter et al., 2001; Slewinski, 2012) and a more stress-resilient plant might conserve these carbohydrates more efficiently.

Two other *PMI* genes are predicted in maize, thus, functional redundancy or involvement in different pathways is possible. The expression of *ZmPMI1* and *ZmPMI2* was found to be low during regular growth and transcript levels were not increased during salt or drought stress, unlike other key genes involved in the Smirnoff/Wheeler pathway, like *ZmPGI2* (C. Yu et al., 2021). However, *ZmPMI3* was not assessed in that study, potentially because the two individual gene fragments lack features of a functional PMI. Thus, it is possible that *ZmPMI3* is involved in mediating stress responses of the Smirnoff/Wheeler pathway. Expression analysis of *ZmPMI3* during regular and stress conditions, like prolonged light or darkness, would help to clarify if it is involved in a stress response pathway. In *A. thaliana*, increased expression was obtained for *Atpmi1* during continuous lights, while *Atpmi2* showed increased expression during extensive darkness (Maruta et al., 2008), suggesting isoform-specific regulation that could also occur in maize.

In maize, several mutant lines (BonnMu0205675::Mu to BonnMu0205677::Mu; BonnMu0498735::Mu and BonnMu0498736::Mu) with insertions in the *ZmPMI3* exons

are available from the Bonn mutant project (Marcon et al., 2020), which could be used to monitor the influence of *ZmPMI3* knock-out or knock-down on stem carbohydrate content. Further, the abiotic stress resistance mediated via AsA of these mutants could be monitored and would help to identify a potential involvement of *ZmPMI3*. Following the same approach as hypothesized for the other gene candidates, these knock-out mutants could be used to study phenotype complementation of the different *ZmPMI3*_haplotypes. Of the identified SNPs in, especially SNP1, distinguishing *ZmPMI3*_hap1 and *ZmPMI3*_hap2 (Figure 23 B), is interesting, as it is located in the predicted catalytic domain and the mutated protein exhibited significantly increased Vmax for F6P synthesis activity. It would help to further study the protein in a purified state. Purification could be achieved via GST- or His-tag purification after *E. coli* expression, as previously shown for other plant PMIs (Hu et al., 2016; Maruta et al., 2008). Doing activity assay with the purified proteins would allow the determination of specific kinetic parameters of each haplotype, without background activity, as was the case in this work. This would also help to compare the M6P synthesis activity across all haplotypes and potentially identify different velocities or substrate affinities, which could influence the carbohydrate homeostasis *in planta*.

In conclusion, the results of this work indicate that *Zm*PMI3 is a functional phosphomannose isomerase that could be related to the water-soluble carbohydrate content in corn stover. One superior haplotype was identified (*ZmPMI3*_hap2), which showed increased total water-soluble carbohydrate content and the mutated protein exhibited increased F6P synthesis activity. These findings highlight PMI3 as a promising target for metabolic engineering aimed at improving corn stover biomass composition for bioconversion processes.

5 Conclusions

The aim of this thesis was to determine if and how *U. maydis* utilizes corn stover as a carbon source and how maize genetic diversity shapes the availability of these resources. By combining a microtiter plate cultivation platform with compositional analysis, a genome-wide association study and functional characterization of candidate genes, several key insights emerged, elaborated on in the following.

U. maydis is able to grow on corn stover as the sole carbon source, and its performance can be robustly monitored by coupling online cultivation data with biochemical residue analysis. The major bottleneck lies in the poor fungal utilization of the lignocellulosic fraction. However, combining a lignin mutant (*bm3*) with a lignocellulolytic enzyme pretreatment improved performance by 196 %, reflecting both enhanced lignocellulose degradation and an intrinsically higher water-soluble carbohydrate content in *bm3* stover compared to the B73 wildtype. Across different corn genotypes, the water-soluble carbohydrates emerged as the dominant carbon source for *U. maydis*, with fungal performance correlating strongly with their abundance (R = 0.92).

The water-soluble carbohydrate content in corn stover is a highly variable trait and ranges from 2 – 52 wt% across a European natural variation panel. A genome-wide association study identified 37 QTLs associated with seven water-soluble carbohydrate-related traits. From within these QTLs, three candidate genes were selected for further studies: *ZmSWI3C1*, a subunit of a Switch/Sucrose Non-Fermenting chromatin remodeling complex, the *ZmSWEET2a* sugar transporter and a misannotated *ZmPMI3* phosphomannose isomerase gene involved in sugar metabolism. A superior haplotype of *ZmSWI3C1* was associated with increased Suc content in corn stover, making it an interesting candidate to further investigate transcriptional control of Suc content by chromatin remodeling complexes. The putative carbohydrate transporter *ZmSWEET2a* localized predominantly to the vacuole membrane in heterologous systems, suggesting a direct role in mediating Glc transport across the tonoplast and contributing to vacuolar storage in mature maize stems. Finally, this work reports *ZmPMI3* as the first functionally characterized phosphomannose isomerase in maize. A non-synonymous SNP in the catalytic domain results in increased F6P synthesis activity and SNP-containing varieties exhibited

increased water-soluble carbohydrate content, linking *Zm*PMI3 activity with sugar metabolism and water-soluble carbohydrate accumulation in corn stover.

Together, these findings establish that water-soluble carbohydrates, rather than lignocellulose, are the decisive carbon source influencing fungal bioconversion of corn stover. The strong natural variation and the identification of candidate genes provide entry points for potential breeding of maize varieties with optimized water-soluble carbohydrate content for microbial utilization. More broadly, the platform developed in this work could be expanded to study other bioconversion systems, including other plant biomasses and fungal production organisms, and provides an important first step to scale-up fermentation from laboratory scale to production scales.

6 References

Akter, S., Zabed, H. M., Sahu, J. N., Chowdhury, F. I., Faruq, G., Boyce, A. N., & Qi, X. (2020). Bioethanol production from water-soluble and structural carbohydrates of normal and high sugary corn stovers harvested at three growth stages. *Energy Conversion and Management*, *221*(April), 113104. https://doi.org/10.1016/j.enconman.2020.113104

Alexandrov, N. N., Brover, V. V., Freidin, S., Troukhan, M. E., Tatarinova, T. V., Zhang, H., Swaller, T. J., Lu, Y. P., Bouck, J., Flavell, R. B., & Feldmann, K. A. (2009). Insights into corn genes derived from large-scale cDNA sequencing. *Plant Molecular Biology*, *69*(1–2), 179–194. https://doi.org/10.1007/s11103-008-9415-4

Alves, L. C., Llerena, J. P. P., Mazzafera, P., & Vicentini, R. (2019). Diel oscillations in cell wall components and soluble sugars as a response to short-day in sugarcane (Saccharum sp.). *BMC Plant Biology*, *19*(1), 1–14. https://doi.org/10.1186/s12870-019-1837-4

Andlar, M., Rezić, T., Marđetko, N., Kracher, D., Ludwig, R., & Šantek, B. (2018). Lignocellulose degradation: An overview of fungi and fungal enzymes involved in lignocellulose degradation. *Engineering in Life Sciences*, *18*(11), 768–778. https://doi.org/10.1002/elsc.201800039

Apriyanto, A., Compart, J., & Fettke, J. (2022). A review of starch, a unique biopolymer – Structure, metabolism and in planta modifications. *Plant Science*, *318*(February), 111223. https://doi.org/10.1016/j.plantsci.2022.111223

Baloch, R. I., Mercer, E. I., Wiggins, T. E., & Baldwin, B. C. (1984). Inhibition of ergosterol biosynthesis in saccharomyces cerevisiae and Ustilago maydis by tridemorph, fenpropimorph and fenpropidin. *Phytochemistry*, *23*(10), 2219–2226. https://doi.org/10.1016/S0031-9422(00)80523-3

Banuett, F. (1992). Ustilago maydis, the delightful blight. *Trends in Genetics*, *8*(5), 174–180. https://doi.org/10.1016/0168-9525(92)90220-X

Barrière, Y. (2017). Brown-midrib genes in maize and their efficiency in dairy cow feeding. Perspectives for breeding improved silage maize targeting gene modifications in the monolignol and p-hydroxycinnamate pathways. *Maydica*,

62(2).

Barrière, Y., Chavigneau, H., Delaunay, S., Courtial, A., Bosio, M. A., Lassagne, H., Derory, J., Lapierre, C., Méchin, V., & Tatout, C. (2013). Different mutations in the ZmCAD2 gene underlie the maize brown-midrib1 (bm1) phenotype with similar effects on lignin characteristics and have potential interest for bioenergy production. *Maydica*, *58*(1), 6–20.

Bian, Y., Gu, X., Sun, D., Wang, Y., Yin, Z., Deng, D., Wang, Y., & Li, G. (2015). Mapping dynamic QTL of stalk sugar content at different growth stages in maize. *Euphytica*, *205*(1), 85–94. https://doi.org/10.1007/s10681-015-1397-0

Bian, Y., Sun, D., Gu, X., Wang, Y., Yin, Z., Deng, D., Wang, Y., Wu, F., & Li, G. (2014). Identification of QTL for stalk sugar-related traits in a population of recombinant inbred lines of maize. *Euphytica*, *198*(1), 79–89. https://doi.org/10.1007/s10681-014-1085-5

Bichot, A., Delgenès, J. P., Méchin, V., Carrère, H., Bernet, N., & García-Bernet, D. (2018). Understanding biomass recalcitrance in grasses for their efficient utilization as biorefinery feedstock. *Reviews in Environmental Science and Biotechnology*, *17*(4), 707–748. https://doi.org/10.1007/s11157-018-9485-y

Bihmidine, S., Baker, R. F., Hoffner, C., & Braun, D. M. (2015). Sucrose accumulation in sweet sorghum stems occurs by apoplasmic phloem unloading and does not involve differential Sucrose transporter expression. *BMC Plant Biology*, *15*(1), 1–22. https://doi.org/10.1186/s12870-015-0572-8

Billett, E. E., & Burnett, J. H. (1978). The host-parasite physiology of the maize smut fungus, Ustilago maydis I. The effect of smut infection on maize growth. *Physiological Plant Pathology*, *12*(1), 93–102. https://doi.org/10.1016/0048-4059(78)90022-X

Biswas, G. C. G., Ransom, C., & Sticklen, M. (2006). Expression of biologically active Acidothermus cellulolyticus endoglucanase in transgenic maize plants. *Plant Science*, *171*(5), 617–623. https://doi.org/10.1016/j.plantsci.2006.06.004

Bonangelino, C. J., Chavez, E. M., & Bonifacino, J. S. (2002). Genomic screen for vacuolar protein sorting genes in Saccharomyces cerevisiae. *Molecular Biology of*

the Cell, *13*(7), 2486–2501. https://doi.org/10.1091/mbc.02-01-0005

Bonifacino, J. S., & Traub, L. M. (2003). Signals for sorting of transmembrane proteins to endosomes and lysosomes. *Annual Review of Biochemistry*, *72*, 395–447. https://doi.org/10.1146/annurev.biochem.72.121801.161800

Boyer, L. A., Latek, R. R., & Peterson, C. R. (2004). The SANT domain-a unique histone-tail-binding module? *Nature Reviews Molecular Cell Biology*, *5*(February), 158–163.

Bradbury, P. J., Zhang, Z., Kroon, D. E., Casstevens, T. M., Ramdoss, Y., & Buckler, E. S. (2007). TASSEL: Software for association mapping of complex traits in diverse samples. *Bioinformatics*, *23*(19), 2633–2635. https://doi.org/10.1093/bioinformatics/btm308

Braun, D. M., Wang, L., & Ruan, Y. L. (2014). Understanding and manipulating sucrose phloem loading, unloading, metabolism, and signalling to enhance crop yield and food security. *Journal of Experimental Botany*, *65*(7), 1713–1735. https://doi.org/10.1093/jxb/ert416

Bräutigam, A., & Gowik, U. (2016). Photorespiration connects C3 and C4 photosynthesis. *Journal of Experimental Botany*, *67*(10), 2953–2962. https://doi.org/10.1093/jxb/erw056

Brunecky, R., Selig, M. J., Vinzant, T. B., Himmel, M. E., Lee, D., Blaylock, M. J., & Decker, S. R. (2011). In planta expression of A. cellulolyticus Cel5A endocellulase reduces cell wall recalcitrance in tobacco and maize. *Biotechnology for Biofuels*, *4*(January). https://doi.org/10.1186/1754-6834-4-1

Buanafina, M. M. d. O., Morris, P., Dalton, S., Buanafina, M. F., & Wang, Y. (2025). Late-stage changes in the composition of cell walls of maize plants expressing an apoplast targeted, senescence enhanced fungal ferulic acid esterase, and the subsequent effects on tissue saccharification. *PLoS ONE*, *20*(1 JANUARY), 1–24. https://doi.org/10.1371/journal.pone.0315950

Buanafina, M. M. de O., Buanafina, M. F., Dalton, S., Morris, P., Kowalski, M., Yadav, M. K., & Capper, L. (2020). Probing the role of cell wall feruloylation during maize development by differential expression of an apoplast targeted fungal ferulic acid

esterase. *PLoS ONE*, *15*(10), 1–29. https://doi.org/10.1371/journal.pone.0240369

Bulone, V., Schwerdt, J. G., & Fincher, G. B. (2019). Co-evolution of Enzymes Involved in Plant Cell Wall Metabolism in the Grasses. *Frontiers in Plant Science*, *10*(August). https://doi.org/10.3389/fpls.2019.01009

Burton, R. A., Collins, H. M., Kibble, N. A. J., Smith, J. A., Shirley, N. J., Jobling, S. A., Henderson, M., Singh, R. R., Pettolino, F., Wilson, S. M., Bird, A. R., Topping, D. L., Bacic, A., & Fincher, G. B. (2011). Over-expression of specific HvCslF cellulose synthase-like genes in transgenic barley increases the levels of cell wall (1,3;1,4)-β-d-glucans and alters their fine structure. *Plant Biotechnology Journal*, *9*(2), 117–135. https://doi.org/10.1111/j.1467-7652.2010.00532.x

Busse-Wicher, M., Gomes, T. C. F., Tryfona, T., Nikolovski, N., Stott, K., Grantham, N. J., Bolam, D. N., Skaf, M. S., & Dupree, P. (2014). The pattern of xylan acetylation suggests xylan may interact with cellulose microfibrils as a twofold helical screw in the secondary plant cell wall of Arabidopsis thaliana. *Plant Journal*, *79*(3), 492–506. https://doi.org/10.1111/tpj.12575

Cano-Canchola, C., Acevedo, L., Ponce-Noyola, P., Flores-Martínez, A., Flores-Carreón, A., & Leal-Morales, C. A. (2000). Induction of lytic enzymes by the interaction of Ustilago maydis with zea mays tissues. *Fungal Genetics and Biology*, *29*(3), 145–151. https://doi.org/10.1006/fgbi.2000.1196

Carpita, N. C. (1996). Structure and biogenesis of the cell walls of grasses. *Annual Review of Plant Physiology and Plant Molecular Biology*, *47*(1), 445–476. https://doi.org/10.1146/annurev.arplant.47.1.445

Carpita, N. C., & McCann, M. C. (2010). The maize mixed-linkage (1→3),(1→4)-β-D-glucan polysaccharide is synthesized at the golgi membrane. *Plant Physiology*, *153*(3), 1362–1371. https://doi.org/10.1104/pp.110.156158

Cazetta, J. O., & Revoredo, M. D. (2018). Non-structural carbohydrate metabolism, growth, and productivity of maize by increasing plant density. *Agronomy*, *8*(11), 1–15. https://doi.org/10.3390/agronomy8110243

Chandrakanth, N. N., Zhang, C., Freeman, J., de Souza, W. R., Bartley, L. E., & Mitchell, R. A. C. (2023). Modification of plant cell walls with hydroxycinnamic

acids by BAHD acyltransferases. *Frontiers in Plant Science*, *13*(January), 1–15. https://doi.org/10.3389/fpls.2022.1088879

Chang, V. S., & Holtzapple, M. T. (2000). Fundamental factors affecting biomass enzymatic reactivity. *Applied Biochemistry and Biotechnology*, *84–86*(1), 5–37. https://doi.org/10.1385/abab:84-86:1-9:5

Chen, C., Zhao, X., Wang, X., Wang, B., Li, H., Feng, J., & Wu, A. (2021). Mutagenesis of UDP-xylose epimerase and xylan arabinosyl-transferase decreases arabinose content and improves saccharification of rice straw. *Plant Biotechnology Journal*, *19*(5), 863–865. https://doi.org/10.1111/pbi.13552

Chen, H. Y., Huh, J. H., Yu, Y. C., Ho, L. H., Chen, L. Q., Tholl, D., Frommer, W. B., & Guo, W. J. (2015). The Arabidopsis vacuolar sugar transporter SWEET2 limits carbon sequestration from roots and restricts Pythium infection. *Plant Journal*, *83*(6), 1046–1058. https://doi.org/10.1111/tpj.12948

Chen, L. Q., Cheung, L. S., Feng, L., Tanner, W., & Frommer, W. B. (2015). Transport of sugars. *Annual Review of Biochemistry*, *84*, 865–894. https://doi.org/10.1146/annurev-biochem-060614-033904

Chen, L. Q., Hou, B. H., Lalonde, S., Takanaga, H., Hartung, M. L., Qu, X. Q., Guo, W. J., Kim, J. G., Underwood, W., Chaudhuri, B., Chermak, D., Antony, G., White, F. F., Somerville, S. C., Mudgett, M. B., & Frommer, W. B. (2010). Sugar transporters for intercellular exchange and nutrition of pathogens. *Nature*, *468*(7323), 527–532. https://doi.org/10.1038/nature09606

Chen, S. F., Mowery, R. A., Scarlata, C. J., & Chambliss, C. K. (2007). Compositional analysis of water-soluble materials in corn stover. *Journal of Agricultural and Food Chemistry*, *55*(15), 5912–5918. https://doi.org/10.1021/jf0700327

Chen, X., He, C., Xu, H., Zeng, G., Huang, Q., Deng, Z., Qin, X., Shen, X., & Hu, Y. (2024). Characterization of the SWI/SNF complex and nucleosome organization in sorghum. *Frontiers in Plant Science*, *15*(June), 1–15. https://doi.org/10.3389/fpls.2024.1430467

Chen, Y., Stevens, M. A., Zhu, Y., Holmes, J., & Xu, H. (2013). Understanding of alkaline pretreatment parameters for corn stover enzymatic saccharification.

Biotechnology for Biofuels, *6*(8). https://doi.org/10.1186/1754-6834-6-8

Christensen, C. S. L., & Rasmussen, S. K. (2019). Low lignin mutants and reduction of lignin content in grasses for increased utilisation of lignocellulose. In *Agronomy* (Vol. 9, Issue 5). https://doi.org/10.3390/agronomy9050256

Cleasby, A., Wonacott, A., Skarzynski, T., Hubbard, R. E., Davies, G. J., Proudfoot, A. E. I., Bernard, A. R., Payton, M. A., & Wells, T. N. C. (1996). The X-ray crystal structure of phosphomannose isomerase from Candida albicans at 1.7 Å resolution. *Nature Structural Biology*, *3*(5), 470–479. https://doi.org/10.1038/nsb0596-470

Coomey, J. H., Sibout, R., & Hazen, S. P. (2020). Grass secondary cell walls, Brachypodium distachyon as a model for discovery. *New Phytologist*, *227*(6), 1649–1667. https://doi.org/10.1111/nph.16603

Cosgrove, D. J. (2014). Re-constructing our models of cellulose and primary cell wall assembly. *Current Opinion in Plant Biology*, *22*, 122–131. https://doi.org/10.1016/j.pbi.2014.11.001

Cosgrove, D. J. (2024). Structure and growth of plant cell walls. *Nature Reviews Molecular Cell Biology*, *25*(5), 340–358. https://doi.org/10.1038/s41580-023-00691-y

Coulin, F., Magnenat, E., Proudfoot, A. E. I., Payton, M. A., Scully, P., & Wells, T. N. C. (1993). Identification of Cys-150 in the Active Site of Phosphomannose Isomerase from Candida albicans. *Biochemistry*, *32*(51), 14139–14144. https://doi.org/10.1021/bi00214a010

Couturier, M., Navarro, D., Olivé, C., Chevret, D., Haon, M., Favel, A., Lesage-Meessen, L., Henrissat, B., Coutinho, P. M., & Berrin, J. G. (2012). Post-genomic analyses of fungal lignocellulosic biomass degradation reveal the unexpected potential of the plant pathogen Ustilago maydis. *BMC Genomics*, *13*(1). https://doi.org/10.1186/1471-2164-13-57

Da Silva, A. S. A., Inoue, H., Endo, T., Yano, S., & Bon, E. P. S. (2010). Milling pretreatment of sugarcane bagasse and straw for enzymatic hydrolysis and ethanol fermentation. *Bioresource Technology*, *101*(19), 7402–7409.

https://doi.org/10.1016/j.biortech.2010.05.008

Depge-Fargeix, N., Javelle, M., Chambrier, P., Frangne, N., Gerentes, D., Perez, P., Rogowsky, P. M., & Vernoud, V. (2011). Functional characterization of the HD-ZIP IV transcription factor OCL1 from maize. *Journal of Experimental Botany*, *62*(1), 293–305. https://doi.org/10.1093/jxb/erq267

Desfougères, Y., Vavassori, S., Rompf, M., Gerasimaite, R., & Mayer, A. (2016). Organelle acidification negatively regulates vacuole membrane fusion in vivo. *Scientific Reports*, *6*(July), 1–16. https://doi.org/10.1038/srep29045

Doehlemann, G., Wahl, R., Vranes, M., de Vries, R. P., Kämper, J., & Kahmann, R. (2008). Establishment of compatibility in the Ustilago maydis/maize pathosystem. *Journal of Plant Physiology*, *165*(1), 29–40. https://doi.org/10.1016/j.jplph.2007.05.016

Drula, E., Garron, M. L., Dogan, S., Lombard, V., Henrissat, B., & Terrapon, N. (2022). The carbohydrate-active enzyme database: functions and literature. *Nucleic Acids Research*, *50*(D1), D571–D577. https://doi.org/10.1093/nar/gkab1045

Duguid, K. B., Montross, M. D., Radtke, C. W., Crofcheck, C. L., Wendt, L. M., & Shearer, S. A. (2009). Effect of anatomical fractionation on the enzymatic hydrolysis of acid and alkaline pretreated corn stover. *Bioresource Technology*, *100*(21), 5189–5195. https://doi.org/10.1016/j.biortech.2009.03.082

Duong, H. L., Paufler, S., Harms, H., Schlosser, D., & Maskow, T. (2022). Fungal Lignocellulose Utilisation Strategies from a Bioenergetic Perspective: Quantification of Related Functional Traits Using Biocalorimetry. *Microorganisms*, *10*(8). https://doi.org/10.3390/microorganisms10081675

Eom, J. S., Chen, L. Q., Sosso, D., Julius, B. T., Lin, I. W., Qu, X. Q., Braun, D. M., & Frommer, W. B. (2015). SWEETs, transporters for intracellular and intercellular sugar translocation. *Current Opinion in Plant Biology*, *25*(May), 53–62. https://doi.org/10.1016/j.pbi.2015.04.005

Fanelli, A., Rancour, D. M., Sullivan, M., Karlen, S. D., Ralph, J., Riaño-Pachón, D. M., Vicentini, R., Silva, T. da F., Ferraz, A., Hatfield, R. D., & Romanel, E. (2021). Overexpression of a Sugarcane BAHD Acyltransferase Alters Hydroxycinnamate

Content in Maize Cell Wall. *Frontiers in Plant Science*, *12*(April), 1–14. https://doi.org/10.3389/fpls.2021.626168

Fansuri, H., Purwandari, U., Putra, S., Adhiksana, A., Junianto, I. D., Oktavian, R., & Cordiner, J. (2024). A Review of the Technological Aspects and Process Optimization of Bioethanol Production From Corn Stover Biomass: Pretreatment Process, Hydrolysis, Fermentation, Purification Process, and Future Perspective. *Environmental Quality Management*, *34*(2), e22336. https://doi.org/https://doi.org/10.1002/tqem.22336

FAO. (2025). *Food and Agriculture Organization of the United Nations, Data, Crops and livestock products.* https://www.fao.org/faostat/en/#data/QCL

Feijao, C., Morreel, K., Anders, N., Tryfona, T., Busse-Wicher, M., Kotake, T., Boerjan, W., & Dupree, P. (2022). Hydroxycinnamic acid-modified xylan side chains and their cross-linking products in rice cell walls are reduced in the Xylosyl arabinosyl substitution of xylan 1 mutant. *Plant Journal*, *109*(5), 1152–1167. https://doi.org/10.1111/tpj.15620

Feldbrügge, M., Kellner, R., & Schipper, K. (2013). The biotechnological use and potential of plant pathogenic smut fungi. In *Applied Microbiology and Biotechnology* (Vol. 97, Issue 8, pp. 3253–3265). https://doi.org/10.1007/s00253-013-4777-1

Fincher, G. B. (2009). Exploring the evolution of (1,3;1,4)-β-d-glucans in plant cell walls: comparative genomics can help! *Current Opinion in Plant Biology*, *12*(2), 140–147. https://doi.org/10.1016/j.pbi.2009.01.002

Forestan, C., Aiese Cigliano, R., Farinati, S., Lunardon, A., Sanseverino, W., & Varotto, S. (2016). Stress-induced and epigenetic-mediated maize transcriptome regulation study by means of transcriptome reannotation and differential expression analysis. *Scientific Reports*, *6*(June), 1–20. https://doi.org/10.1038/srep30446

Fornalé, S., Capellades, M., Encina, A., Wang, K., Irar, S., Lapierre, C., Ruel, K., Joseleau, J. P., Berenguer, J., Puigdomènech, P., Rigau, J., & Caparrós-Ruiz, D. (2012). Altered lignin biosynthesis improves cellulosic bioethanol production in transgenic maize plants down-regulated for cinnamyl alcohol dehydrogenase.

Molecular Plant, *5*(4), 817–830. https://doi.org/10.1093/mp/ssr097

Foster, C. E., Martin, T. M., & Pauly, M. (2010a). Comprehensive compositional analysis of plant cell walls (Lignocellulosic biomass) part I: Lignin. *Journal of Visualized Experiments*, *37*, 5–8. https://doi.org/10.3791/1745

Foster, C. E., Martin, T. M., & Pauly, M. (2010b). Comprehensive compositional analysis of plant cell walls (Lignocellulosic biomass) part II: Carbohydrates. *Journal of Visualized Experiments*, *37*, 10–13. https://doi.org/10.3791/1837

Galbe, M., & Wallberg, O. (2019). Pretreatment for biorefineries: a review of common methods for efficient utilisation of lignocellulosic materials. *Biotechnology for Biofuels*, *12*(1), 294. https://doi.org/10.1186/s13068-019-1634-1

Gao, Y., Lipton, A. S., Wittmer, Y., Murray, D. T., & Mortimer, J. C. (2020). A grass-specific cellulose–xylan interaction dominates in sorghum secondary cell walls. *Nature Communications*, *11*(1), 6081. https://doi.org/10.1038/s41467-020-19837-z

Geiser, E., Reindl, M., Blank, L. M., Feldbrügge, M., Wierckx, N., & Schipper, K. (2016). Activating intrinsic carbohydrate-active enzymes of the smut fungus Ustilago maydis for the degradation of plant cell wall components. *Applied and Environmental Microbiology*, *82*(17), 5174–5185. https://doi.org/10.1128/AEM.00713-16

Geiser, E., Wiebach, V., Wierckx, N., & Blank, L. M. (2014). Prospecting the biodiversity of the fungal family Ustilaginaceae for the production of value-added chemicals. *Fungal Biology and Biotechnology*, *1*(1), 1–10. https://doi.org/10.1186/s40694-014-0002-y

Geiser, E., Wierckx, N., Zimmermann, M., & Blank, L. M. (2013). Identification of an endo-1,4-beta-xylanase of Ustilago maydis. *BMC Biotechnology*, *13*, 1. https://doi.org/10.1186/1472-6750-13-59

Gietz, R. D., & Schiestl, R. H. (2007). Large-scale high-efficiency yeast transformation using the LiAc/SS carrier DNA/PEG method. *Nature Protocols*, *2*(1), 38–41. https://doi.org/10.1038/nprot.2007.15

Gille, S., Cheng, K., Skinner, M. E., Liepman, A. H., Wilkerson, C. G., & Pauly, M.

(2011). Deep sequencing of voodoo lily (Amorphophallus konjac): An approach to identify relevant genes involved in the synthesis of the hemicellulose glucomannan. *Planta*, *234*(3), 515–526. https://doi.org/10.1007/s00425-011-1422-z

Gille, S., & Pauly, M. (2012). O-acetylation of plant cell wall polysaccharides. *Frontiers in Plant Science*, *3*(JAN), 1–7. https://doi.org/10.3389/fpls.2012.00012

Glass, N. L., Schmoll, M., Cate, J. H. D., & Coradetti, S. (2013). Plant cell wall deconstruction by ascomycete fungi. *Annual Review of Microbiology*, *67*, 477–498. https://doi.org/10.1146/annurev-micro-092611-150044

Glassop, D., Ryan, L. P., Bonnett, G. D., & Rae, A. L. (2010). The complement of soluble sugars in the Saccharum complex. *Tropical Plant Biology*, *3*(2), 110–122. https://doi.org/10.1007/s12042-010-9049-y

Gombos, S., Miras, M., Howe, V., Xi, L., Pottier, M., Kazemein Jasemi, N. S., Schladt, M., Ejike, J. O., Neumann, U., Hänsch, S., Kuttig, F., Zhang, Z., Dickmanns, M., Xu, P., Stefan, T., Baumeister, W., Frommer, W. B., Simon, R., & Schulze, W. X. (2023). A high-confidence Physcomitrium patens plasmodesmata proteome by iterative scoring and validation reveals diversification of cell wall proteins during evolution. *New Phytologist*, *238*(2), 637–653. https://doi.org/10.1111/nph.18730

Goñi, A. M., Fernández, J. A., Demarco, P. A., Secchi, M. A., Carcedo, A. J. P., & Ciampitti, I. A. (2024). Determination of water-soluble carbohydrates by near-infrared spectroscopy for canola, maize, and sorghum stem fractions. *Spectrochimica Acta - Part A: Molecular and Biomolecular Spectroscopy*, *304*(August 2023). https://doi.org/10.1016/j.saa.2023.123320

Gowik, U., & Westhoff, P. (2011). The Path from C3 to C4 photosynthesis. *Plant Physiology*, *155*(1), 56–63. https://doi.org/10.1104/pp.110.165308

Granot, D., Kelly, G., Stein, O., & David-Schwartz, R. (2014). Substantial roles of hexokinase and fructokinase in the effects of sugars on plant physiology and development. *Journal of Experimental Botany*, *65*(3), 809–819. https://doi.org/10.1093/jxb/ert400

Grebe, L. A., Richter, P., Altenkirch, T., Mann, M., Müller, M. J., Büchs, J., & Magnus,

J. B. (2024). Sampling-free investigation of microbial carbon source preferences on renewable feedstocks via online monitoring of oxygen transfer rate. *Bioprocess and Biosystems Engineering*, *48*(3), 413–425. https://doi.org/10.1007/s00449-024-03117-x

Grzybowski, M. W., Mural, R. V., Xu, G., Turkus, J., Yang, J., & Schnable, J. C. (2023). A common resequencing-based genetic marker data set for global maize diversity. *Plant Journal*, *113*(6), 1109–1121. https://doi.org/10.1111/tpj.16123

Halpin, C., Holt, K., Chojecki, J., Oliver, D., Chabbert, B., Monties, B., Edwards, K., Barakate, A., & Foxon, G. A. (1998). Brown-midrib maize (bm1) - A mutation affecting the cinnamyl alcohol dehydrogenase gene. *Plant Journal*, *14*(5), 545–553. https://doi.org/10.1046/j.1365-313X.1998.00153.x

Han, Y., Reyes, A. A., Malik, S., & He, Y. (2020). Cryo-EM structure of SWI/SNF complex bound to a nucleosome. *Nature*, *579*(7799), 452–455. https://doi.org/10.1038/s41586-020-2087-1

Harris, D., Bulone, V., Ding, S. Y., & DeBolt, S. (2010). Tools for cellulose analysis in plant cell walls. *Plant Physiology*, *153*(2), 420–426. https://doi.org/10.1104/pp.110.154203

Harris, D. M., Corbin, K., Wang, T., Gutierrez, R., Bertolo, A. L., Petti, C., Smilgies, D. M., Estevez, J. M., Bonetta, D., Urbanowicz, B. R., Ehrhardt, D. W., Somerville, C. R., Rose, J. K. C., Hong, M., & DeBolt, S. (2012). Cellulose microfibril crystallinity is reduced by mutating C-terminal transmembrane region residues CESA1 A903V and CESA3 T942I of cellulose synthase. *Proceedings of the National Academy of Sciences of the United States of America*, *109*(11), 4098–4103. https://doi.org/10.1073/pnas.1200352109

Hartmann, S. K., Stockdreher, Y., Wandrey, G., Hosseinpour Tehrani, H., Zambanini, T., Meyer, A. J., Büchs, J., Blank, L. M., Schwarzländer, M., & Wierckx, N. (2018). Online in vivo monitoring of cytosolic NAD redox dynamics in Ustilago maydis. *Biochimica et Biophysica Acta - Bioenergetics*, *1859*(10), 1015–1024. https://doi.org/10.1016/j.bbabio.2018.05.012

Hatfield, R. D., Rancour, D. M., & Marita, J. M. (2017). Grass cell walls: A story of cross-linking. *Frontiers in Plant Science*, *7*, 204954.

https://doi.org/10.3389/fpls.2016.02056

He, X., Hall, M. B., Gallo-Meagher, M., & Smith, R. L. (2003). Improvement of Forage Quality by Downregulation of Maize O-Methyltransferase. *Crop Science*, *43*(6), 2240–2251. https://doi.org/https://doi.org/10.2135/cropsci2003.2240

He, Y., Pang, Y., Liu, Y., Li, X., & Wang, K. (2008). Physicochemical characterization of rice straw pretreated with sodium hydroxide in the solid state for enhancing biogas production. *Energy and Fuels*, *22*(4), 2775–2781. https://doi.org/10.1021/ef8000967

Holliday, R. (1974). Ustilago maydis. *Bacteria, Bacteriophages, and Fungi*, *93*(3), 575–595. https://doi.org/10.1007/978-1-4899-1710-2_31

Horst, R. J., Engelsdorf, T., Sonnewald, U., & Voll, L. M. (2008). Infection of maize leaves with Ustilago maydis prevents establishment of C4 photosynthesis. *Journal of Plant Physiology*, *165*(1), 19–28. https://doi.org/10.1016/j.jplph.2007.05.008

Hu, L., Li, H., Qin, R., Xu, R., Li, J., Li, L., Wei, P., & Yang, J. (2016). Plant phosphomannose isomerase as a selectable marker for rice transformation. *Scientific Reports*, *6*(May), 1–10. https://doi.org/10.1038/srep25921

Hussnaetter, K. P., Philipp, M., Müntjes, K., Feldbrügge, M., & Schipper, K. (2021). Controlling unconventional secretion for production of heterologous proteins in Ustilago maydis through transcriptional regulation and chemical inhibition of the kinase Don3. *Journal of Fungi*, *7*(3), 1–21. https://doi.org/10.3390/jof7030179

Isett, K., George, H., Herber, W., & Amanullah, A. (2007). Twenty-four-well plate miniature bioreactor high-throughput system: Assessment for microbial cultivations. *Biotechnology and Bioengineering*, *98*(5), 1017–1028. https://doi.org/https://doi.org/10.1002/bit.21484

Ivanov, B., Asada, K., & Edwards, G. E. (2007). Analysis of donors of electrons to photosystem I and cyclic electron flow by redox kinetics of P700 in chloroplasts of isolated bundle sheath strands of maize. *Photosynthesis Research*, *92*(1), 65–74. https://doi.org/10.1007/s11120-007-9166-0

Jablonowski, N. D., Pauly, M., & Dama, M. (2022). Microwave Assisted Pretreatment of Szarvasi (Agropyron elongatum) Biomass to Enhance Enzymatic

Saccharification and Direct Glucose Production. *Frontiers in Plant Science*, *12*(January), 1–12. https://doi.org/10.3389/fpls.2021.767254

Jiang, S. Y., Chi, Y. H., Wang, J. Z., Zhou, J. X., Cheng, Y. S., Zhang, B. L., Ma, A., Vanitha, J., & Ramachandran, S. (2015). Sucrose metabolism gene families and their biological functions. *Scientific Reports*, *5*, 1–24. https://doi.org/10.1038/srep17583

Jilani, S. B., & Olson, D. G. (2023). Mechanism of furfural toxicity and metabolic strategies to engineer tolerance in microbial strains. *Microbial Cell Factories*, *22*(1), 1–20. https://doi.org/10.1186/s12934-023-02223-x

Kaderbek, T., Huang, L., Yue, Y., Wang, Z., Lian, J., Ma, Y., Li, J., Zhuang, J., Chen, J., Lai, J., Song, W., Bian, C., Liu, Q., & Shen, X. (2025). Identification of the maize drought-resistant gene Zinc-finger Inflorescence Meristem 23 through high-resolution temporal transcriptome analysis. *International Journal of Biological Macromolecules*, *308*(September 2024). https://doi.org/10.1016/j.ijbiomac.2025.142347

Kämper, J., Kahmann, R., Bölker, M., Ma, L. J., Brefort, T., Saville, B. J., Banuett, F., Kronstad, J. W., Gold, S. E., Müller, O., Perlin, M. H., Wösten, H. A. B., De Vries, R., Ruiz-Herrera, J., Reynaga-Peña, C. G., Snetselaar, K., McCann, M., Pérez-Martín, J., Feldbrügge, M., … Birren, B. W. (2006). Insights from the genome of the biotrophic fungal plant pathogen Ustilago maydis. *Nature*, *444*(7115), 97–101. https://doi.org/10.1038/nature05248

Kanehisa, M. (2019). Toward understanding the origin and evolution of cellular organisms. *Protein Science*, *28*(11), 1947–1951. https://doi.org/https://doi.org/10.1002/pro.3715

Kanehisa, M., Furumichi, M., Sato, Y., Matsuura, Y., & Ishiguro-Watanabe, M. (2024). KEGG: biological systems database as a model of the real world. *Nucleic Acids Research*, *53*(D1), D672–D677. https://doi.org/10.1093/nar/gkae909

Kanehisa, M., & Goto, S. (2000). KEGG: Kyoto Encyclopedia of Genes and Genomes. *Nucleic Acids Research*, *28*(1), 27–30. https://doi.org/10.1093/nar/28.1.27

Kang, X., Kirui, A., Dickwella Widanage, M. C., Mentink-Vigier, F., Cosgrove, D. J., &

Wang, T. (2019). Lignin-polysaccharide interactions in plant secondary cell walls revealed by solid-state NMR. *Nature Communications*, *10*(1), 347. https://doi.org/10.1038/s41467-018-08252-0

Keegstra, K. (2010). Plant cell walls. *Plant Physiology*, *154*(2), 483–486. https://doi.org/10.1104/pp.110.161240

Kensy, F., Engelbrecht, C., & Büchs, J. (2009). Scale-up from microtiter plate to laboratory fermenter: Evaluation by online monitoring techniques of growth and protein expression in Escherichia coli and Hansenula polymorpha fermentations. *Microbial Cell Factories*, *8*, 1–15. https://doi.org/10.1186/1475-2859-8-68

Kim, S. J., Zemelis-Durfee, S., Jensen, J. K., Wilkerson, C. G., Keegstra, K., & Brandizzi, F. (2018). In the grass species Brachypodium distachyon, the production of mixed-linkage (1,3;1,4)-β-glucan (MLG) occurs in the Golgi apparatus. *Plant Journal*, *93*(6), 1062–1075. https://doi.org/10.1111/tpj.13830

King, B. C., Waxman, K. D., Nenni, N. V., Walker, L. P., Bergstrom, G. C., & Gibson, D. M. (2011). Arsenal of plant cell wall degrading enzymes reflects host preference among plant pathogenic fungi. *Biotechnology for Biofuels*, *4*, 1–14. https://doi.org/10.1186/1754-6834-4-4

Knežević, A., Milovanović, I., Stajić, M., Lončar, N., Brčeski, I., Vukojević, J., & Ćilerdžić, J. (2013). Lignin degradation by selected fungal species. *Bioresource Technology*, *138*, 117–123. https://doi.org/10.1016/j.biortech.2013.03.182

Koressaar, T., Lepamets, M., Kaplinski, L., Raime, K., Andreson, R., & Remm, M. (2018). Primer3_masker: integrating masking of template sequence with primer design software. *Bioinformatics (Oxford, England)*, *34*(11), 1937–1938. https://doi.org/10.1093/bioinformatics/bty036

Koressaar, T., & Remm, M. (2007). Enhancements and modifications of primer design program Primer3. *Bioinformatics (Oxford, England)*, *23*(10), 1289–1291. https://doi.org/10.1093/bioinformatics/btm091

Kraemer, F. J., Lunde, C., Koch, M., Kuhn, B. M., Ruehl, C., Brown, P. J., Hoffmann, P., Go hre, V., Hake, S., Pauly, M., & Ramírez, V. (2021). A mixed-linkage (1,3;1,4)-b-D-glucan specific hydrolase mediates dark-triggered degradation of

this plant cell wall polysaccharide. *Plant Physiology*, *185*(4), 1559–1573. https://doi.org/10.1093/plphys/kiab009

Kumar, B., Bhardwaj, N., Agrawal, K., Chaturvedi, V., & Verma, P. (2020). Current perspective on pretreatment technologies using lignocellulosic biomass: An emerging biorefinery concept. *Fuel Processing Technology*, *199*(July 2019). https://doi.org/10.1016/j.fuproc.2019.106244

Kunze, M., Roth, S., Gartz, E., & Büchs, J. (2014). Pitfalls in optical on-line monitoring for high-throughput screening of microbial systems. *Microbial Cell Factories*, *13*(1). https://doi.org/10.1186/1475-2859-13-53

Lacey, J. A., Emerson, R. M., Thompson, D. N., & Westover, T. L. (2016). Ash reduction strategies in corn stover facilitated by anatomical and size fractionation. *Biomass and Bioenergy*, *90*, 173–180. https://doi.org/10.1016/j.biombioe.2016.04.006

Ladner, T., Held, M., Flitsch, D., Beckers, M., & Büchs, J. (2016). Quasi-continuous parallel online scattered light, fluorescence and dissolved oxygen tension measurement combined with monitoring of the oxygen transfer rate in each well of a shaken microtiter plate. *Microbial Cell Factories*, *15*(1), 1–15. https://doi.org/10.1186/s12934-016-0608-2

Lanver, D., Berndt, P., Tollot, M., Naik, V., Vranes, M., Warmann, T., Münch, K., Rössel, N., & Kahmann, R. (2014). Plant Surface Cues Prime Ustilago maydis for Biotrophic Development. *PLoS Pathogens*, *10*(7). https://doi.org/10.1371/journal.ppat.1004272

Laussel, C., Albanèse, V., Javier, F., Rodríguez, G., Ballin, A., Defenouillère, Q., & Léon, S. (2022). 2-deoxyglucose transiently inhibits yeast AMPK signaling and triggers glucose transporter endocytosis, potentiating the drug toxicity. *PLoS Genetics*, *18*(8), 1–28. https://doi.org/10.1371/journal.pgen.1010169

Leroy, A., Falourd, X., Foucat, L., Méchin, V., Guillon, F., & Paës, G. (2021). Evaluating polymer interplay after hot water pretreatment to investigate maize stem internode recalcitrance. *Biotechnology for Biofuels*, *14*(1), 1–18. https://doi.org/10.1186/s13068-021-02015-8

Li, C., Mao, H., Fan, X., Yu, M., & Yu, X. (2025). Transcriptomic analysis revealed that short-day treatment of seedlings promotes flowering in maize (Zea mays L.). *Genes and Genomics*. https://doi.org/10.1007/s13258-025-01640-z

Li, F., Shahsavarani, M., Handy-Hart, C.-J., Côté, A., Brasseur-Trottier, X., Montgomery, V., Beech, R., Liu, L., Bayen, S., Qu, Y., De Luca, V., & Dastmalchi, M. (2024). Characterization of a vacuolar importer of secologanin in Catharanthus roseus. *Communications Biology*, *7*. https://doi.org/10.1038/s42003-024-06624-5

Li, S. C., & Kane, P. M. (2009). The yeast lysosome-like vacuole: Endpoint and crossroads. *Biochimica et Biophysica Acta - Molecular Cell Research*, *1793*(4), 650–663. https://doi.org/10.1016/j.bbamcr.2008.08.003

Li, X., Dilokpimol, A., Kabel, M. A., & de Vries, R. P. (2022). Fungal xylanolytic enzymes: Diversity and applications. *Bioresource Technology*, *344*(PB), 126290. https://doi.org/10.1016/j.biortech.2021.126290

Li, Y., Wadsö, L., Larsson, L., & Bjurman, J. (2007). Correlating two methods of quantifying fungal activity: Heat production by isothermal calorimetry and ergosterol amount by gas chromatography-tandem mass spectrometry. *Thermochimica Acta*, *458*(1–2), 77–83. https://doi.org/10.1016/j.tca.2007.01.005

Liang, X. G., Gao, Z., Zhang, L., Shen, S., Zhao, X., Liu, Y. P., Zhou, L. L., Paul, M. J., & Zhou, S. L. (2019). Seasonal and diurnal patterns of non-structural carbohydrates in source and sink tissues in field maize. *BMC Plant Biology*, *19*(1), 1–11. https://doi.org/10.1186/s12870-019-2068-4

Lin, I. W., Sosso, D., Chen, L. Q., Gase, K., Kim, S. G., Kessler, D., Klinkenberg, P. M., Gorder, M. K., Hou, B. H., Qu, X. Q., Carter, C. J., Baldwin, I. T., & Frommer, W. B. (2014). Nectar secretion requires sucrose phosphate synthases and the sugar transporter SWEET9. *Nature*, *508*(7497), 546–549. https://doi.org/10.1038/nature13082

Liu, G., Zhang, L., Wei, X., Zou, G., Qin, Y., Ma, L., Li, J., Zheng, H., Wang, S., Wang, C., Xun, L., Zhao, G. P., Zhou, Z., & Qu, Y. (2013). Genomic and Secretomic Analyses Reveal Unique Features of the Lignocellulolytic Enzyme System of Penicillium decumbens. *PLoS ONE*, *8*(2). https://doi.org/10.1371/journal.pone.0055185

Liu, Y., Yu, L., & Wang, R. (2011). Level of ascorbic acid in transgenic rice for l-galactono-1,4-lactone dehydrogenase overexpressing or suppressed is associated with plant growth and seed set. *Acta Physiologiae Plantarum*, *33*(4), 1353–1363. https://doi.org/10.1007/s11738-010-0669-5

López-González, C., Juárez-Colunga, S., Trachsel, S., Marsch-Martínez, N., Stewart Gillmor, C., & Tiessen, A. (2022). Analysis of Global Gene Expression in Maize (Zea mays) Vegetative and Reproductive Tissues That Differ in Accumulation of Starch and Sucrose. *Plants*, *11*(3), 238. https://doi.org/10.3390/plants11030238

Loqué, D., Lalonde, S., Looger, L. L., Von Wirén, N., & Frommer, W. B. (2007). A cytosolic trans-activation domain essential for ammonium uptake. *Nature*, *446*(7132), 195–198. https://doi.org/10.1038/nature05579

Loqué, D., Scheller, H. V., & Pauly, M. (2015). Engineering of plant cell walls for enhanced biofuel production. In *Current Opinion in Plant Biology* (Vol. 25, pp. 151–161). Elsevier Ltd. https://doi.org/10.1016/j.pbi.2015.05.018

Lorenci Woiciechowski, A., Dalmas Neto, C. J., Porto de Souza Vandenberghe, L., de Carvalho Neto, D. P., Novak Sydney, A. C., Letti, L. A. J., Karp, S. G., Zevallos Torres, L. A., & Soccol, C. R. (2020). Lignocellulosic biomass: Acid and alkaline pretreatments and their effects on biomass recalcitrance – Conventional processing and recent advances. *Bioresource Technology*, *304*(January), 122848. https://doi.org/10.1016/j.biortech.2020.122848

Lunn, J. E. (2016). Sucrose Metabolism. In *Encyclopedia of Life Science* (Vol. 110, Issue 1037, pp. 1–9). John Wiley & Sons, Ltd. https://doi.org/https://doi.org/10.1002/9780470015902.a0021259.pub2

Ma, B. L., Zheng, Z. M., & Morrison, M. J. (2017). Does increasing plant population density alter sugar yield in high stalk-sugar maize hybrids? *Crop and Pasture Science*, *68*(1), 1–10. https://doi.org/10.1071/CP16393

Ma, H., Liu, W. W., Chen, X., Wu, Y. J., & Yu, Z. L. (2009). Enhanced enzymatic saccharification of rice straw by microwave pretreatment. *Bioresource Technology*, *100*(3), 1279–1284. https://doi.org/10.1016/j.biortech.2008.08.045

Madeira, F., Madhusoodanan, N., Lee, J., Eusebi, A., Niewielska, A., Tivey, A. R. N.,

Lopez, R., & Butcher, S. (2024). The EMBL-EBI Job Dispatcher sequence analysis tools framework in 2024. *Nucleic Acids Research*, *52*(W1), W521–W525. https://doi.org/10.1093/nar/gkae241

Manter, Kelsey, & Stone. (2001). Quantification of Phaeocryptopus gaeumannii colonization in Douglas-fir needles by ergosterol analysis. *Forest Pathology*, *31*(4), 229–240. https://doi.org/10.1046/j.1439-0329.2001.00243.x

Marcon, C., Altrogge, L., Win, Y. N., Stöcker, T., Gardiner, J. M., Portwood, J. L., Opitz, N., Kortz, A., Baldauf, J. A., Hunter, C. T., McCarty, D. R., Koch, K. E., Schoof, H., & Hochholdinger, F. (2020). BonnMu: A sequence-indexed resource of transposon-induced maize mutations for functional genomics studies. *Plant Physiology*, *184*(2), 620–631. https://doi.org/10.1104/pp.20.00478

Marita, J. M., Vermerris, W., Ralph, J., & Hatfield, R. D. (2003). Variations in the cell wall composition of maize brown midrib mutants. *Journal of Agricultural and Food Chemistry*, *51*(5), 1313–1321. https://doi.org/10.1021/jf0260592

Marriott, P. E., Gómez, L. D., & Mcqueen-Mason, S. J. (2016). Unlocking the potential of lignocellulosic biomass through plant science. *New Phytologist*, *209*(4), 1366–1381. https://doi.org/10.1111/nph.13684

Marten, G. C., & Westerberg, P. M. (1972). Maize Fodder—Influence of Barrenness on Yield and Quality. *Crop Science*, *12*(3), cropsci1972.0011183X001200030033x. https://doi.org/https://doi.org/10.2135/cropsci1972.0011183X001200030033x

Maruta, T., Yonemitsu, M., Yabuta, Y., Tamoi, M., Ishikawa, T., & Shigeoka, S. (2008). Arabidopsis phosphomannose isomerase 1, but not phosphomannose isomerase 2, is essential for ascorbic acid biosynthesis. *Journal of Biological Chemistry*, *283*(43), 28842–28851. https://doi.org/10.1074/jbc.M805538200

Mazaheri, M., Heckwolf, M., Vaillancourt, B., Gage, J. L., Burdo, B., Heckwolf, S., Barry, K., Lipzen, A., Ribeiro, C. B., Kono, T. J. Y., Kaeppler, H. F., Spalding, E. P., Hirsch, C. N., Robin Buell, C., de Leon, N., & Kaeppler, S. M. (2019). Genome-wide association analysis of stalk biomass and anatomical traits in maize. *BMC Plant Biology*, *19*(1), 1–17. https://doi.org/10.1186/s12870-019-1653-x

Mitchell, D. A., Berovič, M., & Krieger, N. (2006). Introduction to solid-state fermentation bioreactors. In *Solid-State Fermentation Bioreactors: Fundamentals of Design and Operation*. https://doi.org/10.1007/3-540-31286-2_3

Miyake, H. (2016). Starch Accumulation in the Bundle Sheaths of C3 Plants: A Possible Pre-Condition for C4 Photosynthesis. *Plant and Cell Physiology*, *57*(5), 890–896. https://doi.org/10.1093/pcp/pcw046

Mueller, O., Kahmann, R., Aguilar, G., Trejo-Aguilar, B., Wu, A., & de Vries, R. P. (2008). The secretome of the maize pathogen Ustilago maydis. *Fungal Genetics and Biology*, *45*(SUPPL. 1). https://doi.org/10.1016/j.fgb.2008.03.012

Mustafa, A. M., Poulsen, T. G., & Sheng, K. (2016). Fungal pretreatment of rice straw with Pleurotus ostreatus and Trichoderma reesei to enhance methane production under solid-state anaerobic digestion. *Applied Energy*, *180*, 661–671. https://doi.org/10.1016/j.apenergy.2016.07.135

Nelissen, H., Eeckhout, D., Demuynck, K., Persiau, G., Walton, A., van Bel, M., Vervoort, M., Candaele, J., De Block, J., Aesaert, S., Van Lijsebettens, M., Goormachtig, S., Vandepoele, K., Van Leene, J., Muszynski, M., Gevaert, K., Inzé, D., & De Jaeger, G. (2015). Dynamic changes in ANGUSTIFOLIA3 complex composition reveal a growth regulatory mechanism in the maize leaf. *Plant Cell*, *27*(6), 1605–1619. https://doi.org/10.1105/tpc.15.00269

Nieter, A., Haase-Aschoff, P., Kelle, S., Linke, D., Krings, U., Popper, L., & Berger, R. G. (2015). A chlorogenic acid esterase with a unique substrate specificity from Ustilago maydis. *Applied and Environmental Microbiology*, *81*(5), 1679–1688. https://doi.org/10.1128/AEM.02911-14

Park, S. H., Mei, C., Pauly, M., Ong, R. G., Dale, B. E., Sabzikar, R., Fotoh, H., Nguyen, T., & Sticklen, M. (2012). Downregulation of maize cinnamoyl-coenzyme a reductase via RNA interference technology causes brown midrib and improves ammonia fiber expansion-pretreated conversion into fermentable sugars for biofuels. *Crop Science*, *52*(6), 2687–2701. https://doi.org/10.2135/cropsci2012.04.0253

Paulino, B. N., Pessôa, M. G., Molina, G., Kaupert Neto, A. A., Oliveira, J. V. C., Mano, M. C. R., & Pastore, G. M. (2017). Biotechnological production of value-added

compounds by ustilaginomycetous yeasts. *Applied Microbiology and Biotechnology*, *101*(21), 7789–7809. https://doi.org/10.1007/s00253-017-8516-x

Pauly, M., Gawenda, N., Wagner, C., Fischbach, P., Ramírez, V., Axmann, I. M., & Voiniciuc, C. (2019). The suitability of orthogonal hosts to study plant cell wall biosynthesis. *Plants*, *8*(11), 1–18. https://doi.org/10.3390/plants8110516

Pauly, M., Gille, S., Liu, L., Mansoori, N., de Souza, A., Schultink, A., & Xiong, G. (2013). Hemicellulose biosynthesis. *Planta*, *238*(4), 627–642. https://doi.org/10.1007/s00425-013-1921-1

Peña, M. J., Kulkarni, A. R., Backe, J., Boyd, M., O'Neill, M. A., & York, W. S. (2016). Structural diversity of xylans in the cell walls of monocots. *Planta*, *244*(3), 589–606. https://doi.org/10.1007/s00425-016-2527-1

Pérez, S., & Bertoft, E. (2010). The molecular structures of starch components and their contribution to the architecture of starch granules: A comprehensive review. *Starch/Staerke*, *62*(8), 389–420. https://doi.org/10.1002/star.201000013

Perrot, T., Pauly, M., & Ramírez, V. (2022). Emerging Roles of β-Glucanases in Plant Development and Adaptative Responses. *Plants*, *11*(9). https://doi.org/10.3390/plants11091119

Philipp, M., Hussnaetter, K. P., Reindl, M., Müntjes, K., Feldbrügge, M., & Schipper, K. (2022). A Novel Potent Carrier for Unconventional Protein Export in Ustilago maydis. *Frontiers in Cell and Developmental Biology*, *9*(January), 1–13. https://doi.org/10.3389/fcell.2021.816335

Piquemal, J., Chamayou, S., Nadaud, I., Beckert, M., Barrière, Y., Mila, I., Lapierre, C., Rigau, J., Puigdomenech, P., Jauneau, A., Digonnet, C., Boudet, A.-M., Goffner, D., & Pichon, M. (2002). Down-Regulation of Caffeic Acid O-Methyltransferase in Maize Revisited Using a Transgenic Approach. *Plant Physiology*, *130*(4), 1675–1685. https://doi.org/10.1104/pp.012237

Pordesimo, L. O., Hames, B. R., Sokhansanj, S., & Edens, W. C. (2005). Variation in corn stover composition and energy content with crop maturity. *Biomass and Bioenergy*, *28*(4), 366–374. https://doi.org/10.1016/j.biombioe.2004.09.003

Ralph, J., Lapierre, C., & Boerjan, W. (2019). Lignin structure and its engineering.

Current Opinion in Biotechnology, *56*, 240–249. https://doi.org/10.1016/j.copbio.2019.02.019

Ralph Singleton, W. (1948). Sucrose in the stalks of maize inbreds. *Science*, *107*(2772), 174. https://doi.org/10.1126/science.107.2772.174

Ramírez, V., Xiong, G., Mashiguchi, K., Yamaguchi, S., & Pauly, M. (2018). Growth- and stress-related defects associated with wall hypoacetylation are strigolactone-dependent. *Plant Direct*, *2*(6). https://doi.org/10.1002/pld3.62

Rao, X., & Dixon, R. A. (2018). Current models for transcriptional regulation of secondary cell wall biosynthesis in grasses. *Frontiers in Plant Science*, *9*(April), 1–11. https://doi.org/10.3389/fpls.2018.00399

Reed, J., Privalle, L., Powell, M. L., Meghji, M., Dawson, J., Dunder, E., Suttie, J., Wenck, A., Launis, K., Kramer, C., Chang, Y.-F., Hansen, G., & Wright, M. (2001). Phosphomannose Isomerase: An Efficient Selectable Marker for Plant Transformation. *In Vitro Cellular & Developmental Biology. Plant*, *37*(2), 127–132. https://doi.org/10.1079/IVP2000162

Regestein, L., Klement, T., Grande, P., Kreyenschulte, D., Heyman, B., Maßmann, T., Eggert, A., Sengpiel, R., Wang, Y., Wierckx, N., Blank, L. M., Spiess, A., Leitner, W., Bolm, C., Wessling, M., Jupke, A., Rosenbaum, M., & Büchs, J. (2018). From beech wood to itaconic acid: Case study on biorefinery process integration. *Biotechnology for Biofuels*, *11*(1), 1–11. https://doi.org/10.1186/s13068-018-1273-y

Reiter, W. D., & Vanzin, G. F. (2001). Molecular genetics of nucleotide sugar interconversion pathways in plants. *Plant Molecular Biology*, *47*(1–2), 95–113. https://doi.org/10.1023/A:1010671129803

Ren, F., Wu, F., Wu, X., Bao, T., Jie, Y., & Gao, L. (2024). Fungal systems for lignocellulose deconstruction: From enzymatic mechanisms to hydrolysis optimization. *GCB Bioenergy*, *16*(5), 1–23. https://doi.org/10.1111/gcbb.13130

Ren, X., & Zhang, J. (2013). Research progresses on the key enzymes involved in sucrose metabolism in maize. *Carbohydrate Research*, *368*, 29–34. https://doi.org/10.1016/j.carres.2012.10.016

Rennie, E. A., & Scheller, H. V. (2014). Xylan biosynthesis. *Current Opinion in Biotechnology*, *26*, 100–107. https://doi.org/10.1016/J.COPBIO.2013.11.013

Reyre, J. Lou, Grisel, S., Haon, M., Navarro, D., Ropartz, D., Le Gall, S., Record, E., Sciara, G., Tranquet, O., Berrin, J. G., & Bissaro, B. (2022). The Maize Pathogen Ustilago maydis Secretes Glycoside Hydrolases and Carbohydrate Oxidases Directed toward Components of the Fungal Cell Wall. *Applied and Environmental Microbiology*, *88*(23). https://doi.org/10.1128/aem.01581-22

Richter, P., Panchalingam, J., Miebach, K., Schipper, K., Feldbrügge, M., & Mann, M. (2024). Studying microbial triglyceride production from corn stover saccharides unveils insights into the galactose metabolism of Ustilago maydis. *Microbial Cell Factories*, *23*(1), 1–13. https://doi.org/10.1186/s12934-024-02483-1

Robertz, S., Philipp, M., Schipper, K., Richter, P., Miebach, K., Magnus, J., Pauly, M., & Ramírez, V. (2024). Monitoring corn stover processing by the fungus Ustilago maydis. *Bioresources and Bioprocessing*, *11*(87). https://doi.org/10.1186/s40643-024-00802-3

Rongpipi, S., Ye, D., Gomez, E. D., & Gomez, E. W. (2019). Progress and opportunities in the characterization of cellulose – an important regulator of cell wall growth and mechanics. *Frontiers in Plant Science*, *9*(March), 1–28. https://doi.org/10.3389/fpls.2018.01894

Ruan, Y. L. (2014). Sucrose metabolism: Gateway to diverse carbon use and sugar signaling. *Annual Review of Plant Biology*, *65*, 33–67. https://doi.org/10.1146/annurev-arplant-050213-040251

Saleem, M. E., Omar, R., Kamal, S. M. M., & Biak, D. R. A. (2015). Microwave-assisted pretreatment of lignocellulosic biomass: A review. *Journal of Engineering Science and Technology*, *10*, 97–109.

Samorski, M., Müller-Newen, G., & Büchs, J. (2005). Quasi-continuous combined scattered light and fluorescence measurements: A novel measurement technique for shaken microtiter plates. *Biotechnology and Bioengineering*, *92*(1), 61–68. https://doi.org/10.1002/bit.20573

Sánchez-Arreguin, J. A., Ortiz-Castellanos, M. L., Robledo-Briones, A. M., León-

Ramírez, C. G., Martínez-Soto, D., & Ruiz-Herrera, J. (2022). Chitosan Is Necessary for the Structure of the Cell Wall, and Full Virulence of Ustilago maydis. *Journal of Fungi*, *8*(8). https://doi.org/10.3390/jof8080813

Sarnowski, T. J., Rios, G., Jásik, J., Świezewski, S., Kaczanowski, S., Li, Y., Kwiatkowska, A., Pawlikowska, K., Koźbiał, M., Koźbiał, P., Koncz, C., & Jerzmanowski, A. (2005). SWI3 subunits of putative SWI/SNF chromatin-remodeling complexes play distinct roles during Arabidopsis development. *Plant Cell*, *17*(9), 2454–2472. https://doi.org/10.1105/tpc.105.031203

Saulnier, L., Vigouroux, J., & Thibault, J. F. (1995). Isolation and partial characterization of feruloylated oligosaccharides from maize bran. *Carbohydrate Research*, *272*(2), 241–253. https://doi.org/10.1016/0008-6215(95)00053-V

Sawaguchi, A., Ide, S., Goto, Y., Kawano, J., Oinuma, T., & Suganuma, T. (2001). A simple contrast enhancement by potassium permanganate oxidation for Lowicryl K4M ultrathin sections prepared by high pressure freezing/freeze substitution. *Journal of Microscopy*, *201*(Pt 1), 77–83. https://doi.org/10.1046/j.1365-2818.2001.00787.x

Scarlat, N., Martinov, M., & Dallemand, J. F. (2010). Assessment of the availability of agricultural crop residues in the European Union: Potential and limitations for bioenergy use. *Waste Management*, *30*(10), 1889–1897. https://doi.org/10.1016/j.wasman.2010.04.016

Schlembach, I., Hosseinpour Tehrani, H., Blank, L. M., Büchs, J., Wierckx, N., Regestein, L., & Rosenbaum, M. A. (2020). Consolidated bioprocessing of cellulose to itaconic acid by a co-culture of Trichoderma reesei and Ustilago maydis. *Biotechnology for Biofuels*, *13*(1). https://doi.org/10.1186/s13068-020-01835-4

Schlüter, U., & Weber, A. P. M. (2020). Regulation and Evolution of C4 Photosynthesis. *Annual Review of Plant Biology*, *71*(Volume 71, 2020), 183–215. https://doi.org/https://doi.org/10.1146/annurev-arplant-042916-040915

Seifert, G. J. (2004). Nucleotide sugar interconversions and cell wall biosynthesis: How to bring the inside to the outside. *Current Opinion in Plant Biology*, *7*(3), 277–284. https://doi.org/10.1016/j.pbi.2004.03.004

Sekhon, R. S., Breitzman, M. W., Silva, R. R., Santoro, N., Rooney, W. L., De Leon, N., & Kaeppler, S. M. (2016). Stover composition in maize and sorghum reveals remarkable genetic variation and plasticity for carbohydrate accumulation. *Frontiers in Plant Science*, *7*(June2016), 822. https://doi.org/10.3389/fpls.2016.00822

Setter, T. L., & Flannigan, B. A. (1986). Sugar and Starch Redistribution in Maize in Response to Shade and Ear Temperature Treatment. *Crop Science*, *26*(3), 575–579. https://doi.org/cropsci1986.0011183X002600030031x

Setter, T. L., Flannigan, B. A., & Melkonian, J. (2001). Loss of kernel set due to water deficit and shade in maize: Carbohydrate supplies, abscisic acid, and cytokinins. *Crop Science*, *41*(5), 1530–1540. https://doi.org/10.2135/cropsci2001.4151530x

Sharma, H. K., Xu, C., & Qin, W. (2019). Biological Pretreatment of Lignocellulosic Biomass for Biofuels and Bioproducts: An Overview. *Waste and Biomass Valorization*, *10*(2), 235–251. https://doi.org/10.1007/s12649-017-0059-y

Simmons, T. J., Mortimer, J. C., Bernardinelli, O. D., Pöppler, A. C., Brown, S. P., DeAzevedo, E. R., Dupree, R., & Dupree, P. (2016). Folding of xylan onto cellulose fibrils in plant cell walls revealed by solid-state NMR. *Nature Communications*, *7*, 1–9. https://doi.org/10.1038/ncomms13902

Sindhu, R., Binod, P., & Pandey, A. (2016). Biological pretreatment of lignocellulosic biomass - An overview. *Bioresource Technology*, *199*, 76–82. https://doi.org/10.1016/j.biortech.2015.08.030

Slewinski, T. L. (2012). Non-structural carbohydrate partitioning in grass stems: a target to increase yield stability, stress tolerance, and biofuel production. *Journal of Experimental Botany*, *63*(13), 4647–4670. https://doi.org/10.1093/jxb/ers124

Soderlund, C., Descour, A., Kudrna, D., Bomhoff, M., Boyd, L., Currie, J., Angelova, A., Collura, K., Wissotski, M., Ashley, E., Morrow, D., Fernandes, J., Walbot, V., & Yu, Y. (2009). Sequencing, mapping, and analysis of 27,455 maize full-length cDNAs. *PLoS Genetics*, *5*(11). https://doi.org/10.1371/journal.pgen.1000740

Somerville, C. (2006). Cellulose synthesis in higher plants. *Annual Review of Cell and Developmental Biology*, *22*, 53–78.

https://doi.org/10.1146/annurev.cellbio.22.022206.160206

Song, L., Yu, H., Ma, F., & Zhang, X. (2013). Biological Pretreatment under Non-sterile Conditions for Enzymatic Hydrolysis of Corn Stover. *BioResources*, *8*(2), 3802–3816. https://doi.org/10.15376/biores.8.3.3802-3816

Soreng, R. J., Peterson, P. M., Zuloaga, F. O., Romaschenko, K., Clark, L. G., Teisher, J. K., Gillespie, L. J., Barberá, P., Welker, C. A. D., Kellogg, E. A., Li, D. Z., & Davidse, G. (2022). A worldwide phylogenetic classification of the Poaceae (Gramineae) III: An update. *Journal of Systematics and Evolution*, *60*(3), 476–521. https://doi.org/10.1111/jse.12847

Sosso, D., Luo, D., Li, Q. B., Sasse, J., Yang, J., Gendrot, G., Suzuki, M., Koch, K. E., McCarty, D. R., Chourey, P. S., Rogowsky, P. M., Ross-Ibarra, J., Yang, B., & Frommer, W. B. (2015). Seed filling in domesticated maize and rice depends on SWEET-mediated hexose transport. *Nature Genetics*, *47*(12), 1489–1493. https://doi.org/10.1038/ng.3422

Spellig, T., Bottin, A., & Kahmann, R. (1996). Green fluorescent protein (GFP) as a new vital marker in the phytopathogenic fungus Ustilago maydis. *Molecular & General Genetics : MGG*, *252*(5), 503–509. https://doi.org/10.1007/BF02172396

Stein, O., & Granot, D. (2019). An overview of sucrose synthases in plants. *Frontiers in Plant Science*, *10*(February), 1–14. https://doi.org/10.3389/fpls.2019.00095

Stelpflug, S. C., Sekhon, R. S., Vaillancourt, B., Hirsch, C. N., Buell, C. R., de Leon, N., & Kaeppler, S. M. (2016). An Expanded Maize Gene Expression Atlas based on RNA Sequencing and its Use to Explore Root Development. *The Plant Genome*, *9*(1). https://doi.org/10.3835/plantgenome2015.04.0025

Steudler, S., & Bley, T. (2015). Better One-Eyed than Blind---Challenges and Opportunities of Biomass Measurement During Solid-State Fermentation of Basidiomycetes. In R. Krull & T. Bley (Eds.), *Filaments in Bioprocesses* (Vol. 149, pp. 223–252). Springer International Publishing. https://doi.org/10.1007/10_2014_300

Stitt, M., & Zeeman, S. C. (2012). Starch turnover: Pathways, regulation and role in growth. *Current Opinion in Plant Biology*, *15*(3), 282–292.

https://doi.org/10.1016/j.pbi.2012.03.016

Stock, J., Sarkari, P., Kreibich, S., Brefort, T., Feldbrügge, M., & Schipper, K. (2012). Applying unconventional secretion of the endochitinase Cts1 to export heterologous proteins in Ustilago maydis. *Journal of Biotechnology*, *161*(2), 80–91. https://doi.org/10.1016/j.jbiotec.2012.03.004

Stoykova, P., & Stoeva-Popova, P. (2011). PMI (manA) as a nonantibiotic selectable marker gene in plant biotechnology. *Plant Cell, Tissue and Organ Culture*, *105*(2), 141–148. https://doi.org/10.1007/s11240-010-9858-6

Sun, Y., Zhang, J., Li, W., Xu, Z., Wang, S., Zhao, M., Shen, J., & Cheng, L. (2024). Regulation of maize root growth by local phosphorus availability, sucrose metabolism, and partitioning. *Annals of Botany*, mcae169. https://doi.org/10.1093/aob/mcae169

Tanaka, S., Brefort, T., Neidig, N., Djamei, A., Kahnt, J., Vermerris, W., Koenig, S., Feussner, K., Feussner, I., & Kahmann, R. (2014). A secreted Ustilago maydis effector promotes virulence by targeting anthocyanin biosynthesis in maize. *ELife*, *3*, 1–27. https://doi.org/10.7554/elife.01355

Taniguchi, M., Suzuki, H., Watanabe, D., Sakai, K., Hoshino, K., & Tanaka, T. (2005). Evaluation of pretreatment with Pleurotus ostreatus for enzymatic hydrolysis of rice straw. *Journal of Bioscience and Bioengineering*, *100*(6), 637–643. https://doi.org/https://doi.org/10.1263/jbb.100.637

Tao, Y., Cheung, L. S., Li, S., Eom, J. S., Chen, L. Q., Xu, Y., Perry, K., Frommer, W. B., & Feng, L. (2015). Structure of a eukaryotic SWEET transporter in a homotrimeric complex. *Nature*, *527*(7577), 259–263. https://doi.org/10.1038/nature15391

Templeton, D. W., Sluiter, A. D., Hayward, T. K., Hames, B. R., & Thomas, S. R. (2009). Assessing corn stover composition and sources of variability via NIRS. *Cellulose*, *16*(4), 621–639. https://doi.org/10.1007/s10570-009-9325-x

Terfrüchte, M., Joehnk, B., Fajardo-Somera, R., Braus, G. H., Riquelme, M., Schipper, K., & Feldbrügge, M. (2014). Establishing a versatile Golden Gate cloning system for genetic engineering in fungi. *Fungal Genetics and Biology*, *62*, 1–10.

https://doi.org/https://doi.org/10.1016/j.fgb.2013.10.012

Terfrüchte, M., Wewetzer, S., Sarkari, P., Stollewerk, D., Franz-Wachtel, M., Macek, B., Schlepütz, T., Feldbrügge, M., Büchs, J., & Schipper, K. (2018). Tackling destructive proteolysis of unconventionally secreted heterologous proteins in Ustilago maydis. *Journal of Biotechnology*, *284*, 37–51. https://doi.org/10.1016/J.JBIOTEC.2018.07.035

Tryfona, T., Bourdon, M., Delgado Marques, R., Busse-Wicher, M., Vilaplana, F., Stott, K., & Dupree, P. (2023). Grass xylan structural variation suggests functional specialization and distinctive interaction with cellulose and lignin. *Plant Journal*, *113*(5), 1004–1020. https://doi.org/10.1111/tpj.16096

Untergasser, A., Cutcutache, I., Koressaar, T., Ye, J., Faircloth, B. C., Remm, M., & Rozen, S. G. (2012). Primer3--new capabilities and interfaces. *Nucleic Acids Research*, *40*(15), e115. https://doi.org/10.1093/nar/gks596

Van Den Brink, J., & De Vries, R. P. (2011). Fungal enzyme sets for plant polysaccharide degradation. *Applied Microbiology and Biotechnology*, *91*(6), 1477–1492. https://doi.org/10.1007/s00253-011-3473-2

van der Weijde, T., Alvim Kamei, C. L., Torres, A. F., Vermerris, W., Dolstra, O., Visser, R. G. F., & Trindade, L. M. (2013). The potential of C4 grasses for cellulosic biofuel production. *Frontiers in Plant Science*, *4*(MAY), 1–18. https://doi.org/10.3389/fpls.2013.00107

Van Reen, R., & Singleton, W. R. (1952). Sucrose Content in the Stalks of Maize Inbreds. *Agronomy Journal*, *44*(12), 610–614. https://doi.org/https://doi.org/10.2134/agronj1952.00021962004400120003x

Van Vleet, J. H., & Jeffries, T. W. (2009). Yeast metabolic engineering for hemicellulosic ethanol production. *Current Opinion in Biotechnology*, *20*(3), 300–306. https://doi.org/10.1016/j.copbio.2009.06.001

Van Zyl, W. H., Bloom, M., & Viktor, M. J. (2012). Engineering yeasts for raw starch conversion. *Applied Microbiology and Biotechnology*, *95*(6), 1377–1388. https://doi.org/10.1007/s00253-012-4248-0

Vanhevel, Y., De Moor, A., Muylle, H., Vanholme, R., & Boerjan, W. (2024). Breeding

for improved digestibility and processing of lignocellulosic biomass in Zea mays. *Frontiers in Plant Science*, *15*(July), 1–21. https://doi.org/10.3389/fpls.2024.1419796

Vanholme, R., De Meester, B., Ralph, J., & Boerjan, W. (2019). Lignin biosynthesis and its integration into metabolism. *Current Opinion in Biotechnology*, *56*, 230–239. https://doi.org/10.1016/j.copbio.2019.02.018

Vasco-Correa, J., Ge, X., & Li, Y. (2016). Fungal pretreatment of non-sterile miscanthus for enhanced enzymatic hydrolysis. *Bioresource Technology*, *203*, 118–123. https://doi.org/https://doi.org/10.1016/j.biortech.2015.12.018

Vega-Sánchez, M. E., Loqué, D., Lao, J., Catena, M., Verhertbruggen, Y., Herter, T., Yang, F., Harholt, J., Ebert, B., Baidoo, E. E. K., Keasling, J. D., Scheller, H. V., Heazlewood, J. L., & Ronald, P. C. (2015). Engineering temporal accumulation of a low recalcitrance polysaccharide leads to increased C6 sugar content in plant cell walls. *Plant Biotechnology Journal*, *13*(7), 903–914. https://doi.org/10.1111/pbi.12326

Vega-Sánchez, M. E., Verhertbruggen, Y., Scheller, H. V, & Ronald, P. C. (2013). Abundance of mixed linkage glucan in mature tissues and secondary cell walls of grasses. *Plant Signaling & Behavior*, *8*(February), 8–11.

Venkatesh, J., & Park, S. W. (2014). Role of L-ascorbate in alleviating abiotic stresses in crop plants. *Botanical Studies*, *55*(1), 1–19. https://doi.org/10.1186/1999-3110-55-38

Verbančič, J., Lunn, J. E., Stitt, M., & Persson, S. (2018). Carbon Supply and the Regulation of Cell Wall Synthesis. *Molecular Plant*, *11*(1), 75–94. https://doi.org/10.1016/j.molp.2017.10.004

Verbruggen, M. A., Beldman, G., & Voragen, A. G. J. (1998). Enzymic degradation of sorghum glucuronoarabinoxylans leading to tentative structures. *Carbohydrate Research*, *306*(1–2), 275–282. https://doi.org/10.1016/S0008-6215(97)10065-9

Vercruyssen, L., Verkest, A., Gonzalez, N., Heyndrickx, K. S., Eeckhout, D., Han, S. K., Jégu, T., Archacki, R., Van Leene, J., Andriankaja, M., De Bodt, S., Abeel, T., Coppens, F., Dhondt, S., De Milde, L., Vermeersch, M., Maleux, K., Gevaert, K.,

Jerzmanowski, A., … Inzé, D. (2014). ANGUSTIFOLIA3 binds to SWI/SNF chromatin remodeling complexes to regulate transcription during Arabidopsis leaf development. *Plant Cell*, *26*(1), 210–229. https://doi.org/10.1105/tpc.113.115907

Vermerris, W., Sherman, D. M., & McIntyre, L. M. (2010). Phenotypic plasticity in cell walls of maize brown midrib mutants is limited by lignin composition. *Journal of Experimental Botany*, *61*(9), 2479–2490. https://doi.org/10.1093/jxb/erq093

Vignols, F., Rigau, J., Torres, M. A., Capellades, M., & Puigdomènech, P. (1995). The brown midrib3 (bm3) mutation in maize occurs in the gene encoding caffeic acid O-methyltransferase. *Plant Cell*, *7*(4), 407–416. https://doi.org/10.2307/3870079

Vinodh Kumar, P. N., Mallikarjuna, M. G., Jha, S. K., Mahato, A., Lal, S. K., Yathish, K. R., Lohithaswa, H. C., & Chinnusamy, V. (2023). Unravelling structural, functional, evolutionary and genetic basis of SWEET transporters regulating abiotic stress tolerance in maize. *International Journal of Biological Macromolecules*, *229*(January), 539–560. https://doi.org/10.1016/j.ijbiomac.2022.12.326

Vogel, J. (2008). Unique aspects of the grass cell wall. In *Current Opinion in Plant Biology* (Vol. 11, Issue 3, pp. 301–307). Elsevier Current Trends. https://doi.org/10.1016/j.pbi.2008.03.002

Volkmar, M., Maus, A. L., Weisbrodt, M., Bohlender, J., Langsdorf, A., Holtmann, D., & Ulber, R. (2023). Municipal green waste as substrate for the microbial production of platform chemicals. *Bioresources and Bioprocessing*, *10*(1). https://doi.org/10.1186/s40643-023-00663-2

Voll, L. M., Horst, R. J., Voitsik, A. M., Zajic, D., Samans, B., Pons-Kühnemann, J., Doehlemann, G., Münch, S., Wahl, R., Molitor, A., Hofmann, J., Schmiedl, A., Waller, F., Deising, H. B., Kahmann, R., Kämper, J., Kogel, K. H., & Sonnewald, U. (2011). Common motifs in the response of cereal primary metabolism to fungal pathogens are not based on similar transcriptional reprogramming. *Frontiers in Plant Science*, *2*(AUG), 1–17. https://doi.org/10.3389/fpls.2011.00039

Vu, H. P., Nguyen, L. N., Vu, M. T., Johir, M. A. H., McLaughlan, R., & Nghiem, L. D. (2020). A comprehensive review on the framework to valorise lignocellulosic biomass as biorefinery feedstocks. *Science of the Total Environment*, *743*,

140630. https://doi.org/10.1016/j.scitotenv.2020.140630

Wahl, R., Wippel, K., Goos, S., Kämper, J., & Sauer, N. (2010). A novel high-affinity sucrose transporter is required for virulence of the plant pathogen Ustilago maydis. *PLoS Biology*, *8*(2), 1000303. https://doi.org/10.1371/journal.pbio.1000303

Wang, D. R., Han, R., Wolfrum, E. J., & McCouch, S. R. (2017). The buffering capacity of stems: genetic architecture of nonstructural carbohydrates in cultivated Asian rice, Oryza sativa. *New Phytologist*, *215*(2), 658–671. https://doi.org/10.1111/nph.14614

Wang, L., Fan, J., Gan, L., Zeng, X., Lin, L., & Liu, J. (2024). Thermostatic microwave-assisted pretreatment of corn stover at atmospheric pressure to enhance saccharification. *Biomass and Bioenergy*, *188*, 107343. https://doi.org/https://doi.org/10.1016/j.biombioe.2024.107343

Wang, S., Robertz, S., Seven, M., Kraemer, F., Kuhn, B. M., Liu, L., Lunde, C., Pauly, M., & Ramírez, V. (2023). A large-scale forward genetic screen for maize mutants with altered lignocellulosic properties. *Frontiers in Plant Science*, *14*(March), 1–12. https://doi.org/10.3389/fpls.2023.1099009

Wewetzer, S. J., Kunze, M., Ladner, T., Luchterhand, B., Roth, S., Rahmen, N., Kloß, R., & Silva, A. C. (2015). Parallel use of shake flask and microtiter plate online measuring devices (RAMOS and BioLector) reduces the number of experiments in laboratory-scale stirred tank bioreactors Parallel use of shake flask and microtiter plate online measuring devices (RA. *Journal of Biological Engineering*, 0–18. https://doi.org/10.1186/s13036-015-0005-0

Wheeler, G. L., Jones, M. A., & Smirnoff, N. (1998). The biosynthetic pathway of vitamin C in higher plants. *Nature*, *393*(6683), 365–369. https://doi.org/10.1038/30728

Wieczorke, R., Krampe, S., Weierstall, T., Freidel, K., Hollenberg, C. P., & Boles, E. (1999). Concurrent knock-out of at least 20 transporter genes is required to block uptake of hexoses in Saccharomyces cerevisiae. *FEBS Letters*, *464*(3), 123–128. https://doi.org/10.1016/S0014-5793(99)01698-1

Wierckx, N., Miebach, K., Ihling, N., Hussnaetter, K. P., Büchs, J., & Schipper, K. (2021). Perspectives for the application of Ustilaginaceae as biotech cell factories. In *Essays in Biochemistry* (Vol. 65, Issue 2, p. 365). Portland Press. https://doi.org/10.1042/EBC20200141

Wilson, S. M., Ho, Y. Y., Lampugnani, E. R., Van De Meene, A. M. L., Bain, M. P., Bacic, A., & Doblin, M. S. (2015). Determining the Subcellular Location of Synthesis and Assembly of the Cell Wall Polysaccharide (1,3; 1,4)-beta-D-Glucan in Grasses. *Plant Cell*, *27*(3), 754–771. https://doi.org/10.1105/tpc.114.135970

Wolfenstetter, S., Wirsching, P., Dotzauer, D., Schneider, S., & Sauer, N. (2012). Routes to the tonoplast: The sorting of tonoplast transporters in Arabidopsis mesophyll protoplasts. *Plant Cell*, *24*(1), 215–232. https://doi.org/10.1105/tpc.111.090415

Woodhouse, M. R., Cannon, E. K., Portwood, J. L., Harper, L. C., Gardiner, J. M., Schaeffer, M. L., & Andorf, C. M. (2021). A pan-genomic approach to genome databases using maize as a model system. *BMC Plant Biology*, *21*(1), 1–10. https://doi.org/10.1186/s12870-021-03173-5

Xiong, W., Li, Y., Wu, Z., Ma, L., Liu, Y., Qin, L., Liu, J., Hu, Z., Guo, S., Sun, J., Yang, G., Chai, M., Zhang, C., Lu, X., & Fu, C. (2020). Characterization of Two New brown midrib1 Mutations From an EMS-Mutagenic Maize Population for Lignocellulosic Biomass Utilization. *Frontiers in Plant Science*, *11*. https://doi.org/10.3389/fpls.2020.594798

Xu, J. (2015). Microwave Pretreatment. *Pretreatment of Biomass: Processes and Technologies*, 157–172. https://doi.org/10.1016/B978-0-12-800080-9.00009-8

Xuan, Y. H., Hu, Y. B., Chen, L. Q., Sosso, D., Ducat, D. C., Hou, B. H., & Frommer, W. B. (2013). Functional role of oligomerization for bacterial and plant SWEET sugar transporter family. *Proceedings of the National Academy of Sciences of the United States of America*, *110*(39). https://doi.org/10.1073/pnas.1311244110

Yates, A. D., Allen, J., Amode, R. M., Azov, A. G., Barba, M., Becerra, A., Bhai, J., Campbell, L. I., Carbajo Martinez, M., Chakiachvili, M., Chougule, K., Christensen, M., Contreras-Moreira, B., Cuzick, A., Da Rin Fioretto, L., Davis, P., De Silva, N. H., Diamantakis, S., Dyer, S., … Flicek, P. (2022). Ensembl Genomes 2022: An

expanding genome resource for non-vertebrates. *Nucleic Acids Research*, *50*(D1), D996–D1003. https://doi.org/10.1093/nar/gkab1007

Yu, C., Yan, M., Dong, H., Luo, J., Ke, Y., Guo, A., Chen, Y., Zhang, J., & Huang, X. (2021). Maize bHLH55 functions positively in salt tolerance through modulation of AsA biosynthesis by directly regulating GDP-mannose pathway genes. *Plant Science*, *302*(1), 110676. https://doi.org/10.1016/j.plantsci.2020.110676

Yu, X., Jiang, L., Wu, R., Meng, X., Zhang, A., Li, N., Xia, Q., Qi, X., Pang, J., Xu, Z. Y., & Liu, B. (2016). The Core Subunit of A Chromatin-Remodeling Complex, ZmCHB101, Plays Essential Roles in Maize Growth and Development. *Scientific Reports*, *6*(November), 1–13. https://doi.org/10.1038/srep38504

Zhang, B., Zhang, L., Li, F., Zhang, D., Liu, X., Wang, H., Xu, Z., Chu, C., & Zhou, Y. (2017). Control of secondary cell wall patterning involves xylan deacetylation by a GDSL esterase. *Nature Plants*, *3*(March). https://doi.org/10.1038/nplants.2017.17

Zhang, D., VanFossen, A. L., Pagano, R. M., Johnson, J. S., Parker, M. H., Pan, S., Gray, B. N., Hancock, E., Hagen, D. J., Lucero, H. A., Shen, B., Lessard, P. A., Ely, C., Moriarty, M., Ekborg, N. A., Bougri, O., Samoylov, V., Lazar, G., & Raab, R. M. (2011). Consolidated Pretreatment and Hydrolysis of Plant Biomass Expressing Cell Wall Degrading Enzymes. *Bioenergy Research*, *4*(4), 276–286. https://doi.org/10.1007/s12155-011-9138-2

Zhang, L., Wang, L., Zhang, J., Song, C., Li, Y., Li, J., & Lu, M. (2021). Expression and localization of SWEETs in Populus and the effect of SWEET7 overexpression in secondary growth. *Tree Physiology*, *41*(5), 882–899. https://doi.org/10.1093/treephys/tpaa145

Zhang, R., Hu, H., Wang, Y., Hu, Z., Ren, S., Li, J., He, B., Wang, Y., Xia, T., Chen, P., Xie, G., Peng, L., & Turner, S. (2020). A novel rice fragile culm 24 mutant encodes a UDP-glucose epimerase that affects cell wall properties and photosynthesis. *Journal of Experimental Botany*, *71*(10), 2956–2969. https://doi.org/10.1093/jxb/eraa044

Zhang, X., Feng, C., Wang, M., Li, T., Liu, X., & Jiang, J. (2021). Plasma membrane-localized SlSWEET7a and SlSWEET14 regulate sugar transport and storage in tomato fruits. *Horticulture Research*, *8*(1). https://doi.org/10.1038/s41438-021-

00624-w

Zhang, X., Jiang, X., Hao, Z., & Qu, K. (2019). Advances in online methods for monitoring microbial growth. *Biosensors and Bioelectronics*, *126*(October 2018), 433–447. https://doi.org/10.1016/j.bios.2018.10.035

Zhong, R., Cui, D., & Ye, Z. H. (2019). Secondary cell wall biosynthesis. *New Phytologist*, *221*(4), 1703–1723. https://doi.org/10.1111/nph.15537

Zhong, W., Zhang, Z., Luo, Y., Sun, S., Qiao, W., & Xiao, M. (2011). Effect of biological pretreatments in enhancing corn straw biogas production. *Bioresource Technology*, *102*(24), 11177–11182. https://doi.org/10.1016/j.biortech.2011.09.077

Zhu, J., Zhou, L., Li, T., Ruan, Y., Zhang, A., Dong, X., Zhu, Y., Li, C., & Fan, J. (2022). Genome-Wide Investigation and Characterization of SWEET Gene Family with Focus on Their Evolution and Expression during Hormone and Abiotic Stress Response in Maize. *Genes*, *13*(10). https://doi.org/10.3390/genes13101682

Zieger, M., & Mayer, A. (2012). Yeast vacuoles fragment in an asymmetrical two-phase process with distinct protein requirements. *Molecular Biology of the Cell*, *23*(17), 3438–3449. https://doi.org/10.1091/mbc.E12-05-0347

Zuo, J., Niu, Q. W., & Chua, N. H. (2001). Technical advance: An estrogen receptor-based transactivator XVE mediates highly inducible gene expression in transgenic plants. *The Plant Journal : For Cell and Molecular Biology*, *24*(2), 265–273. https://doi.org/10.1046/j.1365-313x.2000.00868.x

7 Appendix

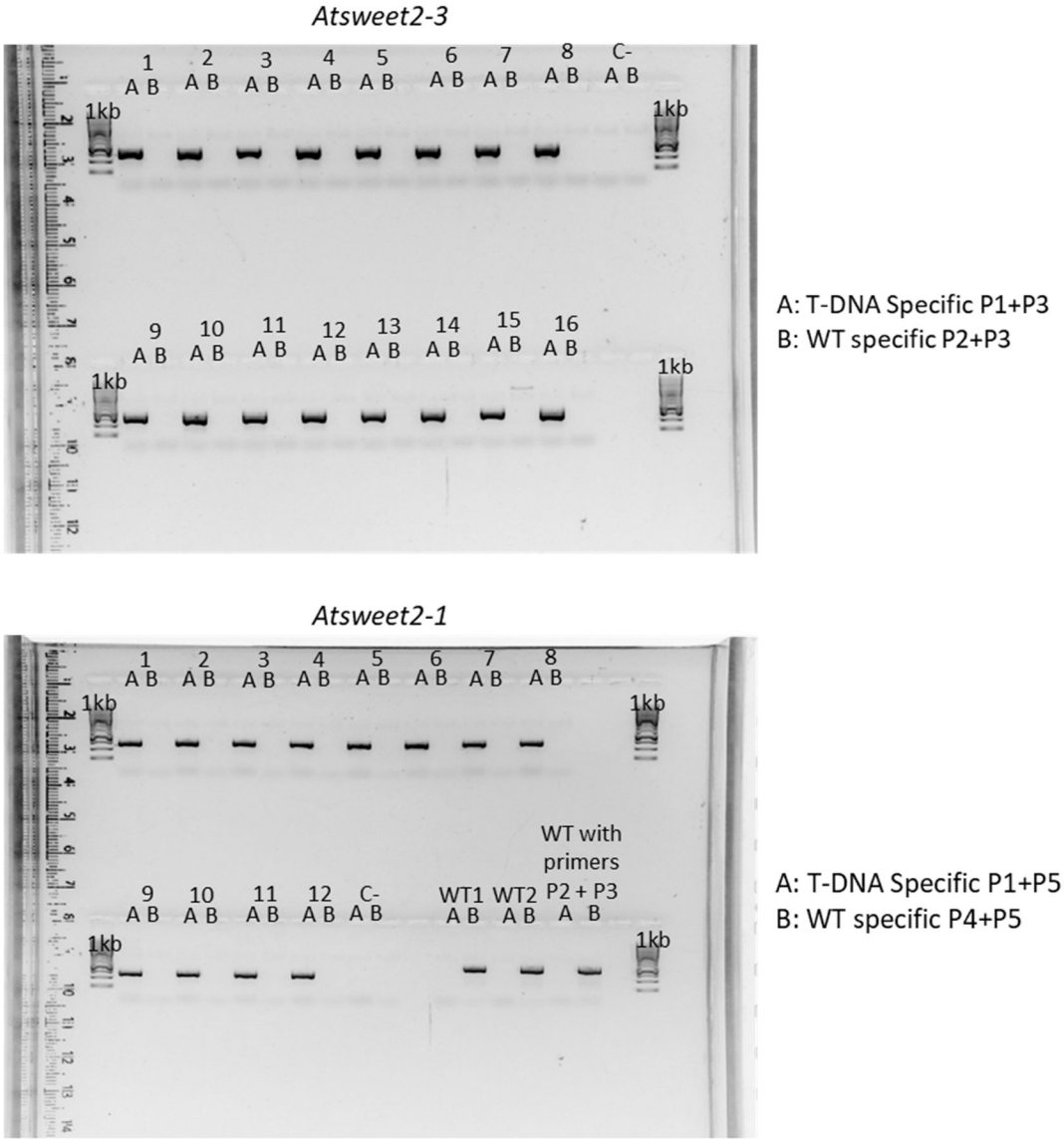

Figure 26: **Genotyping of *A. thaliana* T-DNA mutant lines *Atsweet2-3* and *Atsweet2-1* used in chapter 4 (section 4.4).** Numbers refer to individual plants, 1kb refers to the DNA ladder used as marker, WT refers to *A. thaliana* Col-0 and C- refers to no template control. Only amplification in sample A indicates a homozygous mutant line, amplification in B indicates wildtype and amplification in A and B indicates heterozygous mutant plants. Note: the wildtype control for the *Atsweet2-3* primer combination was run on the gel for *Atsweet2-1* and is indicated by “WT with primers P2 + P3”. Primer sequences can be found in Table 29.

Table 28: **Complete medium components.**

Component	Final concentration
Casaminoacids (Difco)	0.25 % (w/v)
Yeast extract (Difco)	0.1 % (w/v)
vitamin solution	1.0 % (v/v)
salt solution	6.25 % (v/v)
DNA degr. Free acid (Sigma, D-3159)	0.05 % (w/v)
NH_4NO_3 (Sigma, A9642)	0.15 % (w/v)
Glucose	1.0 % (w/v)

vitamin solution **Component**	**Concentration [‰ (w/v)]**
Thiamine (Hydrochlorid, Serva 36020)	0.1
Riboflavin (Sigma R-4500)	0.05
Pyridoxine (Monohydr.chl., Sigma p-9755)	0.05
Ca-Pantothenat (Hemi-Ca.salt, Sigma P-2250)	0.2
Aminobenzoic acid (Free Acid, Sigma A-9878)	0.05
Nicotinic acid (Free Acid, Sigma N-4126)	0.2
Cholinchlorid (Sigma C-1879)	0.2
myo-Inositol (Sigma I-5125)	1

Salt solution **Component**	**Concentration [‰ (w/v)]**
KH_2PO_4	16.00
Na_2SO4	4.00
KCl	8.00
$CaCl_2*2H_2O$	1.32
Trace elements solution	8.00
$MgSO_4$ (Waterfree)	2.00

Trace elements solution **Component**	**Concentration [‰ (w/v)]**
H_3BO_3	0.06
$MnCl*4H_2O$	0.14
ZnCl2	0.4
$Na_2MoO_4*2H_2O$	0.4
$FeCl_3*6H_2O$	0.1
$CuSO_4*5H_2O$	0.04

Table 29: **Primers used in this work.**

#	Primer sequence (5´-> 3´)	Purpose (FW refers to forward primer and REV to reverse primer)
P1	ATTTTGCCGATTTCGGAAC	FW for SALK T-DNA mutants
P2	CGTACACATTCAGCCTTTTGC	FW for SALK_048430C
P3	ATCACTCCAACCACAGCAAAC	REV for SALK_048430C
P4	CCACACAAAAACAAAACCCAC	FW for SALK_044600C
P5	ATCATGAGGAACAAATCGACG	REV for SALK_044600C
P6	TTAGGGCTTGTGCTACAATGG	FW for SALK_053545C
P7	ACGTCATCCATTTCTTCGTTG	REV for SALK_053545C
P8	CTCCAACTGTTCAGCATCTCC	FW for SALK_001774.38.20.x and for SALK_007346.50.40.x
P9	CAAGCACAGATGCATTTCATG	REV for SALK_001774.38.20.x
P10	CAGCAAGATTTGGATCTCCTG	REV for SALK_007346.50.40.x
P11	TTCTGAGAAAATTTCATCCCAAC	FW for SALK_126880C
P12	ATTCAACATGACTCGGTCCAG	REV for SALK_126880C
P13	ATGGCCCAAATCCAAATTAAG	FW for SALK_070922.54.50.x
P14	CGTGAACTGTCGGAGAAAGAG	REV for SALK_070922.54.50.x
P15	CCCCGACCCTACCCGCCCCTACGCAGAGC	Gibson assembly FW primer for PMI3_hap2
P16	AGGGGCGGGTAGGGTCGGGGTTGTTGTGG	Gibson assembly REV primer for PMI3_hap2
P17	CGGGTTTGCCTGTATTGAGGAGCTCAAGGATGTCCTG	Gibson assembly FW primer for PMI3_hap3
P18	CCTCAATACAGGCAAACCCGCAAAGCGC	Gibson assembly REV primer for PMI3_hap3
P19	TTCTTCGTCCAAGCATACACTGAGGTTAAG	Gibson assembly FW primer for PMI3_hap4
P20	GTGTATGCTTGGACGAAGAAAACATCAC	Gibson assembly REV primer for PMI3_hap4
P21	GAGGCGGATAAAGTTGCAGGACCACTTC	Gibson assembly FW primer for pF3A WG (BYDV) Flexi® backbone
P22	CCTGCAACTTTATCCGCCTCCATCCAGTC	Gibson assembly REV primer for pF3A WG (BYDV) Flexi® backbone
P23	GGTCCCCTTATTGCCTGACA	Vector backbone forward primer for pF3A
P24	GAAATACAGGAACGCACGCT	FW for sequencing backbone SNP in pF3A-PMI3 hap4
P25	GCTTCGCAACGTTCAAATCC	FW for sequencing backbone SNP in pF3A-PMI3 hap4
P26	GCAGCGGCCATCATGAATTA	pDRf1-GW backbone REV
P27	GCTCCCCTCCATTAGTTTCG	pDRf1-GW backbone FW
P28	GGGGACAAGTTTGTACAAAAAAGCAGGCTC	Primer to create the 5´ overhang for recombination into pDONR221 vector
P29	GGGGACCACTTTGTACAAGAAAGCTGGGTC	Primer to create the 3´ overhang for recombination into pDONR221 vector
P30	CAAGAAAGCTGGGTCTCAGGCAAGCAACGGTGCTG	Sweet2 REV with stop
P31	CAAGAAAGCTGGGTCGGCAAGCAACGGTGCTGACG	Sweet2 REV without stop
P32	TACAAAAAAGCAGGCTTCATGAGCTCCCTGTACGACGT	Sweet2 hap1 FW with overhang
P33	TACAAAAAAGCAGGCTTCATGAACTCCCTGTACGACGT	Sweet2 hap2 FW with overhang
P34	ATGAGCTCCCTGTACGACGT	Sweet2 5´end primer FW
P35	TCAGGCAAGCAACGGTGCT	Sweet2 3`end primer REV
P36	CCGACCCTACCCGCCC	FW PMI3 hap2
P37	GGGCGGGTAGGGTCGG	REV PMI3 hap2
P38	CGGGTTTGCCTGTATTGAGGA	FW PMI3 hap3
P39	TCCTCAATACAGGCAAACCCG	REV PMI3 hap3
P40	TTTTCTTCGTCCAAGCATACAC	FW PMI3 hap4
P41	GTGTATGCTTGGACGAAGAAAA	REV PMI3 hap4
P42	GCTGAACTTGTGGCCGTTTA	REV pRD04 i. mVenus in pAB111 backbone specific
P43	AAGGGCATCGACTTCAAGGA	FW pMDC7NtmVenus backbone specific
P44	TCCTGCAACTTTATCCGCCTC	Vector backbone reverse primer for pF3A

pDRf1-GFP-GW sequence

ttgagatccttttttctgcgcgtaatctgctgcttgcaaacaaaaaaaccaccgctaccagcggtggtttgtttgccggatcaagagctaccaactctttttccgaag
gtaactggcttcagcagagcgcagataccaaatactgttcttctagtgtagccgtagttaggccaccacttcaagaactctgtagcaccgcctacatacctcgctct
gctaatcctgttaccagtggctgctgccagtggcgataagtcgtgtcttaccgggttggactcaagacgatagttaccggataaggcgcagcggtcgggctgaac
gggggttcgtgcacacagcccagcttggagcgaacgacctacaccgaactgagatacctacagcgtgagctatgagaaagcgccacgcttcccgaagggg
agaaaggcggacaggtatccggtaagcggcagggtcggaacaggagagcgcacgagggagcttccagggggaaacgcctggtatctttatagtcctgtcg
ggtttcgccacctctgacttgagcgtcgatttttgtgatgctcgtcaggggggcggagcctatggaaaaacgccagcaacgcggccttttacggttcctggccttttt
gctggccttttgctcacatgttctttcctgcgttatcccctgattctgtggataaccgtattaccgcctttgagtgagctgataccgctcgccgcagccgaacgaccgag
cgcagcgagtcagtgagcgaggaagcggaagagcgcccaatacgcaaaccgcctctccccgcgcgttggccgattcattaatgcagctggcacgacaggtt
tcccgactggaaagcgggcagtgagcgcaacgcaattaatgtgagttagctcactcattaggcaccccaggctttacactttatgcttccggctcgtatgttgtgtg
gaattgtgagcggataacaatttcacacaggaaacagctatgaccatgattacgccaagcttcctgaaacggagaaacataaacaggcattgctgggatcac
ccatacatcactctgttttgcctgacctttccggtaatttgaaaacaaacccggtctcgaagcggagatccggcgataattaccgcagaaataaacccatacacg
agacgtagaaccagccgcacatggccggagaaactcctgcgagaatttcgtaaactcgcgcgcattgcatctgtatttcctaatgcggcacttccaggcctcgat
cgagaccgtttatccattgctttttgttgtctttttccctcgttcacagaaagtctgaagaagctatagtagaactatgagctttttttgtttctgttttccttttttttttttacctct
gtggaaattgttactctcacactctttagttcgtttgtttgttttgtttattccaattatgaccggtgacgaaacgtggtcgatggtgggtaccgcttatgctcccctccattag
tttcgattatataaaaaggccaaatattgtattattttcaaatgtcctatcattatcgtctaacatctaatttctcttaaatttttttctctttctttcctataacaccaatagtgaaa
atctttttttcttctatatctacaaaaactttttttttctatcaacctcgttgataaatttttttctttaacaatcgttaataattaattaattggaaaataaccatttttttctctctttttata
cacacattcaaaagaaagaaaaaaaatataccccagcctcgactagtggatccccctacagtttgtacaaaaaagctgaacgagaaacgtaaaatgatata
aatatcaatatattaaattagattttgcataaaaaacagactacataatactgtaaaacacaacatatccagtcactatggcggcccctcgaggggccgcattag
gcaccccaggctttacactttatgcttccggctcgtataatgtgtggattttgagttaggatccgtcgagattttcaggagctaaggaagctaaaatggagaaaaaa
atcactggatataccaccgttgatatatcccaatggcatcgtaaagaacattttgaggcatttcagtcagttgctcaatgtacctataaccagaccgttcagctggat
attacggccttttaaagaccgtaaagaaaaataagcacaagttttatccggcctttattcacattcttgcccgcctgatgaatgctcatccggaattccgtatggcaa
tgaaagacggtgagctggtgatatgggatagtgttcacccttgttacaccgttttccatgagcaaactgaaacgttttcatcgctctggagtgaataccacgacgatt
tccggcagtttctacacatatattcgcaagatgtggcgtgttacggtgaaaacctggcctatttccctaaagggtttattgagaatatgtttttcgtctcagccaatccct
gggtgagtttcaccagttttgatttaaacgtggccaatatggacaacttcttcgcccccgttttcaccatgggcaaatattatacgcaaggcgacaaggtgctgatgc
cgctggcgattcaggttcatcatgccgtttgtgatggcttccatgtcggcagaatgcttaatgaattacaacagtactgcgatgagtggcaggcggggcgtaatcta
gaggatccggcttactaaaagccagataacagtatgcgtatttgcgcgctgatttttgcggtataagaatatatactgatatgtatacccgaagtatgtcaaaaaga
ggtatgctatgaagcagcgtattacagcgacagttgacagcgacagctatcagttgctcaaggcatatatgatgtcaatatctccggtctggtaagcacaaccat
gcagaatgaagcccgtcgtctgcgtgccgaacgctggaaagcggaaaatcaggaagggatggctgaggtcgcccggtttattgaaatgaacggctcttttgct
gacgagaacaggggctggtgaaatgcagtttaaggtttacacctataaaagagagagccgttatcgtctgtttgtggatgtacagagtgatattattgacacgccc
gggcgacggatggtgatccccctggccagtgcacgtctgctgtcagataaagtcccccgtgaactttacccggtggtgcatatcggggatgaaagctggcgcat
gatgaccaccgatatggccagtgtgccggtctccgttatcggggaagaagtggctgatctcagccaccgcgaaaatgacatcaaaaacgccattaacctgatg
ttctggggaatataaatgtcaggctcccttatacacagccagtctgcaggtcgaccatagtgactggatatgttgtgttttacagtattatgtagtctgttttttatgcaaa
atctaatttaatatattgatatttatatcattttacgtttctcgttcagctttcttgtacaaagtggtgaagcttatggtgagcaagggcgaggagctgttcaccggggtggt
gcccatcctggtcgagctggacggcgacgtaaacggccacaagttcagcgtgtccggcgagggcgagggcgatgccacctacggcaagctgaccttgaagt
tcatctgcaccaccggcaagctgcccgtgccctggcccaccctcgtgaccaccctgacctacggcgtgcagtgcttcagccgctaccccgaccacatgaagca
gcacgacttcttcaagtccgccatgcccgaaggctacgtccaggagcgcaccatcttcttcaaggacgacggcaactacaagacccgcgccgaggtgaagtt
cgagggcgacaccctggtgaaccgcatcgagctgaagggcatcgacttcaaggaggacggcaacatcctggggcacaagctggagtacaactacaacag
ccacaacgtctatatcatggccgacaagcagaagaacggcatcaaggtgaacttcaagatccgccacaacatcgaggacggcagcgtgcagctcgccgac
cactaccagcagaacaccccccatcggcgacggccccgtgctgctgcccgacaaccactacctgagcacccagtccgccctgagcaaagaccccaacgag
aagcgcgatcacatggtcctgctggagttcgtgaccgccgccgggatcactctcggcatggacgagctgtacaagtaactcgaggggggggcccggtacccaa
ttcgccctatagtgagtcgtattacgcgcggatccagctttggacttcttcgccagaggtttggtcaagtctccaatcaaggttgtcggcttgtctaccttgccagaaat
ttacgaaaagatggaaaagggtcaaatcgttggtagatacgttgttgacacttctaaataagcgaatttcttatgatttatgatttttattattaaataagttataaaaaa
aataagtgtatacaaattttaaagtgactcttaggttttaaaacgaaaattcttattcttgagtaactctttcctgtaggtcaggttgctttctcaggtatagcatgaggtcg
ctcttattgaccacacctctaccggcatgccaattcactggccgtcgttttacaacgtcgtgactgggaaaaccctggcgttacccaacttaatcgccttgcagcac
atccccctttcgccagctggcgtaatagcgaagaggcccgcaccgatcgcccttcccaacagttgcgcagcctgaatggcgaatggcgcctgatgcggtattttc
tccttacgcatctgtgcggtatttcacaccgcataatcggatcgtacttgttacccatcattgaattttgaacatccgaacctgggagttttccctgaaacagatagtat
atttgaacctgtataataatatatagtctagcgctttacggaagacaatgtatgtatttcggttcctggagaaactattgcatctattgcataggtaatcttgcacgtcgc
atccccggttcattttctgcgtttccatcttgcacttcaatagcatatctttgttaacgaagcatctgtgcttcattttgtagaacaaaaatgcaacgcgagagcgctaatt
tttcaaacaaagaatctgagctgcatttttacagaacagaaatgcaacgcgaaagcgctatttttaccaacgaagaatctgtgcttcatttttgtaaaacaaaaatgc
aacgcgagagcgctaatttttcaaacaaagaatctgagctgcatttttacagaacagaaatgcaacgcgagagcgctatttttaccaacaaagaatctatacttctt
ttttgttctacaaaaatgcatcccgagagcgctatttttctaacaaagcatcttagattactttttttctcctttgtgcgctctataatgcagtctcttgataacttttgcactgt
aggtccgttaaggttagaagaaggctactttggtgtctattttctcttccataaaaaaagcctgactccacttcccgcgtttactgattactagcgaagctgcgggtgc
atttttcaagataaaggcatccccgattatattctataccgatgtggattgcgcatactttgtgaacagaaagtgatagcgttgatgattcttcattggtcagaaaatta
tgaacggtttcttctattttgtctctatatactacgtataggaaatgtttacattttcgtattgttttcgattcactctatgaatagttcttactacaatttttttgtctaaagagtaat
actagagataaacataaaaaatgtagaggtcgagtttagatgcaagttcaaggagcgaaaggtggatgggtaggttatatagggatatagcacagagatatat
agcaaagagatactttgagcaatgtttgtggaagcggtattcgcaatattttagtagctcgttacagtccggtgcgtttttggttttttgaaagtgcgtcttcagagcgct
tttggttttcaaaagcgctctgaagttcctatactttctagctagagaataggaacttcggaataggaacttcaaagcgtttccgaaaacgagcgcttccgaaaatg
caacgcgagctgcgcacatacagctcactgttcacgtcgcacctatatctgcgtgttgcctgtatatatatatacatgagaagaacggcatagtgcgtgtttatgctt
aaatgcgtacttatatgcgtctatttatgtaggatgaaaggtagtctagtacctcctgtgatattatcccattccatgcggggtatcgtatgcttccttcagcactacccttt
agctgttctatatgctgccactcctcaattggattagtctcatccttcaatgctatcatttcctttgatattggatcgatccgatgataagctgtcaaacatgagaattgggt
aataactgatataattaaattgaagctctaatttgtgagtttagtatacatgcatttacttatataatacagttttttagttttgctggccgcatcttctcaaatatgcttcccagc
ctgcttttctgtaacgttcaccctctaccttagcatcccttcccttgcaaatagtcctcttccaacaataataatgtcagatcctgtagagaccacatcatccacggttct
atactgttgacccaatgcgtctcccttgtcatctaaacccacaccgggtgtcataatcaaccaatcgtaaccttcatctcttccacccatgtctctttgagcaataaag
ccgataacaaaatctttgtcgctcttcgcaatgtcaacagtacccttagtatattctccagtagatagggagcccttgcatgacaattctgctaacatcaaaaggcct

ctaggttcctttgttacttcttctgccgcctgcttcaaaccgctaacaatacctgggcccaccacaccgtgtgcattcgtaatgtctgcccattctgctattctgtatacac
ccgcagagtactgcaatttgactgtattaccaatgtcagcaaatttctgtcttcgaagagtaaaaaattgtacttggcggataatgcctttagcggcttaactgtgcc
ctccatggaaaaatcagtcaagatatccacatgtgtttttagtaaacaaatttgggacctaatgcttcaactaactccagtaattccttggtggtacgaacatccaat
gaagcacacaagtttgtttgcttttcgtgcatgatattaaatagcttggcagcaacaggactaggatgagtagcagcacgttccttatatgtagctttcgacatgattta
tcttcgtttcctgcatgtttttgttctgtgcagttgggttaagaatactgggcaatttcatgtttcttcaacactacatatgcgtatatataccaatctaagtctgtgctccttcct
tcgttcttccttctgttcggagattaccgaatcaaaaaaatttcaaggaaaccgaaatcaaaaaaaagaataaaaaaaaaaatgatgaattgaaaagctaattctt
gaagacgaaagggcctcgtgatacgcctatttttataggttaatgtcatgataataatggtttcttagacgtcaggtggcacttttcggggaaatgtgcgcggaaccc
ctatttgtttatttttctaaatacattcaaatatgtatccgctcatgagacaataaccctgataaatgcttcaataatattgaaaaaggaagagtatgagtattcaacattt
ccgtgtcgcccttattcccttttttgcggcattttgccttcctgtttttgctcacccagaaacgctggtgaaagtaaaagatgctgaagatcagttgggtgcacgagtgg
gttacatcgaactggatctcaacagcggtaagatccttgagagttttcgccccgaagaacgttttccaatgatgagcacttttaaagttctgctatgtggcgcggtatt
atcccgtattgacgccgggcaagagcaactcggtcgccgcatacactattctcagaatgacttggttgagtactcaccagtcacagaaaagcatcttacggatg
gcatgacagtaagagaattatgcagtgctgccataaccatgagtgataacactgcggccaacttacttctgacaacgatcggaggaccgaaggagctaaccg
ctttttgcacaacatgggggatcatgtaactcgccttgatcgttgggaaccggagctgaatgaagccataccaaacgacgagcgtgacaccacgatgcctgta
gcaatggcaacaacgttgcgcaaactattaactggcgaactacttactctagcttcccggcaacaattaatagactggatggaggcggataaagttgcaggacc
acttctgcgctcggcccttccggctggctggtttattgctgataaatctggagccggtgagcgtgggtctcgcggtatcattgcagcactggggccagatggtaagc
cctcccgtatcgtagttatctacacgacggggagtcaggcaactatggatgaacgaaatagacagatcgctgagataggtgcctcactgattaagcattggtaa
ctgtcagaccaagtttactcatatatactttagattgatttaaaacttcatttttaatttaaaaggatctaggtgaagatccttttgataatctcatgaccaaaatcccttaa
cgtgagttttcgttccactgagcgtcagaccccgtagaaaagatcaaaggatcttc

pMDC7NtmVenus sequence

ctggacctaccaaggcaacgctatgttctcttgcttttgtcagcaagatagccagatcaatgtcgatcgtggctggctcgaagatacctgcaagaatgtcattgcgc
tgccattctccaaattgcagttcgcgcttagctggataacgccacggaatgatgtcgtcgtgcacaacaatggtgacttctacagcgcggagaatctcgctctctcc
aggggaagccgaagtttccaaaaggtcgttgatcaaagctcgccgcgttgtttcatcaagccttacggtcaccgtaaccagcaaatcaatatcactgtgtggcttc
aggccgccatccactgcggagccgtacaaatgtacggccagcaacgtcggttcgagatggcgctcgatgacgccaactacctctgatagttgagtcgatacttc
ggcgatcaccgcttcccccatgatgtttaactttgttttagggcgactgccctgctgcgtaacatcgttgctgctccataacatcaaacatcgacccacggcgtaacg
cgcttgctgcttggatgcccgaggcatagactgtaccccaaaaaaacagtcataacaagccatgaaaaccgccactgcgccgttaccaccgctgcgttcggtc
aaggttctggaccagttgcgtgagcgcatacgctacttgcattacagcttacgaaccgaacaggcttatgtccactgggttcgtgcccgaattgatcacaggcag
caacgctctgtcatcgttacaatcaacatgctaccctccgcgagatcatccgtgtttcaaacccggcagcttagttgccgttcttccgaatagcatcggtaacatga
gcaaagtctgccgccttacaacggctctcccgctgacgccgtcccggactgatgggctgcctgtatcgagtggtgattttgtgccgagctgccggtcggggagct
gttggctggctggtggcaggatatattgtggtgtaaacaaattgacgcttagacaacttaataacacattgcggacgtttttaatgtactgaattaacgccgaattga
attcgagctcggtacccgccattcaggctgcgcaactgttgggaagggcgatcggtgcgggcctcttcgctattacgccagctggcgaaaggggatgtgctgc
aaggcgattaagttgggtaacgccagggttttcccagtcacgacgttgtaaaacgacggccagtgaattcctcgactcggtacccctcgacacaaaaagccta
tactgtacttaacttgattgcataattacttgatcatagactcatagtaaacttgattacacagataagtgaagaaacaaaccaattcaagacataaccaaagaga
ggtgaaagactgttttatatgtctaacattgcaccttaatatcacactgttagttcctttcttacttaaattcaacccattaaagtaaaaacaacagataataataatttga
gaatgaacaaaaggaccatatcatttattaactcttatccatccatttgcattttgatgtccgaaaacaaaaactgaaagaacacagtaaattacaagcagaaca
aatgatagaagaaaacagcttttccaatgccataatactcaaacttagtaggattctggtgtgtgggcaatgaaactgatgcattgaacttgacgaacgttgtcga
aaccgatgatacggacgaaagctgggaggcctggatcgactagttaattaagaattatcaaccactttgtacaagaaagctgaacgagaaacgtaaaatgat
ataaatatcaatatattaaattagattttgcataaaaaacagactacataatactgtaaaacacaacatatccagtcactatggtcgacctgcagactggctgtgtat
aagggagcctgacatttatattccccagaacatcaggttaatggcgtttttgatgtcattttcgcggtggctgagatcagccacttcttccccgataacggagaccgg
cacactggccatatcggtggtcatcatgcgccagctttcatccccgatatgcaccaccgggtaaagttcacgggagactttatctgacagcagacgtgcactggc
caggggggatcaccatccgtcgcccgggcgtgtcaataatatcactctgtacatccacaaacagacgataacggctctctcttttataggtgtaaaccttaaactgc
atttcaccagcccctgttctcgtcagcaaaagagccgttcatttcaataaaccgggcgacctcagccatcccttcctgattttccgctttccagcgttcggcacgcag
acgacgggcttcattctgcatggttgtgcttaccagaccggagatattgacatcatatatgccttgagcaactgatagctgtcgctgtcaactgtcactgtaatacgct
gcttcatagcatacctctttttgacatacttcgggtatacatatcagtatatattcttataccgcaaaaatcagcgcgcaaatacgcatactgttatctggcttttagtaag
ccggatccagatctttacgcccgccctgccactcatcgcagtactgttgtaattcattaagcattctgccgacatggaagccatcacaaacggcatgatgaacct
gaatcgccagcggcatcagcaccttgtcgccttgcgtataatatttgcccatggtgaaaacgggggcgaagaagttgtccatattggccacgtttaaatcaaaact
ggtgaaactcacccagggattggctgagacgaaaaacatattctcaataaaccctttagggaaataggccaggttttcaccgtaacacgccacatcttgcgaat
atatgtgtagaaactgccggaaatcgtcgtggtattcactccagagcgatgaaaacgtttcagtttgctcatggaaaacggtgtaacaagggtgaacactatccc
atatcaccagctcaccgtctttcattgccatacggaattccggatgagcattcatcaggcgggcaagaatgtgaataaaggccggataaaacttgtgcttatttttctt
tacggtctttaaaaaggccgtaatatccagctgaacggtctggttataggtacattgagcaactgactgaaatgcctcaaaatgttctttacgatgccattgggatat
atcaacggtggtatatccagtgatttttttctccattttagcttccttagctcctgaaaatctcgacggatcctaactcaaaatccacacattatacgagccggaagcat
aaagtgtaaagcctggggtgcctaatgcggccgccatagtgactggatatgttgtgttttacagtattatgtagtctgttttttatgcaaaatctaatttaatatattgatatt
tatatcatttacgtttctcgttcagctttttgtacaaacttgtacctccgccgcttccaccgcctcccttgtacagctcgtccatgccgagagtgatcccggcggcggtc
acgaactccagcaggaccatgtgatcgcgcttctcgttggggtctttgctcagggcggactggtagctcaggtagtggttgtcgggcagcagcacggggccgtc
gccgatgggggtgttctgctggtagtggtcggcgagctgcacgccgccgtcctcgatgttgtggcggatcttgaagttggccttgatgccgttcttctgcttgtcggcg
gtgatatagacgttgtggctgttgtagttgtactccagcttgtgccccaggatgttgccgtcctccttgaagtcgatgcccttcagctcgatgcggttcaccagggtgtc
gccctcgaacttcacctcggcgcgggtcttgtagttgccgtcgtccttgaagaagatggtgcgctcctggacgtagccttcgggcatggcggacttgaagaagtcg
tgctgcttcatgtggtcggggtagcgggcgaagcactgcaggccgtagcccagggtggtcacgagggtgggccagggcacgggcagcttgccggtggtgca
gatcagcttcagggtcagcttgccgtaggtggcatcgccctcgccctcgccggacacgctgaacttgtggccgtttacgtcgccgtccagctcgaccaggatggg
caccaccccggtgaacagctcctcgcccttgctcaccatggtgaagggtcttgcgaagatcctagagtcgagcatattacatggcattaccaccatatacatatcc
atatacatatccatatctaatcttacctcgactgctgtatataaaaccagtggttatatgtacagtactgctgtatataaaaccagtggttatatgtacagtacgtcgag
gggatgataatgcgattagttttttagcctcgacctgcagcccaagcggcatgcaagctgtcgaggggggatcaattcccgatctagtaacatagatgacaccgc

gcgcgataatttatcctagtttgcgcgctatattttgttttctatcgcgtattaaatgtataattgcgggactctaatcataaaaacccatctcataaataacgtcatgcatt
acatgttaattattacatgcttaacgtaattcaacagaaattatatgataatcatcgcaagaccggcaacaggattcaatcttaagaaactttattgccaaatgtttga
acgatcggggaaattcgggggatcagcttgtgatcatgttacatcacctccaagatcccggacgagtgctggggcgtcggtttccactatcggcgagtacttctac
acagccatcggtccagacggccgcgcttctgcgggcgatttgtgtacgcccgacagtcccggctccggatcggacgattgcgtcgcatcgaccctgcgcccaa
gctgcatcatcgaaattgccgtcaaccaagctctgatagagttggtcaagaccaatgcggagcatatacgcccggagccgcggcgatcctgcaagctccggat
gcctccgctcgaagtagcgcgtctgctgctccatacaagccaaccacggcctccagaagaagatgttggcgacctcgtattgggaatccccgaacatcgcctc
gctccagtcaatgaccgctgttatgcggccattgtccgtcaggacattgttggagccgaaatccgcgtgcacgaggtgccggacttcggggcagtcctcggccc
aaagcatcagctcatcgagagcctgcgcgacggacgcactgacggtgtcgtccatcacagtttgccagtgatacacatggggatcagcaatcgcgcatatga
aatcacgccatgtagtgtattgaccgattccttgcggtccgaatgggccgaacccgctcgtctggctaagatcggccgcagcgatcgcatccatggcctccgcga
ccggctgcagaacagcgggcagttcggtttcaggcaggtcttgcaacgtgacaccctgtgcacggcgggagatgcaataggtcaggctctcgctgaattcccc
aatgtcaagcacttccggaatcgggagcgcggccgatgcaaagtgccgataaacataacgatctttgtagaaaccatcggcgcagctatttacccgcaggac
atatccacgccctcctacatcgaagctgaaagcacgagattcttcgccctccgagagctgcatcaggtcggagacgctgtcgaacttttcgatcagaaacttctc
gacagacgtcgcggtgagttcaggctttttcatatctcattgccccccgggatcttgcaggtcgagatcctctagcggatccggtgcagattatttggattgagagtg
aatatgagactctaattggataccgaggggaatttatggaacgtcagtggagcatttttgacaagaaatatttgctagctgatagtgaccttaggcgacttttgaacg
cgcaataatggtttctgacgtatgtgcttagctcattaaactccagaaacccgcggctgagtggctccttcaacgttgcggttctgtcagttccaaacgtaaaacgg
cttgtcccgcgtcatcggcgggggtcataacgtgactcccttaattctccgctcatgatcagattgtcgtttcccgccttcagtttcaagcttgtttggggatctagtgtttt
actcctcatattaacttcggtcattagaggccacgatttgacacatttttactcaaaacaaaatgtttgcatatctcttataatttcaaattcaacacacaacaaataag
agaaaaaacaaataatattaatttgagaatgaacaaaaggaccatatcattcattaactcttctccatccatttccatttcacagttcgatagcgaaaaccgaataa
aaaacacagtaaattacaagcacaacaaatggtacaagaaaaacagttttcccaatgccataatactcgaacaagctagcttactcagttaggtcgagtcatttt
tgatgaaacagaagctttttgatatttccatttgaatattttggtatctgattagtgatgatttcagctaacatctctgggaattccgccagggagctctcagactgtggca
gggaaaccctctgcctcccccgtgatgtaatacttttgcaaggaatgcgatgaagtagagcccgcagtggccaagtggctttggtccgtctcctccacggatgcc
cctccacggctagtgggcgcatgtaggcggtgggcgtccagcatctccagcagcaggtcatagaggggcaccacgttcttgcacttcatgctgtacagatgctc
catgcctttgttactcatgtgcctgatgtgggagaggatgaggaggagctgggccagccgctggtgctgctgctgcagggtcaggcctgccttggccatcaggtg
gatcaaagtgtctgtgatcttgtccaggactcggtggatatggtccttctcttccagagacttcagggtgctggacagaaatgtgtacactccagaattaagcaaaa
taatagatttgaggcacacaaactcctctccctgcagattcatcatgcggaaccgagatgatgtagccagcagcatgtcgaagatctccaccatgccctctacac
attttccctggttcctgtccaagagcaagttaggagcaaacagtagcttccctgggtgctccatggagcgccagacgagaccaatcatcaggatctctagccagg
cacattctagaaggtggacctgatcatggagggtcaaatccacaaagcctggcaccctcttcgcccagttgatcatgtgaaccagctccctgtctgccaggttggt
cagtaagcccatcatcgaagcttcactgaagggtctggtaggatcatactcggaatagagtatgggggctcagcatccaacaaggcactgaccatctggtcg
gccgtcagggacaaggccaggctgttcttcttagagcgtttgatcatgagcgggcttggccaaaggttggcagctctcatgtctccagcagacggatccccaccg
tactcgtcaattccaagggcatcggtaaacatctgctcaaactcgaagtcggccatatccagagcgccgtagggggcggagtcgtgggggtaaatcccgga
cccggggaatccccgtcccccaacatgtccagatcgaaatcgtctagcgcgtcggcatgcgccatcgccacgtcctcgccgtctaagtggagctcgtccccca
ggctgacatcggtcgggggggcgctcgacggttcaccggcagccacacgacctaccagcggcaacccttcttcctcttcctgcaacagacgaatcccgcgtg
atgcgccggaaacaatttcaataacgcctttgcgtgccagcgccttcagatgttcttcagccgcgtttggggaacggaaccccaaacgctgcgcgatttccgcac
gcgtcggcggcatacctgtctggctgatgtgatcacggatgagatcaaacacctcttgttgcctggccgttaacgctttcattccgcccggaattggggatcccagc
gtgtcctctccaaatgaaatgaacttccttatatagaggaagggtcttgcgaaggatagtgggattgtgcgtcatcccttacgtcagtggagatggatcctctagag
gcacgtggcggcacgtggcggcacgtggcggcacgtggcaagcttggatccacgatatcctgcaggcatgcaagcttagcttgagcttggatcagattgtcgttt
cccgccttcagtttaaactatcagtgtttgacaggatatattggcgggtaaacctaagagaaaagagcgtttattagaataatcggatatttaaaagggcgtgaaa
aggtttatccgttcgtccatttgtatgtgcatgccaaccacagggttcccctcgggatcaaagtactttaaagtactttaaagtactttaaagtactttgatccaacccct
ccgctgctatagtgcagtcggcttctgacgttcagtgcagccgtcttctgaaaacgacatgtcgcacaagtcctaagttacgcgacaggctgccgccctgccctttt
cctggcgttttcttgtcgcgtgttttagtcgcataaagtagaatacttgcgactagaaccggagacattacgccatgaacaagagcgccgccgctggcctgctggg
ctatgcccgcgtcagcaccgacgaccaggacttgaccaaccaacgggccgaactgcacgcggccggctgcaccaagctgttttccgagaagatcaccggc
accaggcgcgaccgcccggagctggccaggatgcttgaccacctacgccctggcgacgttgtgacagtgaccaggctagaccgcctggcccgcagcaccc
gcgacctactggacattgccgagcgcatccaggaggccggcgcgggcctgcgtagcctggcagagccgtgggccgacaccaccacgccggccggccgc
atggtgttgaccgtgttcgccggcattgccgagttcgagcgttccctaatcatcgaccgcacccggagcgggcgcgaggccgccaaggcccgaggcgtgaag
tttggcccccgccctaccctcaccccggcacagatcgcgcacgcccgcgagctgatcgaccaggaaggccgcaccgtgaaagaggcggctgcactgcttgg
cgtgcatcgctcgaccctgtaccgcgcacttgagcgcagcgaggaagtgacgcccaccgaggccaggcggcgcggtgccttccgtgaggacgcattgaccg
aggccgacgccctggcggccgccgagaatgaacgccaagaggaacaagcatgaaaccgcaccaggacggccaggacgaaccgtttttcattaccgaag
agatcgaggcggagatgatcgcggccgggtacgtgttcgagccgcccgcgcacgtctcaaccgtgcggctgcatgaaatcctggccggtttgtctgatgccaa
gctggcggcctggccggccagcttggccgctgaagaaaccgagcgccgccgtctaaaaaggtgatgtgtatttgagtaaaacagcttgcgtcatgcggtcgct
gcgtatatgatgcgatgagtaaataaacaaatacgcaaggggaacgcatgaaggttatcgctgtacttaaccagaaaggcgggtcaggcaagacgaccatc
gcaacccatctagcccgcgccctgcaactcgccggggccgatgttctgttagtcgattccgatccccagggcagtgcccgcgattgggcggccgtgcgggaag
atcaaccgctaaccgttgtcggcatcgaccgcccgacgattgaccgcgacgtgaaggccatcggccggcgcgacttcgtagtgatcgacggagcgccccag
gcggcggacttggctgtgtccgcgatcaaggcagccgacttcgtgctgattccggtgcagccaagcccttacgacatatgggccaccgccgacctggtggagc
tggttaagcagcgcattgaggtcacggatggaaggctacaagcggcctttgtcgtgtcgcgggcgatcaaaggcacgcgcatcggcggtgaggttgccgagg
cgctggccgggtacgagctgcccattcttgagtcccgtatcacgcagcgcgtgagctacccaggcactgccgccgccggcacaaccgttcttgaatcagaacc
cgagggcgacgctgcccgcgaggtccaggcgctggccgctgaaattaaatcaaaactcatttgagttaatgaggtaaagagaaaatgagcaaaagcacaa
acacgctaagtgccggccgtccgagcgcacgcagcagcaaggctgcaacgttggccagcctggcagacacgccagccatgaagcgggtcaactttcagtt
gccggcggaggatcacaccaagctgaagatgtacgcggtacgccaaggcaagaccattaccgagctgctatctgaatacatcgcgcagctaccagagtaa
atgagcaaatgaataaatgagtagatgaattttagcggctaaaggaggcggcatggaaaatcaagaacaaccaggcaccgacgccgtggaatgccccatgt
gtggaggaacgggcggttggccaggcgtaagcggctgggttgtctgccggccctgcaatggcactggaaccccaagcccgaggaatcggcgtgagcggt
cgcaaaccatccggcccggtacaaatcggcgcggcgctgggtgatgacctggtggagaagttgaaggccgcgcaggccgcccagcggcaacgcatcgag
gcagaagcacgccccggtgaatcgtggcaagcggccgctgatcgaatccgcaaagaatcccggcaaccgccggcagccggtgcgccgtcgattaggaag
ccgcccaagggcgacgagcaaccagatttttcgttccgatgctctatgacgtgggcacccgcgatagtcgcagcatcatggacgtggccgttttccgtctgtcga
agcgtgaccgacgagctggcgaggtgatccgctacgagcttccagacgggcacgtagaggtttccgcagggccggccggcatggccagtgtgtgggattac
gacctggtactgatggcggtttcccatctaaccgaatccatgaaccgataccgggaagggaagggagacaagcccggccgcgtgttccgtccacacgttgcg
gacgtactcaagttctgccggcgagccgatggcggaaagcagaaagacgacctggtagaaacctgcattcggttaaacaccacgcacgttgccatgcagcg
tacgaagaaggccaagaacggccgcctggtgacggtatccgagggtgaagccttgattagccgctacaagatcgtaaagagcgaaaccgggcggccgga

gtacatcgagatcgagctagctgattggatgtaccgcgagatcacagaaggcaagaacccggacgtgctgacggttcaccccgattacttttttgatcgatcccg
gcatcggccgttttctctaccgcctggcacgccgcgccgcaggcaaggcagaagccagatggttgttcaagacgatctacgaacgcagtggcagcgccgga
gagttcaagaagttctgtttcaccgtgcgcaagctgatcgggtcaaatgacctgccggagtacgatttgaaggaggaggcggggcaggctggcccgatcctag
tcatgcgctaccgcaacctgatcgagggcgaagcatccgccggttcctaatgtacggagcagatgctagggcaaattgccctagcaggggaaaaaggtcga
aaaggtctctttcctgtggatagcacgtacattgggaacccaaagccgtacattgggaaccggaacccgtacattgggaacccaaagccgtacattgggaacc
ggtcacacatgtaagtgactgatataaaagagaaaaaaggcgatttttccgcctaaaactctttaaaacttattaaaactcttaaaacccgcctggcctgtgcata
actgtctggccagcgcacagccgaagagctgcaaaaagcgcctacccttcggtcgctgcgctccctacgccccgccgcttcgcgtcggcctatcgcggccgct
ggccgctcaaaaatggctggcctacggccaggcaatctaccagggcgcggacaagccgcgccgtcgccactcgaccgccggcgcccacatcaaggcacc
ctgcctcgcgcgtttcggtgatgacggtgaaaacctctgacacatgcagctcccggagacggtcacagcttgtctgtaagcggatgccgggagcagacaagcc
cgtcagggcgcgtcagcgggtgttggcgggtgtcggggcgcagccatgacccagtcacgtagcgatagcggagtgtatactggcttaactatgcggcatcaga
gcagattgtactgagagtgcaccatatgcggtgtgaaataccgcacagatgcgtaaggagaaaataccgcatcaggcgctcttccgcttcctcgctcactgactc
gctgcgctcggtcgttcggctgcggcgagcggtatcagctcactcaaaggcggtaatacggttatccacagaatcaggggataacgcaggaaagaacatgtg
agcaaaaggccagcaaaaggccaggaaccgtaaaaaggccgcgttgctggcgtttttccataggctccgcccccctgacgagcatcacaaaaatcgacgct
caagtcagaggtggcgaaacccgacaggactataaagataccaggcgtttcccccctggaagctccctcgtgcgctctcctgttccgaccctgccgcttaccgga
tacctgtccgcctttctcccttcgggaagcgtggcgctttctcatagctcacgctgtaggtatctcagttcggtgtaggtcgttcgctccaagctgggctgtgtgcacga
acccccgttcagcccgaccgctgcgccttatccggtaactatcgtcttgagtccaacccggtaagacacgacttatcgccactggcagcagccactggtaaca
ggattagcagagcgaggtatgtaggcggtgctacagagttcttgaagtggtggcctaactacggctacactagaaggacagtatttggtatctgcgctctgctgaa
gccagttaccttcggaaaaagagttggtagctcttgatccggcaaacaaaccaccgctggtagcggtggttttttgtttgcaagcagcagattacgcgcagaaa
aaaaggatctcaagaagatcctttgatcttttctacggggtctgacgctcagtggaacgaaaactcacgttaagggattttggtcatgcatgatatatctcccaatttg
tgtagggcttattatgcacgcttaaaaataataaagcagacttgacctgatagtttggctgtgagcaattatgtgcttagtgcatctaacgcttgagttaagccgcgc
cgcgaagcggcgtcggcttgaacgaatttctagctagacattatttgccgactaccttggtgatctcgcctttcacgtagtggacaaattcttccaactgatctgcgcg
cgaggccaagcgatcttcttcttgtccaagataagcctgtctagcttcaagtatgacgggctgatactgggccggcaggcgctccattgcccagtcggcagcgac
atccttcggcgcgattttgccggttactgcgctgtaccaaatgcgggacaacgtaagcactacatttcgctcatcgccagcccagtcgggcggcgagttccatag
cgttaaggtttcatttagcgcctcaaatagatcctgttcaggaaccggatcaaagagttcctccgccg

pRD04 i. mVenus in pAB111 sequence

taagcacatacgtcagaaaccattattgcgcgttcaaaagtcgcctaaggtcactatcagctagcaaatatttcttgtcaaaaatgctccactgacgttccataaatt
cccctcggtatccaattagagtctcatattcactctcaatccaaataatctgcaccggatccgctagaggatctcgacctgcaagatcccgggggggcaatgagat
atgaaaaagcctgaactcaccgcgacgtctgtcgagaagtttctgatcgaaaagttcgacagcgtctccgacctgatgcagctctcggagggcgaagaatctc
gtgctttcagcttcgatgtaggagggcgtggatatgtcctgcgggtaaatagctgcgccgatggtttctacaaagatcgttatgtttatcggcactttgcatcggccgc
gctcccgattccggaagtgcttgacattggggaattcagcgagagcctgacctattgcatctcccgccgtgcacagggtgtcacgttgcaagacctgcctgaaac
cgaactgcccgctgttctgcagccggtcgcggaggccatggatgcgatcgctgcggccgatcttagccagacgagcgggttcggcccattcggaccgcaagg
aatcggtcaatacactacatggcgtgatttcatatgcgcgattgctgatccccatgtgtatcactggcaaactgtgatggacgacaccgtcagtgcgtccgtcgcgc
aggctctcgatgagctgatgctttgggccgaggactgccccgaagtccggcacctcgtgcacgcggatttcggctccaacaatgtcctgacggacaatggccg
cataacagcggtcattgactggagcgaggcgatgttcggggattcccaatacgaggtcgccaacatcttcttctggaggccgtggttggcttgtatggagcagca
gacgcgctacttcgagcggaggcatccggagcttgcaggatcgccgcggctccgggcgtatatgctccgcattggtcttgaccaactctatcagagcttggttga
cggcaatttcgatgatgcagcttgggcgcagggtcgatgcgacgcaatcgtccgatccggagccgggactgtcgggcgtacacaaatcgcccgcagaagcg
cggccgtctggaccgatggctgtgtagaagtactcgccgatagtggaaaccgacgccccagcactcgtccgggatcttggaggtgatgtaacatgatcacaag
ctgatccccgaatttccccgatcgttcaaacatttggcaataaagtttcttaagattgaatcctgttgccggtcttgcgatgattatcatataatttctgttgaattacgtta
agcatgtaataattaacatgtaatgcatgacgttatttatgagatgggtttttatgattagagtcccgcaattatacatttaatacgcgatagaaaacaaaatatagcg
cgcaaactaggataaattatcgcgcgcggtgtcatctatgttactagatcgggaattgatccccccctcgacagcttgcatgccgcttgggctgcaggtcgaggcta
aaaaactaatcgcattatcatcccctcgacgtactgtacatataaccactggttttatatacagcagtactgtacatataaccactggttttatatacagcagtcgacg
tactgtacatataaccactggttttatatacagcagtactgtacatataaccactggttttatatacagcagtcgaggtaagattagatatggatatgtatatggatatgt
atatggtggtaatgccatgtaatatgctcgactctaggatcttcgcaagacccttcctctatataaggaagttcatttcatttggagaggacacgctgaagctagtcg
actctagcctcgaggcgcgccaagctatcaacaagtttgtacaaaaaagctgaacgagaaacgtaaaatgatataaatatcaatatattaaattagattttgcat
aaaaaacagactacataatactgtaaaacacaacatatccagtcactatggcggccgcattaggcaccccaggctttacactttatgcttccggctcgtataatgt
gtggattttgagttaggatccgtcgagattttcaggagctaaggaagctaaaatggagaaaaaaatcactggatataccaccgttgatatatcccaatggcatcgt
aaagaacattttgaggcatttcagtcagttgctcaatgtacctataaccagaccgttcagctggatattacggccttttaaagaccgtaaagaaaaataagcaca
agttttatccggcctttattcacattcttgcccgcctgatgaatgctcatccggaattccgtatggcaatgaaagacggtgagctggtgatatgggatagtgttcaccct
tgttacaccgttttccatgagcaaactgaaacgttttcatcgctctggagtgaataccacgacgatttccggcagtttctacacatatattcgcaagatgtggcgtgtta
cggtgaaaacctggcctatttccctaaagggtttattgagaatatgtttttcgtctcagccaatccctgggtgagtttcaccagttttgatttaaacgtggccaatatgga
caacttcttcgcccccgttttcaccatgggcaaatattatacgcaaggcgacaaggtgctgatgccgctggcgattcaggttcatcatgccgtttgtgatggcttccat
gtcggcagaatgcttaatgaattacaacagtactgcgatgagtggcagggcggggcgtaaagatctggatccggcttactaaaagccagataacagtatgcgt
atttgcgcgctgatttttgcggtataagaatatatactgatatgtatacccgaagtatgtcaaaaagaggtatgctatgaagcagcgtattacagtgacagttgacag
cgacagctatcagttgctcaaggcatatatgatgtcaatatctccggtctggtaagcacaaccatgcagaatgaagcccgtcgtctgcgtgccgaacgctggaa
agcggaaaatcaggaagggatggctgaggtcgcccggtttattgaaatgaacggctcttttgctgacgagaacaggggctggtgaaatgcagtttaaggtttac
acctataaaagagagagccgttatcgtctgtttgtggatgtacagagtgatattattgacacgcccgggcgacggatggtgatcccctggccagtgcacgtctgc
tgtcagataaagtctcccgtgaactttacccggtggtgcatatcggggatgaaagctggcgcatgatgaccaccgatatggccagtgtgccggtctccgttatcgg
ggaagaagtggctgatctcagccaccgcgaaaatgacatcaaaaacgccattaacctgatgttctggggaatataaatgtcaggctcccttatacacagccagt
ctgcaggtcgaccatagtgactggatatgttgtgttttacagtattatgtagtctgtttttttatgcaaaatctaatttaatatattgatatttatatcattttacgtttctcgttcag
ctttcttgtacaaagtggttgatcattccttaattaaaatggtgagcaagggcgaggagctgttcaccggggtggtgcccatcctggtcgagctggacggcgacgt
aaacggccacaagttcagcgtgtccggcgagggcgagggcgatgccacctacggcaagctgaccctgaagctcatctgcaccaccggcaagctgcccgtg

ccctggcccaccctcgtgaccaccctcggctacggcctgcagtgcttcgcccgctaccccgaccacatgaagcagcacgacttcttcaagtccgccatgcccg
aaggctacgtccaggagcgcaccatcttcttcaaggacgacggcaactacaagacccgcgccgaggtgaagttcgagggcgacaccctggtgaaccgcat
cgagctgaagggcatcgacttcaaggaggacggcaacatcctggggcacaagctggagtacaactacaacagccacaacgtctatatcaccgccgacaag
cagaagaacggcatcaaggccaacttcaagatccgccacaacatcgaggacggcggcgtgcagctcgccgaccactaccagcagaacaccccccatcgg
cgacggccccgtgctgctgcccgacaaccactacctgagctaccagtccaagctgagcaaagaccccaacgagaagcgcgatcacatggtcctgctggagt
tcgtgaccgccgccgggatcactctcggcatggacgagctgtacaagtaactagtcgatccaggcctcccagctttcgtccgtatcatcggtttcgacaacgttcgt
caagttcaatgcatcagtttcattgcccacacaccagaatcctactaagtttgagtattatggcattggaaaagctgttttcttctatcatttgttctgcttgtaatttactgt
gttctttcagtttttgttttcggacatcaaaatgcaaatggatggataagagttaataaatgatatggtccttttgttcattctcaaattattattatctgttgtttttacttttaatg
ggttgaatttaagtaagaaaggaactaacagtgtgatattaaggtgcaatgttagacatataaaacagtctttcacctctctttggttatgtcttgaattggtttgtttcttc
acttatctgtgtaatcaagtttactatgagtctatgatcaagtaattatgcaatcaagttaagtacagtataggctttttgtgtcgaggggggtaccgagtcgaggaattc
actggccgtcgttttacaacgtcgtgactgggaaaaccctggcgttacccaacttaatcgccttgcagcacatcccccctttcgccagctggcgtaatagcgaaga
ggcccgcaccgatcgcccttcccaacagttgcgcagcctgaatggcgggtaccgagctcgaattcaattcggcgttaattcagtacattaaaaacgtccgcaat
gtgttattaagttgtctaagcgtcaatttgtttacaccacaatatatcctgccaccagccagccaacagctccccgaccggcagctcggcacaaaatcaccactcg
atacaggcagcccatcagtccgggacggcgtcagcgggagagccgttgtaaggcggcagactttgctcatgttaccgatgctattcggaagaacggcaacta
agctgccgggtttgaaacacggatgatctcgcggagggtagcatgttgattgtaacgatgacagagcgttgctgcctgtgatcaattcgggcacgaacccagtg
gacataagcctgttcggttcgtaagctgtaatgcaagtagcgtatgcgctcacgcaactggtccagaaccttgaccgaacgcagcggtggtaacggcgcagtg
gcggttttcatggcttgttatgactgtttttttggggtacagtctatgcctcgggcatccaagcagcaagcgcgttacgccgtgggtcgatgtttgatgttatggagcag
caacgatgttacgcagcagggcagtcgccctaaaacaaagttaaacatcatgggggaagcggtgatcgccgaagtatcgactcaactatcagaggtagttgg
cgtcatcgagcgccatctcgaaccgacgttgctggccgtacatttgtacggctccgcagtggatggcggcctgaagccacacagtgatattgatttgctggttacg
gtgaccgtaaggcttgatgaaacaacgcggcgagctttgatcaacgacctttttggaaacttcggcttcccctggagagagcgagattctccgcgctgtagaagtc
accattgttgtgcacgacgacatcattccgtggcgttatccagctaagcgcgaactgcaatttggagaatggcagcgcaatgacattcttgcaggtatcttcgagc
cagccacgatcgacattgatctggctatcttgctgacaaaagcaagagaacatagcgttgccttggtaggtccagcggcggaggaactctttgatccggttcctg
aacaggatctatttgaggcgctaaatgaaaccttaacgctatggaactcgccgcccgactgggctggcgatgagcgaaatgtagtgcttacgttgtcccgcatttg
gtacagcgcagtaaccggcaaaatcgcgccgaaggatgtcgctgccgactgggcaatggagcgcctgccggcccagtatcagcccgtcatacttgaagcta
gacaggcttatcttggacaagaagaagatcgcttggcctcgcgcgcagatcagttggaagaatttgtccactacgtgaaaggcgagatcaccaaggtagtcgg
caaataatgtctagctagaaattcgttcaagccgacgccgcttcgcggcgcggcttaactcaagcgttagatgcactaagcacataattgctcacagccaaacta
tcaggtcaagtctgcttttattatttttaagcgtgcataataagccctacacaaattgggagatatatcatgcatgaccaaaatcccttaacgtgagttttcgttccactg
agcgtcagaccccgtagaaaagatcaaaggatcttcttgagatccttttttttctgcgcgtaatctgctgcttgcaaacaaaaaaaccaccgctaccagcggtggttt
gtttgccggatcaagagctaccaactctttttccgaaggtaactggcttcagcagagcgcagataccaaatactgtccttctagtgtagccgtagttaggccaccac
ttcaagaactctgtagcaccgcctacatacctcgctctgctaatcctgttaccagtggctgctgccagtggcgataagtcgtgtcttaccgggttggactcaagacg
atagttaccggataaggcgcagcggtcgggctgaacgggggttcgtgcacacagcccagcttggagcgaacgacctacaccgaactgagatacctacag
cgtgagctatgagaaagcgccacgcttcccgaagggagaaaggcggacaggtatccggtaagcggcagggtcggaacaggagagcgcacgagggagc
ttccagggggaaacgcctggtatctttatagtcctgtcgggtttcgccacctctgacttgagcgtcgatttttgtgatgctcgtcaggggggcggagcctatggaaaa
acgccagcaacgcggccttttacggttcctggccttttgctggccttttgctcacatgttctttcctgcgttatcccctgattctgtggataaccgtattaccgcctttgagt
gagctgataccgctcgccgcagccgaacgaccgagcgcagcgagtcagtgagcgaggaagcggaagagcgcctgatgcggtattttctccttacgcatctgt
gcggtatttcacaccgcatatggtgcactctcagtacaatctgctctgatgccgcatagttaagccagtatacactccgctatcgctacgtgactgggtcatggctgc
gccccgacacccgccaacacccgctgacgcgccctgacgggcttgtctgctcccggcatccgcttacagacaagctgtgaccgtctccgggagctgcatgtgt
cagaggttttcaccgtcatcaccgaaacgcgcgaggcagggtgccttgatgtgggcgccggcggtcgagtggcgacggcgcggcttgtccgcgccctggtag
attgcctggccgtaggccagccatttttgagcggccagcggccgcgataggccgacgcgaagcggcggggcgtagggagcgcagcgaccgaagggtagg
cgcttttgcagctcttcggctgtgcgctggccagacagttatgcacaggccaggcgggttttaagagttttaataagttttaaagagttttaggcggaaaaatcgcct
ttttctcttttatatcagtcacttacatgtgtgaccggttcccaatgtacggctttgggttcccaatgtacgggttccggttcccaatgtacggctttgggttcccaatgtac
gtgctatccacaggaaagagacctttcgacctttttcccctgctagggcaatttgccctagcatctgctccgtacattaggaaccggcggatgcttcgccctcgatc
aggttgcggtagcgcatgactaggatcgggccagcctgccccgcctcctccttcaaatcgtactccggcaggtcatttgacccgatcagcttgcgcacggtgaaa
cagaacttcttgaactctccggcgctgccactgcgttcgtagatcgtcttgaacaaccatctggcttctgccttgcctgcggcgcggcgtgccaggcggtagagaa
aacggccgatgccgggatcgatcaaaaagtaatcggggtgaaccgtcagcacgtccgggttcttgccttctgtgatctcgcggtacatccaatcagctagctcga
tctcgatgtactccggccgcccggtttcgctctttacgatcttgtagcggctaatcaaggcttcaccctcggataccgtcaccaggcggccgttcttggccttcttcgta
cgctgcatggcaacgtgcgtggtgtttaaccgaatgcaggtttctaccaggtcgtctttctgctttccgccatcggctcgccggcagaacttgagtacgtccgcaac
gtgtggacggaacacgcggccgggcttgtctcccttccttcccggtatcggttcatggattcggttagatgggaaaccgccatcagtaccaggtcgtaatcccac
acactggccatgccggccggccctgcggaaacctctacgtgcccgtctggaagctcgtagcggatcacctcgccagctcgtcggtcacgcttcgacagacgg
aaaacggccacgtccatgatgctgcgactatcgcgggtgcccacgtcatagagcatcggaacgaaaaaatctggttgctcgtcgcccttgggcggcttcctaat
cgacggcgcaccggctgccggcggttgccgggattctttgcggattcgatcagcggccgcttgccacgattcaccggggcgtgcttctgcctcgatgcgttgccg
ctgggcggcctgcgcggccttcaacttctccaccaggtcatcacccagcgccgcgccgatttgtaccgggccggatggtttgcgaccgctcacgccgattcctcg
ggcttgggggttccagtgccattgcagggccggcagacaacccagccgcttacgcctggccaaccgcccgttcctccacacatggggcattccacggcgtcg
gtgcctggttgttcttgattttccatgccgcctcctttagccgctaaaattcatctactcatttattcatttgctcatttactctggtagctgcgcgatgtattcagatagcagct
cggtaatggtcttgccttggcgtaccgcgtacatcttcagcttggtgtgatcctccgccggcaactgaaagttgacccgcttcatggctggcgtgtctgccaggctgg
ccaacgttgcagccttgctgctgcgtgcgctcggacggccggcacttagcgtgtttgtgcttttgctcattttctctttacctcattaactcaaatgagttttgatttaatttca
gcggccagcgcctggacctcgcgggcagcgtcgccctcgggttctgattcaagaacggttgtgccggcggcggcagtgcctgggtagctcacgcgctgcgtg
atacgggactcaagaatgggcagctcgtacccggccagcgcctcggcaacctcaccgccgatgcgcgtgcctttgatcgcccgcgacacgacaaaggccg
cttgtagccttccatccgtgacctcaatgcgctgcttaaccagctccaccaggtcggcggtggcccatatgtcgtaagggcttggctgcaccggaatcagcacga
agtcggctgccttgatcgcggacacagccaagtccgccgcctggggcgctccgtcgatcactacgaagtcgcgccggccgatggccttcacgtcgcggtcaat
cgtcgggcggtcgatgccgacaacggttagcggttgatcttcccgcacggccgcccaatcgcgggcactgccctggggatcggaatcgactaacagaacatc
ggccccggcgagttgcagggcgcgggctagatgggttgcgatggtcgtcttgcctgacccgcctttctggttaagtacagcgataaccttcatgcgttcccccttgcg
tatttgtttatttactcatcgcatcatatacgcagcgaccgcatgacgcaagctgttttactcaaatacacatcacctttttagacggcggcgctcggtttcttcagcggc
caagctggccggccaggccgccagcttggcatcagacaaaccggccaggatttcatgcagccgcacggttgagacgtgcgcgggcggctcgaacacgtac
ccggccgcgatcatctccgcctcgatctcttcggtaatgaaaaacggttcgtcctggccgtcctggtgcggtttcatgcttgttcctcttggcgttcattctcggcggcc
gccagggcgtcggcctcggtcaatgcgtcctcacggaaggcaccgcgccgcctggcctcggtgggcgtcacttcctcgctgcgctcaagtgcgcggtacagg
gtcgagcgatgcacgccaagcagtgcagccgcctctttcacggtgcggccttcctggtcgatcagctcgcgggcgtgcgcgatctgtgccggggtgagggtag

ggcgggggccaaacttcacgcctcgggccttggcggcctcgcgcccgctccgggtgcggtcgatgattagggaacgctcgaactcggcaatgccggcgaac
acggtcaacaccatgcggccggccggcgtggtggtgtcggcccacggctctgccaggctacgcaggcccgcgccggcctcctggatgcgctcggcaatgtcc
agtaggtcgcgggtgctgcgggccaggcggtctagcctggtcactgtcacaacgtcgccagggcgtaggtggtcaagcatcctggccagctccgggcggtcg
cgcctggtgccggtgatcttctcggaaaacagcttggtgcagccggccgcgtgcagttcggcccgttggttggtcaagtcctggtcgtcggtgctgacgcgggcat
agcccagcaggccagcggcggcgctcttgttcatggcgtaatgtctccggttctagtcgcaagtattctactttatgcgactaaaacacgcgacaagaaaacgcc
aggaaaagggcagggcggcagcctgtcgcgtaacttaggacttgtgcgacatgtcgttttcagaagacggctgcactgaacgtcagaagccgactgcactata
gcagcggaggggttggatcaaagtactttaaagtactttaaagtactttaaagtactttgatcccgaggggaaccctgtggttggcatgcacatacaaatggacg
aacggataaaccttttcacgccctttaaatatccgattattctaataaacgctcttttctcttaggtttacccgccaatatatcctgtcaaacactgatagtttaaactga
aggcgggaaacgacaatctgatccaagctcaagctaagcttgcatgcctgcaggatatcgtggatccaagcttgccacgtgccgccacgtgccgccacgtgc
cgccacgtgcctctagaggatccatctccactgacgtaagggatgacgcacaatcccactatccttcgcaagacccttcctctatataaggaagttcatttcatttg
gagaggacacgctgggatccccaattccgggcggaatgaaagcgttaacggccaggcaacaagaggtgtttgatctcatccgtgatcacatcagccagaca
ggtatgccgccgacgcgtgcggaaatcgcgcagcgtttggggttccgttccccaaacgcggctgaagaacatctgaaggcgctggcacgcaaaggcgttatt
gaaattgtttccggcgcatcacgcgggattcgtctgttgcaggaagaggaagaagggttgccgctggtaggtcgtgtggctgccggtgaaccgtcgagcgcccc
cccgaccgatgtcagcctgggggacgagctccacttagacggcgaggacgtggcgatggcgcatgccgacgcgctagacgatttcgatctggacatgttggg
ggacggggattccccgggtccgggatttacccccacgactccgccccctacggcgctctggatatggccgacttcgagtttgagcagatgtttaccgatgccctt
ggaattgacgagtacggtggggatccgtctgctggagacatgagagctgccaacctttggccaagcccgctcatgatcaaacgctctaagaagaacagcctg
gccttgtccctgacggccgaccagatggtcagtgccttgttggatgctgagccccccatactctattccgagtatgatcctaccagaccttcagtgaagcttcgatg
atgggcttactgaccaacctggcagacagggagctggttcacatgatcaactgggcgaagagggtgccaggctttgtggatttgaccctccatgatcaggtcca
ccttctagaatgtgcctggctagagatcctgatgattggtctcgtctggcgctccatggagcacccagggaagctactgtttgctcctaacttgctcttggacaggaa
ccagggaaaatgtgtagagggcatggtggagatcttcgacatgctgctggctacatcatctcggttccgcatgatgaatctgcagggagaggagtttgtgtgcctc
aaatctattattttgcttaattctggagtgtacacatttctgtccagcaccctgaagtctctggaagagaaggaccatatccaccgagtcctggacaagatcacaga
cactttgatccacctgatggccaaggcaggcctgaccctgcagcagcagcaccagcggctggcccagctcctcctcatcctctcccacatcaggcacatgagt
aacaaaggcatggagcatctgtacagcatgaagtgcaagaacgtggtgcccctctatgacctgctgctggagatgctggacgcccaccgcctacatgcgccc
actagccgtggaggggcatccgtggaggagacggaccaaagccacttggccactgcgggctctacttcatcgcattccttgcaaaagtattacatcacggggg
aggcagagggtttccctgccacagtctgagagctccctggcggaattcccagagatgttagctgaaatcatcactaatcagataccaaaatattcaaatggaaat
atcaaaaagcttctgtttcatcaaaaatgactcgacctaactgagtaagctagcttgttcgagtattatggcattgggaaaactgtttttcttgtaccatttgttgtgcttgt
aatttactgtgtttttattcggttttcgctatcgaactgtgaaatggaaatggatggagaagagttaatgaatgatatggtccttttgttcattctcaaattaatattatttgttt
tttctcttatttgttgtgtgttgaatttgaaattataagagatatgcaaacattttgttttgagtaaaaatgtgtcaaatcgtggcctctaatgaccgaagttaatatgagga
gtaaaacactagatccccaaacaagcttgaaactgaaggcgggaaacgacaatctgatcatgagcggagaattaagggagtcacgttatgacccccgccga
tgacgcgggacaagccgttttacgtttggaactgacagaaccgcaacgttgaaggagccactcagccgcgggtttctggagtttaatgagc

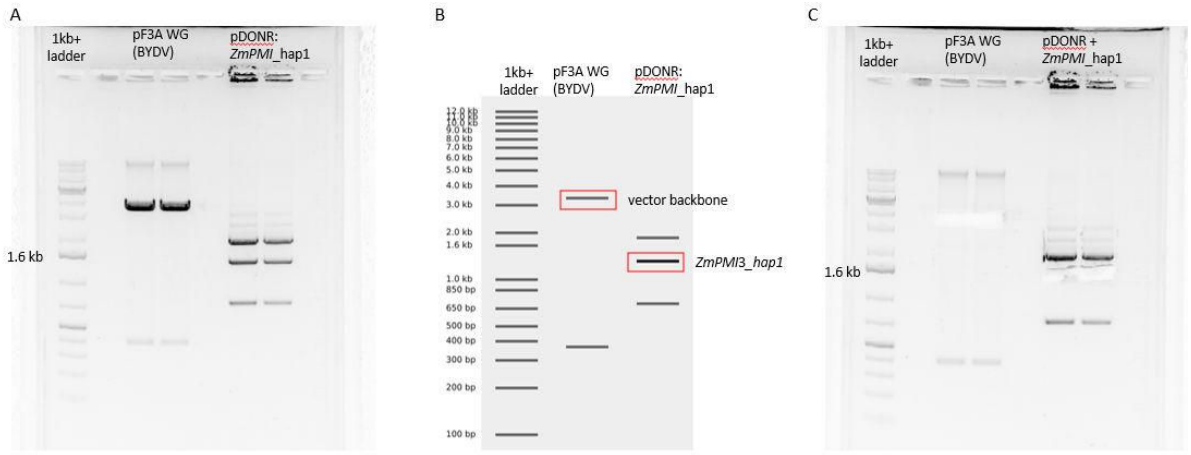

Figure 27: **Restriction enzyme digest of pF3A WG (BYDV) and pDONR:*ZmPMI3*_hap1.** Both vectors were digested with the enzymes SfaAI and MssI for 2 h. The resulting DNA fragments were separated via gel electrophoresis (A) and compared to the virtual digest prepared in Benchling (B). Accordingly, the respective bands of the pF3A WG (BYDV) vector backbone and the *ZmPMI3*_hap1 were cut out and used for molecular cloning (C).

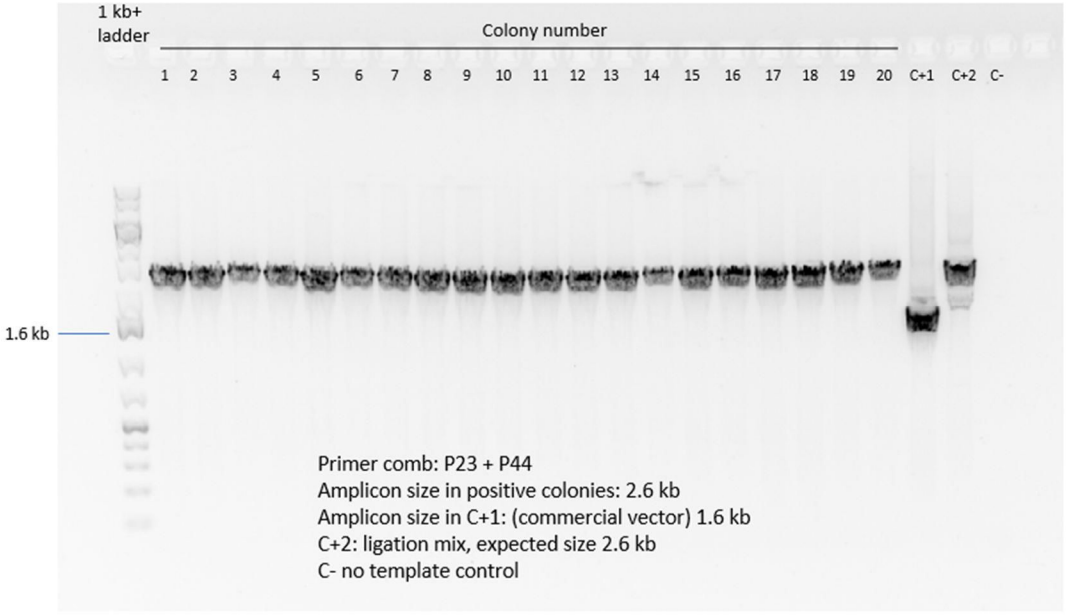

Figure 28: **Colony PCR of *E. coli* transformed with the ligated pF3A WG (BYDV) Flexi®::PMI_hap1 vector.** The P23 and P44 primers (Table 29) bind to the vector backbone flanking the insertion site for *PMI3*_hap1. The expected amplicon size in positive colonies is 2.6 kb; in C+1 (the commercial pF3A WG (BYDV) Flexi® vector) the amplicon size is 1.6 kb; in C+2, the ligation mixture used initially to transform *E. coli*, the expected amplicon size is 2.6 kb; no amplification was expected in C-.

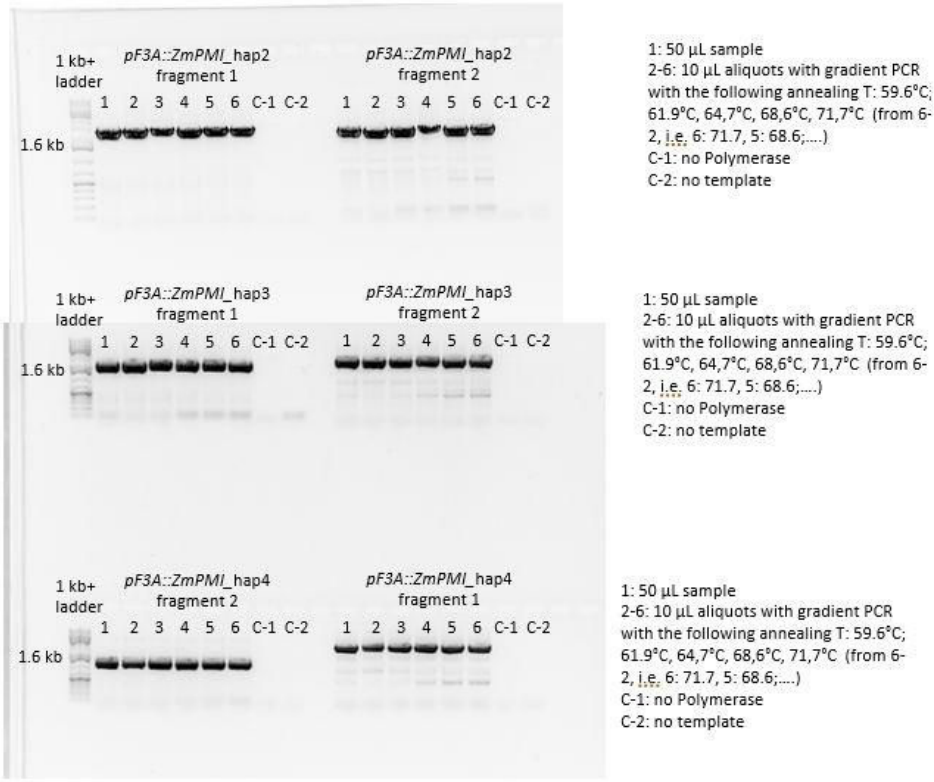

Haplotype	Primer combination fragment 1	Primer combination fragment 2
pF3A::PMI3_hap2	P21 + P16; amplicon 2228 bp	P22 + P15; amplicon 2409 bp
pF3A::PMI3_hap3	P21 + P18; amplicon 2549 bp	P22 + P17; amplicon 2088 bp
pF3A::PMI3_hap4	P21 + P20; amplicon 3273 bp	P22 + P19; amplicon 1364 bp

Figure 29: **Separation of the amplified Gibson fragments for pF3A::PMI3_hap2 to pF3A::PMI3_hap4 via gel electrophoresis.** C-1 is always the no Polymerase control, where no Phusion polymerase was added and C-2 is the no template control. Primer combinations and expected amplicon sizes are given below the gels, as well as in table Table 9 (section 3.8). Details regarding PCR protocol and primer generation are additionally provided in section 3.8 and all primer sequences are listed in Table 29.

Table 30: **Average temperatures (°C) and rainfall (mm) during the planting season of 2023 and 2024 in Düsseldorf.** Corn plants were grown outdoors in the botanical garden at HHU Düsseldorf and were used in chapter 2 (section 4.2). Data from meteostat.net.

	Year 2023		Year 2024	
Month	T (°C)	Rainfall (mm)	T (°C)	Rainfall (mm)
May	14.4	44.6	15.9	144.3
June	20.7	66.2	17.0	102.1
July	19.4	130.2	19.3	80.3
August	18.6	148.2	20.7	66.9
September	18.8	85.4	16.6	63.6
October	13.8	108.3	12.7	66.3

Table 31: **Distribution of water-soluble carbohydrates and lignocellulosic components among corn varieties digested by *U. maydis* (section 4.2.2).** Relative distribution based on the minimum and maximum detected for the whole data set. "+ + +" indicates the highest 10 %, "+ +" indicates the highest 30℅, "+" indicates lower than 30 % but higher than 50 % ; "-"indicates lower than 50 %, but higher than the lowest 30 % ("- -") and "- - -" indicates the lowest 10℅. Table is sorted by total water-soluble carbohydrate content.

Variety	Glucose	Fructose	Sucrose	Total	Xylose	HC	Cellulose	Lignin	*U. maydis* performance
B76	+	+	+	+ + +	- -	- -	+ +	-	+ + +
CI64	+	+	+	+ + +	+	+	+	-	+ +
F886	-	-	+ +	+ + +	+	+ +	+	+	+ +
FC13	-	- -	+ + +	+ + +	+	-	+	+	+ + +
Mo17	+ + +	+ + +	- -	+ +	-	-	-	-	+ +
FC1819	- -	- -	+ + +	+ +	+ +	+	+	+	+ + +
A619	- -	- -	+ + +	+ +	+	+ +	-	+	+ + +
NC232	- -	- -	+ + +	+ +	-	-	-	-	+ + +
F2834T	+	-	+	+ +	-	-	+ + +	- -	+ +
MoG	+	+	+	+ +	- -	-	+ + +	- -	+ + +
CI28A	-	-	+	+ +	-	+	+	- -	+ +
AR210	-	-	+ +	+ +	- - -	- -	+	-	+ +
NC306	- -	- -	+ +	+ +	+	+	+	- -	+ +
F918	+	+	+	+ +	-	-	+	-	+ + +
NC222	+ +	+ + +	- - -	+	-	-	+	-	-
NC314	+ +	+ + +	- - -	+	+	+	+	-	+
FC352	- - -	- - -	+ +	+	+	+ +	-	+	-
H49	+	+ + +	- - -	+	-	-	+	-	+
NC326	-	-	-	+	+ +	+ +	- -	+	+
B46	+ +	+ +	- - -	+	- -	- -	+	+	+
CML9	-	-	- -	+	- -	- -	-	- -	-
A251	-	-	+	+	+	+	+ + +	-	+
H91	+	+ +	- - -	+	+	+	- - -	-	-
NC320	-	-	-	+	+ +	+ +	- -	-	+
FAP1360A_1	- -	- -	+	+	+ +	+	+ +	+ + +	+
NC356	-	- -	+	+	+	+	+ +	+ + +	+
SC357	- -	- -	+ +	+	- -	- -	-	- -	+
F916	+	-	-	+	-	+	+	- -	+
F335	- - -	- - -	+	+	+	+	+	+	-
CO125	-	-	+	+	-	-	+	- -	+ +
F331	- -	+	- - -	-	-	+	+	+	- - -
F9003	+	+	- - -	-	-	+	+	-	-
F284	- - -	- -	-	-	+ + +	+ +	+	-	- - -
B52	- -	-	- - -	-	- - -	- - -	+	+	- - -
H95	+	-	- -	-	+	+	- - -	-	-
FAP1360A_2	- -	- -	-	-	+ +	+	+ +	+ + +	-
CH10	-	- -	- -	-	+	-	+	- -	-
4226	-	- -	- -	-	-	- -	+ +	-	- - -
F7	- -	- -	- - -	- -	+ +	+	+	-	- - -
F345	- -	- -	- - -	- -	-	-	+	-	- - -
F7	- - -	- - -	- - -	- - -	+ +	+	-	+	- - -
F268	- - -	- - -	- - -	- - -	+	+	+	+	- - -
FP1	- - -	- - -	- - -	- - -	+	+	-	-	- - -
F292	- - -	- - -	- - -	- - -	+ + +	+ + +	-	+	- - -
F76	- - -	- - -	- - -	- - -	+	-	- -	+	- - -

r = Pearson coefficient; Total = sum of water-soluble carbohydrates; HC = sum of hemicellulosic components; CC = crystalline cellulose

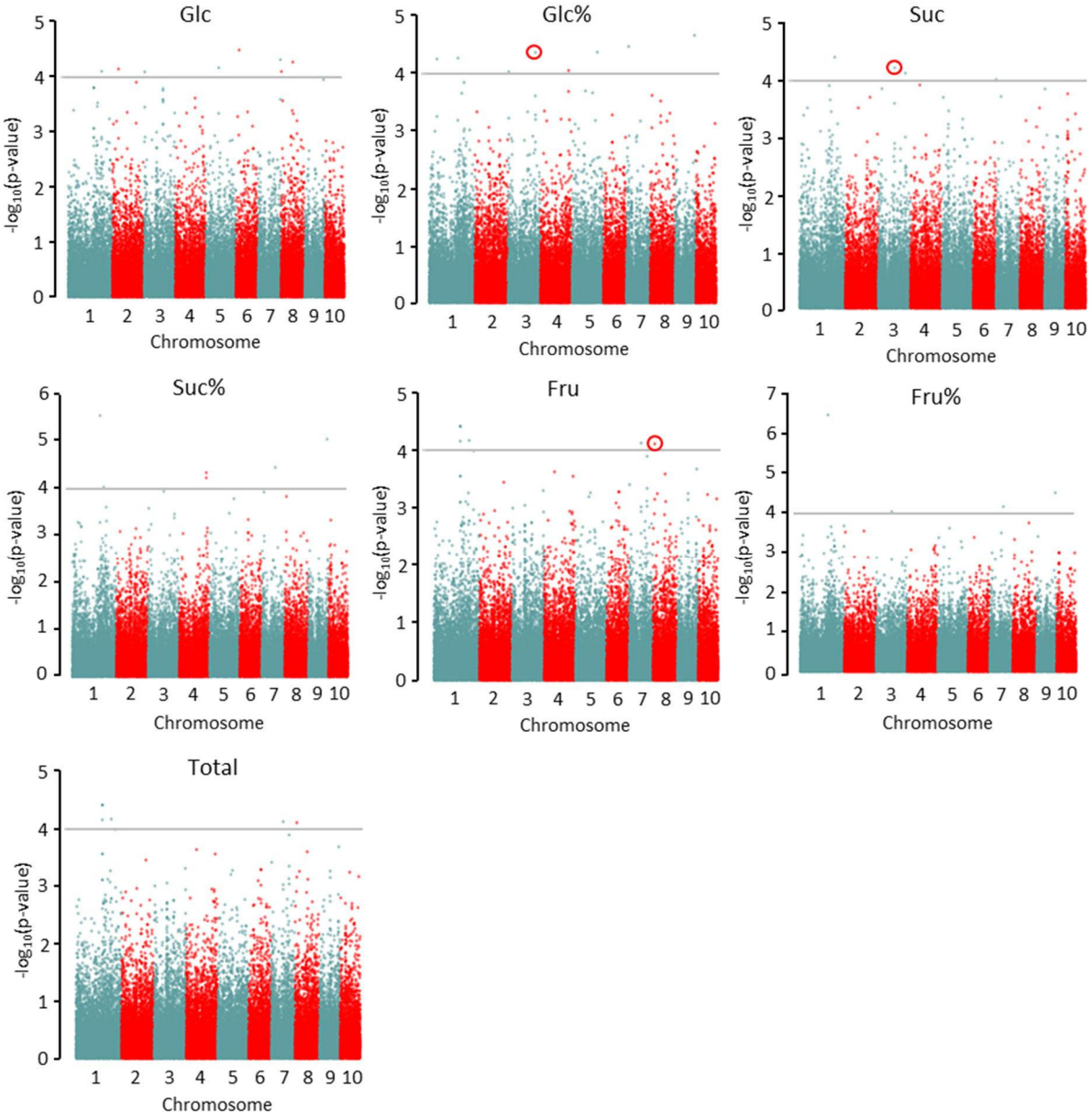

Figure 30: **Manhattan-plots of genome-wide association study (section 4.2.2).** The plots display the negative logarithm of the p-values for 44,293 SNPs across 212 corn varieties. Each dot represents one SNP, whose physical location in the genome is shown on the x-axis. Different colors distinguish the individual chromosomes. The horizontal line indicates the significance threshold of $p < 0.0001$. The traits are glucose (Glc), fructose (Fru), sucrose (Suc) in total and relative (%) abundance and the total water-soluble carbohydrates (Total). Red circles indicate the SNPs that define the QTLs which contain the selected candidate genes.

Table 32: **Significant SNPs correlating to the 7 traits and their physical position in B73 RefGen_v2 and RefGen_v5 (section 4.2.2).** The analyzed traits are absolute content of glucose (Glc), fructose (Fru), sucrose (Suc) and total soluble carbohydrate content (Total), as well as their relative composition (Glc%, Fru%, Suc%).

Trait	SNP ID/Locus	Chr	Physical position (bp) B73v2	-log(P-value)	Synonyms		Physical position (bp) B73v5
Glc	PZE.101192764	1	239535224	4.10	rs131868092	ss196431219	245178795
Glc	SYN19476	2	31830162	4.14	rs131181960	ss196508254	33385853
Glc	SYN6755	3	3701505	4.09	rs131186087	ss196526637	3755532
Glc	PZE.105075111	5	82881987	4.16	rs131538537	ss196463853	84814765
Glc	SYN26542	6	35091333	4.48	rs130247068	ss196513963	42964540
Glc	PZE.107134586	7	173482344	4.31	rs132449772	ss196481431	182524830
Glc	PZE.108002910	8	3159216	4.09	rs131640778	ss196481646	3467614
Glc	PZE.108056460	8	101409730	4.26	rs130826224	ss196485451	103380217
Glc%	PZE.100001759	1	202758306	4.27	rs128290545	ss196422021	207273252
Glc%	SYN2604	1	43062814	4.25	rs128425899	ss196513566	42913701
Glc%	PZE.103151399	3	205260873	4.36	rs129589441	ss196450046	210746242
Glc%	SYN6756	3	3700793	4.03	rs129536762	ss196526639	3754820
Glc%	PUT.163a.74232765.3578	4	224036678	4.05	rs129938789	ss196420761	231257952
Glc%	PZE.105128384	5	185626663	4.37	rs132256532	ss196467696	189323384
Glc%	PZE.107017579	7	15157101	4.47	No records found in MaizeGDB		
Glc%	PZE.109109692	9	150354622	4.66	rs132566677	ss196494292	156815497
Fru	PZE.101196778	1	244906397	4.22	rs128918254	ss196431418	250699962
Fru	PZE.101219678	1	271111712	4.04	rs131892013	ss196432348	277612674
Fru	SYN28099	1	189586308	4.47	No records found in MaizeGDB		
Fru	SYN28100	1	189588905	4.47	rs131826954	ss196515234	193783734
Fru	SYN28108	1	189589043	4.47	rs131183513	ss196515240	193783872
Fru	SYN3135	1	189359106	4.21	rs131826870	ss196517981	193552471
Fru	PZE.107053846	7	105221578	4.18	rs130599888	ss196478842	109896853
Fru	PZE.108010908	8	11504308	4.16	rs130713930	ss196481916	11956275
Fru%	PZE.100001759	1	202758306	6.47	rs128290545	ss196422021	207273252
Fru%	PZE.103083198	3	137788044	4.04	rs132033286	ss196447284	139390412
Fru%	PZE.107063028	7	120107334	4.17	rs130620836	ss196479442	125330985
Fru%	PZE.109109692	9	150354622	4.52	rs132566677	ss196494292	156815497
Suc	PZE.101195302	1	242541772	4.43	rs128913628	ss196431307	248216003
Suc	PZE.103084194	3	139508679	4.24	rs132034133	ss196447370	141163822
Suc	SYN8972	3	204363992	4.15	rs129395180	ss196528450	209675293
Suc	PZE.107000798	7	988177	4.03	rs131179431	ss196475190	845208
Suc%	PZE.100001759	1	202758306	5.54	rs128290545	ss196422021	207273252
Suc%	SYN21134	1	225041422	4.03	rs131857318	ss196509665	230598209
Suc%	PUT.163a.74232765.3576	4	224036660	4.22	rs129938788	ss196420757	231257934
Suc%	PUT.163a.74232765.3578	4	224036678	4.33	rs129938789	ss196420761	231257952
Suc%	PZE.107063028	7	120107334	4.44	rs130620836	ss196479442	125330985
Suc%	PZE.109109692	9	150354622	5.04	rs132566677	ss196494292	156815497
Total	PZE.101171014	1	214648677	4.26	No records found in MaizeGDB		
Total	PZE.107000798	7	988177	4.25	rs131179431	ss196475190	845208

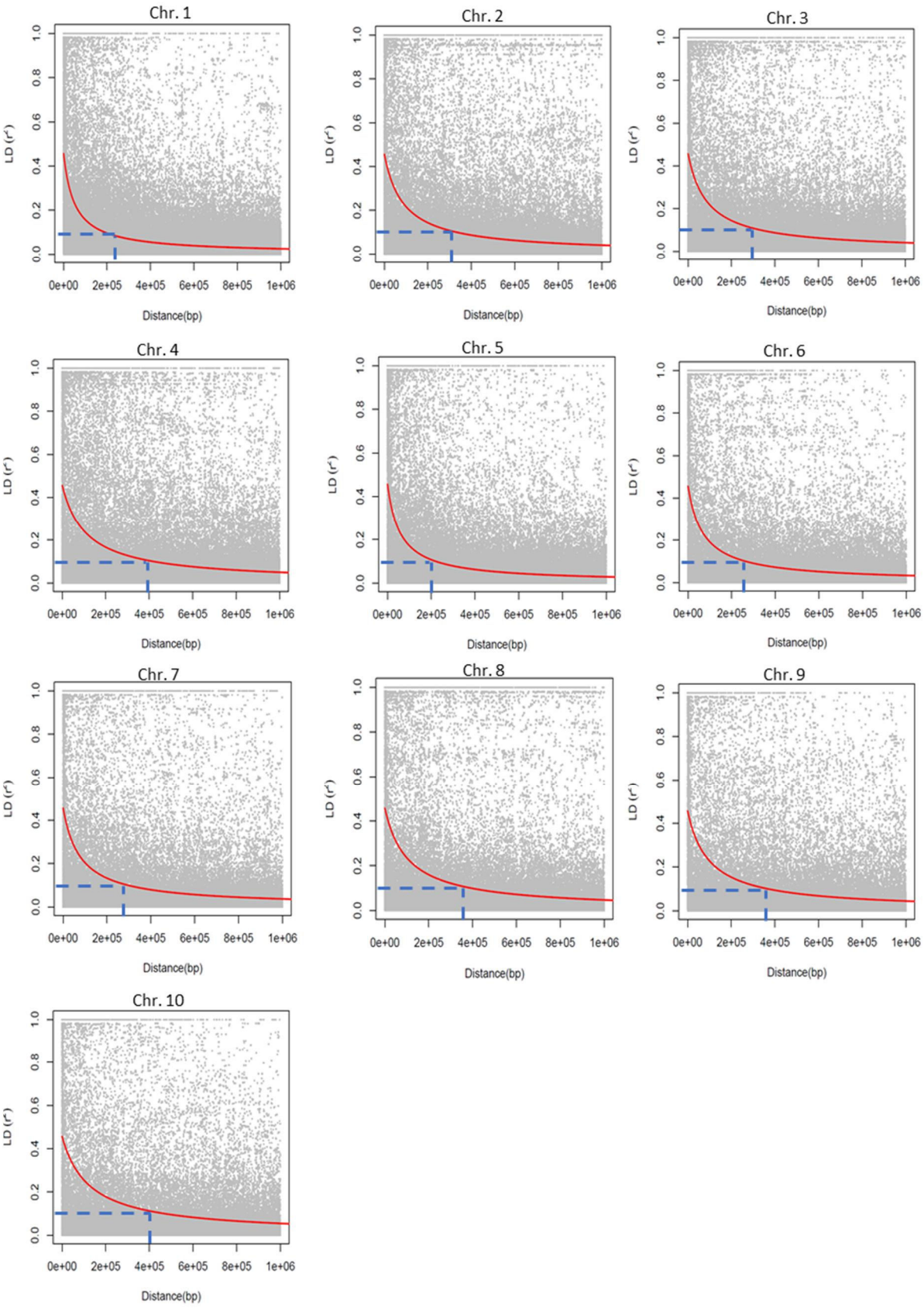

Figure 31: **Chromosome specific linkage disequilibrium decay plots (section 4.2.2).** Plotted is the r^2 between the SNPs against the physical distance between them. The red line shows the linkage disequilibrium decay, and the blue bars show the threshold of 0.1 and its corresponding physical distance.

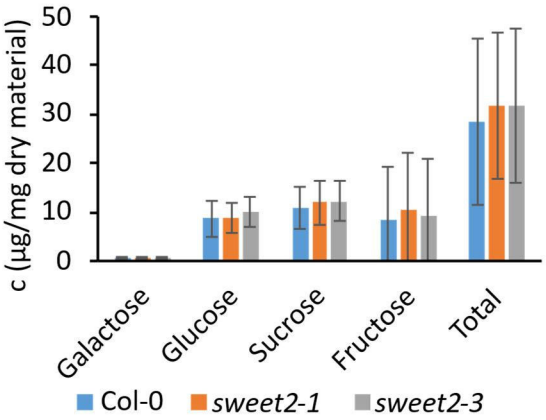

Figure 32: **Water-soluble carbohydrate content stem material of soil-grown *A. thaliana* T-DNA lines and wildtype (Col-0) (section 4.4.2).** Data are shown as average ± SD in µg per mg dry material. The stems of 17 Col-0, 18 *sweet2-1* and 16 *sweet2-3* plants were analyzed after 8 weeks. Significant differences between a T-DNA line (*sweet2-1* or *sweet2-3*) and Col-0 are indicated by an asterisk and determined by a one-way ANOVA followed by Tukey-HSD test with $p < 0.05$. No significant differences were detected.

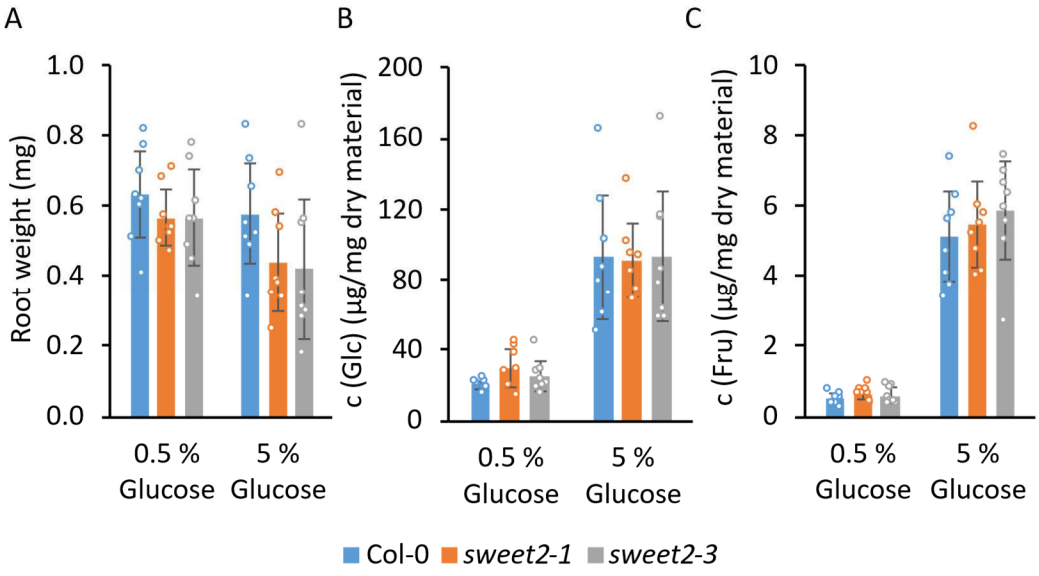

Figure 33: **Root weight and water-soluble carbohydrate content in *A. thaliana* lines (section 4.4.2).** A) Root weight of *A. thaliana* plants grown in hydroponic systems supplemented with 0.5 % or 5 % glucose. Depicted is the average ± SD of the individual root weight, determined by normalization of the pools to the number of roots within the pool. B/C) Soluble glucose (B) and fructose (C) content of these roots. Depicted are the average ± SD of 8 pools of roots (containing 2-3 individual roots) for each genotype. Datapoints represent individual measurements. Significant differences between a T-DNA line (*sweet2-1* or *sweet2-3*) and Col-0 are indicated by an asterisk and determined by a one-way ANOVA followed by Tukey-HSD test with $p < 0.05$. No significant differences were detected.

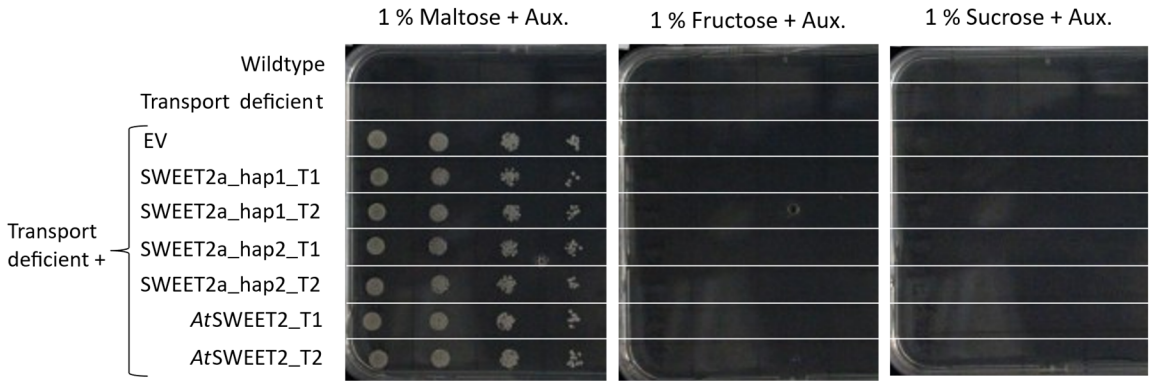

Figure 34: **Growth of *S. cerevisiae* strains on different carbohydrate containing media (section 4.4.2).** Different yeast strains *i.e.*, the wildtype strain, the transport deficient strain and the transport deficient strain transformed with ZmSWEET2a_hap1, _hap2, AtSWEET2 or the empty pDRf1-vector (EV) were spotted on synthetic medium containing different carbon sources. T1 and T2 refer to individual transformants. The amino acids histidine, tryptophan and leucine were added to the media. Uracil was used as selection marker for the pDRf1 vector and not added to the media, as indicated by Aux. The plates were incubated at 28℃ for four days before taking pictures. Individual spots from left to right show 10-fold dilutions. Neither the wildtype nor the transport deficient strain can grow on any media due to the absence of uracil, while the pDRf1-containing yeast strains grow only on maltose containing media, due to the absence of Fructose or Sucrose transport ability.

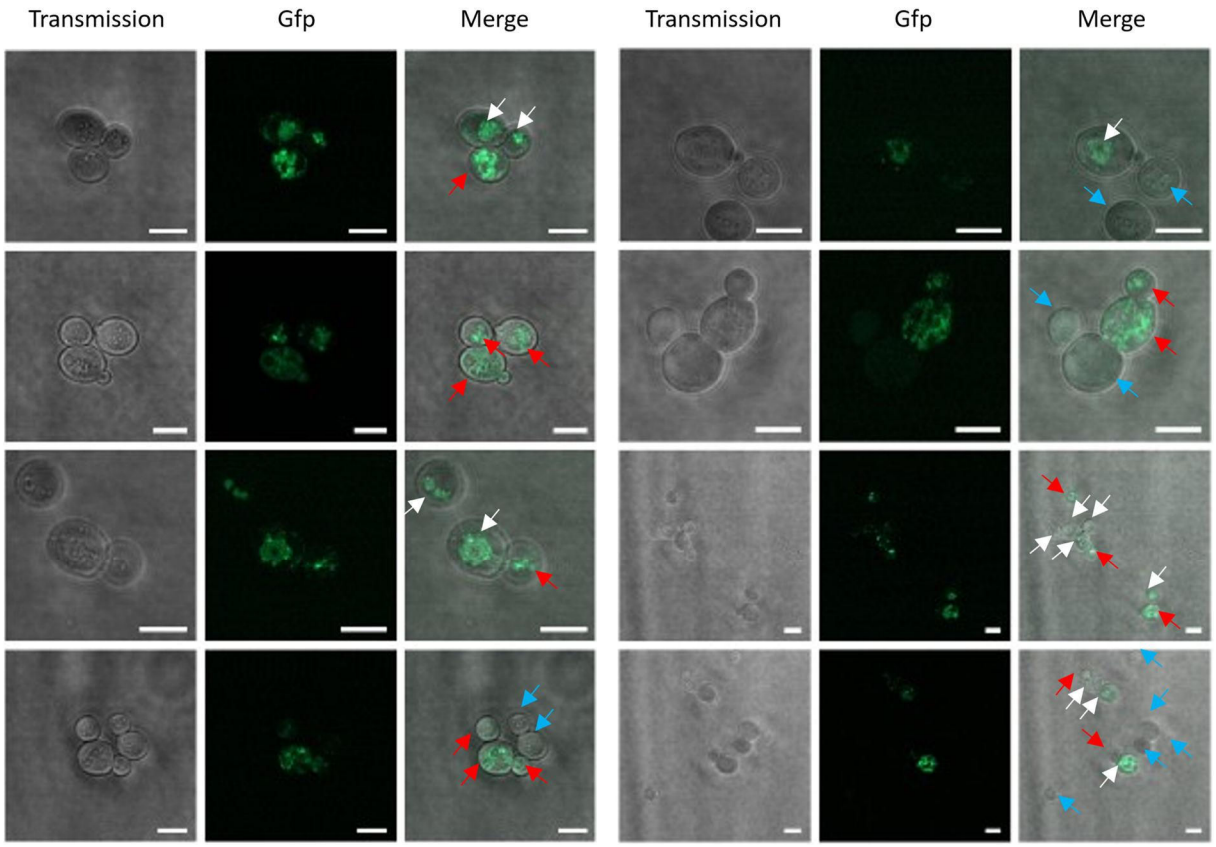

Figure 35: **Localization of GFP tagged ZmSWEET2a_hap1 in transport deficient *S. cerevisiae* strain (section 4.4.2).** Transmission and GFP pictures were taken by laser scanning confocal microscopy. White arrows indicate clear vacuolar localization, red arrows indicate diffuse localization, and blue arrows indicate not expressing cells. Scale bar: 5 µm.

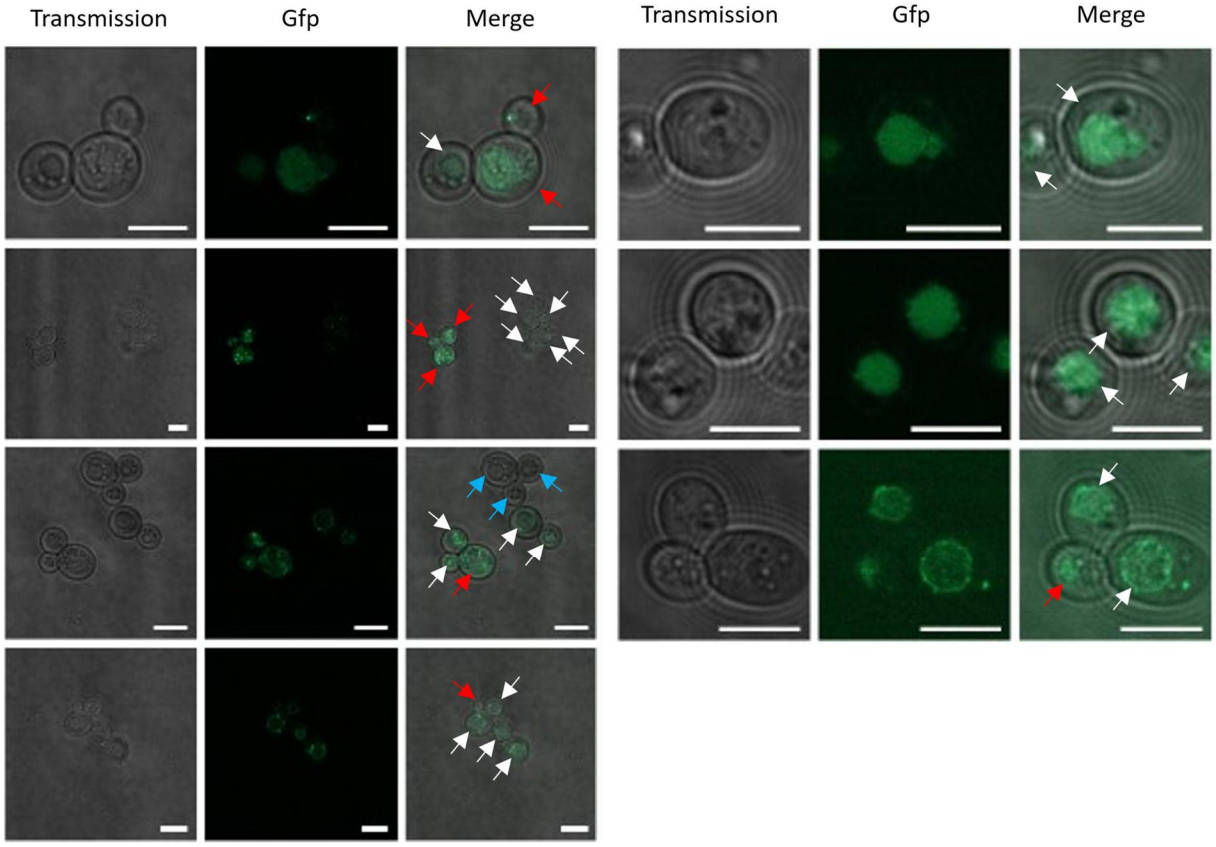

Figure 36: **Localization of GFP tagged ZmSWEET2a_hap2 in transport deficient *S. cerevisiae* strain (section 4.4.2).** Transmission and GFP images were taken by laser scanning confocal microscopy. White arrows indicate clear vacuolar localization, red arrows indicate diffuse localization, and blue arrows indicate not expressing cells. Scale bar: 5 µm.

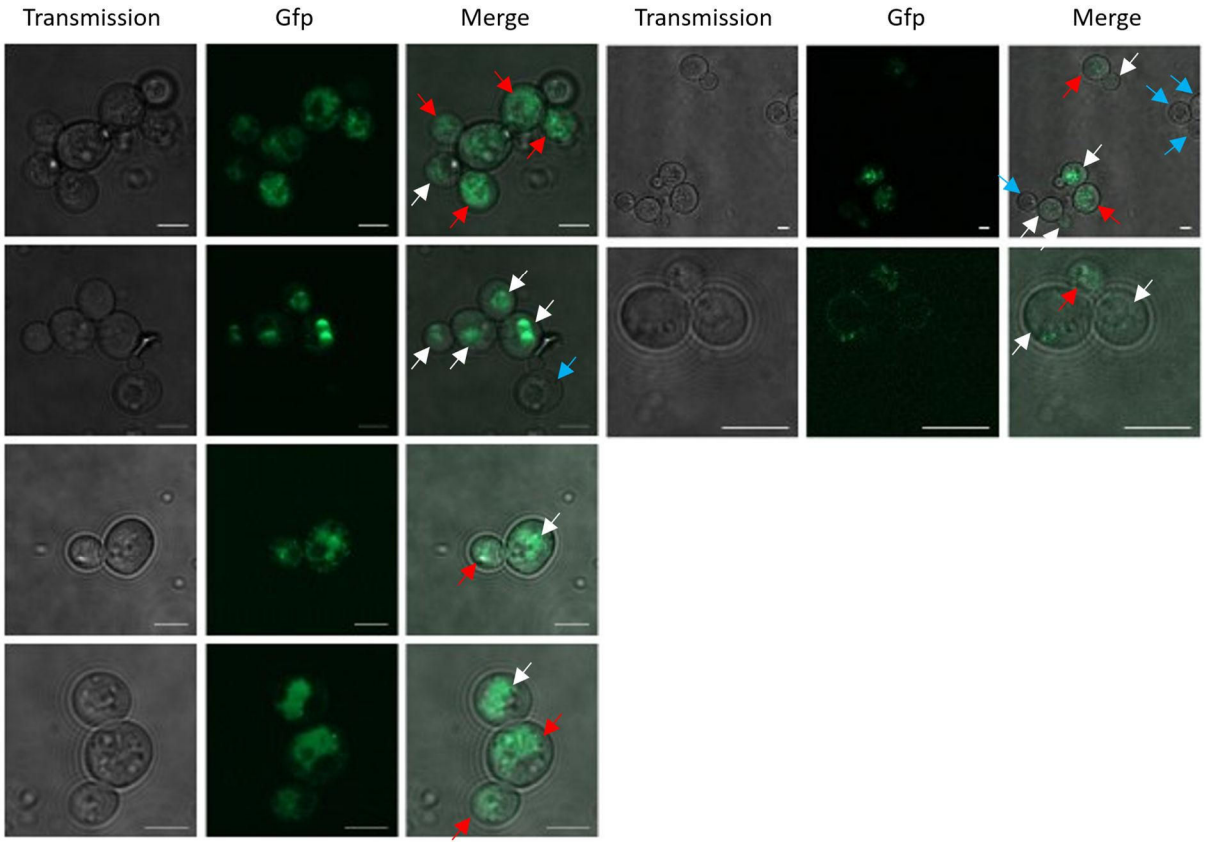

Figure 37: **Localization of GFP tagged *Os*SWEET2b in transport deficient *S. cerevisiae* strain (section 4.4.2).** Transmission and GFP pictures were taken by laser scanning confocal microscopy. White arrows indicate clear vacuolar localization, red arrows indicate diffuse localization, and blue arrows indicate not expressing cells. Scale bar: 5 µm.

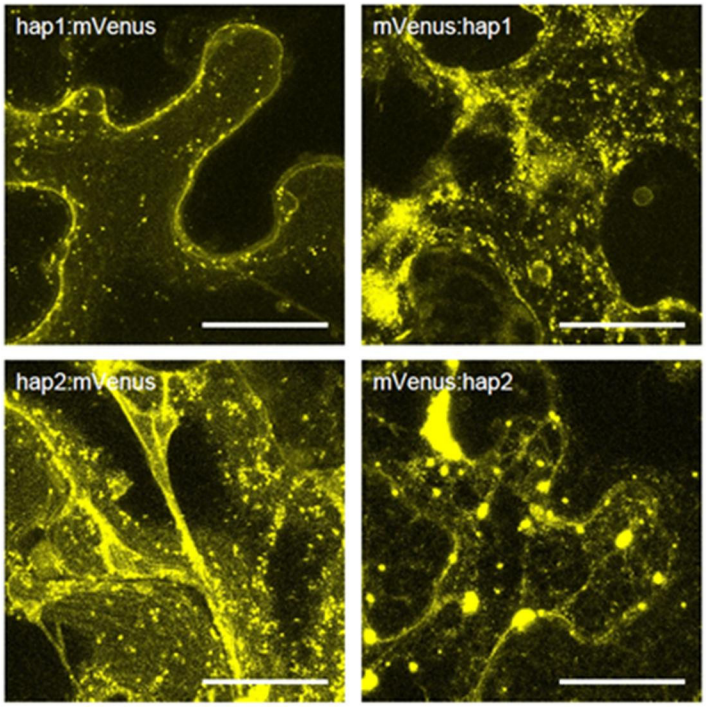

Figure 38: **Subcellular localization of mVenus tagged SWEET2a_hap1 and SWEET2a_hap2 in *N. benthamiana* leaf cells (section 4.4.2).** Pictures were taken 3 days post infiltration and 5 h post induction with laser scanning confocal microscopy. Pictures are the overlay of multiple z-stacks. Scale bar = 50 µm.

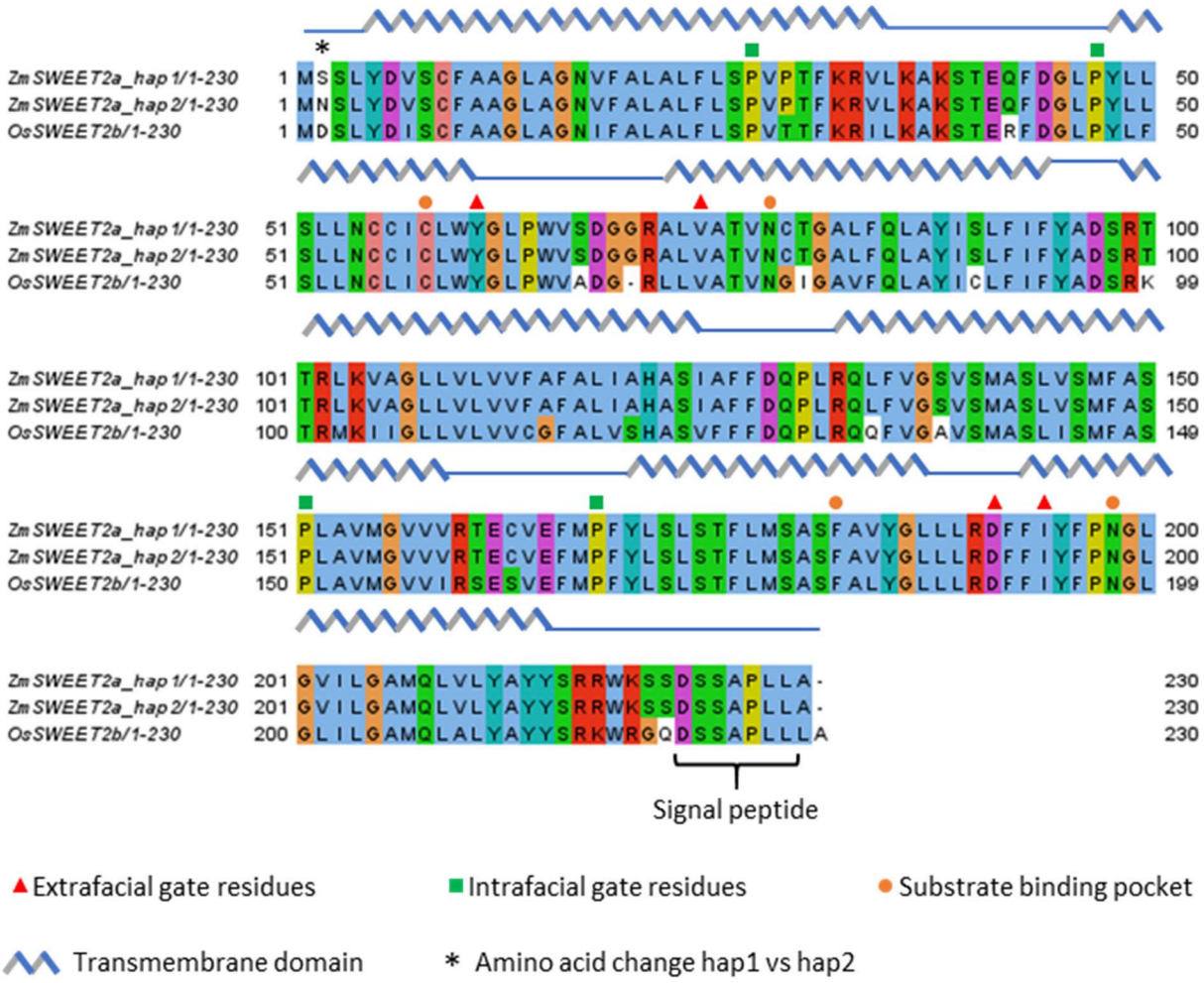

Figure 39: **Primary sequence alignment of ZmSWEET2a hap1 and 2 and OsSWEET2b proteins (section 4.4.2).** The alignment was done with Clustal Omega (1.2.4) (Madeira et al., 2024) using the default parameters and visualized with Jalview (2.11.4.1). Extra-/Intrafacial gate, substrate binding pocket and transmembrane domain were marked based on the *Os*SWEET2b sequence (Tao et al., 2015). The position of the signal peptide was predicted with DeepLoc (2.0).

Table 33: **Bradford assay of PMI3 haplotypes and a no protein control (section 4.5.2).** Protein concentrations were calculated with a bovine serum albumin standard curve.

Sample	c (total protein) (µg/µL)
ZmPMI3_hap1	6.15
ZmPMI3_hap2	6.27
ZmPMI3_hap3	6.66
ZmPMI3_hap4	7.13
No protein	7.15

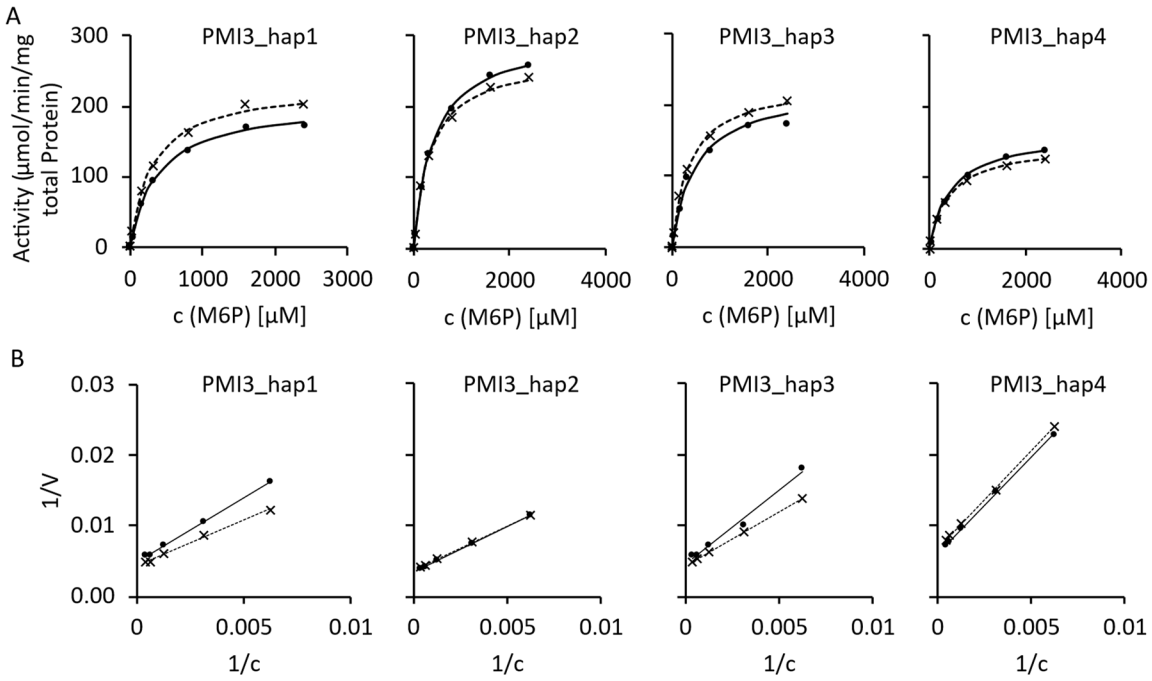

Figure 40: **Kinetics of F6P synthesis of *Zm*PMI3 haplotypes (section 4.5.2).** For the Michaelis-Menten plots (A), the results are depicted as the individual measurements of two different protein concentrations (points and crosses). The curves are calculated based on the Vmax and Km values determined with the Lineweaver Burk plots (B).

Licence to Publish - Open Access

SPRINGER NATURE

Licensee:	State Key Laboratory of Bioreactor Engineering, East China University of Science and Technology	(the 'Licensee')
Journal Name:	Bioresources and Bioprocessing	(the 'Journal')
Manuscript Number:	BIOB-D-24-00159R1	
Proposed Title of Article:	Monitoring corn stover processing by the fungus Ustilago maydis	(the 'Article')
Author(s) [Please list all named Authors]:	Stefan Robertz, Magnus Philipp, Kerstin Schipper, Paul Richter, Katharina Miebach, Jorgen Magnus, Markus Pauly, Vicente Ramírez	(the 'Author')
Corresponding Author Name:	Vicente Ramírez	

Licence Applicable to the Article:

Creative Commons licence CC BY: This licence allows readers to copy, distribute and transmit the Article as long as it is attributed back to the author. Readers are permitted to alter, transform or build upon the Article, and to use the Article for commercial purposes. Please read the full licence for further details at - http://creativecommons.org/licenses/by/4.0/

Subject to editorial acceptance of the Article, it will be published under the Creative Commons licence shown above.

1 Grant of Rights

a) For good and valuable consideration, the Author hereby grants to the Licensee the perpetual, non-exclusive, irrevocable, world-wide, assignable, sublicensable and unlimited right to: publish, reproduce, copy, distribute, communicate, display publicly, sell, rent and/ or otherwise make available the article identified above, including any supplementary information and graphic elements therein (e.g. illustrations, charts, moving images) (the "Article") in any language, in any versions or editions in any and all forms and/or media of expression (including without limitation in connection with any and all end-user devices), whether now known or developed in the future. Without limitation, the above grant includes: (i) the right to edit, alter, adapt, adjust and prepare derivative works; (ii) all commercial use, advertising, and marketing rights, including without limitation graphic elements on the cover of the journal and in relation to social media; (iii) rights for any training, educational and/or instructional purposes; (iv) the right to add and/or remove links or combinations with other media/works; and (v) the right to create, use and/or license and/or sublicense content data or metadata of any kind in relation to the Article (including abstracts and summaries) without restriction. The above rights are granted in relation to the Article as a whole or any part and with or in relation to any other works.

b) Without limiting the rights granted above, Licensee is granted the rights to use the Article for the purposes of analysis, testing, and development of publishing- and research-related workflows, systems, products, projects, and services; to confidentially share the Article with select third parties to do the same; and to retain and store the Article and any associated correspondence/files/forms to maintain the historical record, and to facilitate research integrity investigations. The grant of rights set forth in this clause (b) is irrevocable.

c) The Licensee will have the right, but not the obligation, to exercise any or all of the rights granted herein. If the Licensee elects not to publish the Article for any reason, all publishing rights under this Agreement as set forth in clause 1.a) above will revert to the Author.

2 Copyright

Ownership of copyright in the Article will be vested in the name of the Author. When reproducing the Article or extracts from it, the Author will acknowledge and reference first publication in the Journal.

3 Use of Article Versions

a) For purposes of this Agreement: (i) references to the "Article" include all versions of the Article; (ii) "Submitted Manuscript" means the version of the Article as first submitted by the Author; (iii) "Accepted Manuscript" means the version of the Article accepted for publication, but prior to copy-editing and typesetting; and (iv) "Version of Record" means the version of the Article published by the Licensee, after copy-editing and typesetting. Rights to all versions of the Manuscript are granted on a non-exclusive basis.

b) The Author may make the Submitted Manuscript available at any time and under any terms (including, but not limited to, under a CC BY licence), at the Author's discretion. Once the Article has been published, the Author will include an acknowledgement and provide a link to the Version of Record on the publisher's website: "This preprint has not undergone peer review (when applicable) or any post-submission improvements or corrections. The Version of Record of this article is published in [insert journal title], and is available online at https://doi.org/[insert DOI]".

c) Immediately after acceptance the Author may deposit the Accepted Manuscript to any location, and under any terms (including, but not limited to, under a CC BY licence), provided it is not made publicly available until after publication. The Author will include an acknowledgement in the Accepted Manuscript, together with a link to the Version of Record on the publisher's website: "This version of the article has been accepted for publication, after peer review (when applicable) but is not the Version of Record and does not reflect post-acceptance improvements, or any corrections. The Version of Record is available online at: http://dx.doi.org/[insert DOI]".

4 Warranties & Representations

Author warrants and represents that:

a)

i. the Author is the sole copyright owner or has been authorised by any additional copyright owner(s) to grant the rights defined in clause 1,

ii. the Article does not infringe any intellectual property rights (including without limitation copyright, database rights or trade mark rights) or other third party rights and no licence from or payments to a third party are required to publish the Article,

iii. the Article has not been previously published, nor has the Author committed to licensing any version of the Article under a licence inconsistent with the terms of this Agreement,

iv. if the Article contains materials from other sources (e.g. illustrations, tables, text quotations), Author has obtained written permissions to the extent necessary from the copyright holder(s), to license to the Licensee the same rights as set out in clause 1 and has cited any such materials correctly;

b) all of the facts contained in the Article are according to the current body of research true and accurate;

c) nothing in the Article is obscene, defamatory, violates any right of privacy or publicity, infringes any other human, personal or other rights of any person or entity or is otherwise unlawful and that informed consent to publish has been obtained for any research participants;

d) nothing in the Article infringes any duty of confidentiality owed to any third party or violates any contract, express or implied, of the Author;

e) all institutional, governmental, and/or other approvals which may be required in connection with the research reflected in the Article have been obtained and continue in effect;

f) all statements and declarations made by the Author in connection with the Article are true and correct; and

g) the signatory who has signed this agreement has full right, power and authority to enter into this agreement on behalf of all of the Authors.

5 Cooperation

a) The Author will cooperate fully with the Licensee in relation to any legal action that might arise from the publication of the Article, and the Author will give the Licensee access at reasonable times to any relevant accounts, documents and records within the power or control of the Author. The Author agrees that any Licensee affiliate through which the Licensee exercises any rights or performs any obligations under this Agreement is intended to have the benefit of and will have the right to enforce the terms of this Agreement.

b) Author authorises the Licensee to take such steps as it considers necessary at its own expense in the Author's name(s) and on their behalf if the Licensee believes that a third party is infringing or is likely to infringe copyright in the Article including but not limited to initiating legal proceedings.

6 Author List

Changes of authorship, including, but not limited to, changes in the corresponding author or the sequence of authors, are not permitted after acceptance of a manuscript.

7 Post Publication Actions

The Author agrees that the Licensee may remove or retract the Article or publish a correction or other notice in relation to the Article if the Licensee determines that such actions are appropriate from an editorial, research integrity, or legal perspective.

8 Controlling Terms

The terms of this Agreement will supersede any other inconsistent terms that the Author or any third party may assert apply to any version of the Article.

9 Governing Law

This Agreement will be governed by, and construed in accordance with, the laws of the Republic of Singapore. The courts of Singapore, Singapore will have exclusive jurisdiction.

Signed for and on behalf of the Author(s)
Corresponding Author: Vicente Ramírez
Email: ramirezg@hhu.de
IP Address: 134.99.202.33

Time Stamp: 2024-09-10 11:53:33

Figure 41: **Publication License (CC BY) Agreement for the Publication "Monitoring Corn Stover Processing by the fungus *Ustialgo maydis*" (Robertz et al., 2024) granting the right to reuse figures, data and text, if proper attribution is given.**

[Extern] RE: Request for permission to Reuse Published Data in PhD Thesis

Von Frontiers in Plant Science - Journal <plantscience@frontiersin.org>
An robertst@hhu.de <robertst@hhu.de>
Datum 2025-09-05 12:49

Dear Stefan,

Thank you for your message and for outlining your request so clearly.

You are welcome to reuse content from your article published in Frontiers in Plant Science for your PhD thesis. Frontiers articles are published under the Creative Commons Attribution License (CC BY), which allows you to reproduce, distribute, and adapt material, including data and figures, from your own work, as long as you provide appropriate citation to the original article.

Since your thesis may be publicly available via your university's repository, please make sure to include a full citation to the published article in Frontiers and a note indicating it is distributed under the CC BY license. No additional permission or paperwork from Frontiers is needed, as the license already provides the necessary authorization, but this email can serve as a formal confirmation should your institution require it.

If your institution needs a more specific letter or has any formal requirements, please let us know and we would be happy to assist.

Best wishes,

Silvia Ziliotto, PhD
Journal Specialist

Frontiers in Plant Science

Impact Factor 4.8, CiteScore 8.8
900,00+ citations

Senior Journal Manager: Shirley Deng
Journal Manager: Ana Castro

Frontiers
www.frontiersin.org

---------- Original Message ----------
From: Stefan Josef Robertz [robertst@hhu.de]
Sent: 4/9/2025, 19:50
To: plantscience@frontiersin.org
Subject: Request for permission to Reuse Published Data in PhD Thesis

Dear Editorial Office,

I hope this message finds you well.

I am writing to formally request permission to reuse data and figures from my article published in Frontiers in Plant Science, titled "A large-scale forward genetic screen for maize mutants with altered lignocellulosic properties" in my upcoming PhD thesis.
https://doi.org/10.3389/fpls.2023.1099009

I understand that the article is published under the terms of Creative Commons Attribution License (CC BY), which permits reuse of content provided that proper attribution is given. While this license allows for such use, I would like to obtain formal approval from the Journal as a courtesy and to comply with academic best practices, particularly as my institution advises obtaining explicit permission when reusing previously published material in a doctoral thesis.

The thesis will be submitted to Heinrich-Heine-Universität Düsseldorf and may be made publicly available through the university's institutional repository.

Please let me know, if any further information is required, or if there are specific conditions I should observe when reusing this material.

Thank you very much for your time and consideration!

Kind regards,

Stefan Robertz

Institute for Plant Cell Biology and Biotechnology

Figure 42: **Permission to reuse published data, figures and text from the publication "A large-scale forward genetic screen for maize mutants with altered lignocellulosic properties" (S. Wang et al., 2023).**

8 Acknowledgements

First and foremost, I want to thank Prof. Dr. Markus Pauly for giving me the opportunity to pursue my PhD project in his institute. His continuous scientific input, guidance, and support throughout the entire period have been invaluable. I am also sincerely thankful to him for offering me a PostDoc position even before the submission of this thesis. Additionally, I want to thank Prof. Dr. Michael Feldbrügge for taking over the role of the mentor and his scientific input during the project meetings.

I am deeply thankful for all the help from my co-supervisor Dr. Vicente Ramirez Garcia, who supported me from the first day. His openness, patience, and encouragement to think beyond the boundaries of my own project have had a great and lasting impact on my scientific development. I would also like to thank him for motivating me early on to think about my future beyond my PhD.

I would also like to thank Katharina Grosche for her excellent support with all analytical instruments in the lab, for sharing countless long lab days with me, and for all the great conversations both inside and outside the lab. In addition, I would like to thank her for insisting on showing me funny dog videos. Furthermore, I nod to Benjamin Menn for becoming a good friend during our shared PhD suffering. A special thank-you goes to Dr. Shaogan Wang for his support and for sharing his knowledge on plants, genotyping, GWAS, proteins etc. with me. Then I would like to thank Barbara Schulten, Felix Roth and Konstantin Shek for making sure that the everyday work in the lab runs smoothly and for all conversations about lab related and unrelated stuff. I would also like to thank everyone at the Institute for Plant Cell Biology and Biotechnology who was there during my time and contributed to the nice work atmosphere, especially my PhD colleagues Gabriel, Marius, Ronja and Lucas!

In addition, I would like to thank my family and my friends for their moral support. To my parents, my grandfather and my sister, thank you for trying to understand what my project is about and why I am not just making popcorn out of the maize. Special thanks go to Lion Schmitter and Dr. Sophie Weber as my best friends for always being there for me. And finally thank you to all my friends for the countless hours of fun that we spent together talking, playing Leberschuss (of course, not competitively), going to concerts or festivals, or whatever. You know, I´m not a man of many words, so simply Thank you all!